

IEEE

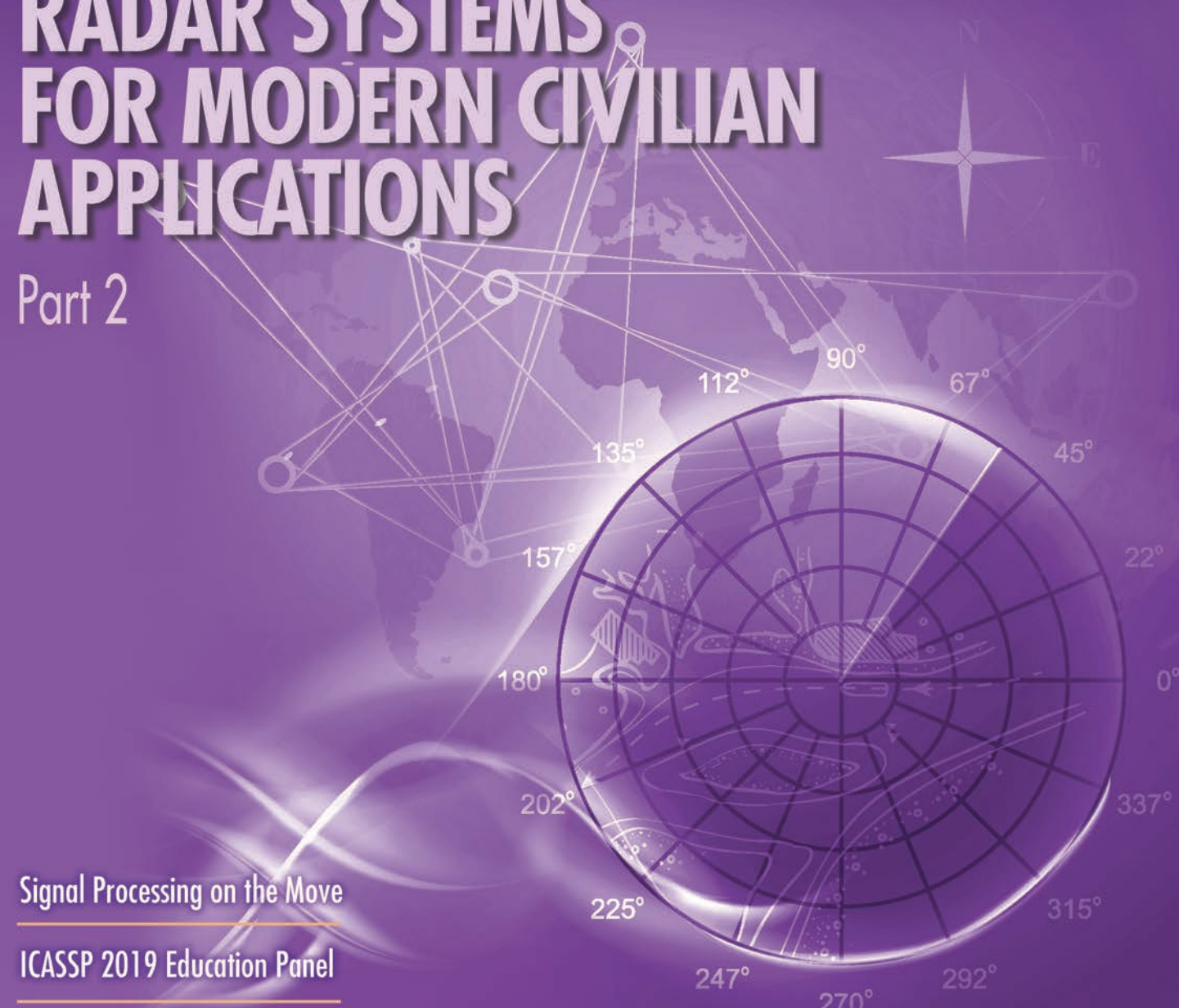
# Signal Processing

Volume 36 | Number 5 | September 2019

MAGAZINE

## RADAR SYSTEMS FOR MODERN CIVILIAN APPLICATIONS

Part 2



---

Signal Processing on the Move

---

ICASSP 2019 Education Panel

---

Perspectives in Autonomous  
Systems Research

**Call for Papers**  
**IEEE Signal Processing Society**  
**IEEE SIGNAL PROCESSING MAGAZINE**

**Special Issue on Graph Signal Processing: Foundations and Emerging Directions**

As modern data is getting more heterogeneous and intricate, identifying and leveraging its intrinsic structure and geometry emerges as a crucial task. The postulation of parsimonious models for the available information and the existing interdependencies is critical not only to understand the data at hand, but also to define effective compression, reconstruction, and inference architectures to process the available information. Graph signal processing (GSP) has approached this problem by modeling the structure of the data using a graph and, then, viewing the available information as a signal defined on top of it. A plethora of graph signals exists, with examples ranging from neurological activity patterns defined on top of brain networks to the spread of epidemics over social networks. Most early GSP efforts assumed that the underlying network was known, and then analyzed how the graph's algebraic and spectral characteristics impact the properties of the graph signals of interest. More recently, the focus has been on setups where the graph is implicit and must be learned from the data itself. While the theoretical and practical success achieved by GSP in the last years has been noticeable, many issues remain open, with, e.g., robust, nonlinear, or higher-dimensional GSP being at their infancy.

This Special Issue aims at introducing recent GSP advances, identifying some of its emerging directions, and presenting relevant practical problems that can be successfully addressed using GSP tools. The overall goal is to provide an overview of the current state of GSP, making it accessible to a broader audience who will ultimately contribute to shape the future of the field.

**Topics of interest include (but are not limited to):**

- Theoretical foundations for GSP: Advanced models for graphs, graph signals and graph filters
- Nonlinear GSP
- Beyond graph models: Hyper-based and tensor-based GSP
- Statistical and robust GSP
- Graph topology inference, including directed graphs and applications to causality
- Machine learning for graph signals and geometric data
- Applications of SP over directed graphs to causal inference
- Deep learning architectures for graph signals and geometric data
- Algorithmic advances, distributed computations and large-scale graphs
- Bioengineering, neuroscience and bioinformatics using GSP-tools
- Communication, power, and transportation networks using GSP-tools
- Finance, economics, and social networks using GSP-tools
- Speech, image and video processing using GSP-tools

**Submission Process**

The Special Issue seeks to offer broad coverage of the field including most recent developments in both theory and applications. Submissions of comprehensive overviews are strongly encouraged, as well as papers dealing with new and emerging applications provided that are accessible for a broad audience. White papers are required, and full articles are invited based on the review of white papers. Submissions will be reviewed according to the IEEE Signal Processing Magazine guidelines, and should not have been published or under review elsewhere.

Manuscripts should be submitted online at <http://mc.manuscriptcentral.com/sps-ieee> using the Manuscript Central interface, see <http://www.signalprocessingsociety.org/publications/periodicals/spm/> for guidelines and information.

**Important Dates**

White papers (4 pages) due: October 7, 2019

Invitation notification: November 15, 2019

Manuscripts due: February 15, 2020

Review results and decision notification: May 1, 2020

Revised manuscripts due: June 7, 2020

Final acceptance notification: July 7, 2020

Final manuscripts due: August 1, 2020

Publication due: **November 1, 2020**

**Guest Editors:**

Antonio G. Marques, King Juan Carlos University, Spain, [antonio.garcia.marques@urjc.es](mailto:antonio.garcia.marques@urjc.es)

José M.F Moura, Carnegie Mellon University, USA, [moura@ece.cmu.edu](mailto:moura@ece.cmu.edu)

Dimitri Van De Ville, EPFL and University of Geneva, Switzerland, [dimitri.vandeville@epfl.ch](mailto:dimitri.vandeville@epfl.ch)

Rebecca Willett, University of Chicago, USA, [willett@uchicago.edu](mailto:willett@uchicago.edu)

Negar Kiyavash, Georgia Institute of Technology, USA, [negar.kiyavash@ece.gatech.edu](mailto:negar.kiyavash@ece.gatech.edu)

# Contents

Volume 36 | Number 5 | September 2019

## SPECIAL SECTION

### ADVANCES IN RADAR SYSTEMS FOR MODERN CIVILIAN AND COMMERCIAL APPLICATIONS: PART 2

#### 16 FROM THE GUEST EDITORS

Maria S. Greco, Jian Li, Teng Long, and Abdelhak Zoubir

#### 20 THE RISE OF RADAR FOR AUTONOMOUS VEHICLES

Igal Bilik, Oren Longman, Shahar Villevan, and Joseph Tabrikian

#### 32 HIGH-PERFORMANCE AUTOMOTIVE RADAR

Gor Hakobyan and Bin Yang

#### 45 INTERFERENCE IN AUTOMOTIVE RADAR SYSTEMS

Stephen Allard, Wayne Stark, Murtaza Ali, and Manju Hegde

#### 60 ON THE SAFE ROAD TOWARD AUTONOMOUS DRIVING

Michael Gerstmair, Alexander Melzer, Alexander Onic, and Mario Huemer



PG. 12



#### ON THE COVER

Part 2 of this special issue of *IEEE Signal Processing Magazine* continues with articles regarding the techniques applied in different scenarios by different systems, focusing particularly on some of the new civil and commercial applications (see the July 2019 issue for Part 1). This issue includes eight special issue articles. Happy reading!

COVER IMAGE: IMAGE LICENSED BY INGRAM PUBLISHING

#### 71 RADAR-ON-CHIP/IN-PACKAGE IN AUTONOMOUS DRIVING VEHICLES AND INTELLIGENT TRANSPORT SYSTEMS

Sergio Saponara, Maria Sabrina Greco, and Fulvio Gini

#### 85 RADAR AND COMMUNICATION COEXISTENCE: AN OVERVIEW

Le Zheng, Marco Lops, Yonina C. Eldar, and Xiaodong Wang

#### 100 TOWARD MILLIMETER-WAVE JOINT RADAR COMMUNICATIONS

Kumar Vijay Mishra, M.R. Bhavani Shankar, Visa Koivunen, Björn Ottersten, and Sergiy A. Vorobyov

#### 115 DUAL-FUNCTION RADAR COMMUNICATION SYSTEMS

Aboulnasr Hassanien, Moeness G. Amin, Elias Aboutanios, and Braham Himed

## COLUMNS

#### 8 Society News

Election of President-Elect, Regional Directors-at-Large, and Members-at-Large  
Rabab K. Ward

#### 9 Reader's Choice

Top Downloads in IEEE Xplore

#### 12 Special Reports

Signal Processing on the Move  
John Edwards

#### 127 Conference Highlights

Quo Vadis ICASSP: Echoes of 2019  
ICASSP in Brighton, United Kingdom  
Danilo P. Mandic, Petar M. Djurić, Andrzej Cichocki, Clive Cheong-Took, Saeid Sanei, and Lajos Hanzo



PG. 127

**IEEE SIGNAL PROCESSING MAGAZINE** (ISSN 1053-5888) (ISPREG) is published bimonthly by the Institute of Electrical and Electronics Engineers, Inc., 3 Park Avenue, 17th Floor, New York, NY 10016-5997 USA (+1 212 419 7900). Responsibility for the contents rests upon the authors and not the IEEE, the Society, or its members. Annual member subscriptions included in Society fee. Nonmember subscriptions available upon request. **Individual copies:** IEEE Members US\$20.00 (first copy only), nonmembers US\$241.00 per copy. Copyright and Reprint Permissions: Abstracting is permitted with credit to the source. Libraries are permitted to photocopy beyond the limits of U.S. Copyright Law for private use of patrons: 1) those post-1977 articles that carry a code at the bottom of the first page, provided the per-copy fee indicated in the code is paid through the Copyright Clearance Center, 222 Rosewood Drive, Danvers, MA 01923 USA; 2) pre-1978 articles without fee. Instructors are permitted to photocopy isolated articles for noncommercial classroom use without fee. For all other copying, reprint, or republication permission, write to IEEE Service Center, 445 Hoes Lane, Piscataway, NJ 08854 USA. Copyright © 2019 by the Institute of Electrical and Electronics Engineers, Inc. All rights reserved. Periodicals postage paid at New York, NY, and at additional mailing offices. **Postmaster:** Send address changes to IEEE Signal Processing Magazine, IEEE, 445 Hoes Lane, Piscataway, NJ 08854 USA. Canadian GST #125634188

Printed in the U.S.A.

Digital Object Identifier 10.1109/MSP.2019.2917974

**135 SP Forum**

Innovation Starts With Education  
*Victor Solo, Maria Sabrina Greco, Danilo Mandic, Petar Djuric, Andreas Spanias, and Mónica F. Bugallo*

**138 SP Competitions**

Audio-Based Search and Rescue With a Drone  
*Antoine Deleforge, Diego Di Carlo, Martin Strauss, Romain Serizel, and Lucio Marcenaro*

**148 In the Spotlight**

Perspectives in Autonomous Systems Research  
*Carlo Regazzoni and Ioannis Pitas*

**DEPARTMENTS****3 From the Editor**

Making a Good Feature Article Submission  
*Robert W. Heath, Jr.*

**5 President's Message**

Losing Your Mind  
*Ali H. Sayed*

**145 Dates Ahead**

©STOCKPHOTO.COM/BR

ICASSP 2020 will be held 4–9 May 2020, in beautiful Barcelona, Spain.

PG. 145

**IEEE Signal Processing Magazine****EDITOR-IN-CHIEF**

Robert W. Heath, Jr.—The University of Texas at Austin, U.S.A.

**AREA EDITORS****Feature Articles**

Matthew McKay—Hong Kong University of Science and Technology, Hong Kong SAR of China

**Special Issues**

Namrata Vaswani—Iowa State University, U.S.A.

**Columns and Forum**

Rodrigo Capobianco Guido—São Paulo State University (UNESP), Brazil

Roberto Tognoni—The University of Western Australia

**e-Newsletter**

Ervin Sejdic—University of Pittsburgh, U.S.A.

**Social Media and Outreach**

Tiago Henrique Falk—INRS, Canada

**Special Initiatives**

Andres Kwasinski—Rochester Institute of Technology, U.S.A.

Nuria Gonzalez Prelcic—Universidade de Vigo, Spain

**EDITORIAL BOARD**

Daniel Bliss—Arizona State University, U.S.A.

Daniela Cabric—University of California, U.S.A.

Volkan Cevher—École polytechnique fédérale de Lausanne, Switzerland

Mrityunjay Chakraborty—Indian Institute of Technology, Kharagpur, India

George Chrisikos—Qualcomm, Inc., U.S.A.

Elza Erkip—New York University, U.S.A.

Alfonso Farina—Leonardo S.p.A., Italy

B. Vikram Gowreesunker—Texas Instruments Inc., U.S.A.

Joseph Guerci—Information Systems Laboratories, Inc., U.S.A.

Nageen Himayat—Intel, U.S.A.

Clem Karl—Boston University, U.S.A.

C.-C. Jay Kuo—University of Southern California, U.S.A.

Erik Larsson—Linköping University, Sweden

David Love—Purdue University, U.S.A.

Maria G. Martini—Kingston University, U.K.

Helen Meng—The Chinese University of Hong Kong, China

Meinard Mueller—Friedrich-Alexander Universität Erlangen-Nürnberg, Germany

Phillip A. Regalia—U.S. National Science Foundation

Alejandro Ribeiro—University of Pennsylvania, U.S.A.

Douglas O'Shaughnessy—INRS Université de Recherche, Canada

Osvaldo Simeone—Kings College London, U.K.

Milica Stojanovic—Northeastern University, U.S.A.

Ananthram Swami, Army Research Labs, U.S.A.

Jong Chul Ye—KAIST, South Korea

Qing Zhao—Cornell University, U.S.A.

Josiane Zerubia—INRIA Sophia-Antipolis Mediterranee, France

**ASSOCIATE EDITORS—COLUMNS AND FORUM**

Ivan Bajic—Simon Fraser University, Canada  
 Balázs Bank—Budapest University of Technology and Economics, Hungary

Panayiotis (Panos) Georgiou—University of Southern California, U.S.A.

Hande Godrich—Rutgers University, U.S.A.

Yuan-Hao Huang—National Tsing Hua University, Taiwan

Euee Seon Jang—Hanyang University, South Korea

Vishal M. Patel—Rutgers University, U.S.A.

Christian Ritz—University of Wollongong, Australia

Changshui Zhang—Tsinghua University, China

H. Vicky Zhao—Tsinghua University, China

**ASSOCIATE EDITORS—e-NEWSLETTER**

Nesreen Ahmed—Intel, U.S.A.

Behnaz Ghoraani—Florida Atlantic University, U.S.A.

Anubha Gupta—IIT Delhi, India

Yang Li—Harbin Institute of Technology, China

Alessio Medda—Georgia Tech Research Institute, U.S.A.

Irena Orovic—University of Montenegro, Podgorica

Sarah Ostadabbas—Northeastern University, U.S.A.

Ronen Talmon—Technion, Israel

**ASSOCIATE EDITOR—SOCIAL MEDIA/OUTREACH**

Guijin Wang—Tsinghua University, China

**IEEE SIGNAL PROCESSING SOCIETY**

Ali H. Sayed—President

Ahmed Tewfik—President-Elect

Fernando Pereira—Vice President, Conferences

Nikos D. Sidiropoulos—Vice President, Membership

Sergio Theodoridis—Vice President, Publications

Tülay Adalı—Vice President, Technical Directions

**IEEE SIGNAL PROCESSING SOCIETY STAFF**

William Colaccchio—Senior Manager, Publications and Education Strategy and Services

Rebecca Wollman—Publications Administrator

**IEEE PERIODICALS MAGAZINES DEPARTMENT**

Jessica Welsh, *Managing Editor*

Geraldine Krolin-Taylor, *Senior Managing Editor*

Janet Dudar, *Senior Art Director*

Gail A. Schnitzer, *Associate Art Director*

Theresa L. Smith, *Production Coordinator*

Mark David, *Director, Business Development - Media & Advertising*

Felicia Spagnoli, *Advertising Production Manager*

Peter M. Tuohy, *Production Director*

Kevin Lisankie, *Editorial Services Director*

Dawn M. Melley, *Staff Director, Publishing Operations*

*Digital Object Identifier 10.1109/MSP.2019.2917995*

**SCOPE:** IEEE Signal Processing Magazine publishes tutorial-style articles on signal processing research and applications as well as columns and forums on issues of interest. Its coverage ranges from fundamental principles to practical implementation, reflecting the multidimensional facets of interests and concerns of the community. Its mission is to bring up-to-date, emerging and active technical developments, issues, and events to the research, educational, and professional communities. It is also the main Society communication platform addressing important issues concerning all members.



IEEE prohibits discrimination, harassment, and bullying.  
 For more information, visit  
<http://www.ieee.org/web/aboutus/whatis/policies/p9-26.html>

Robert W. Heath, Jr. | Editor-in-Chief | rheath@utexas.edu



## Making a Good Feature Article Submission

**I**ne of the main items of feedback during our recent IEEE Periodicals Review and Advisory Committee (PRAC) meeting was that *IEEE Signal Processing Magazine* (*SPM*) rejected too many feature article white papers as being “out of scope.” In this editorial, I attempt to outline the key features of a good feature article. I hope that you readers—as potential feature article authors—will also consider these tips when you prepare your submissions.

I will start the description by providing some basic background. First and foremost, a feature article is a tutorial paper not associated with a special issue. In particular, it should not include new ideas or fundamental results, as might appear in *IEEE Transactions on Signal Processing*, for example. Any article that features new results is not in the scope of a feature article and will be rejected.

A typical feature article is focused on a topic that is narrow enough to be adequately covered within the page and reference limits of the article (more on this later), with enough breadth to be inclusive of the perspectives from different authors. Good articles will provide an introduction to the area, provide a novel perspective on different technical directions, and, most importantly, will highlight directions for future work. The key relevant contributions of a feature article lie in the careful selection of references, thoughtful perspectives on them, and ideas for future work.

Graphics should not be overlooked. Having insightful illustrations, and simulations that combine perspectives from different work, can be very useful for future readers.

Feature articles focus on a hot topic or may provide a new perspective on an established topic. For example, an article that reviews fundamentals and highlights new applications of a tool would be a good fit for a feature article. Articles that focus purely on history or on teaching a mathematical tool may be a better fit for a column in the magazine.

Submitting a feature article is a two-step process. The first step involves the submission of what is called a *white paper*. The paper is sent by Area Editor Matthew McKay for review to the Senior Editorial Board. Normally, about ten short reviews are received, which are used to indicate whether the full paper should be invited, if the white paper should be revised, or if a full paper is declined. Of course, being invited for a full paper is not a guarantee that the paper will be accepted eventually. The paper will be sent out to reviewers for detailed feedback, who are not, in general, on the editorial board.

While it may seem like a hassle to prepare a white paper, it is actually a service for potential authors. The effort to prepare a white paper should be much lower than preparing the entire paper draft. The white paper stage is an opportunity for the authors to get early feedback, for example, that their article is not a good fit for the magazine. This avoids spending time on a tutorial paper

that cannot be resubmitted to a different publication with different requirements.

A white paper is usually five pages (or fewer) and must include several components. I enumerate each component and explain how this information is used in the following.

- Proposed title: this is important to set the stage for the scope of the article. Good titles should not be too long, but they should not be too generic. Be sure to check the titles of related papers and be sure to differentiate your title.
- Author list including biographies: the list is used to determine if the authors have expertise in the area. Good feature articles will be coauthored by different research groups. This helps to ensure the diverse perspective on different research lines as expected in tutorial and overview papers.
- History, motivation, and significance of the topic: this is the place to make your case that a feature article will be of broad interest to the signal processing community. It is useful to cite some references in this section. It is also important to highlight differences with other tutorial, overview, or survey papers on related topics.
- An outline of the proposed paper: here you provide a section and subsection outline of the final paper. It is useful to briefly mention the content of each section and also to list the papers that you plan to cite in this section.

■ References: these are the references you have cited in your white paper, which will (with some exceptions) also be present in the full paper. The reference list is an important way to gauge the balance of the coverage, meaning that the paper goes beyond citing the authors' own work.

In most cases, the outcome of the first white paper review is either a rejection or a major revision. Assuming the latter, you need to revise your white paper to address the comments from the editorial board. As I mentioned, there are usually around 10 sets of reviews, sometimes conflicting. Address all of the reviews to the best of your ability, revise the white paper, and also provide a summary document about how you addressed the changes in your white paper. The summary document, or *reply-to-reviewers* as it is usually called, is uploaded as a separate PDF file. The review of white papers is quick, normally lasting a few weeks in each round.

Once your white paper is accepted, you have the opportunity to submit a full paper. It is important to note that this is not an open-ended invitation: the full paper must be submitted in two months. Occasional short extensions are granted; long extensions require resubmission of a white paper. Having a deadline on the submission motivates authors to actually write the paper (after the whole process, some feature article papers never get written). The deadline also serves as a way to temporarily reserve a topic. For example, if a second white paper is submitted on a similar topic, preference would be given to the feature article that was already in process.

Feature articles may be up to 40 double-spaced pages, 11-point font size, including figures, tables, and references. Of course, the figures should not be shrunk to the size of a postage stamp to accommodate the page length. They should also be centered in the page with space on either side, not embedded in the text. You may not have more than 15 figures in total, including subfigures. Margins of 1.25-in on the left and right

and 1-in on the top and bottom are expected. Of critical importance: only 50 references are allowed without a special exception.

The formatting guidelines are useful to ponder even when preparing your white paper. For example, if you absolutely need 100 references to adequately survey the prior work or cannot squeeze your contribution to 40 pages, then *SPM* may not be the best fit for your paper. Think about the limits as the size of the canvas, and make a painting to fit the piece. Note that you should put your creativity into writing a compelling paper to fit the limits, not in finding new ways to trick the word processing program into fitting more text on a page.

There are no guidelines on equations for a feature article. Given the importance of mathematics in signal processing, it would be unusual to find a feature article without any equations. Due to the tutorial nature of the papers, though, it would not be typical to see the pages filled with equations either. Most feature articles tend to have around 30 equations to highlight key results (proofs would be referenced in other papers). You should feel free to use mathematics as needed to make your paper compelling. Having equations is one of the distinguishing features of *SPM* compared to magazines from other Societies.

Put a lot of thought into the figures. *SPM* is received by most of our readers in hardcopy form, printed in color. Please take advantage of color in your graphics, including the block diagrams, performance plots, and other illustrations. Also note that it is possible to have offset text boxes to make side notes or highlight different ideas. You may like to indicate this in your submission as well.

This is also a good place to make a comment about the abstract of a feature article. If you look at a typical feature article in the magazine, you will see that there is no separate abstract. Yet if you search in *IEEE Xplore*, there is an abstract listed. What happens? Essentially, the abstract of your submitted paper

becomes the first paragraph of the published and formatted paper. You should keep this in mind the relationship between the abstract and introduction in your final printed article.

Upon full submission, feature articles are assigned to an associate editor for further review. The associate editor is normally selected from one of the editorial board members. At this point, the article begins the formal review process. External reviewers are solicited by experts to provide feedback on the article. The associate editor then makes a decision based on his or her own reading of the paper and the input from the reviewers. Manuscripts may be rejected at this stage or given an opportunity for a revision. If you are encouraged to revise, it is critical that you address the comments from the reviewers in the paper and provide a detailed *reply-to-reviewers* as a separate PDF file. Do your best to be thoughtful in your edits and your reply; simply arguing with the reviewers seldom leads to a positive outcome. Usually, there is only one round of major reviews.

If your feature article is accepted, then it will be processed and published on a space-available basis. Be sure to submit your final files in a timely fashion as your place in the feature article queue is determined based on that submission date. The article will appear as soon as possible in the magazine. Sometimes they appear in an issue with several feature articles; other times they appear in an issue that also features articles in a special issue. Because of physical constraints associated with each issue and total yearly page budgets, it may not appear in the most immediate issue.

I hope that this editorial explained the feature article requirements, review process, and best practices for submitting a compelling article. Please consider submitting a paper soon!



SP



## Losing Your Mind

**I**magine sitting in a room where every individual is able to read every other individual's mind. Would you lose your mind?

We are living in an age where many of us have already surrendered our personal privacy to online interfaces either knowingly or by deceptive means. As technology continues to advance, we are likely to lose even more of our personal space and identity, unless legislation catches up to keep pace with the transformative changes around us. Nicholas Carr, author of the 2011 Pulitzer Prize finalist *The Shallows: What the Internet Is Doing to Our Brains*, went further by claiming that the Internet is having detrimental effects on our brains and cognition. According to him, "We become, neurologically, what we think," a fact that is in line with studies in the cognitive sciences showing that our thoughts can change and rewire our brains, thus potentially altering or enhancing some of their functions. Albert Einstein was perhaps perceptive of this cognitive norm when he stated, "It is not that I am so smart, it is just that I stay with problems longer."

The online world we live in is not only altering the personal space around us but is also having an effect on our inner selves. And there is yet more to come! Today, we are moving in new technological directions that can literally "take control" of

our minds and brains, whether for good or bad, with machines that can read our brain waves and infer our thoughts [1]. The technology is taking its first steps but is rapidly building up strength. Many valid ethical and legal ramifications will arise in this domain, in addition to questionable practices and applications. One would expect that common sense would prevail, although this can never be taken for granted. To paraphrase Voltaire, sometimes "common sense is not so common." I will not delve into these issues here. My focus will be on the potential for scientific discoveries and the role our signal processing discipline can play in advancing knowledge.

The ancient Egyptians had little regard for the brain. During mummification, they would remove brain tissues through the nostrils and discard them. We have come a long way since then and now recognize the power and central role of not only the human brain, but also of the human mind and our thought process. One of the most promising and mysterious frontiers for engineering, life sciences, and cognitive sciences is joining forces to explore the human brain and mind. Eric Kandel, the 2000 Nobel Laureate in Physiology from Columbia University declared in his speech at the Nobel Banquet [2] "The biology of the mind will be as scientifically important to this century as the biology of the gene has been to the 20th century." Our signal processing discipline can help perfect the tools and sensors to make this

focus a reality by helping probe the biological environment more thoroughly, analyze massive brain data more closely, and develop inference tools to learn and predict thought patterns, as well as restore or augment neural functionality.

According to the World Health Organization (WHO), an estimated 1 billion people suffer from neurological disorders [3]. These are disorders of the nervous system including brain damage, spinal cord injury, epilepsy, paralysis, Parkinson's disease, Alzheimer's disease, multiple sclerosis, migraines, and other related ailments. Neurotechnology offers great potential to treat patients with such disorders, help restore functionality, and permit healthy aging. Interest and progress in the field will be driven by several ongoing trends in technology that open the way for new discoveries and treatments.

On one hand, our increased ability to design and control miniaturized devices, coupled with advances in sensing and nanotechnologies, is changing the way we probe and interact with living cells. At the same time, progress in invasive and noninvasive procedures, coupled with advances in new materials and wireless technologies, is allowing us to monitor the biological environment ever more closely and continually. Likewise, advances in powerful imaging modalities, coupled with computing power, storage capabilities, and intelligent bio-instruments, are enabling the collection and processing of larger amounts of

biodata, thus enabling better understanding and newer discoveries. Although we have been able to record brain waves for a long time, the recent advances in machine learning and data-analytics are making it possible to interpret these waves more thoroughly, read their “messages” more clearly, and correlate them more directly with actions and behaviors.

Driven by these advances, we are already witnessing important strides toward exploring the complex wilderness of the human brain and mind. This past May, DARPA, the funding agency that is responsible for the advancement of research programs for the U.S. Department of Defense, launched an ambitious multimillion-dollar program in support of mind-control technologies. The program’s objective is to develop solutions that enable the control of defense systems and swarms of drones through a soldier’s thoughts and without requiring surgery [4]. Six research teams have been selected to receive funding under the so-called N3 Program, which stands for the Next-Generation Nonsurgical Neurotechnology Program. The main motivation of the N3 program is to reduce the latency (or delay) that exists between the moment a soldier decides on an action plan and the time it takes for his/her limbs and muscles to act by pressing control buttons or typing commands on a keyboard.

Some will question the devious reason behind the need for launching weapons at faster speeds, even to the point of spending millions of dollars on trying to reduce the action time by milliseconds. Others will argue in favor of such investments to enhance one’s defense capabilities. Regardless of the argument that you are most comfortable with, my intention is to focus purely on the enabling science; namely, on the ability to use one’s thoughts to control machines. It is not clear how successful these efforts will be. However, time and again, we have witnessed how similar ambitious projects in the past, driven initially by purely military considerations, have ended up leading to superb technological advances for society at large.

The most notable modern example is the Internet, which started as a military

project in the mid 1960s called ARPANET (Advanced Research Projects Agency Network). It was funded by the U.S. Department of Defense. The purpose of the project was to develop technology that would enable a network of computers to communicate with each other and to store information in a decentralized manner. A network of this type would be more robust in the face of catastrophic events, such as a nuclear event during the years of the Cold War. We have come a long way since then, with the Internet today defining our modern times. While researching the history of ARPANET, I found the following passage very amusing on the Wikipedia page; it is extracted from [5, p. 9]. The reference is a 1982 manual for users at the MIT AI Laboratory instructing them on the use of their computer network:

“It is considered illegal to use the ARPANET for anything which is not in direct support of Government business ... personal messages to other ARPANET subscribers (for example, to arrange a get-together or check and say a friendly hello) are generally not considered harmful ... Sending electronic mail over the ARPANET for commercial profit or political purposes is both anti-social and illegal.”

Contrast the instruction in the last sentence of this paragraph with the current state of affairs! Using the precursor of the Internet for commercial purposes was considered both “antisocial and illegal.” At the time of this writing, Amazon.com, one of the largest commercial enterprises ever, has just commemorated 25 years of existence, having been launched on July 5th, 1994. This is only one example of the vast online world we live in today, besides email and messaging tools that we cannot live without! The practice of exchanging “friendly hellos” was considered “nonharmful” back then. Today, the practice has evolved into flooding our inboxes with messages for the most trivial reasons, apart of course from the relentless spamming. I love the short emails that say “Hi, can we have a brief chat by phone?” I have used them myself. Why not just pick up the phone? We are becoming mentally

wired to using an electronic medium, perhaps because it is easier nowadays to reach people by email than by phone in an ever-interconnected and busy world. Given our hectic schedules, it is often a necessity to schedule beforehand a time to chat by phone, and we use emails to break through that barrier! The online world is changing our social behavior. Similar effects are likely to occur, and perhaps on a much more pronounced scale, once we start tinkering with our brains and minds! Be prepared.

Similar to what happened with ARPANET, whether successful or not, the recent DARPA efforts may similarly lead to important technological advances of great societal and clinical value. Advances in neurotechnology are likely to have an impact on computing, the consumer industry, and on the pharmaceutical industry. This is because a better control and understanding of the brain functions and its chemistry can suggest more effective drug systems, promote new forms of consumer neurotechnology, and even lead to new computing modalities. For example, the brain is recognized as a more efficient machine, consuming far less power (about 20W), than modern supercomputers (which consume close to 5–10MW). There are several ongoing efforts, including by companies like Intel and IBM, on neuromorphic computing and the design of neuro-chips that imitate the functionality of brain cells. These chips are also embedded with learning abilities [6]. Imagine the devices inside your machines becoming more powerful and wiser as they age based on experience!

Advances in neurotechnology will further lead to hybrid brain-machine interfaces to augment human capabilities and to assist with disabilities. There already exist prototypes of headsets that allow users to control electronic devices such as their TVs using thought commands [7]. Facebook is also apparently working on a brain-machine interface that would read people’s thoughts and allow them to navigate and interact with an augmented reality environment in that manner alone, without the need for keyboards, remote controls, or gestures [8]. It is estimated that Facebook

has over 60 developers working on this technology alone. Just imagine how much more privacy users will give up if and when this Facebook interface becomes a reality!

In yet another recent development [9], researchers at the University of Washington demonstrated a setup where two individuals sitting in separate rooms can communicate clues through their thoughts to a third person in another room. The thought commands are meant to help the third individual move a falling block on a computer screen to the right or left in a Tetris-like game until it fits into the proper location on the bottom row. The third individual does not see the bottom row but only sees the falling block and deciphers the “mind” commands that arrive from the other two individuals. Advances of this type open up the possibility of communicating without language or gestures. They may also enable transmitting thought commands from one healthy individual to a patient.

We are often enamored by the wonders of technology, and gasp at demonstrations reading our thoughts. Yet, we

need to remain vigilant and conscious of how technology is invading our personal space and altering our own humanity. Tinkering with the minds and brains of individuals can alter these individuals forever! Social norms and behavior will change; no question about that. Similar to what has happened with the online medium, we should avoid immersing ourselves uncontrollably into new technologies without considering the implications on our personal space, privacy, and behavior. We should approach advances of this magnitude with a mind of our own and have a more inquisitive approach. As the Spanish proverb goes, “A wise man changes his mind, a fool never.”

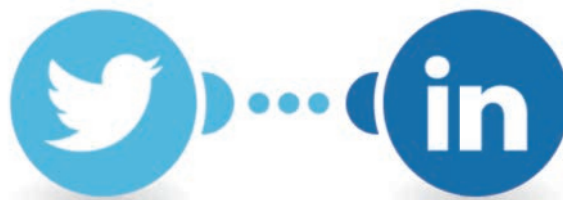
## References

- [1] W. Roush, “Machines that read your brain waves,” *Scientific American*, Apr. 1, 2019. [Online]. Available: <https://www.scientificamerican.com/article/machines-that-read-your-brain-waves/>
- [2] The Nobel Foundation, “The Nobel Prize in physiology or medicine.” Accessed on: July 8, 2019. [Online]. Available: <https://www.nobelprize.org/prizes/medicine/2000/kandel/speech/>
- [3] World Health Organization, “Neurological disorders: Public health challenges.” Accessed on: July 11, 2019. [Online]. Available: [https://www.who.int/mental\\_health/neurology/neurodiso/en/](https://www.who.int/mental_health/neurology/neurodiso/en/)
- [4] Defense Advanced Research Projects Agency, “Six paths to the nonsurgical future of brain-machine interfaces.” Accessed on: May 20, 2019. [Online]. Available: <https://www.darpa.mil/news-events/2019-05-20>
- [5] C. C. Stacy. Sept. 1982. “Getting started computing at the AI lab MIT Artificial Intelligence Laboratory,” Working Paper 235, MIT Libraries, Sept. [Online]. Available: <https://dspace.mit.edu/handle/1721.1/41180>
- [6] S. Ravindran, “Building a silicon brain,” *The Scientist*, May 1, 2019. [Online]. Available: <https://www.the-scientist.com/features/building-a-silicon-brain-65738>
- [7] S. Curtis, “Brainwave-reading headset lets you control your TV with your mind.” *The Telegraph*, June 19, 2015. [Online]. Available: <https://www.telegraph.co.uk/technology/news/11685928/Brainwave-reading-headset-lets-you-control-your-TV-with-your-mind.html>
- [8] N. Cohen, “Zuckerberg wants Facebook to build a mind-reading machine,” *Wired*, Mar. 7, 2019. [Online]. Available: <https://www.wired.com/story/zuckerberg-wants-facebook-to-build-mind-reading-machine/>
- [9] Technology Networks, “Brain-computer interface lets three people play video games using their minds,” July 2, 2019. [Online]. Available: <https://www.technologynetworks.com/neuroscience/news/brain-computer-interface-lets-three-people-play-video-games-using-their-minds-321268>



SP

# IEEE Signal Processing Magazine



Twitter

LinkedIn

**Interested in learning about upcoming SPM issues or open calls for papers?  
Want to know what the SPM community is up to?**

**Follow us on twitter (@IEEEspm) and/or join our LinkedIn group  
([www.linkedin.com/groups/8277416/](https://www.linkedin.com/groups/8277416/)) to stay in the know and share your ideas!**



## Election of President-Elect, Regional Directors-at-Large, and Members-at-Large

Your vote is more important than ever! It is my pleasure to announce that the IEEE Signal Processing Society (SPS) annual election commenced on 15 August 2019. Beginning this year, all eligible SPS members will now vote for the next president-elect (the term is 1 January 2020 through 31 December 2021) in addition to the regional directors-at-large for Regions 7, 9, and 10 (term 1 January 2020 through 31 December 2021) and members-at-large (term 1 January 2020 through 31 December 2022) of the IEEE SPS Board of Governors (BoG).

Ballots will be mailed to SPS members. Each ballot includes a diverse slate of candidates (who were vetted by the SPS Nominations and Appointments Committee) for all elections as well as a space for write-in candidates. This year's election offers SPS members the

opportunity to cast their votes via the web at <https://eballot4.votenet.com/> IEEE for up to one president-elect, one regional director-at-large for your corresponding Region, Regions 7 and 9 (Canada and Latin America) and Region 10 (Asia and Pacific), and three member-at-large candidates. Ballots must be received at the IEEE no later than 1 October 2019 to be counted. Members must meet the eligibility requirements at the time the ballot data are generated to be eligible to vote. To be eligible to vote in this year's Society election, you had to have been an active SPS member, affiliate, or graduate student member as of 30 June 2019. This is the date when the list of eligible Society voting members was compiled.

The candidates for president-elect are

- V. John Mathews
- Athina P. Petropulu.

The candidates for regional director-at-large are

### ■ *Regions 7 and 9*

- Charles Casimiro Cavalcante
- Timothy Norman Davidson

### ■ *Region 10*

- Kin-Man Lam
- Wing-Kin (Ken) Ma.

The candidates for member-at-large are

- Eric Fosler-Lussier
- Pascale Fung
- Fa-Long Luo
- Marc Moonen
- Patrick A. Naylor
- Roxana Saint-Nom
- Bjoern W. Schuller
- Gaurav Sharma.

The BoG is the governing body that oversees the activities of the SPS. The SPS BoG has the responsibility of establishing and implementing policy and receiving reports from its standing boards and committees and comprises 22 Society members: the president and president-elect who are elected by the

(continued on page 15)

Digital Object Identifier 10.1109/MSP.2019.2922459  
Date of publication: 9 September 2019

### The candidates for president-elect



V. John Mathews



Athina P. Petropulu

### The candidates for regional director-at-large

#### Regions 7 and 9



Charles Casimiro Cavalcante



Timothy Norman Davidson

#### Region 10



Kin-Man Lam



Wing-Kin (Ken) Ma

## Top Downloads in IEEE Xplore

Each “Reader’s Choice” column focuses on a different publication of the IEEE Signal Processing Society (SPS). This month we are highlighting articles in *IEEE Transactions on Multimedia* (*T-MM*). The scope of the periodical is the various aspects of research in multimedia technology and applications of multimedia, including, but not limited to, circuits, networking, signal processing, systems, software, and systems integration, as represented by the fields of interest of the sponsors. This issue’s “Reader’s Choice” column lists the 15 *T-MM* articles that were downloaded the most from January 2017 to May 2019. Your suggestions and comments are welcome and should be sent to Associate Editor H. Vicky Zhao (vzhao@tsinghua.edu.cn).

## Detection and Classification of Acoustic Scenes and Events

*Recent Books and Items*

This paper describes the IEEE Audio and Acoustic Signal Processing Technical Committee Challenge on Detection and Classification of Acoustic Scenes and Events. The challenge focuses on recognition of the general audio environment type (the acoustic scene) and detection and classification of audio events occurring within a scene. The state-of-the-art works in machine lis-

taining are reviewed, and details on the experimental design of the tasks in the challenge, the evaluation approach, and the collected data are provided. Issues emerging from results in the challenge and future directions are also discussed.

October 2015

# Social Attribute Aware Incentive Mechanism for Device-to-Device Video Distribution

*Wu, D.; Yan, J.; Wang, H.; Wu, D.;  
Wang, R.*



An effective pricing-based multicast video distribution system and a grid-based clustering method are proposed to support video distribution over cellular networks. Users' mobility and social characteristics are explored to select core users, who cooperate with the base station to distribute videos to other users through an intracluster device-to-device multicast. A Stackelberg-game-based pricing mechanism is proposed to motivate core users to help distribute videos and enhance the



system resource utilization. Simulation results show that the proposed system can effectively alleviate the traffic load at the base stations and improve the effectiveness and reliability of video transmission.

August 2017

### Socially Aware Energy-Efficient Mobile Edge Collaboration for Video Distribution

Wu, D.; Liu, Q.; Wang, H.; Wu, D.; Wang, R.

A social-attribute-based scalable video coding mechanism is presented for video distribution at the edge of mobile networks. First, coalition games are used to dynamically divide users into different virtual communities based on their preference for video content. Then, based on their geographical locations, a grid-based clustering method is used to select a set of cooperative transmission users who help forward video packets to other users. A user-attribute-aware video distribution mechanism using scalable video coding is then proposed. It improves the reliability and adaptability of video distribution through user collaboration and effectively reduces transmission energy consumptions.

October 2017

### Multipath Cooperative Communications Networks for Augmented and Virtual Reality Transmission

Ge, X.; Pan, L.; Li, Q.; Mao, G.; Tu, S. To meet the requirements of low latency and massive data transmission in

augmented-reality and virtual-reality applications, a software-defined networking architecture is described for 5G small-cell networks. A multipath-cooperative route scheme is proposed to facilitate fast wireless transmissions from multiple edge data centers to the desired user, and the delay is analytically studied. Furthermore, a service effective management optimization algorithm is designed to minimize the network energy consumption while guaranteeing the delay requirement.

October 2017

### A Survey of Audio-Based Music Classification and Annotation

Fu, Z.; Lu, G.; Ting, K.M.; Zhang, D. Classification is a fundamental problem in music information retrieval. This survey offers a comprehensive review of audio-based classification and systematically summarizes the state-of-the-art techniques for music classification. An up-to-date discussion of audio features and classification techniques used in the literature is provided. Also, individual tasks for music classification and annotation are reviewed, and the difference in the features and the types of classifiers used for different classification tasks is identified.

April 2011

### Scale-Aware Fast R-CNN for Pedestrian Detection

Li, J.; Liang, X.; Shen, S.; Xu, T.; Feng, J.; Yan, S.

In this work, a novel scale-aware fast region-based convolutional neural network model is proposed to address the large

variance in spatial scales in pedestrian detection. The proposed framework includes a large-size subnetwork and a small-size subnetwork to capture and detect the unique characteristics of large-size and small-size pedestrian instances, respectively. A scale-aware weighting mechanism is proposed to adaptively combine outputs from both subnets and generate the final detection results. Extensive experiments demonstrate that the proposed framework is superior in detecting small-size pedestrian instances and achieves top performance on several challenging benchmarks.

August 2018

### Deep Head Pose: Gaze-Direction Estimation in Multimodal Video

Mukherjee, S.S.; Robertson, N.M.

This paper presents a convolutional-neural-network-based model for human head pose estimation in low-resolution multimodal red-green-blue depth data. The problem is formulated as classification of human gazing direction, and the learned deep classifier is further fine-tuned into a regressor. The classification and the regression models are then combined to estimate approximate regression confidence. Simulation results show that the proposed framework can achieve state-of-the-art results in both high-resolution human–robot interaction and low-resolution surveillance data sets.

November 2015

### Robust Part-Based Hand Gesture Recognition Using Kinect Sensor

Ren, Z.; Yuan, J.; Meng, J.; Zhang, Z.

Presented in this paper is a robust part-based hand gesture recognition system using Kinect sensors. A new distance metric, finger-earth mover's distance, is proposed to measure the dissimilarity between hand shapes. It is robust to orientation, scale, and articulation changes as well as local distortions of hand shapes. Extensive experiments, including two real-life human–computer-interaction applications, show that the proposed system is accurate, efficient, robust to different distortions and orientation or scale changes, and can work in uncontrolled environments.

August 2013

## **Video Captioning With Attention-Based LSTM and Semantic Consistency**

*Gao, L.; Guo, Z.; Zhang, H.; Xu, X.; Shen, H.T.*

A novel end-to-end attention-based long short-term memory (LSTM) framework is proposed to transfer videos to natural sentences in video captioning applications. The proposed framework incorporates an attention mechanism that uses the dynamic weighted sum of local two-dimensional convolutional-neural-network representations at the frame level. An LSTM visual decoder takes those feature vectors as inputs and exploits temporal information to generate important words. Multimodal embedding is used to map the visual and sentence features into a joint space to guarantee the semantic consistency of the sentence description and the visual content.

*September 2017*

## **A Deep Neural Network-Driven Feature Learning Method for Multiview Facial Expression Recognition**

*Zhang, T.; Zheng, W.; Cui, Z.; Zong, Y.; Yan, J.; Yan, K.*

A novel deep-neural-network-driven feature learning method for multiview facial expression recognition is proposed. Scale-invariant feature transform features corresponding to a set of landmark points are first extracted from each facial image. In sequent, based on the structure of the low-level input features, the proposed projection and the convolutional layers are designed to adaptively learn spatial discriminative information as well as to extract more robust high-level features. The two layers can significantly reduce the space complexity of parameters and further alleviate the overfitting phenomenon, especially on small data sets.

*December 2016*

## **Multimodal 2D + 3D Facial Expression Recognition With Deep Fusion Convolutional Neural Network**

*Li, H.; Sun, J.; Xu, Z.; Chen, L.*

This paper details a novel and efficient deep-fusion convolutional neural net-

work (DF-CNN) for multimodal 2D and 3D facial expression recognition. Each textured 3D face scan is represented as six types of 2D facial attribute maps, all of which are jointly fed into a DF-CNN for feature learning and fusion learning. A deep-fusion net is used to learn the optimal combination weights of 2D and 3D facial representations for multimodal facial expression recognition. The proposed DF-CNN combines feature learning and fusion learning into a unified end-to-end training framework and consistently outperforms prior methods.

*December 2017*

## **Barcode Modulation Method for Data Transmission in Mobile Devices**

*Motahari, A.; Adjouadi, M.*

Considered in this paper is wireless data transmission between handheld devices using 2D bar codes, where a file on a cell phone is transferred to a second cell phone through a series of 2D bar-code images captured and decoded by the camera of the second cell phone. A new approach for data modulation of 2D bar codes is introduced, where orthogonal frequency-division multiplexing modulation is used together with differential phase-shift keying over adjacent frequency-domain elements. Simulation results show that the proposed method can significantly reduce error rates caused by camera movements.

*January 2015*

## **Edge Computing Framework for Cooperative Video Processing in Multimedia IoT Systems**

*Long, C.; Cao, Y.; Jiang, T.; Zhang, Q.*  
For delay-sensitive multimedia Internet of Things tasks, an edge computing framework is proposed to enable cooperative processing on resource-abundant mobile devices. The key challenges are identified as the optimal formation of mobile devices into video processing groups and the dispatch of video chunks to proper video processing groups. Simulation results show that the proposed group formation algorithm and the heuristic algorithm for

video-group matching can significantly reduce the computation complexity and achieve suboptimal performance in terms of human detection accuracy.

*May 2018*

## **Ultrasonic Communication Using Consumer Hardware**

*Getreuer, P.; Gnevy, C.; Lyon, R.F.; Saurous, R.F.*

A communication protocol is proposed for transmitting small amounts of data as inaudible near-ultrasonic sound in the 18.5–20-kHz band over a short distance. The system is based on direct-sequence spread-spectrum modulation and resistant to reverberation, background interference, and Doppler shift due to motion. In real indoor environments, transmission between mobile devices is reliable at 2 m and often works at 10 m. To achieve low latency, synchronization is determined by an exhaustive but computationally efficient search over a finely sampled grid of time and frequency offset.

*June 2018*

## **Speech Emotion Recognition Using Deep Convolutional Neural Network and Discriminant Temporal Pyramid Matching**

*Zhang, S.; Zhang, S.; Huang, T.; Gao, W.*  
This work explores how to utilize a deep convolutional neural network to bridge the affective gap between the subjective emotions and low-level features in speech signals. Three channels of log-mel spectrograms are first extracted from the speech signal and inputted into the AlexNet model to learn high-level feature representations on each segment divided from an utterance. The discriminant temporal pyramid matching strategy is then used to combine temporal pyramid matching and optimal  $L_p$ -norm pooling to form a global utterance-level feature representation, followed by the linear support vector machines for emotion classification. Experiments on public data sets show promising results of the proposed system.

*June 2018*



## Signal Processing on the Move

*Research leads to innovations in multiple forms of mobile technologies*

The world is moving faster, and signal processing is helping to lead the way, making mobile technologies faster, safer, and more functional on land and even under the sea.

At the Massachusetts Institute of Technology (MIT), engineers have created an algorithm that allows autonomous underwater vehicles (AUVs) to weigh the risks and potential rewards of exploring unknown deep-sea sites in real time. An AUV dispatched to investigate an underwater oil leak, for example, could rely on the algorithm to calculate the danger level of pinpointing the discharge against the probability that the AUV might smash into a nearby cliff or other potentially destructive obstacle.

The technology, which researchers in the lab of Brian Williams, an MIT professor of aeronautics and astronautics, have affectionately dubbed *Spock*, is an adaptive science system. “That means it’s tasked with exploring environments that we know little about and directs the underwater vehicle to locations that will best assist the system and user in understanding that environment and finding locations they are interested in,” explains Benjamin Ayton, a graduate student in MIT’s Department of Aeronautics and Astronautics.

Spock was born from the understanding that undersea exploration is inherently dangerous and that equipping an

AUV with human-like risk/reward compromise behavior might be a good way to enhance both vehicle safety and productivity. Spock is one piece of a larger architecture called *Enterprise*, which handles overall AUV dynamics, scheduling, and user interaction. The system has been in development for about three to four years, Ayton says. “In that time, we’ve moved it from basic concept through to several successful demonstrations.”

Spock promises to help scientists more effectively investigate hard-to-reach marine environments. It will also be useful for businesses and government organizations to autonomously monitor deeply submerged assets, such as oil pipelines, seismic detectors, and under-sea cables. The algorithm also has the potential to assist in the exploration of liquid environments on extraterrestrial bodies, such as Europa, a Jupiter moon that’s believed to harbor a huge ocean beneath its icy shell.

The new algorithm is the first to allow risk-bounded adaptive sampling. The approach, Ayton notes, enables the AUV to rapidly and intelligently hone-in on whatever it’s trying to find. “This type of reasoning has been done before, but that [prior] technology could not be readily deployed because it had no reasoning over the potential dangers, so you would see reckless behaviors that threaten collisions between the vehicle and what it’s trying to monitor,” he explains. “By reasoning over the risks the system takes, we’re able to balance

danger against the capability for the vehicle to perform its task.”

Spock automatically ingests data about the area topography, including any nearby obstacles, as well as the vehicle’s dynamics and inertial measurements, to compute the level of risk for a specific anticipated path. The algorithm also evaluates all of the previous measurements the AUV has taken to determine the probability that any high-reward measurements may exist along the proposed path. If the risk-to-reward ratio meets a value determined by the vehicle’s project team beforehand, the AUV will proceed along its planned course, collecting even more measurements that feed back into the algorithm to help it evaluate the risk and reward of other paths as the vehicle proceeds.

“Generally, we’re trying to use measurements to construct a world model and then decide what additional measurements [are necessary] to both refine the model and find features of interest,” Ayton says. “Signal processing is really essential to the first step, where we need to decide what signals to fold in, transform that into a simple form we can reason over, smooth the data, and perform predictions about new locations.”

Reasoning about risk and reward required an entirely new method of producing policies that can also satisfy technical constraints, Ayton notes. “Exploring all outcomes explicitly was simply impossible because there may be  $10^{40}$  or more, so we showed that this

could be done in an alternative, albeit slightly suboptimal way, by only examining a small number of outcomes and by constructing approximating problems that converge to the true solution.”

Managing scale is the biggest challenge the researchers currently face. “We want to be able to incorporate as many measurements as possible from multiple vehicles across large spatial scales,” Ayton explains. “We address this in part using hierarchical reasoning, so that the impact of many measurements far away is condensed into few data points.” The team also combines subsamples with methods derived from sparse Gaussian processes to maintain accuracy, he notes.

The Gaussian processes, which handle most of the project’s difficult work, are commonly used for this particular type of adaptive science task, Ayton observes. “They give us a number of desirable properties, including global predictions, probability distributions for predictions, which are critical for the probabilistic reasoning we perform, explicit inclusion of uncertainties in all input measurements, and guarantees of smoothness,” he says. “They also allow measures of informativeness of measurements to be expressed and computed easily.” Ayton notes that the team briefly explored other techniques, mostly drawn from the machine-learning community, including neural networks and support vector machines, but these approaches either didn’t provide the capability required or were not suitable for predicting model changes with new data.

Last December, Spock was used by an AUV in Costa Rica to help geologists quickly discover the locations of underwater hydrocarbon seepage. In January, Spock was deployed in Hawaii for coral reef monitoring. “Short term, we are preparing for a deployment in Greece, searching for hydrothermal activity,” Ayton says. “We hope to run the system for longer [periods] autonomously and move some processing and decision-making capability to low-power processors on board.” Long-term plans call for developing a fleet of vehicles that can do persistent exploration and monitoring in a safe and coordinated manner.

Multivehicle planning introduces a range of new challenges, however. These include the problem of how vehicles should maneuver safely relative to each other as well as how they should cooperate for reasoning tasks and when they should communicate. “We have only scraped the surface on this challenge,” Ayton says. The researchers also hope to give Spock the ability to run on low-power vehicles without requiring computationally intensive planning and signal processing on a ship or on shore. “This means everything needs to be made more efficient, and capable of being run on low-power hardware,” he notes.

The research is supported, in part, by Exxon Mobile for the MIT Energy Initiative, and by NASA.

### Navigation bugs

Swarming insects, which can create a traffic hazard if they obscure a driver’s view of the road, are now playing a key role in a global research project focused on developing a new type of collision-avoidance system for terrestrial autonomous vehicles.

The Ultralayered Perception Project (ULTRACEPT), headed by Shigang Yue, a professor of computer science at the U.K.’s University of Lincoln, aims to create a compact, reliable collision-detection sensor system based on

a microchip (Figure 1). The system is being designed to provide an alternative to current vehicle collision-detection technologies, which are often unsatisfactory in terms of reliability, cost, energy consumption, and size.

Inspired by the ability of many insects to respond rapidly to new situations and incorporating near-range collision-detection technology, long-range hazard perception, and thermal-based collision-detection tools, ULTRACEPT aims to produce a technology that works equally well day or night and can rapidly adapt to unexpected hazards and various weather and lighting situations.

Current laser-based lidar (light detection and ranging) systems can be fooled or hacked, leading to potentially disastrous consequences. Similarly, vision-based systems are primarily based on situational training and therefore often experience difficulty coping with unknown or unusual situations.

Nature gives autonomous-vehicle researchers a deep pool of inspiration for artificial visual systems that can be applied to collision-detection and collision-avoidance technologies. Locusts, for instance, can fly for hundreds of miles in dense swarms without any risk of collision. Many nocturnal insects successfully navigate through the forest at night without bumping into each other.

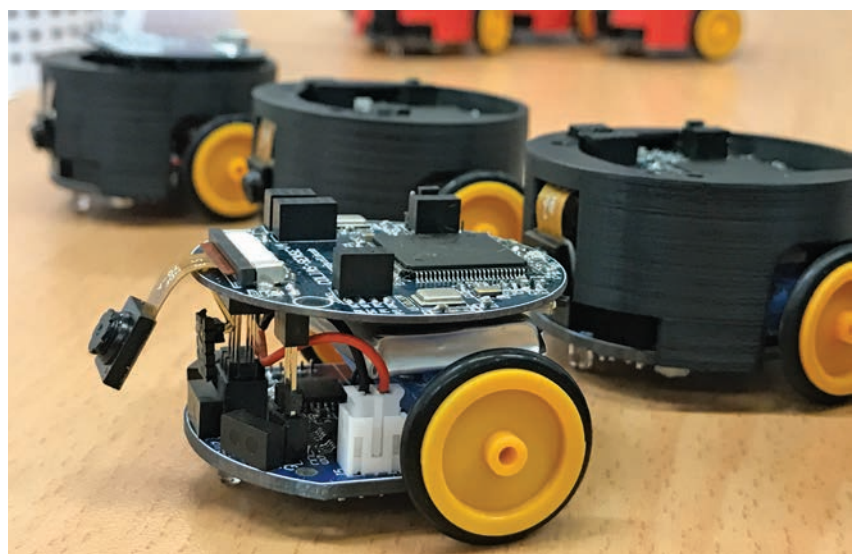


**FIGURE 1.** This sensor system based on a microchip is a creation of ULTRACEPT, a project that aims to provide a more reliable alternative to current vehicle collision-detection technologies. (Source: University of Lincoln; used with permission.)

"These naturally evolved vision systems provide ideal models to develop an artificial system for collision detection and avoidance, and we hope that, in the future, each vehicle, with or without a driver, will be well equipped with an innovative sensor to navigate as effectively as animals do," Yue reports.

ULTRACEPT researchers plan to create enhanced visual neural systems inspired by insect navigation, Yue says. "Also, a 2D map generated from sound could be fed to the system in certain circumstances to make detection possible," he adds.

For the technology's visual component, the researchers will rely on bioinspired algorithms. "Traditional signal processing techniques will be used in sound-related inputs... algorithms such as visual neural network lobula giant movement detectors, elementary motion detectors or small-target motion detectors on visual information processing with some commonly used high-pass/low-pass filters in the early signal processing stage," Yu explains. "For example, the input images are filtered with low/high pass filters first, then processed with lateral inhibition, and then summed together to form a time series output signal," Yue says. "This output signal is then turned into spiking trains to trigger the alarm signal, depending on the number of spikes over time for collision detection."

Traditional signal processing methods will be used to collect and process the technology's sound inputs, Yue notes. The project unites experts from universities in the United Kingdom, Germany, China, Japan, Malaysia, and South America, including experts in hardware, software, and robotics. Team members include invertebrate visual neuroscientists, invertebrate vision modelers, mixed-signal chip designers, robotics platform providers, and brain-inspired pattern-recognition specialists.

"The biologically plausible methods are the result of evolution and tested over time for fast-moving animals in the real world," Yue says. "The signal and image processing algorithms inspired by biological systems are therefore robust and also easy to be realized into chips."

ULTRACEPT's integrated computer vision system, besides being used in autonomous vehicles, will be applicable

to a number of other industries, including robotics, video game development, and health care. The project is funded by a €1.8 million grant from the E.U.'s Horizon 2020 research and innovation program.

### Smart wheelchairs

Electric wheelchairs provide both mobility and independence to walking-impaired individuals. However, such devices have their limitations. Even today's most sophisticated wheelchairs can't respond to voice commands or alert its user to approaching obstacles.

Konstantinos Sirlantzis, an associate professor in intelligent systems at the U.K.'s University of Kent, plans to change this situation. He foresees a smart wheelchair and hopes that the Assistive Devices for Empowering Disabled People Through Robotic Technologies (ADAPT) project will play a major role in making such a technology an everyday reality. ADAPT's aim is to develop various smart wheelchair-oriented technologies that can enhance the independence and quality of life for people coping with mobility challenges. Funding is being provided by the European Regional Development Fund.

Sirlantzis notes that assistive technology addresses the needs of an increasing number of elderly and disabled people currently excluded from a variety of activities. "I realized many years ago that methods I was developing in the field of signal processing, computer vision, and related pattern-recognition methods can be transferred directly, or with small modifications, to develop novel assistive technologies that could make a difference in people's lives," he says. "Specifically, my work on iris recognition is now used in our head-tracking algorithms for driving and navigating a wheelchair for users who cannot use a joystick or other conventional means."

Working with over a dozen partner institutions, as well as with Paul Oprea, a University of Kent postdoctoral research fellow, Sirlantzis and his ADAPT core-researchers plan to share control hardware and algorithms based on their work in artificial intelligence and sensor signal processing. One current ADAPT project involves the development of a smart

garment that can be integrated into an exoskeleton to assess its wearer's user comfort and stress levels. "For this [technology], signal processing of user physiology—measurements such as electromyography, electrocardiography, and skin galvanic response data—need to be collected, filtered, amplified and subsequently processed using AI learning algorithms," Sirlantzis explains.

ADAPT's ultimate goal is to create a framework of intelligent and modular systems that can provide different functionalities in a plug-and-play context to suit the unique needs of individual users. "We aim to create a system that will not cost more than is required by being able to integrate seamlessly diverse subsystems [that] will collaborate and learn from the user's behaviors and conditions," Sirlantzis says. "We aim to create a well-being enhancement tool."

The project is focused on developing new technologies that can be added to existing wheelchairs at an affordable cost (Figure 2). "Within this context, our current shared control technology, based on artificial-intelligence algorithms applied to sensor and visual data, helps with avoiding obstacles and navigating difficult paths with uneven surfaces, such as ramps and pavement curbs," Sirlantzis explains.

Signal processing is an essential part of most ADAPT technologies. "Every component of the systems we design and implement is based on some level of signal generated, captured, or recorded in some way," Sirlantzis reports. "The quality of these signals—noise filtering, appropriate amplification, sampling frequency, and so on—is the foundation on which the successful operation of our systems is based."

Sirlantzis says the greatest signal processing challenge the researchers face when working with biosignals is filtering out the noise that can be generated by skin-surface static electricity, sensor movement, muscle flexes, loss of sensor connectivity, and environmental electric or magnetic fields. "Quality of the signal recorded and authentic representational power of the signal for the activity you are interested in, are paramount for successfully applying second stage processing and obtaining state-of-the-art level of performance," says Sirlantzis.



**FIGURE 2.** The aim of the ADAPT project is to develop affordable technologies that can be added to wheelchairs to give wheelchair users more independence and a better quality of life. (Source: University of Kent; used with permission.)

Sirlantzis is looking forward to the widespread deployment of 5G cellular wireless technology. “By increasing the speed of wireless and mobile communication, and reducing latency, 5G technology opens a wide range of possibilities for enhancing the quality of life and well-being of people with disabilities,” he observes. “It can, for example, improve accessibility by providing visual and navigation information about routes, and accessibility options and services available to specific buildings or urban locations,” he notes.

### Author

**John Edwards** ([jedwards@johnedwardsmedia.com](mailto:jedwards@johnedwardsmedia.com)) is a technology writer based in the Phoenix, Arizona, area. Follow him on Twitter @TechJohnEdwards.

SP

## SOCIETY NEWS *(continued from page 8)*

### The candidates for member-at-large



Eric Fosler-Lussier



Pascale Fung



Fa-Long Luo



Marc Moonen



Patrick A. Naylor



Roxana Saint-Nom



Bjoern W. Schuller



Gaurav Sharma

of the Society shall serve ex-officio, without vote.

The president-elect is an IEEE SPS member elected by the Society’s membership via the annual election, to serve as an officer and as a voting member on the Society’s BoG, executive committee, Conferences Board, Education Board, Membership Board, and Publications Board. The president-elect position automatically succeeds to president.

Regional directors-at-large are SPS members who are elected locally by Society voting members of their corresponding Region via the annual election to serve on the Society’s BoG as nonvoting and voting members of the Society’s Membership Board.

Members-at-large represent the member viewpoint in the board’s decision making. They typically review, discuss, and act upon a wide range of items affecting the actions, activities, and health of the Society. More information on the IEEE SPS can be found at <https://signalprocessingsociety.org/>.

SP

voting members of the Society, five vice president officers of the Society who are elected by the BoG, nine members-at-large elected by the voting members of the Society, four regional directors-at-large elected locally by Society voting members of the corresponding Region,

as well as the Awards Board chair. The seven officers are the president, president-elect, the vice president-Conferences, vice president-Education, vice president-Membership, vice president-Publications, and vice president-Technical Directions. The executive director

## Advances in Radar Systems for Modern Civilian and Commercial Applications: Part 2

Part 1 of the special issue “Advances in Radar Systems for Modern Civilian and Commercial Applications,” published in the July 2019 issue of *IEEE Signal Processing Magazine (SPM)*, described advances in signal processing for radar systems involving a wide range of applications, including health care, archeology, and weather forecasting, to mention a few. This second part of the special issue is dedicated to automotive radar because the topic is so timely and continues to be an area of daunting challenges. Also, the topic has attracted a large number of submissions.

For several decades, engineers have been wrestling with the signal processing challenges associated with automotive applications. With all this attention, the number of advanced signal processing algorithms used in various automotive applications continues to increase [1]–[3]. In the November 2016 and March 2017 issues, *SPM* published the two-part special section “Signal Processing for Smart Vehicle Technologies” under the guidance of guest editors J.H.L. Hansen et al. [4], [5]. That special section addressed many signal processing challenges in a variety of automotive areas and on such topics as “the future of automotive localization algorithms” [4]. However, only two articles in the special section dealt with automotive radar [5]. Since then, this field has developed with remarkable speed as engineers take on

the challenge of exploiting the technology’s full potential.

Soon, automated driving will become a reality. Already, many cars are equipped with assistance systems that automatically enhance driver safety and comfort. One of the most dynamic areas in research and development in the automotive industry is the field of advanced driver assistance systems (ADASs) for highly automated driving (HAD). The performance and reliability of these systems strongly depend on the ability to sense the environment. Radar technology is far more important for HAD than alternative technologies, such as cameras and lidar. Long-range radar systems for forward-looking functions especially developed for HAD are commercially available and widely used today. Radar is typically used in current ADASs, such as adaptive cruise control, forward collision avoidance, lane change assist, and evasion assist, to name a few [3]. Radar works reliably in bad weather and lighting conditions; can provide accurate and direct measurements of range, relative velocity, and angle of multiple targets; and can provide a high range coverage.

With nearly 1.25 million road fatalities worldwide each year, safety remains a focus of the automotive industry. Fully autonomous cars of the future will rely on the great capabilities of radar, but the demands by automobile manufacturers on sensor reliability are very high with the goal of reaching the zero-casualties objective. The

signal processing community is in a great position to play an important role in tackling this challenge.

We were very careful in the selection of articles for this second part. Not only did we consider novelty and tutorial-style writing, a decision supported by expert reviewers, but we also made every attempt to avoid large overlaps.

Part 2 of this special issue opens with an overview on conventional techniques for signal processing in automotive radar, “The Rise of Radar for Autonomous Vehicles” by Bilik et al. The authors emphasize the limitations of conventional processing approaches in practical automotive scenarios, present alternatives, and suggest future directions. They suggest that one solution for the future could be based on cognitive sensing because both the scene of operation and the tasks of radar change continuously in automotive applications.

The second article, “High-Performance Automotive Radar,” by Hakobyan and Yang, provides an overview of challenges for developers of automotive radar as they refashion the technology from a sensor for ADASs to a core component of self-driving cars. The authors discuss the specific shortcomings of classical signal processing algorithms, and they present a signal processing framework that overcomes these limitations. They also discuss digital modulations for automotive radar and interference mitigation methods that are adaptive, cognitive, and/or coordinated.

Alland et al.'s article, "Interference in Automotive Radar Systems," focuses on the effects of an interfering radar on a so-called victim radar. The authors review the already deployed state-of-the-art interference mitigation techniques as well as areas of ongoing research. They also suggest directions for future research, such as alternative modulation techniques and decentralized multiple-access protocols known from communications.

"On the Safe Road Toward Autonomous Driving," by Gerstmair et al., explains that the most limiting factors of a frequency-modulated continuous wave (FMCW) radar is phase noise that affects the sensitivity and range of a radar system. Thus, it is important to monitor phase noise throughout the lifecycle of a radar system. The authors address the problem of estimating phase noise and phase noise monitoring for automotive FMCW radar to fulfill the functional safety requirements.

The article "Radar-on-Chip/in-Package in Autonomous Driving Vehicles and Intelligent Transport Systems," by Saponara, Greco, and Gini, focuses on signal processing techniques for a cheap and power-efficient radar sensor that operates in real time while ensuring that the automotive coverage-range needs are met. They discuss signal processing techniques for velocity-range estimation, direction estimation, waveform design, and beamforming, with particular emphasis on the radar–physical layer codesign. They envision the evolution of embedded computing platforms wherein advanced signal processing techniques are enabled. These could include multiple-input, multiple-output and cognitive radars, with adaptive waveforms to solve interference and spectrum-scarcity issues.

Engineers in recent years have conducted considerable research associated with vehicle-to-vehicle communication and vehicular ad hoc networks. Applications relate to areas ranging from safety to navigation and law enforcement. One of the biggest challenges is to ensure a suitable radio spectrum, which needs to be shared with other applications,

such as, for example, high-speed Internet. Three articles in this Part 2 address some challenges, possible solutions, and future directions.

The article "Radar and Communication Coexistence: An Overview," by Zheng et al., reviews recent work on coexistence between radar and communication systems, including work related to signal models, waveform design, and signal processing techniques. The authors survey contributions in this area, which serves as a primary starting point for new researchers interested in these problems. The strategies proposed so far have been grouped into three major categories. The first one allows spectral overlap between the signal transmitted by the radar and communication systems, while the other two avoid mutual interference either by cognitively assigning disjoint subbands to the different services or by allowing just one transmitter at a time to be active. The authors discuss advantages and disadvantages and offer some examples to illustrate.

Next, Mishra et al.'s article, "Toward Millimeter-Wave Joint Radar Communications," concerns millimeter-wave (mm-wave) communications, which emerged as a technology for short-distance wireless links because it provides transmission bandwidth that is several gigahertz wide. This band is also promising for short-range radar applications as large transmit signal bandwidths imply high range resolution. Signal processing techniques are critical in implementing mm-wave joint radar–communications systems. The article emphasizes the challenge of identifying the best joint waveform design and performance criteria, which must be balanced between communications and radar functionalities.

Hassanien et al.'s article, "Dual-Function Radar Communication Systems," reviews the principles of dual-function radar communication (DFRC) systems and describes the progress made to date in devising different forms of signal embedding. Various approaches to DFRC system design, including downlink and uplink signaling schemes, are discussed along with their respective

advantages and limitations. Tangible applications of DFRC systems and a delineation of their design requirements and challenges are presented. Future trends and open research problems are also highlighted.

We hope that you enjoy reading this second part of the special issue and that the discussed challenges and future directions will spark interest among signal processing practitioners in finding practical and efficient solutions.

## Acknowledgments

We thank all of the contributors for sharing their work with our community. We are indebted to the reviewers for their careful and critical reading of the manuscripts. Our gratitude goes to *SPM*'s Editor-in-Chief Robert Heath and IEEE Signal Processing Society Publications Administrator Rebecca Wollman for their continual support and assistance.

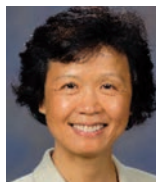
## Guest Editors



**Maria S. Greco**

(m.greco@iet.unipi.it)  
received her M.S. degree in electronic engineering in 1993 and her Ph.D. degree

in information engineering in 1998. She is a full professor in the Department of Information Engineering, University of Pisa, Italy. She is a corecipient of the 2001 and 2012 IEEE Aerospace and Electronic Systems Society's (AECC's) Barry Carlton Award for Best Paper and a recipient of the IEEE AECC 2008 Fred Nathanson Young Engineer of the Year award. She has been general chair, technical program chair, and organizing committee member of many international conferences. She is an associate editor of *IET Radar, Sonar & Navigation*, and Springer's *Journal of Advances in Signal Processing*; a senior editorial board member of *IEEE Journal of Selected Topics in Signal Processing*; and a senior area editor of *IEEE Transactions on Signal Processing*. Her general interests are in the areas of statistical signal processing, estimation, and detection theory. She is a Fellow of the IEEE.



**Jian Li** (li@ dsp.ufl.edu) received her M.Sc. and Ph.D. degrees in electrical engineering from The Ohio State University, Columbus, in 1987 and 1991, respectively. She is currently a professor in the Department of Electrical and Computer Engineering, University of Florida, Gainesville. She received the 1994 National Science Foundation Young Investigator Award and the 1996 Office of Naval Research Young Investigator Award, the M. Barry Carlton Award for the best paper published in *IEEE Transactions on Aerospace and Electronic Systems* in 2005, and the Best Paper Award in 2013 from the IEEE Signal Processing Society. Her research interests include spectral estimation; statistical and array signal processing; and their applications to radar, sonar, and biomedical engineering. She is a Fellow of the IEEE as well as of the Institution of Engineering and Technology and the European Academy of Sciences (Brussels).



**Teng Long** (longteng@bit.edu.cn) received his M.S. and Ph.D. degrees in electrical engineering from the Beijing Institute of

Technology (BIT) in 1991 and 1995, respectively. He has been a full professor with the Department of Electrical Engineering, BIT, since 2000. Since 2008, he has been dean of the School of Information and Electronics. He was a visiting scholar with Stanford University, California, in 1999 and University College London in 2002. He has authored or coauthored more than 300 papers. He has received many awards for his contributions to research and invention in China. His research interests include synthetic aperture radar systems and real-time digital signal processing, with applications to radar and communication systems. He is a Fellow of the IEEE as well as of the Institute of Electronic and Technology and the Chinese Institute of Electronics.



**Abdelhak Zoubir** (zoubir@spg.tu-darmstadt.de) received his Dr.-Ing. degree from Ruhr-Universität Bochum, Germany, in 1992. He was with Queensland University of Technology, Australia, from 1992 to 1998, where he was an associate professor. In 1999, he joined Curtin University of Technology, Australia, as a professor of telecommunications. In 2003, he moved to Technische

Universität Darmstadt, Germany, as a professor of signal processing and the head of the Signal Processing Group. His research interest lies in statistical methods for signal processing with emphasis on bootstrap techniques; robust detection and estimation; and array processing applied to telecommunications, radar, sonar, automotive monitoring and safety, and biomedicine. He has served on publication boards of various publications, most notably as the editor-in-chief of *IEEE Signal Processing Magazine* (2012–2014). He is a Fellow of the IEEE and was an IEEE Distinguished Lecturer (class of 2010–2011).

## References

- [1] F. Gustafsson, "Automotive safety systems," *IEEE Signal Process. Mag.*, vol. 26, no. 4, pp. 32–47, July 2009.
- [2] K. Bengler, K. Dietmayer, B. Farber, M. Maurer, C. Stiller, and H. Winnert, "Three decades of driver assistance systems: Review and future perspectives," *IEEE Intell. Transp. Syst. Mag.*, vol. 6, no. 4, pp. 6–22, Oct. 2014.
- [3] A. Eskandarian, *Handbook of Intelligent Vehicles*. New York: Springer, 2012.
- [4] J. H. L. Hansen, K. Takeda, S. M. Naik, M. M. Trivedi, G. U. Schmidt, and Y. Chan, "Signal processing for smart vehicle technologies: Part 1," *IEEE Signal Process. Mag.*, vol. 33, no. 6, pp. 12–13, Nov. 2016.
- [5] J. H. L. Hansen, K. Takeda, S. M. Naik, M. M. Trivedi, G. U. Schmidt, Y. Chan, and W. Trappe, "Signal processing for smart vehicle technologies: Part 2," *IEEE Signal Proc. Mag.*, vol. 34, no. 2, pp. 18–21, Mar. 2017.

SP

We want  
to hear  
from you!

Do you like what you're reading?  
Your feedback is important.  
Let us know—send the editor-in-chief an e-mail!

 IEEE



**One dollar.  
Endless opportunity.**

## **Join SPS as a Student Member for \$1**

IEEE Signal Processing Society membership gives you access to the educational tools, career development resources, and professional network you need to begin your career in signal and data science.

**Join Now:**  
[signalprocessingsociety.org](http://signalprocessingsociety.org)



Igal Bilik, Oren Longman, Shahar Villeval,  
and Joseph Tabrikian

# The Rise of Radar for Autonomous Vehicles

*Signal processing solutions and future research directions*



©ISTOCKPHOTO.COM/TALAJ

**A**utomotive radar is the most promising and fastest-growing civilian application of radar technology. Vehicular radars provide the key enabling technology for the autonomous driving revolution that will have a dramatic impact on everyone's day-to-day lives. They play a central role in the autonomous sensing suite because of the significant progress in the radio-frequency (RF) CMOS technology that enables high-level radar-on-chip integration and thus reduces the automotive radar cost to the level of consumer mass production. However, this would not be sufficient without high spatial resolution performance, which can be obtained by multiple-input, multiple-output (MIMO) and cognitive approaches at a lower cost.

The uniqueness of automotive radar scenarios mandates the formulation and derivation of new signal processing approaches beyond classical military radar concepts. The reformulation of vehicular radar tasks, along with new performance requirements, provides an opportunity to develop innovative signal processing methods. In this article, we first revise conventional techniques for signal processing in automotive radar. Then, we emphasize the limitations of the historically driven conventional processing approaches in practical roadway scenarios and present alternative signal processing solutions. Finally, we propose several future research directions to enhance vehicular radar performance.

## Introduction

Autonomous driving is one of the megatrends in the automotive industry, and a majority of car manufacturers are already introducing various levels of autonomy into commercially available vehicles. Autonomous conveyances need to substitute for a human driver in both sensing and decision making. The main task of the sensing suite in autonomous vehicles is to provide the most reliable and dense information on the vehicular surroundings. Specifically, it is necessary to acquire information on drivable areas on the road and to report all objects above the road level as obstacles to be avoided. Thus, the sensors need to detect, localize, and classify a variety of typical objects, such as vehicles, pedestrians, poles, and guardrails. Since the major benefits

of autonomous vehicles are expected in urban environments, the variety of obstacles' appearance and the short response time required pose the major challenges to the sensing suite. Comprehensive and accurate information on vehicle surroundings cannot be achieved by any single practical sensor. Therefore, all autonomous vehicles are typically equipped with multiple sensors of multiple modalities: radars, cameras, and lidars.

Because cameras resemble human driver vision, they can be the most natural sensors for autonomous driving. They are low in cost and have a small form factor, providing dense and rich information on the environment, along with the color and texture of objects. However, cameras have significant shortcomings: they are sensitive to illumination and weather conditions, have to be mounted behind an optically transparent surface, and do not provide direct range and velocity measurements. On the contrary, radars are robust to adverse weather conditions, are insensitive to lighting variations, provide long and accurate range measurements, and can be packaged behind optically nontransparent fascia.

The first attempts at automotive radar applications were reported a few decades ago [1]–[3]. However, the mass deployment of radars in commercial vehicles began only recently. The autonomous driving megatrend is the major factor in automotive radar mass production. The technological progress of the 77-GHz RF CMOS with integrated digital CMOS and further packaging advances enable low-cost radar-on-chip and antenna-on-chip systems. The continuously shrinking vehicular radar form factor enables novel on-platform integration possibilities and, consequently, new applications [4].

Historically, automotive radars were classified into long-range radars (LRRs), short-range radars (SRRs), and side-blind zone radars (SBZAs) [5]. This was driven by a variety of applications and performance requirements, such as operation range, field of view (FOV), and object of interest. Thus, LRR is mainly used for adaptive cruise control and, therefore, is required to detect, localize, track, and classify vehicles at longer ranges, with a narrow FOV. SRR needs to provide information on a vehicle's surroundings at ranges of up to 100 m, with an FOV of more than 120°, where the reference target can be any object above the road level. The simplest automotive radar, SBZA, is required to detect only objects within the lanes adjacent to the host vehicle.

The reduced radar size and advanced capabilities have opened the door for completely new radar application segments. Thus, ultrashort-range radar (USRR) was recently introduced for autonomous parking and side-looking applications at a wide FOV of 120° and ranges of up to 30 m [6]. The multimode radar [7], where the same hardware configures its operation (antenna configuration, waveform, radar echo processing, and so forth) to various operational modes, is another automotive radar trend.

Vehicular radars are required to provide sensing capabilities starting from zero range and, therefore, are continuous wave (CW) and, because of low-cost requirements, employ linear-frequency modulation (LFM) ([8, Ch. 16]). Other waveforms, such as phase modulation [9] and step frequency [10], were also introduced for automotive radars.

The most dramatic transformation of the vehicular radar system is now occurring because of its role shift from a sensor that detects to one that images [5], [11]. Autonomous driving requires high-resolution sensing capabilities, and thus automotive radars must provide high-resolution information on the vehicle environment in the range–Doppler–azimuth–elevation domains. Range resolution is inversely proportional to the radar bandwidth. In 77-GHz radars, the available bandwidth is 4 GHz, which provides sufficient range resolution. Doppler resolution is limited by the coherent observation time and depends on the transmitted waveform, receiver processing, and target dynamics. Angular resolution is contingent upon the antenna aperture and thus is determined by the number and geometry of the transmit and receive channels, limited by the radar cost and packaging size.

Automotive radars are required to operate in dense urban environments with distributed objects. Therefore, the applicability of conventional superresolution methods, such as multiple signal classification (MUSIC) and minimum-variance distortionless response (MVDR) [12], relying on spatial sparsity, is limited. The requirements for high-angular resolution in both azimuth and elevation, using a small number of channels, turns the MIMO radar concept [13] into an attractive alternative to the full sensor array. Thus, the majority of state-of-the-art automotive radars use some variant of MIMO radar.

In automotive radar applications, a novel interpretation of the target and clutter notions is required because all of the dynamic or static objects above the road level are targets of interest, and detailed information on them is needed for autonomous driving. This operational scenario poses additional challenges for the radar processing and limits the applicability of conventional radar techniques to automotive radar.

This work overviews the conventional fast LFM–CW automotive radar signal processing flow, emphasizes its limited applicability to vehicular radar scenarios, and proposes a few novel approaches for key performance improvements. In particular, novel range–Doppler processing, detection, clustering, and dynamic range (DR) enhancement methods are required, specifically designed for high-resolution automotive radar. Thus, one of the challenges in vehicular radar operation is the discernment of small objects (e.g., child pedestrians) as well as large ones (e.g., semitrailers). Conventional implementation of detection methods, such as constant false-alarm rate (CFAR), are suboptimal in the automotive environment since objects occupy multiple range–Doppler–azimuth–elevation cells. Therefore, novel detection methods for target recognition that use information from adjacent range–Doppler cells are required.

High-resolution automotive radars can generate multiple detections from the same object. Thus, data association methods are required. Detections originated by the same object have similar properties and, therefore, can be associated into clusters. Data similarity is determined by specific criteria and metrics, such as distribution in the range–Doppler–azimuth–elevation space.

## Automotive radar operation challenges

The main role of the sensing suite in autonomous driving is to be a substitute for human driver vision and thus provide

reliable information on a moving vehicle's surroundings to enable a prompt reaction to the dynamically changing scene and threats to the vehicle being driven. The autonomous sensing capabilities are well beyond those of human eyes, compensating for the limited artificial intelligence in comparison with human cognition.

The radar, along with cameras, plays a central role in autonomous vehicles oriented toward mass production. Automotive radars have multiple advantages over cameras and lidars, such as long operation ranges, immunity to lighting and weather influences, ability to operate behind optically nontransparent fascia, and direct measurement of targets' radial velocity. Therefore, radars have been given a key role in autonomous vehicles. Both the advantages and challenges of automotive radars stem from the properties of their associated electromagnetic waves and their wavelength, which is determined by regulations. The main issue for automotive radar systems is to provide high-resolution information about multiple dynamic targets in an extremely cluttered automotive scene with a high update rate.

Figure 1 shows a typical urban scenario as an example of the automotive radar challenges described in this section. The radar is required to perceive this scene of a vehicle passing near a pedestrian. To achieve this task, high-resolution sensing in range–Doppler–azimuth–elevation and a sensitive detector, followed by clustering, tracking, and classification algorithms, are required. This section describes the major challenges of the vehicular radar that determine its design guidelines.

### Scene variety

Many automotive radar challenges stem from the requirement to operate across a variety of scenes, ranging from urban and metropolitan to rural and freeway environments. These settings are characterized by a wide spectrum of targets and infrastructures, varying by radar cross section (RCS), velocity, and motion pattern: road debris, animals, pedestrians, vehicles, bridges, and so on. As a result, an automotive radar needs to be designed to detect, localize, track, and classify everything from slowly moving children and animals in parking lot scenarios to fast-moving vehicles on freeways. Consequently,

the necessity to support this wide range of velocities challenges the waveform design in terms of chirp duration, duty cycle, and frame size. Moreover, the tradeoff between Doppler ambiguity, maximal range, and range resolution makes demands upon the automotive radar system design.

The large variety in target size, ranging from small RCS targets, such as on-road debris, to large RCS structures, such as bridges, requires a high DR. Another reason for the high DR requirement is the simultaneous detection of far and small targets and close and large objects. As a result, a high DR dictates the required effective number of bits (ENOB), limiting the sampling rate. The cost of the analog-to-digital converters (ADCs) increases with the DR according to  $DR = 6.021 \text{ ENOB} + 1.763 \text{ dB}$  [14].

Operation in typical urban scenes is characterized by a large number of targets that create a continuum of radar echoes across the FOV, which poses a computational complexity challenge to the detector and the beamformer processing algorithms. Moreover, when designing a high-resolution radar, typical automotive radar targets are spatially distributed and can be observed as a superposition of multiple point reflectors, complicating the detector design. In addition, the superposition of multiple point scatterers is observed by the radar as a single target with a highly variable RCS.

For typical autonomous scenarios, the radar is required to provide high-resolution 4D information regarding the host vehicle's surroundings. These data are then used to identify obstacles above the road level. Thus, high angular resolution in elevation is required to recognize any obstacle 10 cm above the road surface. Identification of the drivable path further requires the detection of overhead objects, such as bridges and signs, that may interfere with the moving vehicle. Finally, the automotive radar needs to support a variety of active safety features, under a wide spectrum of operational conditions, that challenge the optimization of the radar parameters.

In dense urban environments, the vehicular radar experiences multipath from the surrounding surfaces. The multipath effect increases estimation errors and generates ghost targets, which are considered to be false alarms [15]. Multipath mitigation involves processing with additional computational complexity.

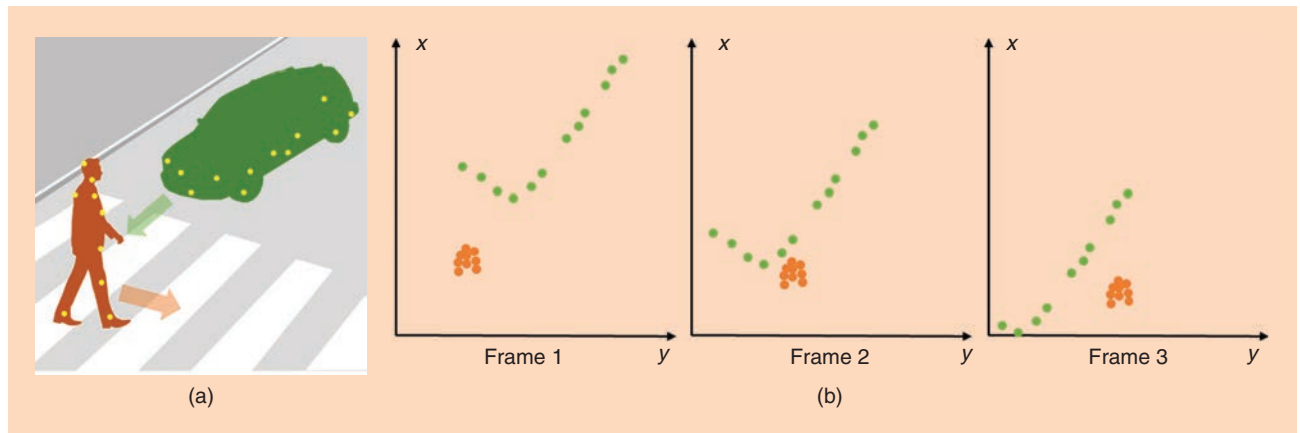


**FIGURE 1.** An example of the urban environment, demonstrating some of the automotive radar challenges. (a) A vehicle passing near a pedestrian. Each target consists of several detections, generating a point cloud. (b) Adjacent point clouds of a pedestrian and vehicle, over several frames.

## High resolution

Autonomous driving requires information on all obstacles surrounding the host vehicle above the ground level. Thus, an automotive radar needs not only to localize the surrounding objects but to provide information on their extent (and, preferably, shape) and classify them. These tasks require high resolution in range, Doppler, azimuth, and elevation to attain lidar-like performance. The high-resolution requirement increases the computational complexity of radar signal processing and requires the development of computationally efficient algorithms to provide real-time (or low-latency) solutions to the high-dimensional and extensive data.

The range resolution is given by  $\Delta R = c/2B$ , where  $B$  is the transmitted signal bandwidth. In LFM signals,  $B = \tau b$ , where  $b$  denotes the chirp slope, and  $\tau$  is the chirp duration. The Doppler resolution is given by  $\Delta D = 1/TOT$ , where TOT is the time on target. The TOT is limited by the overall maximal allowed system latency and by the maximal coherent integration interval, determined by the target's radial velocity  $V$  as follows:  $TOT < \Delta R/V$ . Beyond this limit, an increase in TOT does not contribute to the target intensity or to Doppler resolution because of the target migration to other range cells.

Figure 2 shows a scenario in which the target's dynamics exceed this limit, creating the range migration phenomenon. The Doppler information in a typical fast LFM automotive radar is extracted via an additional fast Fourier transform (FFT). High Doppler resolution requires a long integration time, and low Doppler ambiguity necessitates a high chirp rate, resulting in a large number of chirps during the observation time. Therefore, high resolution in the range–Doppler domain needs the implementation of a large 2D FFT. Conventionally, in automotive radars, the FFT is performed by dedicated processing accelerators. The implementation of a large 2D FFT increases the processor cost, requires a larger on-chip fast memory, and challenges the heat dissipation design.

A high angular resolution in azimuth and elevation requires a large antenna array aperture and thus a large number of transmit and/or receive channels. Therefore, computational resources are demanded to process the generated data. In addition, the need for a large antenna aperture challenges its integration in the automotive platform and drives the system cost as the number of transmit and receive channels increases.

## Clutter

The operational environment of automotive radar differs from that of conventional military radars in the sense that all objects above the ground level are targets that need to be detected, localized, and classified. In automotive radar, any obstacle above the ground level is considered to be a threat, if located in the planned driving path of the host vehicle. Therefore, the conventional clutter returns are actually targets of interest. Typically, clutter returns are weak because of low aspect angles and high operational frequencies. However, ground returns from a close proximity to the host vehicle determine the requirements for antenna sidelobe levels in elevation since road echoes received through sidelobes can be stronger than echoes from far and weak targets at the antenna main beam.

In scenarios with a moving host vehicle, static clutter echoes from the road are received at different Doppler shifts, which is a function of the road angle  $D = V\cos\theta\cos\varphi$ , where  $V$  is the host vehicle speed and  $\theta$  and  $\varphi$  are the elevation and azimuth, respectively, of the clutter return. The detection of weak and far targets within strong Doppler-spread clutter challenges the automotive radar detector design. Figure 3 illustrates a scenario of a target adjacent to clutter, where the target is a pedestrian and clutter originates from a fire hydrant, potentially masking the target.

## Interference

One of the future challenges of automotive radars is interference mitigation [16], [17]. Vehicular radar is subject to three types of interference: self-interference, cross interference from other radars on the same vehicle, and interference from other vehicles' radars. Self-interference originates from strong radar echoes reflected by the vehicle platform, painted fascia, and the radome itself. These echoes mask short ranges of the automotive radar and thus degrade the detection performance on close targets. In addition, they contribute to increasing the probability of false alarms and reducing the radar DR, as the self-interference often determines the saturation limit. Furthermore, the computational complexity increases because of the requirement for mitigation algorithms.

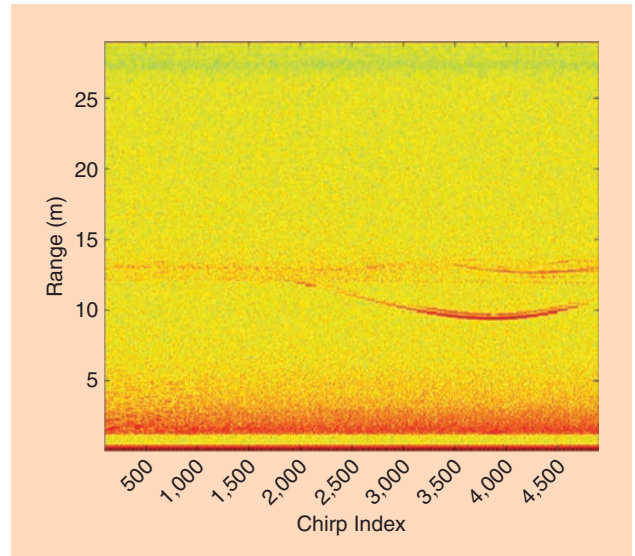


**FIGURE 2.** A range–chirp map showing target migration in a range over a long observation time.

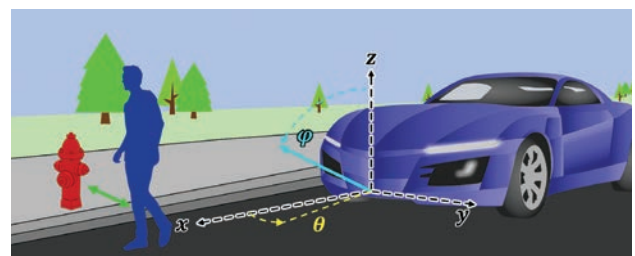


**FIGURE 3.** A cluttered roadway scenario.

Autonomous vehicles need surround coverage, which is achieved by mounting multiple radars around the vehicle. The radars have overlapping FOVs, which might cause mutual interference. The interference is both direct and reflected from targets. Thus, innovative algorithms for interference mitigation are required.

When most vehicles are equipped with automotive radars, multiple interferences are to be expected between radars of adjacent vehicles. Direct and reflected interference sources are expected to occur in dense-traffic scenarios, where the level of interference depends on the distance between radars, beam pattern, orientation, waveform, and the signal processing scheme. Interference sources increase the probability of false alarms, create ghost targets, and can mask true targets. Mitigation schemes will increase the computational complexity.

### State-of-the-art automotive radar technology

State-of-the-art vehicular radar is designed to address automotive environment challenges. This is reflected in the radar's hardware, system design, waveform, antenna, and processing chain.

#### Concept

To tackle the automotive environment issues, as described in the "Automotive Radar Operation Challenges" section, the following technologies have been commonly adopted for vehicular radars: CW-LFM MIMO, high carrier frequency, solid state, CMOS, and RF integrated circuit. Pulse-Doppler radars have minimal detectable range (blind range) since the radar's receiver is turned off during the transmission interval. Automotive radars are required to detect targets at close proximity (starting from zero range), making the pulse-Doppler radar operation concept inappropriate for vehicular applications. Another advantage of CW operation is the low transmission peak power, which is important for operation in close proximity to the general public and which is strictly regulated by health authorities. Pulse-Doppler radars conventionally operate with up to a  $D_{dc} = 10\%$  duty cycle, and, therefore, to achieve the required average power  $P_{avg} = P_{peak} D_{dc}$ , they need to transmit higher peak power  $P_{peak}$  compared with CW radars. The latter have modulated signals to obtain a target's range information. The LFM waveform is the most common CW modulation scheme since it has high range resolution and allows simple and low-cost fabrication.

State-of-the-art automotive radars have adopted the MIMO operation concept to achieve high angular resolution at a wide 2D

azimuth–elevation FOV, with a high update rate. The MIMO vehicular radar illuminates the entire FOV with a wide and static transmit beam, where the angular information is obtained using the MIMO scheme at the receiver [13]. Common alternatives of direction-of-arrival (DOA) estimation are scanning phased array and monopulse (see [8, Ch. I]). Scanned-based DOA estimation and monopulse are infeasible in automotive radars because of the low update rate and low angular resolution.

High angular resolution, determined by the antenna beamwidth at a wide FOV, can be achieved via a multibeam beamforming. Analog beamforming implementation requires multiple circuitries for each generated beam, followed by multiple samplers. The large number of beams prohibits its analog implementation, which becomes complex, expensive, and cumbersome.

An alternative approach is digital beamforming, where each antenna element is sampled, and digitally steered beams can be obtained via a discrete Fourier transform [18]. In digital beamforming, there is no physical constraint on the number of beams, which is limited only by the computational power. This process is applicable at the receiver in a single-input, multiple-output system. In a MIMO system, this concept is extended from physical elements to virtual elements by transmitting orthogonal signals and decoding them at each receiver element [13].

#### FOV

Autonomous driving requires surround coverage of the host vehicle to provide reliable information about the static and dynamic obstacles that can be threats for the vehicle. The requirement of a low-cost system motivates the widest possible azimuth FOV. MIMO radar provides a wide FOV while obtaining narrow beams and a high angular resolution. This is achieved by the effect of virtual sensors. Each combination of receive and transmit elements generates a virtual element, with signal properties determined by the unique transmitter–target–receiver path, as conceptually shown in Figure 4. The MIMO virtual antenna aperture is larger than that of a conventional phased-array antenna, providing higher angular resolution.

Regulated by the authorities, automotive radars are implemented at a high carrier frequency band of 76–81 GHz. The radar antenna size decreases, and the angular resolution, determined by the ratio between the antenna aperture and the carrier frequency, increases with the carrier frequency. Therefore, a higher operational frequency allows smaller and lighter automotive radar implementation, attaining higher angular resolution.

The Doppler resolution  $\Delta D$  improves linearly with increasing carrier frequency  $f_c$ ,

$$\Delta D = \frac{c}{2f_c} \frac{1}{TOT}. \quad (1)$$

The higher operational frequency provides a larger available spectrum bandwidth for a transmitter with a constant fractional bandwidth [19]. Therefore, the range resolution increases at a higher carrier frequency.

High carrier frequency poses a technological challenge to fabricate high-quality and low-loss RF components. Thus, the performance of RF components in terms of noise figure, phase

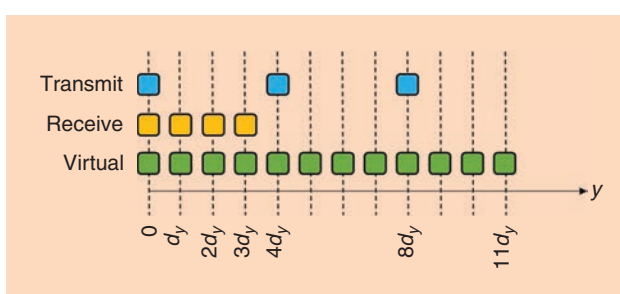


**FIGURE 4.** A MIMO radar antenna array.

noise, antenna gain, and efficiency typically degrades with increasing carrier frequency. Moreover, free-space path loss grows as the carrier frequency increases, resulting in shorter radar detection range (see [8, Ch. 1]).

Automotive radars are expected to be manufactured in high volumes, far greater than conventional military radars. Therefore, certain techniques and materials, e.g., solid-state CMOS, which meet both mass production and low-cost requirements, will be implemented. The most challenging aspect of radar mass production is antenna calibration, which conventionally is a long and costly process, inapplicable to mass production. Efficient innovative methods are required for fast and accurate calibration.

### Waveform

Motivated by the requirement of high angular resolution, state-of-the-art automotive radars adopt a MIMO approach, which requires orthogonal waveform generation. The simplest way to achieve a waveform's orthogonality is time-division multiple access (TDMA), where the number of TDMA cycles  $N_{\text{Tx}}$  equals the number of transmit antennas. For the LFM-TDMA-MIMO automotive radar, the pulse repetition interval is  $T_{\text{cyc}} = T_{\text{c}}N_{\text{Tx}}$ , where  $T_{\text{c}}$  is the chirp period and is equal to the chirp duration. The range resolution and maximal unambiguous Doppler velocity are  $\Delta R = c/2bT_{\text{c}}$  and  $D_{\text{unamb}} = (c/2f_{\text{c}})(1/T_{\text{cyc}})$ , respectively. The overall TOT =  $N_{\text{cyc}}T_{\text{cyc}}$ , determined by the number of cycle repetitions  $N_{\text{cyc}}$ , upper-bounds the update rate of the radar detections FPS  $\leq 1/\text{TOT}$  and defines the Doppler resolution as  $\Delta D = (c/2f_{\text{c}})(1/\text{TOT})$ . Additional approaches for obtaining nearly orthogonal signals have been derived [20], and similar approaches can be adopted for automotive applications.

Conventional vehicular radars are designed for a specific set of active safety features, and, therefore, radar waveform parameters are optimized for this particular array of operational conditions. Thus, an LRR is required to provide long ranges for fast-moving targets (a short chirp duration for increasing the maximal unambiguous Doppler) with lower range resolution. In turn, an SRR operates at shorter ranges, with higher range resolution and smaller unambiguous Doppler. Since the optimal waveform is scenario and mission dependent, the development of a radar that adapts the waveform according to the instantaneous radar mission and environment is required.

### Processing chain

When operated in dense urban environments characterized by multiple objects, the transmitted automotive radar signals are reflected back from the targets and clutter and then received and down-converted as a mixture of multiple radar echoes accompanied by additive receiver noise. The main task of the vehicular radar signal processing chain is to suppress the additive noise and detect, isolate, and classify these multiple mixed echoes from different objects that are prominent and separable in the 4D spectral domain of range, Doppler shift, and 2D DOA. Conventionally, the automotive radar processing chain performs this task by employing multiple integrations along the different dimensions [7].

In the presence of  $M$  targets, the baseband data model at the  $k$ th chirp and the  $n$ th antenna receiver with a single transmitter is given by

$$x_{n,k}(t) = \sum_{m=1}^M A_m s(t - \tau_m) e^{j2\pi f_{\text{dm}} k T_c} e^{j2\pi f_{\text{c}} \Delta\tau_{m,n}} + v_{n,k}(t), \quad (2)$$

where  $s(t)$  is the transmitted signal and  $A_m$ ,  $\tau_m$ , and  $f_{\text{dm}}$  are the amplitude, time delay, and Doppler shift of the  $m$ th target, respectively. The time-delay difference  $\Delta\tau_{m,n}$  denotes the delay difference between the antenna array origin and the  $n$ th antenna for the  $m$ th target, and  $v_{n,k}(t)$  represents the additive receiver noise.

Stretch processing is performed by multiplying the received signal with the conjugated transmitted signal. For an LFM signal  $s(t) = e^{j\pi b t^2}$ , one obtains

$$\tilde{x}_{n,k}(t) = x_{n,k}(t) s^*(t) = \sum_{m=1}^M \tilde{A}_m e^{-j2\pi b \tau_m t} e^{j2\pi T f_{\text{dm}} k} e^{j2\pi f_{\text{c}} \Delta\tau_{m,n}} + \tilde{v}_{n,k}(t), \quad (3)$$

where  $\tilde{A}_m = A_m e^{j\pi b \tau_m^2}$ . It can be seen that the model consists of a product of sinusoids in slow-time  $k$  and fast-time  $t$  data. For uniform planar arrays,  $\tau_{m,n}$  is linear in indices of horizontal and vertical elements. Thus, the model includes a product of sinusoids in these axes as well. This implies that, to extract range–Doppler–azimuth–elevation information, one needs to implement a 4D FFT. Prior to the digital FFT, the signal is sampled with a sampling time of  $T_s$ , yielding  $x[l, k, n] = \tilde{x}_{n,k}(lT_s)$ . The 4D FFT is performed by

$$X[p, q, \theta, \varphi] = \sum_{n_v=1}^N \sum_{n_h=1}^H \sum_{k=1}^K \sum_{l=1}^L x[l, k, n] e^{-j2\pi p \frac{l}{L}} e^{-j2\pi q \frac{k}{K}} e^{j2\pi \frac{d}{\lambda} n_h \sin \theta \cos \varphi} e^{j2\pi \frac{d}{\lambda} n_v \sin \varphi}, \quad (4)$$

where  $n_h$  and  $n_v$  are the horizontal and vertical antenna indices, respectively,  $n = n_h + H(n_v - 1)$  for  $H$  horizontal antennas, and  $d$  is the antenna spacing. The resulting data cube is depicted in Figure 5. Targets that are distinguishable at least in one of these parameters can be resolved.

Leveraging the separation of the received radar echoes from multiple objects in the four domains, the receiver reports the target presence at a particular point in this space by the comparison of the received signal energy to the threshold (detection). Conventionally, automotive radars use CFAR detection, in which a detection is declared for cells that satisfy the following condition:

$$|X[p, q, \theta, \varphi]|^2 > T + \hat{\sigma}_v^2[p, q, \theta, \varphi], \quad \forall p, q, \theta, \varphi, \quad (5)$$

where  $T$  is the CFAR threshold and  $\hat{\sigma}_v^2[p, q, \theta, \varphi]$  is the noise variance, estimated around the cell defined by its arguments. As radar operation in an automotive environment pushes the radar design toward higher sensitivity (longer detection ranges of weaker targets), lowered CFAR thresholds raise the false-alarm rate beyond the desired point. Therefore, additional detection-level

spatiotemporal filtering, denoted as *clustering and tracking*, is conventionally implemented in vehicular radars. The conventional density-based spatial clustering of applications with noise (DBSCAN) [21], [22] takes advantage of the high spatial resolution, groups together closely located detections, and represents them as a single cluster. Groups that contain few detections are marked as noise and removed, leaving the point cloud with an improved detection-to-false-alarm rate. Temporal filtering, which is usually implemented using Kalman, particle, or multimodal filters [23], further increases the fidelity of the output data by associating temporally close clusters into tracks.

Finally, additional information on the detected and tracked target is extracted from the received echoes via classification, which may be performed with extracted micro-Doppler features [24], spatial spread, movement along the space, or other information. These features can be used to characterize the detection or even improve upon the estimation of its parameters. The processing flow is depicted in Figure 6.

### Antenna design

The automotive radar antenna must provide high angular resolution and accuracy while being mass-produced at low cost. To satisfy these criteria, microstrip patch technology is often used for vehicular radars operated at the carrier frequency of 77 GHz (a wavelength of  $\lambda = c/f_c = 39$  mm) with a wide bandwidth of 4 GHz. For this wavelength scale, the required fabrication accuracy is on the order of micrometers, which is higher than currently available fabrication technologies, resulting in suboptimal antenna performance. The majority of modern automotive radars prioritize angular resolution in azimuth over that in elevation. However, the practical implementation of the radar-based active safety features and autonomous driv-

ing requires high angular resolution in both azimuth and elevation. Therefore, a planar antenna layout is needed to provide such resolution. The microstrip antennas on the printed circuit board have an inherently poor isolation between the antennas and therefore provide degraded performance.

### Future solutions

This section describes the performance gaps in state-of-the-art automotive radars and discusses some of the required signal processing improvements. Parts of these topics have been developed and intensively investigated in recent years. These areas have the potential to move vehicular radar technology forward, but adaptation to the special needs of automotive radars is necessary.

### Cognitive radar

Highly dynamic and varying roadway scenarios motivate the adaptive allocation of automotive radar resources. Moreover, the cost reduction requirement drives the consolidation of sensing capabilities to support multiple automated features within a single sensor. Cognitive sensing that introduces feedback between the receiver and the transmitter to improve scene perception can address these challenges. Specifically, the radar waveform needs to be adapted to the scene and mission: different ranges, FOVs, target types, RCSs, and velocities. The array configuration can also be changed according to the tradeoff between angular resolution, FOV, and maximal range.

The basic idea of cognitive radar is presented next (see Figure 7). MIMO radar allows flexibility in the design of the transmit waveform, which may be different for each transmitting element. After the introduction of colocated MIMO radar in [13], the problem of optimal waveform design for various scenarios and under different criteria has been intensively investigated. In automotive radar applications, the radar task and scenario continuously change, and thus the transmit waveform needs to be adaptively modified based on history observations, using a cognitive approach.

The idea of cognitive radar was proposed in [25] and has been investigated in several works. A cognitive radar system adaptively interrogates the environment using the available information from previous observations, external databases, and task priorities. The transmit waveform can be sequentially adapted in the space, time, and frequency domains, based on previous observations, which provide relevant information on the scenario. Adaptive beamforming for cognitive MIMO radar was investigated in [26]. However, in that paper, the focus was on only spatial waveform design, ignoring the range and Doppler dependency.

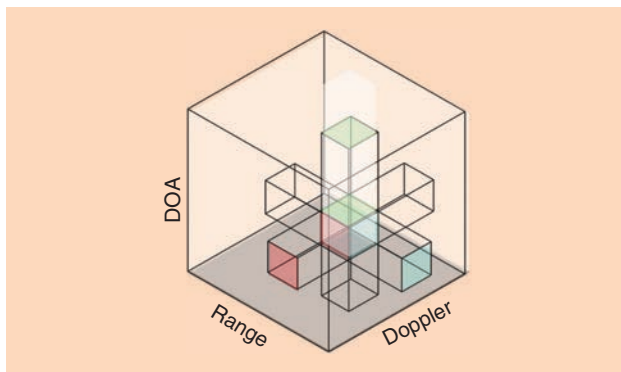


**FIGURE 5.** A range–Doppler–DOA data cube, an output of the 4D FFT.

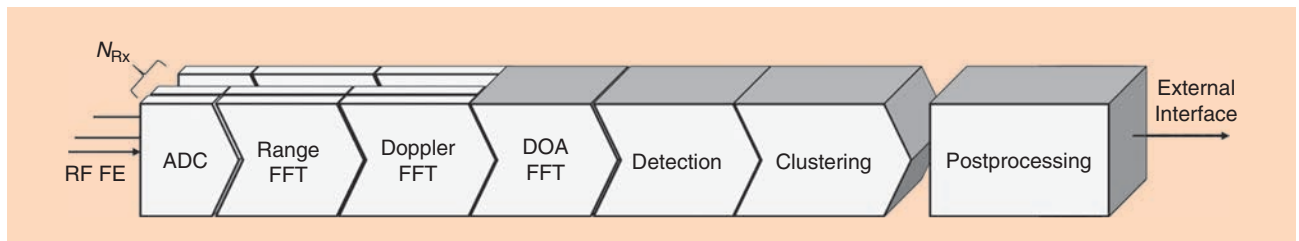


**FIGURE 6.** A conventional automotive radar processing flow. FE: front end.

Consider a monostatic MIMO radar with colocated transmit and receive arrays of  $N_T$  and  $N_R$  elements, respectively. In the presence of  $M$  targets, the received signal model at the  $k$ th pulse/chirp can be expressed as

$$\mathbf{x}_k(t) = \sum_{m=1}^M \alpha_m e^{-j\omega_{Dm} k} \mathbf{a}_R(\varphi_m) \mathbf{a}_T^T(\varphi_m) \mathbf{s}_k(t - \tau_m) + \mathbf{v}_k(t), \\ k = 1, 2, \dots, t \in [0, T], \quad (6)$$

where  $\mathbf{x}_k(t)$ ,  $\mathbf{s}_k(t)$ , and  $\mathbf{v}_k(t)$  denote the vectors of the received data, the transmit signal, and the noise vector, respectively. The parameters  $\alpha_m$ ,  $\varphi_m$ ,  $\tau_m$ , and  $\omega_{Dm}$  are the complex attenuation, direction, propagation delay, and Doppler frequency shift of the  $k$ th target, respectively, and  $\mathbf{a}_T(\cdot)$  and  $\mathbf{a}_R(\cdot)$  are the steering vectors for the transmit and receive arrays, respectively. The Fourier coefficients of the data model in (6) are given by

$$\mathbf{x}_{kl} = \mathbf{H}_{kl}(\theta) \mathbf{s}_{kl} + \mathbf{v}_{kl}, \quad k = 1, 2, \dots, l = 1, \dots, L, \quad (7)$$

where  $\mathbf{x}_{kl}$ ,  $\mathbf{s}_{kl}$ , and  $\mathbf{v}_{kl}$ , are the  $l$ th Fourier coefficients of the received data, transmit signal, and noise vectors, respectively, and

$$\mathbf{H}_{kl}(\theta) = \sum_{m=1}^M \alpha_m e^{-j\omega_{Dm} k} e^{-j\frac{2\pi l}{T} \tau_m} \mathbf{a}_R(\varphi_m) \mathbf{a}_T^T(\varphi_m) \quad (8)$$

is the MIMO transfer function. Let  $\mathbf{X}_k = [\mathbf{x}_{k1}, \dots, \mathbf{x}_{kL}]$  and  $\mathbf{S}_k = [\mathbf{s}_{k1}, \dots, \mathbf{s}_{kL}]$ . A cognitive radar adaptively modifies the transmit signal sequence at the  $k$ th step  $\mathbf{S}_k$ , given observations in previous steps denoted by  $\mathbf{X}^{(k-1)} = [\mathbf{X}_1, \dots, \mathbf{X}_{k-1}]$ .

The transmit signal is usually constrained according to one of the following approaches:

- *Limited total energy:*  $\sum_{l=1}^L \|\mathbf{s}_{kl}\|^2 = \text{const}$
- *Limited energy at each transmitter element:*  $\sum_{l=1}^L \|[\mathbf{s}_{kl}]_n\|^2 = \text{const}, n = 1, \dots, N_T$
- *Limited total energy at each frequency bin:*  $\|\mathbf{s}_{kl}\|^2 = \text{const}, l = 1, \dots, L$ .

The cognitive scheme can be formulated as follows:

$$\begin{aligned} & \underset{\mathbf{s}_k}{\text{optimize}} && C(\mathbf{S}_k, \mathbf{X}^{(k-1)}) \\ & \text{subject to} && \text{signal energy constraint,} \end{aligned}$$

where  $C(\cdot, \cdot)$  denotes the optimization criterion, which reflects a measure of performance. Performance bounds can serve as possible optimization criteria. For cases where one is interested in optimizing the parameter estimation accuracy, lower bounds, such as the Cramér–Rao bound or other large-error

bounds, are usually adopted as optimization criteria. The non-Bayesian framework is not applicable because non-Bayesian bounds are usually parameter dependent. Although the unknown parameter may be substituted by its estimates, this solution usually results in poor performance. To obtain a performance measure independent of the parameters to be estimated, the Bayesian framework is usually preferred. This approach has been proposed for target localization [26].

For detection or classification problems, one may use the sequential hypothesis testing framework. In this approach, one is interested in minimizing the average sample number (ASN) where the decision error probabilities are fixed. Lower ASN bounds are inversely proportional to the Kullback–Leibler divergence (KLD) between the probability density functions under the given hypotheses. This implies that, for detection or classification tasks, one is required to maximize the KLD to optimize the performance.

### Extended target detection

In typical urban scenarios, high-resolution automotive radars with a range resolution of several centimeters are required to detect range-extended targets that occupy multiple range–Doppler cells. At such fine resolution, every single extended target appears as a set of point targets, as shown in Figure 1(a). Single-cell-based detectors do not aggregate the entire spread target energy and, therefore, provide shorter detection ranges. Conventional radar detectors, such as CFAR, offer degraded performance in such scenarios because of contamination of the noise estimation by the interfering cells. Therefore, the development of alternative detectors that are robust to interference from other cells is required. In military applications, detectors for distributed targets were first introduced in [27] and further developed in [28]. These approaches cannot be directly applied to automotive radars, since prior information on the targets in the vehicular domain is typically unavailable because of the vast variety of their types and sizes. Alternatively, what is needed is the development of a detection approach utilizing rigid-body information on the automotive targets to integrate energy spread over multiple cells.

### Doppler ambiguity

TDMA implementation of the state-of-the-art automotive MIMO radars results in a contradiction between the Doppler and the DOA requirements. This occurs because the DOA estimation is performed per range–Doppler cell, and, as a result, the DOA estimation performance directly depends on the Doppler estimation [29]. In TDMA–MIMO radar, as the number

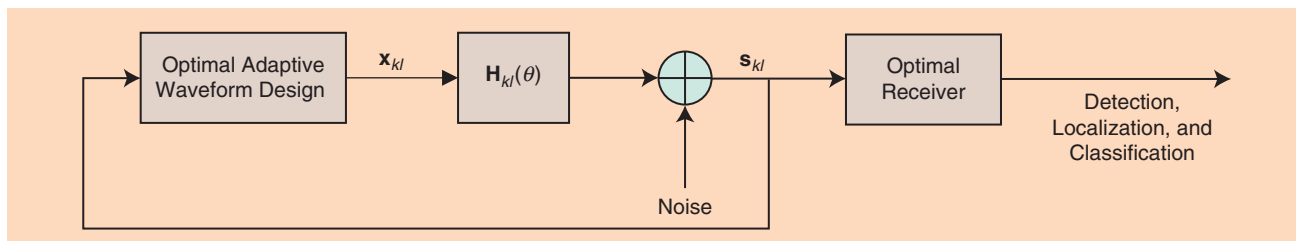


**FIGURE 7.** A cognitive radar configuration.

of transmit antennas increases, the maximal unambiguous Doppler frequency decreases. Therefore, novel methods to resolve the Doppler ambiguity of automotive MIMO radars are required. For this purpose, several approaches may be adopted. One interesting technique is the chirp sequence waveform design presented in [30]. Moreover, at longer operational ranges (e.g., in freeway scenarios), a longer chirp duration is required, which challenges the Doppler ambiguity mitigation methods.

### Multipath mitigation

Flat surfaces on roads, guardrails, buildings, signs, and bridges characterize automotive scenes. The radar transmitted signal reflects from these surfaces and interferes with the direct signal that echoes from targets. Figure 8 shows typical traffic situations, with vertical, road-induced and horizontal, guardrail-induced multipath scenarios.

Indirect signal parameters, such as range, Doppler, azimuth, and elevation, differ from those of the direct signal. If they are similar to those of the direct signal and are beneath resolution, they may interfere with it, potentially disrupting target detection and parameter estimation. Angular information has the highest sensitivity to multipath, and its estimation performance can be greatly degraded. If the indirect signal parameters differ beyond the ability of the radar to resolve, a false target may appear. This phenomenon is difficult to mitigate, and current radars suffer from it.

The indirect signals are determined by radar-target-environment geometry and correlated with the direct path signal. Current mitigation methods utilize the difference between the direct and indirect signals in the time-delay, Doppler, and DOA domains: [15] utilizes the angular difference to filter multipath with MIMO space-time adaptive processing, [31] employs correlation, [32] proposes to track both the direct and indirect signals simultaneously, and [33] takes advantage of the different indirect signal responses for up and down LFM signals to distinguish and mitigate them. All of these methods cannot be directly applied to automotive radars and need to be modified since the use of different waveforms is limited because of several reasons. These include the requirement of low cost, the difference of automotive clutter from that encountered with airborne radars, the occurrence of vehicular multipath in both azimuth and elevation, and the multiple moving objects that induce the large number of multipath returns in dense urban environments.

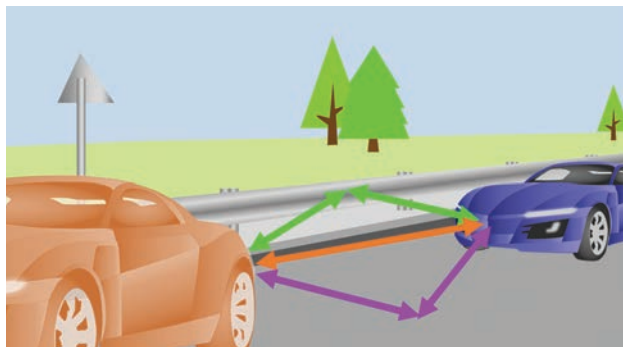


**FIGURE 8.** An illustration of multipath, with the target echo traveling in additional indirect paths, reflected by the road surface and guardrail.

### Angular superresolution

State-of-the-art automotive radars have a low angular resolution determined by the antenna aperture. The resolution attained through conventional beamforming cannot break this physical limitation. Therefore, vehicular radars adopt a MIMO radar approach to achieve higher angular resolution at a smaller aperture and a feasible number of channels [7]. Superresolution methods that are successfully used in military applications, such as MVDR and MUSIC, are expected to be implemented in automotive radars. This task requires the development of low-computational processing algorithms and their adaptation to automotive scenarios with angularly spread targets (short-range and large objects, such as vehicles) that may occupy multiple angular cells.

### Clustering

Because of high range resolution in automotive radars, targets (such as vehicles and pedestrians) appear as a cloud of point targets, and thus the association of these point targets to a single object target, denoted as *clustering*, is required. The clustering process consists of point target association to centroids representing actual objects. Thus, the DBSCAN was shown to be able to generate arbitrarily shaped clusters and to disregard noise-generated detections without a need for a priori knowledge of the number of clusters [21]. The DBSCAN was adapted to a variety of applications and input data characteristics [22]. However, its major shortcoming is its inability to provide centroids that are related to real-life objects. Moreover, in dense automotive environments with multiple adjacent objects, the association task is computationally demanding. Therefore, novel clustering methods are necessitated that take into account point detection densities in the entire range-Doppler-DOA domain and provide an indication of object shapes.

### Waveform optimization

State-of-the-art automotive radars that adopt the MIMO approach achieve the required waveform orthogonality via TDMA operation at the expense of shortened maximal detection range and lower maximal unambiguous Doppler. Therefore, the practical implementation of vehicular MIMO radars requires the development of a more efficient method to achieve waveform orthogonality through code-division multiple access (CDMA) via phase or frequency coding. The CDMA approach was intensively studied in the communications literature, and many efficient codes, such as Gold and Hadamard, were shown to achieve high orthogonality among transmitted sequences [34], [35]. However, the orthogonality provided by these codes degrades with the delay or Doppler shifts that characterize automotive applications. Therefore, new code families need to be developed for efficient implementation of the Doppler- and delay-shift codes that in turn could enable efficient CDMA-MIMO implementation of vehicular radars.

### Synthetic aperture radar

Synthetic aperture radar (SAR) mounted on the moving vehicle platform has a potential to improve automotive radar angular resolution and enhance imaging capabilities [36], [37]. Vehicular SAR is especially efficient for a variety of side-looking applications, such as parking spot detection [38] and road boundary localization

[39]. However, the forward direction is of the greatest interest for automotive radar for autonomous driving, and some preliminary results on forward-looking automotive SAR were shown in [40]. Major challenges in the application of airborne-based SAR methods to vehicular radars are motion compensation, nonlinear host vehicle motion, and low-grazing angles. Therefore, efficient methods for automotive SAR are a subject for future research.

### Multiradar coexistence

The last decade showed an exponential growth in the number of automotive radars deployed in retail vehicles, and a similar tendency is expected in the future. Thus, the density of automotive radars on the road per area is growing. As all vehicular radars share the same spectrum, mutual interference between them is expected to become a major concern. The probability of interference is determined by the radar waveform, transmitted power, beamforming properties, and distance between the radars. The power of the direct interference at the receiver is

$$P_{RH} = \frac{P_{II} G_{II} G_{RH} \lambda_I^2}{(4\pi)^2 R^2 L_H}, \quad (9)$$

where  $P_{RH}$  and  $G_{RH}$  are the received power at the host radar and its gain toward the interfering radar,  $P_{II}$  and  $G_{II}$  are the transmit power of the interfering radar and its gain toward the host radar,  $\lambda_I$  is the signal wavelength,  $R$  is the distance between the radars, and  $L_H$  is the propagation loss between the radars. Notice that, in (9), the interference source experiences one-way propagation loss and thus increases the detection threshold of the host radar, which results in significant detection performance degradation.

State-of-the-art automotive radars rely on frequency, spatial, and directional diversity and thus assume a low probability of interference. However, in the near future, this assumption will not hold, and, therefore, new interference mitigation methods are needed. Interference can be direct or indirect and can be categorized according to the modulation scheme. There are three approaches for interference mitigation:

- 1) resource allocation, e.g., via spectrum allocation, which results in degraded system performance when no interference is present
- 2) synchronization, which requires online coordination between adjacent radars via an additional communication channel
- 3) waveform parameters randomization.

The first approach is the most attractive and easiest to implement (and is currently adopted in the automotive industry), but it might fail as the probability of interference increases. Moreover, fully autonomous vehicles will demand extremely high reliability for the automotive radars, which could be compromised by interference in heavy-traffic scenarios where multiple radars operate closely adjacent. Therefore, implementation of additional interference mitigation approaches will be required.

Synchronization of multiple-platform radars is another approach that is expected to be adopted in the future to address the mutual interference problem in automotive radars. Synchronization and interference mitigation approaches that are widely used in cellular networks, such as orthogonal frequency-division multiplexing (OFDM), which divides the time–frequency resources [41], are expected to be adopted in the dynamic network of vehicular radars. However, these additional countermeasures seem to be insufficient, and additional CDMA-like approaches to achieve higher interference suppression will be needed. Thus, different code families could be used at different time–frequency slots of the OFDM. Communication-based CDMA methods cannot be directly used in automotive radars where higher orthogonality and interference suppression are required for operation in practical roadway scenarios characterized by multipath, delay-Doppler spread, high DR, and range–Doppler–DOA ambiguity. Thus, development of interference-resistant codes and radar network management via ad hoc base stations will be needed. Finally, extensive regulations for vehicular radar operation and resource management will be required.

### Multiple target tracking

Trackers play a significant role in radar signal processing. They improve localization estimation, reduce false alarms, deduce absolute velocity and trajectory, and generate a perception of the host vehicle's surroundings. A typical tracker comprises three main blocks: prediction, association, and update. Since conventional trackers have been developed for sparse, nonmaneuverable aerial and naval environments, they cannot be directly used in highly dynamic and dense urban environments with multiple, closely located, and rapidly maneuvering targets, such as vehicles, motorbikes, bicycles, and pedestrians. Moreover, detection-to-track association methods developed for the military sparse environment, such as nearest neighbors, fail in dense urban scenes. For example, Figure 9 shows one

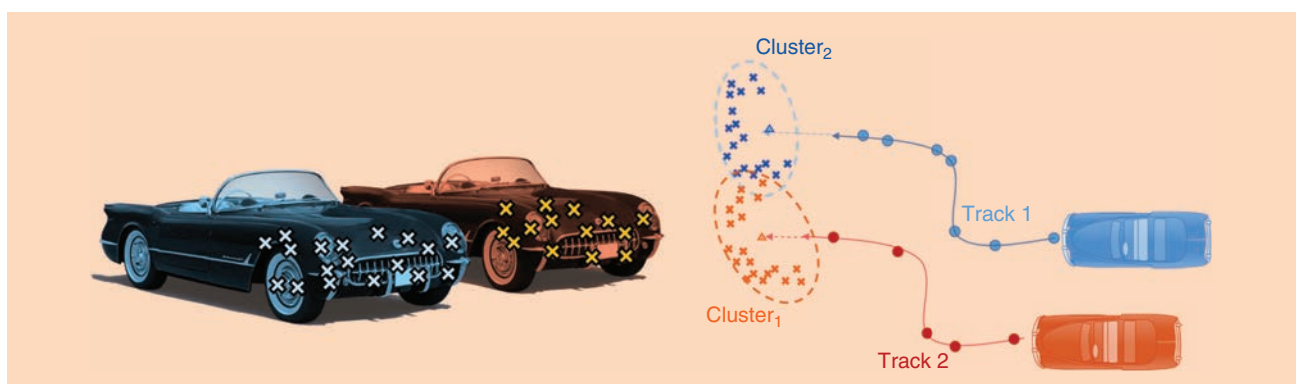


**FIGURE 9.** An interchanging vehicles association challenge.

of the typical traffic scenarios that challenge the conventional detection-to-track association techniques.

Therefore, the application of conventional tracking procedures for automotive radars requires multiple adaptations. Thus, alternative association criteria [42] need to be developed where multiple radars are used in a joint association fashion [43]. In addition, the multihypothesis tracking approach can be more efficient in vehicular radars compared with conventional Kalman tracking [44]. Association can also be improved by expanding the target's feature space. State-of-the-art automotive radars use target position and velocity for detection-to-track association. Features such as class, micro-Doppler signature, and size can be used to improve the solution to the detection-to-track association problem.

### *Classification via micro-Doppler*

Autonomous driving requires reliable knowledge of the vehicle's surroundings. Therefore, scene perception is an important component of vehicle sensing. In particular, classification of the detected targets is needed for threat assessment, sensing resource allocation, and automated control. Currently, target classification is performed mainly using computer vision methods applied to camera images. Typical automotive radar targets, such as pedestrians, cyclists, and vehicles, consist of multiple moving and rotating parts inducing micro-Doppler modulation to the radar echoes [45]. Micro-Doppler was extensively studied in military radar target classification and was suggested for automotive applications [46], [47].

Trends to increase the angular and Doppler resolution of automotive radars motivated recent attempts to use micro-Doppler features for vehicular radar target classification [24], [48]. High angularity and range resolution allows the receipt of the micro-Doppler of multiple moving targets' parts individually and thus the construction of distinctive spatiotemporal signatures of the moving targets, enabling high-fidelity radar-based target classification. Advances in deep-learning methods further enhance the significance of micro-Doppler features for radar target classification [49].

### *Deep learning*

Deep learning is a revolutionary data-driven processing approach first introduced for image processing and lately adopted in other disciplines, such as speech and language recognition [50]. Recently, deep learning was used for radar signal processing, mainly for target classification [51]. Deep learning has a potential for automotive radar processing tasks beyond target classification, such as interference mitigation, extended target detection and localization, design (waveform and antenna), and more specific tasks, such as road estimation [52].

### **Conclusions**

This work reviewed state-of-the-art conventional automotive radar processing and discussed its limitations when used in practical, highly complex automotive scenarios. Requirements for future vehicular radars as a main enabler of autonomous driving were discussed. This overview proposed directions to improve automotive radar performance by the development of alternative processing approaches that are currently missing or being implemented

in conventional military radars and cannot be directly applied to automotive radar without significant adaptations. SAR, micro-Doppler-based classification, extended target detection, super-resolution beamforming, adaptive waveforms, CDMA, and other discussed methods were successfully developed for other applications and thus have the potential to significantly improve the performance of vehicular radars. Novel interference and multipath mitigation methods, Doppler ambiguity elimination, multitarget tracking, cognitive processing, and clustering methods need to be further developed for the unique automotive applications.

### **Authors**

**Igal Bilik** (igal.bilik@gm.com) received his B.Sc., M.Sc., and Ph.D. degrees in electrical and computer engineering from Ben-Gurion University of the Negev, Beer-Sheva, Israel, in 1997, 2003, and 2006, respectively. From 2006 to 2008, he was a postdoctoral research associate in the Department of Electrical and Computer Engineering, Duke University, Durham, North Carolina. From 2008 to 2012, he was an assistant professor in the Department of Electrical and Computer Engineering, University of Massachusetts, Dartmouth. From 2011 to 2018, he was a staff researcher at the General Motors (GM) Advanced Technical Center, Herzliya, Israel. Starting in 2019, he has been leading the Smart Sensing and Vision Group at the GM Advanced Technical Center, conducting research on sensor technology for autonomous driving. He is a Senior Member of the IEEE.

**Oren Longman** (oren.longman@gm.com) received his B.Sc. degree in applied mathematics from the University of Bar Ilan, Ramat Gan, Israel, in 2008. In 2008, he entered the Israeli Navy as an algorithm engineer for phased-array radars. In 2014, he was employed by Elbit Systems as a researcher in the R&D department for radar and electronic intelligence systems. In 2016, he joined the General Motors Advanced Technical Center in Herzliya, Israel as a senior researcher in the R&D radar group. His current research interests include temporal fast linear frequency modulation processing; multiple-input, multiple-output radar signal processing; interference mitigation and management; localization; and estimation theory.

**Shahar Villeval** (shahar.villeval@gm.com) received his B.Sc. and M.Sc. degrees in electrical and computer engineering from Ben-Gurion University of the Negev, Beer-Sheva, Israel, in 2011 and 2012, respectively. Since 2013, he has been working at the General Motors Advanced Technical Center, Herzliya, Israel, currently as a senior researcher. His research interests are cognitive radars, automotive radar signal processing and system design, and array processing.

**Joseph Tabrikian** (joseph@bgu.ac.il) received his B.Sc., M.Sc., and Ph.D. degrees in electrical engineering from Tel-Aviv University, Israel, in 1986, 1992, and 1997, respectively. After a two-year postdoctoral period at Duke University, Durham, North Carolina, he joined the Department of Electrical and Computer Engineering, Ben-Gurion University of the Negev, Beer-Sheva, Israel. He is the founder of the School of Electrical and Computer Engineering, where he has been the department head since 2017. He has served on the editorial boards of *IEEE Transactions on Signal Processing* and *IEEE Signal Processing Letters* in several

positions in addition to being a member of several technical committees: IEEE Sensor Array and Multichannel Technical Committee, IEEE Signal Processing Theory and Methods Technical Committee, and Signal Processing and Multisensor Systems—Special Area Team of the European Association for Signal Processing. He is a coauthor of seven award-winning papers at IEEE conferences and workshops and is a Fellow of the IEEE.

## References

- [1] D. M. Grimes and T. O. Jones, "Automotive radar: A brief review," *Proc. IEEE*, vol. 62, no. 6, pp. 804–822, 1974.
- [2] E. F. Belohoubek, "Radar control for automotive collision mitigation and headway spacing," *IEEE Trans. Veh. Technol.*, vol. 31, no. 2, pp. 89–99, 1982.
- [3] S. M. Patole, M. Torlak, D. Wang, and M. Ali, "Automotive radars: A review of signal processing techniques," *IEEE Signal Process. Mag.*, vol. 34, no. 2, pp. 22–35, 2017.
- [4] J. Wenger, "Automotive radar-status and perspectives," in *Proc. IEEE Compound Semiconductor Integrated Circuit Symp.*, 2005, pp. 21–25.
- [5] M. Murad, I. Bilik, M. Friesen, J. Nickolaou, J. Salinger, K. Geary, and J. Colburn, "Requirements for next generation automotive radars," in *Proc. IEEE Radar Conf.*, 2013, pp. 1–6. doi: 10.1109/RADAR.2013.6586127.
- [6] F. G. Jansen, "Automotive radar sensor for ultra short range applications," in *Proc. 18th Int. Radar Symp.*, 2017, pp. 1–6. doi: 10.23919/IRS.2017.8008134.
- [7] I. Bilik et al., "Automotive multi-mode cascaded radar data processing embedded system," in *Proc. IEEE Radar Conf.*, 2018, pp. 372–376.
- [8] M. I. Skolnik, *Radar Handbook*. New York: McGraw-Hill, 1970.
- [9] A. Bourdoux, U. Ahmad, D. Guermandi, S. Brebels, A. Dewilde, and W. Van Thillo, "PMCW waveform and MIMO technique for a 79 GHz CMOS automotive radar," in *Proc. IEEE Radar Conf.*, 2016, pp. 1–5. doi: 10.1109/RADAR.2016.7485114.
- [10] H. Rohling, F. Fölster, M.-M. Meinecke, and R. Mende, "A new generation of automotive radar waveform design techniques," in *Proc. IEEE Int. Conf. Waveform Diversity and Design*, 2004, pp. 1–5. doi: 10.1109/IWDDC.2004.8317521.
- [11] I. Bilik et al., "Automotive MIMO radar for urban environments," in *Proc. IEEE Radar Conf.*, 2016, pp. 1–6. doi: 10.1109/RADAR.2016.7485215.
- [12] H. Krim and M. Viberg, "Two decades of array signal processing research: The parametric approach," *IEEE Signal Process. Mag.*, vol. 13, no. 4, pp. 67–94, 1996.
- [13] I. Bekerman and J. Tabrikian, "Target detection and localization using MIMO radars and sonars," *IEEE Trans. Signal Process.*, vol. 54, no. 10, pp. 3873–3883, 2006.
- [14] E. B. James, D. Taylor, and A. Borysenko, "Signals, targets, and advanced ultrawideband radar systems," in *Advanced Ultrawideband Radar*. Boca Raton, FL: CRC, 2016, pp. 83–122.
- [15] J. Yu and J. Krolík, "MIMO multipath clutter mitigation for GMTI automotive radar in urban environments," in *Proc. IET Int. Conf. Radar Systems (Radar 2012)*, Oct. 22–25, 2012. doi: 10.1049/cp.2012.1565.
- [16] G. M. Brooker, "Mutual interference of millimeter-wave radar systems," *IEEE Trans. Electromagn. Compat.*, vol. 49, no. 1, pp. 170–181, 2007.
- [17] M. Goppelt, H.-L. Blöcher, and W. Menzel, "Automotive radar—investigation of mutual interference mechanisms," *Adv. Radio Sci.*, vol. 8, no. B3, pp. 55–60, 2010.
- [18] H. Steyskal, "Digital beamforming antennas," *Microw. J.*, vol. 30, no. 1, pp. 107–124, 1987.
- [19] N. Fourikis, *Advanced Array Systems, Applications and RF Technologies*. Amsterdam, The Netherlands: Elsevier, 2000.
- [20] X. Song, S. Zhou, and P. Willett, "Reducing the waveform cross correlation of MIMO Radar with space-time coding," *IEEE Trans. Signal Process.*, vol. 58, no. 8, pp. 4213–4224, 2010.
- [21] M. Ester, H.-P. Kriegel, J. Sander, and X. Xu, "A density-based algorithm for discovering clusters in large spatial databases with noise," in *Proc. 2nd Int. Conf. Knowledge Discovery and Data Mining*, August 2–4, 1996, pp. 226–231.
- [22] V. S. Ware and H. Bharathi, "Study of density based algorithms," *Int. J. Comput. Applicat.*, vol. 69, no. 26, pp. 1–4, 2013. doi: 10.5120/12132-8235.
- [23] Y. Bar-Shalom, X. R. Li, and T. Kirubarajan, *Estimation With Applications to Tracking and Navigation: Theory Algorithms and Software*. Hoboken, NJ: Wiley, 2004.
- [24] D. Belgiovane and C. Chen, "Micro-Doppler characteristics of pedestrians and bicycles for automotive radar sensors at 77 GHz," in *Proc. 11th European Conf. Antennas and Propagation*, 2017, pp. 2912–2916.
- [25] S. Haykin, "Cognitive radar: A way of the future," *IEEE Signal Process. Mag.*, vol. 23, no. 1, pp. 30–40, 2006.
- [26] W. Huleihel, J. Tabrikian, and R. Shavit, "Optimal adaptive waveform design for cognitive MIMO radar," *IEEE Trans. Signal Process.*, vol. 61, no. 20, pp. 5075–5089, 2013.
- [27] P. Hughes, "A high-resolution radar detection strategy," *IEEE Trans. Aerosp. Electron. Syst.*, vol. AES-19, no. 5, pp. 663–667, 1983.
- [28] C.-Y. Chen and P. Vaidyanathan, "MIMO radar waveform optimization with prior information of the extended target and clutter," *IEEE Trans. Signal Process.*, vol. 57, no. 9, pp. 3533–3544, 2009. doi: 10.1109/TSP.2009.2021632.
- [29] S. Villeval, J. Tabrikian, and I. Bilik, "Ambiguity function for sequential antenna selection," in *Proc. IEEE Sensor Array and Multichannel Signal Processing Workshop*, 2016, pp. 1–4. doi: 10.1109/SAM.2016.7569753.
- [30] M. Kronauge and H. Rohling, "New chirp sequence radar waveform," *IEEE Trans. Aerosp. Electron. Syst.*, vol. 50, no. 4, pp. 2870–2877, 2014.
- [31] I.-Y. Son, T. Varslot, C. E. Yarman, A. Pezeshki, B. Yazici, and M. Cheney, "Radar detection using sparsely distributed apertures in urban environment," in *Proc. Signal Processing, Sensor Fusion, and Target Recognition XVI*, vol. 6567, International Society for Optics and Photonics, 2007, p. 65671Q. doi: 10.1117/12.720069.
- [32] L. Li and J. L. Krolík, "Simultaneous target and multipath positioning via multi-hypothesis single-cluster FPD filtering," in *Proc. IEEE Asilomar Conf. Signals, Systems and Computers*, 2013, pp. 461–465.
- [33] S. Roehr, P. Gulden, and M. Vossiek, "Precise distance and velocity measurement for real time locating in multipath environments using a frequency-modulated continuous-wave secondary radar approach," *IEEE Trans. Microw. Theory Techn.*, vol. 56, no. 10, pp. 2329–2339, 2008.
- [34] R. Gold, "Optimal binary sequences for spread spectrum multiplexing [Corresp.]," *IEEE Trans. Inf. Theory*, vol. 13, no. 4, pp. 619–621, 1967.
- [35] S. Tahc�푸ulloh and G. Hendrantoro, "Phased-MIMO radar using Hadamard coded signal," in *Proc. Int. Conf. Radar, Antenna, Microwave, Electronics, and Telecommunications*, 2016, pp. 13–16.
- [36] H. Iqbal, M. B. Sajjad, M. Mueller, and C. Waldschmidt, "SAR imaging in an automotive scenario," in *Proc. IEEE 15th Mediterranean Microwave Symp.*, 2015, pp. 1–4. doi: 10.1109/MMS.2015.7375430.
- [37] T. Zhang and X.-G. Xia, "OFDM synthetic aperture radar imaging with sufficient cyclic prefix," *IEEE Trans. Geosci. Remote Sens.*, vol. 53, no. 1, pp. 394–404, 2015.
- [38] H. Wu and T. Zwick, "Automotive SAR for parking lot detection," in *Proc. German Microwave Conf.*, 2009, pp. 1–8. doi: 10.1109/GEMIC.2009.4815910.
- [39] D. Clarke, D. Andre, and F. Zhang, "Synthetic aperture radar for lane boundary detection in driver assistance systems," in *Proc. IEEE Int. Conf. Multisensor Fusion and Integration Intelligent Systems*, 2016, pp. 238–243.
- [40] S. Gishkori, L. Daniel, M. Gashinova, and B. Mulgrew, "Imaging for a forward scanning automotive synthetic aperture radar," *IEEE Trans. Aerosp. Electron. Syst.*, vol. 55, no. 3, pp. 1420–1434, 2018.
- [41] X.-G. Xia, T. Zhang, and L. Kong, "MIMO OFDM radar IRCI free range reconstruction with sufficient cyclic prefix," *IEEE Trans. Aerosp. Electron. Syst.*, vol. 51, no. 3, pp. 2276–2293, 2015.
- [42] M.-S. Lee and Y.-H. Kim, "New data association method for automotive radar tracking," *IEE Proc.: Radar, Sonar Navigation*, vol. 148, no. 5, 2001, pp. 297–301.
- [43] F. Folster and H. Rohling, "Data association and tracking for automotive radar networks," *IEEE Trans. Intell. Transp. Syst.*, vol. 6, no. 4, pp. 370–377, 2005.
- [44] N. A. Tsokas and K. J. Kyriakopoulos, "Multi-robot multiple hypothesis tracking for pedestrian tracking with detection uncertainty," in *Proc. 19th Mediterranean Conf. Control Automation*, 2011, pp. 315–320.
- [45] V. C. Chen, F. Li, S.-S. Ho, and H. Wechsler, "Micro-Doppler effect in radar: Phenomenon, model, and simulation study," *IEEE Trans. Aerosp. Electron. Syst.*, vol. 42, no. 1, pp. 2–21, 2006.
- [46] S. Villeval, I. Bilik, and S. Z. Gürbüz, "Application of a 24 GHz FMCW automotive radar for urban target classification," in *Proc. IEEE Radar Conf.*, 2014, pp. 1237–1240.
- [47] I. Bilik and P. Khomchuk, "Minimum divergence approaches for robust classification of ground moving targets," *IEEE Trans. Aerosp. Electron. Syst.*, vol. 48, no. 1, pp. 581–603, 2012.
- [48] D. Kellner, M. Barjenbruch, J. Klappstein, J. Dickmann, and K. Dietmayer, "Wheel extraction based on micro doppler distribution using high-resolution radar," in *Proc. IEEE MTT-S Int. Conf. Microwaves Intelligent Mobility*, 2015, pp. 1–4. doi: 10.1109/ICMIM.2015.7117951.
- [49] M. S. Seyfioğlu and S. Z. Gürbüz, "Deep neural network initialization methods for micro-doppler classification with low training sample support," *IEEE Geosci. Remote Sens. Lett.*, vol. 14, no. 12, pp. 2462–2466, 2017.
- [50] A. Krizhevsky, I. Sutskever, and G. E. Hinton, "Imagenet classification with deep convolutional neural networks," in *Advances in Neural Information Processing Systems 25*, F. Pereira, C. J. C. Burges, L. Bottou, and K. Q. Weinberger, Eds. Red Hook, NY: Curran Associates, Inc., 2012, pp. 1097–1105.
- [51] E. Mason, B. Yonet, and B. Yazici, "Deep learning for radar," in *Proc. IEEE Radar Conf.*, 2017, pp. 1703–1708.
- [52] T. Giese, J. Klappstein, J. Dickmann, and C. Wöhler, "Road course estimation using deep learning on radar data," in *Proc. IEEE 18th Int. Radar Symp.*, 2017, pp. 1–7. doi: 10.23919/IRS.2017.8008125.

# High-Performance Automotive Radar

A review of signal processing algorithms and modulation schemes



©ISTOCKPHOTO.COM/TALAJ

The ongoing automation of driving functions in cars results in the evolution of advanced driver assistance systems (ADAS) into ones capable of highly automated driving, which will in turn progress into fully autonomous, self-driving cars. To work properly, these functions first must be able to perceive the car's surroundings by such means as radar, lidar, camera, and ultrasound sensors. As the complexity of such systems increases along with the level of automation, the demands on environment sensors, including radar, grow as well. For radar performance to meet the requirements of self-driving cars, straightforward scaling of the radar parameters is not sufficient. To refine radar capabilities to meet more stringent requirements, fundamentally different approaches may be required, including the use of more sophisticated signal processing algorithms as well as alternative radar waveforms and modulation schemes. In addition, since radar is an active sensor (i.e., it operates by transmitting signals and evaluating their reflections) interference becomes a crucial issue as the number of automotive radar sensors increases. This article gives an overview of the challenges that arise for automotive radar from its development as a sensor for ADAS to a core component of self-driving cars. It summarizes the relevant research and discusses the following topics related to high-performance automotive radar systems: 1) shortcomings of the classical signal processing algorithms due to underlying fundamental assumptions and a signal processing framework that overcomes these limitations, 2) use of digital modulations for automotive radar, and 3) interference-mitigation methods that enable multiple radar sensors to coexist in conditions of increasing market penetration. The overview presented in this article shows that new paradigms arise as automotive radar transitions into a more powerful vehicular sensor, which provides a fertile research ground for further investigation.

## Introduction

When the idea of radar was first explored back in the late-19th and early-20th centuries, it was primarily seen as a technology for military applications. Other applications gradually emerged, however, and in the last four decades, radar has been studied for

use in the automotive sector for such applications as predictive crash sensing, obstacle detection, and braking [1]. The term *radar* is short for *radio detection and ranging*, an indication that radar is used to detect objects (obstacles and other road users) near the vehicle and to estimate their range as well as velocity and angle relative to the radar. For many years, production cars have made use of these capabilities to facilitate various driver-assistance functions, such as emergency brake assist and adaptive cruise control. More complex functions, such as fully autonomous driving, also rely heavily on radar as an environmental sensor [2], as it is capable of direct range and velocity measurements, can sense long distances ahead, is robust to bad weather and poor light conditions, and can be hidden behind a bumper.

A detailed overview of the status of automotive radar during its first several years is presented in [1]. The evolution of automotive radar is discussed in [3]. Other review articles provide overviews of the signal processing architecture and of the millimeter-wave technology for automotive radar [4], [5]. A more recent review article discusses the state-of-the-art signal processing algorithms for automotive radar and gives a bird's-eye view of estimation techniques, radar waveforms, and higher-level processing steps, such as tracking and classification [6].

This article gives an overview of the signal processing and modulation aspects of high-end automotive radar systems and discusses recent advances in these fields. We address the use of digital modulations, such as orthogonal frequency-division multiplexing (OFDM) and phase modulated continuous wave (PMCW) waveforms, for automotive radar and multiple-input, multiple-output (MIMO) radar in particular; discuss their potential benefits and challenges due to increased complexity; and survey recent research in this area. We also point out that classical automotive radar signal processing does not fully accommodate performance improvement through simple upscaling of the radar parameters (e.g., bandwidth, measurement time, antenna aperture) due to underlying fundamental assumptions. We provide a signal processing framework based on a more advanced signal model that surpasses these limits at a feasible computational cost. Next we explore the reliable operation of future automotive radar systems for which interference mitigation is vital and complete the discussion with a survey of interference-mitigation methods. These include some promising paradigms, such as interference-aware cognitive radar [7] and centralized coordination for interference avoidance [8].

## Conventional automotive radar

Today, conventional automotive radar operates with a sequence of frequency-modulated continuous wave (FMCW) signals and is a well-studied research field [6], [9]. These systems transmit a series of analog-generated chirps, which are reflected and then mixed with the transmit (Tx) chirp at the receiver, resulting in a frequency proportional to the target distance and called *beat frequency*. The range processing is based on Fourier transform of the beat frequencies, and the Doppler-induced phase progression over the consecutive chirps is used for velocity estimation. Chirps are commonly designed to be short enough so that the distance-induced component of the

beat frequency predominates, and their Doppler shift, i.e., the velocity component, is negligible (hence the name *fast chirp*). Figure 1(a) illustrates a sequence of identical FMCW chirps, the delayed and Doppler-shifted reflections of which after mixing with the Tx signal result in 2D complex exponentials in the baseband. A subsequent 2D Fourier transform yields the distance–velocity radar image. To localize targets in space, target angles are measured based on direction of arrival (DOA) of reflected signals with array processing techniques, most commonly via digital beamforming. Figure 1(b) shows the DOA-induced phase differences at receive (Rx) channels and the principle of digital beamforming that combines Rx signals with phases that digitally direct the beam to a certain DOA. In the simplest case, all three frequency-estimation tasks are solved jointly by a 3D Fourier transform, followed by power detection [10], parameter estimation, clustering and association of reflexes [11], object classification and tracking [12], data fusion [13], and other calculations.

Typical frequency bands for automotive radar are 24 and 77 GHz, with most of the manufacturers shifting toward 77 GHz for newer radar generations. This is due to larger available bandwidth (76–77 GHz for long-range and 77–81 GHz for short-range applications), higher Doppler sensitivity (and thus higher velocity resolution), and smaller antennas.

Automotive radar performance is measured according to the following main parameters: 1) resolution (ability to separate two closely spaced targets), 2) unambiguously measurable range (the range of parameter values that are unambiguously distinguishable), and 3) dynamic range (power ratio between the strongest and the weakest of detectable targets) in its measurement dimensions, i.e., distance, velocity, azimuth, and elevation angle.

For conventional Fourier-based signal processing, the radar resolution and unambiguous range for all of the aforementioned measurement parameters are directly determined by the sampling frequency and observation length in the corresponding dimension. For distance, the observation length is given by the bandwidth  $B$ , and its inverse determines the resolution with which the round-trip delays  $\tau = 2d/c_0$  are measured, with  $d$  being the target distance and  $c_0$  being the speed of light. Thus, the distance resolution is given by the following bandwidth:  $\Delta d = c_0/(2B)$ . Analogously, in the velocity dimension the Doppler resolution  $\Delta f_D$  is determined by the inverse of the measurement cycle duration  $T_{\text{cycle}}$ , i.e.,  $\Delta f_D = 1/T_{\text{cycle}}$ . With  $\Delta f_D = 2\Delta v f_c/c_0$ , the velocity resolution is  $\Delta v = c_0/(2f_c T_{\text{cycle}})$ . For DOA-induced spatial frequencies, the resolution can be derived analogously from the dimensions of the antenna array [14]. The previous discussion makes apparent that regardless of the radar waveform, a large bandwidth and a long measurement time are required for a high distance and velocity resolution.

To obtain a resolution higher than that of the conventional Fourier processing, superresolution frequency estimation methods can be applied in different radar measurement dimensions. Such methods can be coarsely classified into subspace-based, maximum-likelihood, or compressed-sensing methods. A review of high-resolution methods for array processing and

for multidimensional automotive radar processing can be found in [14] and [15], respectively. An overview of compressed-sensing applications for radar is given in [16].

## Digital radar

In parallel to the described fast-chirp radar, alternative automotive radar concepts based on digital modulations, such as OFDM [17] and PMCW [18], have been studied over the past few years. These concepts differ from FMCW radar in terms of generating waveforms digitally and performing demodulation in the digital domain. Broadly speaking, this is equivalent to operating with arbitrary digitally generated waveforms and matched filter-based processing at the receiver. For OFDM radar, this large degree of flexibility in the waveform choice enables communication and radar capabilities to be combined by embedding communication information into the radar waveform [17]. It further enables fully adaptive, software-defined behavior based on digitally generated waveforms. While more challenging in terms of practical realization—mainly

due to analog-to-digital converters (ADCs) and significantly larger data loads—this opens up new dimensions for radar development and enables advanced radar concepts.

## OFDM radar

The OFDM waveform is composed of a set of orthogonal complex exponentials [subcarriers; see the left-hand side of Figure 2(a)], the complex amplitudes of which are modulated with communication data or radar modulation symbols. The orthogonality of subcarriers results from the constraint of all subcarriers having a whole number of periods during one evaluation interval, called an *OFDM symbol* [see the right-hand side of Figure 2(a)]. As the discrete Fourier transform (DFT) exhibits the same characteristics, OFDM waveforms can be efficiently generated via inverse fast Fourier transform (IFFT) of the modulation symbols, i.e., complex amplitudes of OFDM subcarriers. Conversely, the communication data or radar modulation symbols can be efficiently extracted (demodulated) at the receiver based on FFT. From the communication standpoint,

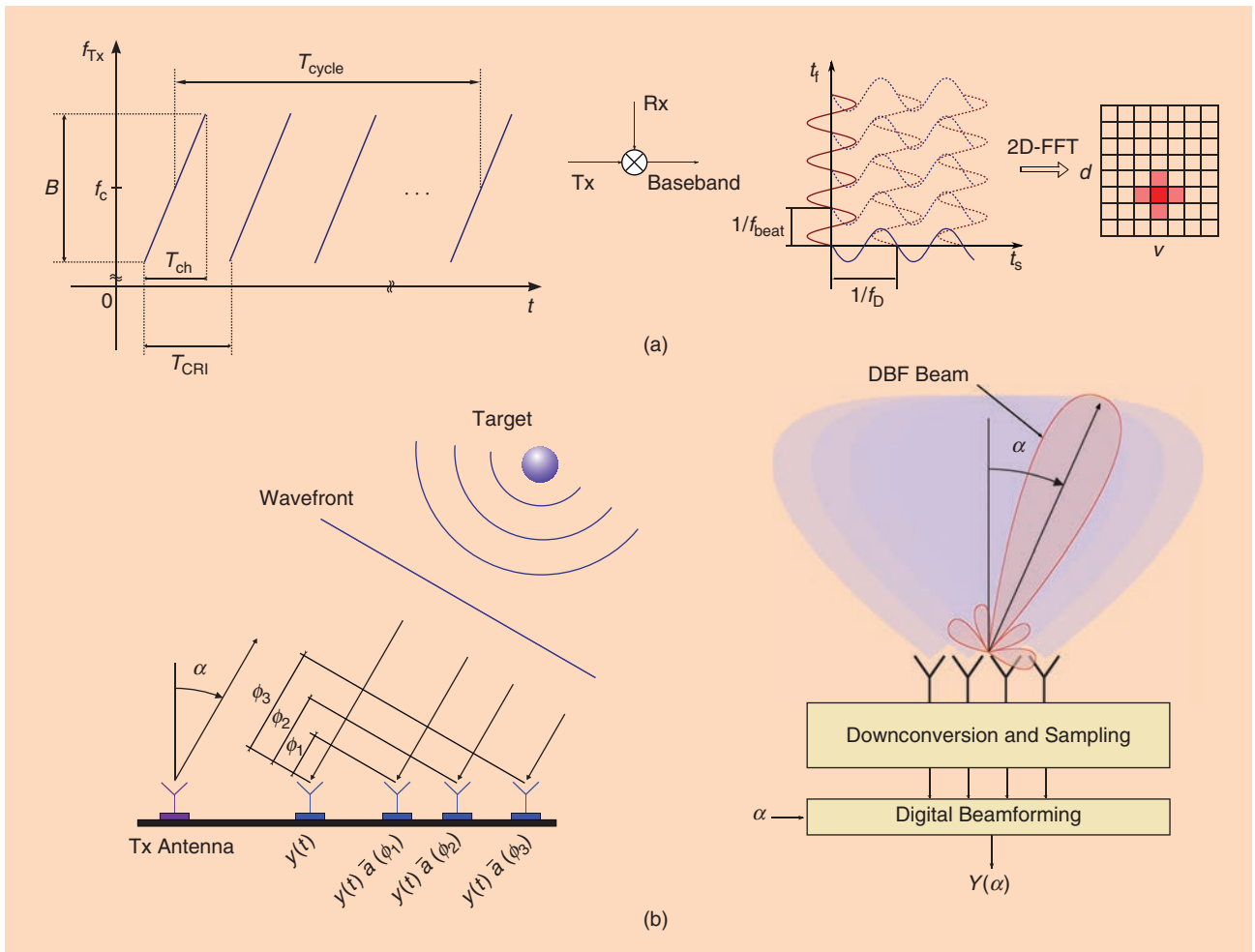


**FIGURE 1.** Graphs and illustrations showing the principle of distance, velocity, and DOA estimation for conventional fast-chirp automotive radar. (a) A sequence of identical FMCW chirps. The delayed and Doppler-shifted reflections of such chirps, after mixing with the Tx signal, result in 2D complex exponentials in the baseband. (b) The DOA-induced phase differences at Rx channels and the principle of digital beamforming that combines Rx signals with phases that digitally direct the beam to a certain DOA.  $B$ : bandwidth;  $f_c$ : carrier frequency;  $T_{CRI}$ : chirp repetition interval;  $T_{ch}$ : chirp duration;  $f_{beat}$ : beat frequency;  $f_D$ : Doppler shift;  $t_s$ : slow-time;  $d$ : distance;  $v$ : velocity;  $\alpha$ : target angle;  $y(\phi_n)$  received signal with a phase shift  $\phi_n$  at the  $n$ th Rx antenna.

this achieves high spectral efficiency as well as simple extraction of communication data. Meanwhile, from the radar standpoint, it enables efficient digital demodulation of the radar waveform. OFDM not only enables favorable modulation for both applications, but it also combines both functionalities via a single waveform. This initially motivated research on OFDM radar. Currently, OFDM is often studied as a means for efficient implementation of digital, software-defined radar—*independent* of the communication aspect.

To prevent interference between consecutive OFDM symbols in a multipath channel, a cyclic prefix (CP) that contains repetition of the end portion of OFDM symbol is transmitted before the symbol [see the right-hand side of Figure 2(a)]. This converts the linear convolutive channel into a cyclic one, and

thus time-of-flight delays result in cyclic shifts of OFDM symbols at the receiver. The block diagram in Figure 2(b) depicts the structure of the OFDM system. The OFDM symbols generated via IFFT are shifted into the radio-frequency (RF) band via a quadrature modulation and transmitted over the channel. From the perspective of radar, the channel represents objects in the vehicle's surroundings, i.e., the driving environment. At the receiver, the CP is removed from the quadrature demodulated signal, and the complex modulation symbols are obtained via an FFT. For OFDM radar signal processing illustrated in Figure 2(c), the subcarrier values of consecutive OFDM symbols are placed into a 2D measurement matrix. The radar waveform is demodulated based on spectral division, which cancels out the transmitted complex modulation symbols by elementwise

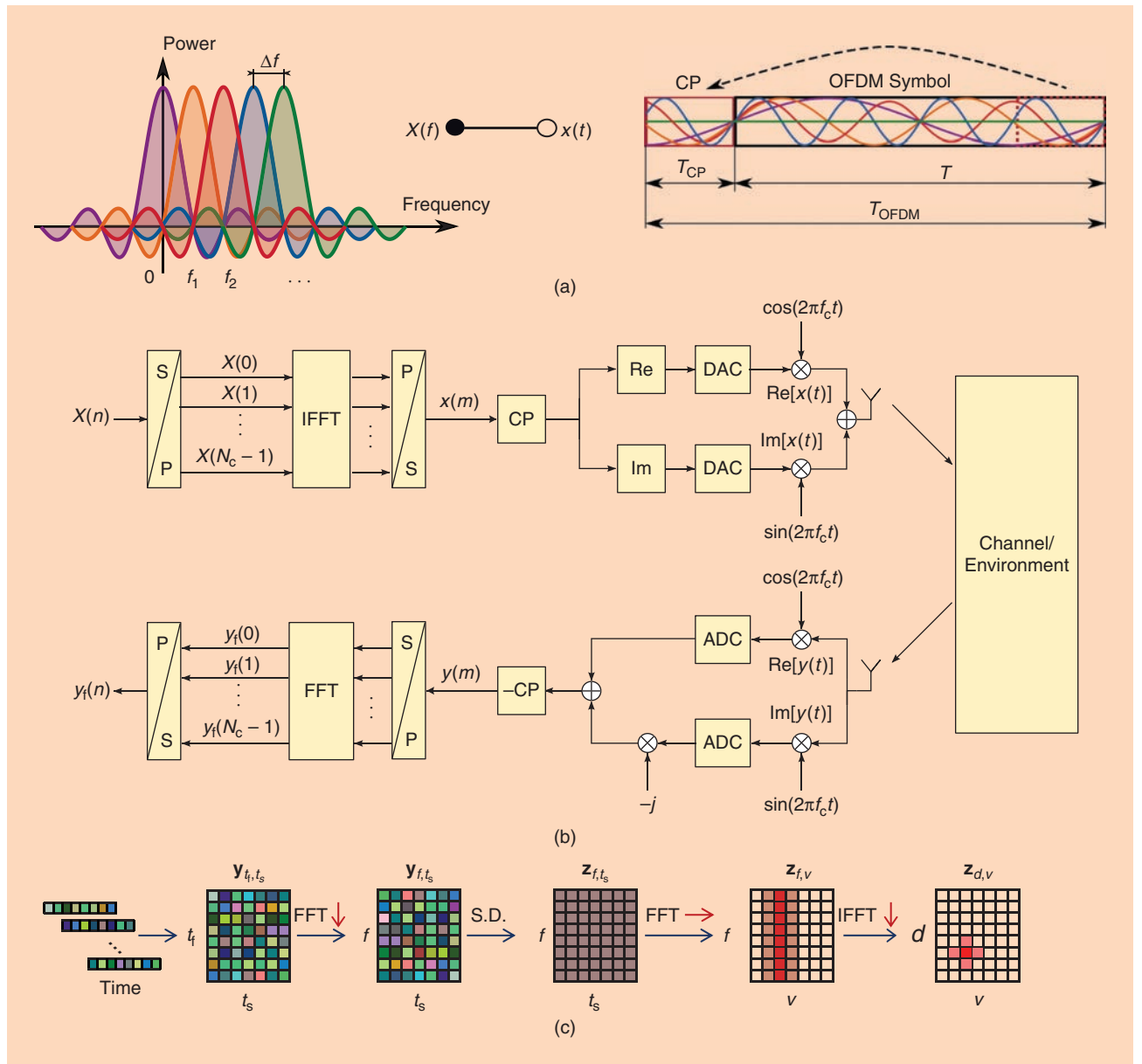


**FIGURE 2.** Illustrations showing the OFDM radar principle. (a) On the left, the OFDM spectrum and its inverse Fourier transform resulting in a time-domain OFDM symbol on the right. (b) The block diagram of the OFDM system. (c) The signal processing steps of OFDM radar. S.D.: spectral division; Re, real, Im, imaginary; P/S, the parallel-to-serial blocks; S/P, the serial-to-parallel blocks.

multiplication with their inverse values (conjugate in case of unitary subcarrier amplitudes). This operation reduces the measurement matrix to a sum of 2D complex exponentials, the frequencies of which over the OFDM subcarriers and symbols correspond to the distances and velocities of the radar targets. Similar to fast-chirp radar, a 2D-FFT processing (IFFT over subcarriers, FFT over symbols) leads to the distance–velocity radar image.

We make the following observations regarding the OFDM radar signal processing.

- For unitary subcarrier amplitudes, the distance processing is equivalent to matched filtering implemented efficiently in the frequency domain.
- The described signal processing neglects the Doppler shift of OFDM subcarriers, which might lead to intercarrier interference (ICI). To limit ICI to a negligible level, the subcarrier spacing  $\Delta f$  must be much larger than the maximum possible Doppler shift  $f_{D,\max}$ , e.g.,  $\Delta f = 10f_{D,\max}$  [17]. This limits, however, the parametrization freedom, especially for long-range and highly dynamic applications, such as front long-range automotive radar.
- Under conditions of unitary subcarrier amplitudes and negligible Doppler shift, the waveform has no influence on the signal processing performance. Thus, it can carry communication data or be optimized with respect to peak-to-average power ratio for radar (e.g., [19]).
- The distance and velocity processing is done in two independent dimensions and no coupling between them is considered. Since the target velocity in practice affects both measurement dimensions, this can be interpreted as simplification of the 2D matched filtering into two separate one-dimensional matched filters, one per each measurement dimension. Analogous to fast-chirp radar, this ignores the range change for moving targets, and thus assumes all OFDM symbols to have the same delay.

Since OFDM radar demodulates the radar waveform in the digital domain, the entire signal bandwidth needs to be sampled, contrary to fast-chirp radar that samples only the bandwidth of beat frequencies. This makes the practical realization of OFDM radar more challenging, imposing high demands on ADCs, memory, and digital signal processing. Some of the ongoing research in [7] and [20]–[22] focuses on methods for limit-

ing the instantaneous bandwidth, and thus the sampling rates. Whereas [20] covers a larger bandwidth by sweeping in multiple steps (called *stepped OFDM*), [7] and [21] combine OFDM waveform with a chirp to increase the effective bandwidth. By randomly occupying smaller portions of the full bandwidth at each time instance, [22] aims to reduce the sampling rates of OFDM radar with a compressed-sensing approach.

### PMCW radar

An alternative implementation of digital radar uses a sequence of waveforms generated by phase modulation of continuous waves [18]. The waveform generation via biphasic modulation of the RF-carrier signal with  $0^\circ$  and  $180^\circ$  phase shifts is particularly simple to implement in CMOS technology [18]. At the receiver, a bank of digitally implemented correlators is used for range processing. The Doppler processing is done via an FFT over a sequence of consecutive coded waveforms, analogous to fast-chirp or OFDM radars. The block diagram of a PMCW radar is shown in Figure 3. For favorable autocorrelation properties and thus high dynamic range in range estimation, the selection of a proper code sequence is essential. Using orthogonal codes, multiple Tx channels can operate simultaneously based on code-domain separation, allowing MIMO processing. Furthermore, a meaningful code selection can provide favorable properties in terms of robustness against interference. As for OFDM radar, Doppler shift has an adverse effect on PMCW waveforms in terms of auto- and cross-correlation properties, and needs to be accounted for by parametrization, code choice, or compensation in signal processing.

### Discussion of modulation schemes

Fast-chirp, OFDM, and PMCW radars share the same principle of distance–velocity measurement: time-of-flight-based coherent distance estimation via pulse compression (fast-time) and Doppler-based velocity estimation via FFT over a series of consecutive waveforms (slow-time). For all three systems, the resolution and unambiguous range depend solely on observation length (i.e., bandwidth in fast-time and measurement time in slow-time) and sampling rate (ADC rate in fast-time and waveform repetition rate in slow-time). In terms of hardware effort, fast-chirp radar has an advantage due to analog mixing, i.e.,

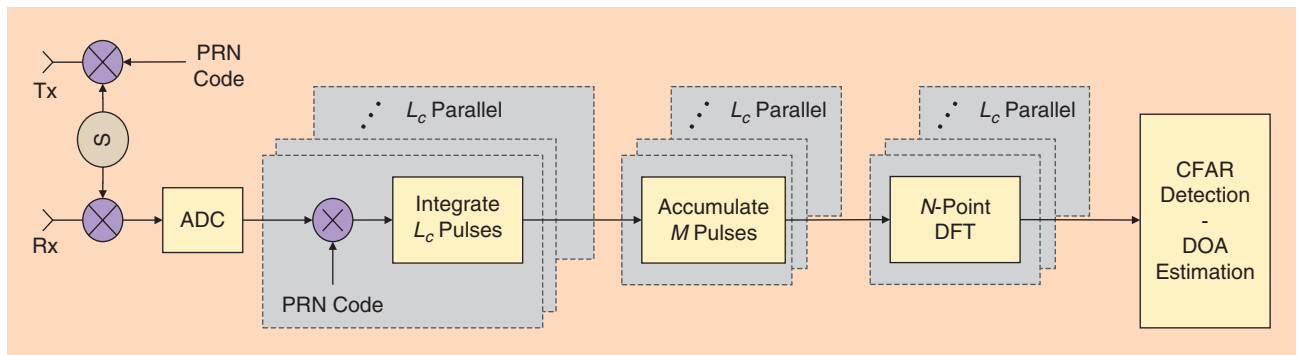


**FIGURE 3.** A schematic view of PMCW radar. The carrier signal is modulated with a pseudorandom noise (PRN) code. The distance processing is based on  $L_c$  digital correlators, followed by DFT-based Doppler processing [18]. CFAR: constant false alarm rate.

demodulation, resulting in significantly reduced sampling rates for beat frequencies. In contrast, digital radar requires sampling of the entire bandwidth, i.e., higher ADC rates, memory, and computational demands. The software-defined capabilities of such radar allow, however, a substantially larger flexibility in operation. As automotive radars become increasingly complex, digital radar with software-defined modulation allows more features with respect to adaptive and multifunction behavior, advantageous MIMO concepts, and robustness against interference based on large waveform diversity.

## MIMO radar

The use of MIMO radar techniques is a well-established approach for improved angle estimation with radar [23]. MIMO radar uses multiple channels at both the Tx and the Rx sides such that the number of paths between the radar and the target is efficiently increased. That is, with the number of paths being the product of the number of Tx and Rx channels, MIMO radar obtains more paths than the number of physical channels. These paths can be arranged into a larger virtual aperture with more elements, as depicted in Figure 4, and thus improve the angular resolution and estimation accuracy of the radar. The resulting virtual aperture can then be processed with conventional array processing techniques. The main challenge for MIMO radar is thus the choice of waveforms such that the signals from different Tx antennas can be clearly distinguished, i.e., the multiplexing of the Tx channels. For high-performance automotive radar, efficient multiplexing of a large Tx array is a key factor for achieving a high angular resolution in both azimuth and elevation. Conventionally, Tx antennas are multiplexed in time [24], frequency [25], or code [26].

Because of its simplicity, time-division multiplexing (TDM) with equidistantly interleaved chirps is the most common multiplexing technique for fast-chirp radar. However, this approach allows only one antenna to be active at a time, and thus limits considerably the number of Tx antennas that can be multiplexed. Some more advanced multiplexing methods for fast-chirp radar include the following [6]:

■ **Beat frequency multiplexing:** Chirps of multiple Tx channels run parallel with an offset in time and/or frequency, such that the beat frequencies of different Tx channels appear as frequency division multiplexed (FDM). Let us denote the base chirp  $x_0 = \exp(j\pi Kt^2)$  with  $K$  being the chirp slope. For chirps with frequency offset, the signal of the  $n$ th Tx channel is  $x_n = \exp(j\pi[Kt^2 + 2n\Delta f_{Tx}t])$ , the offset  $\Delta f_{Tx}$  being larger than the maximum beat frequency  $f_{beat,max}$ . Analogously, for chirps offset in time, the signal of the  $n$ th Tx channel is  $x_n = \exp(j2\pi K[t - n\Delta\tau_{Tx}]^2)$ , with  $\Delta\tau_{Tx}$  being larger than the maximum round-trip delay  $\tau_{max}$ . This allows tighter spacing of chirps than conven-

tional TDM or FDM, e.g., more efficient use of time–frequency resources.

■ **Slope diversity multiplexing:** Multiple Tx channels transmit chirps of the same bandwidth but different duration, i.e., slope. The signal of the  $n$ th Tx antenna is then  $x_n = \exp(j\pi[K + \Delta K_n]t^2)$ , with  $\Delta K_n$  being the slope difference to the base chirp slope  $K$ . At the receiver, the radar signal is demodulated with multiple slopes, each of the signals resulting in beat frequency for the corresponding Tx channel and chirp for other channels. The subsequent FFT processing focuses the signals with constant beat frequency and spreads the remaining chirp signals. This achieves a separation between Tx channels, albeit in a nonorthogonal manner and thus with limited dynamic range.

■ **Slow-time phase modulation based multiplexing:** The phase of each chirp (or any waveform in general) in slow-time is modulated to multiplex Tx channels. That is, for the  $n$ th Tx antenna, the phase over slow-time is modulated with  $\exp(j2\pi C_n(t_s))$ . When modulated with a complex exponential (linear phase progression  $C_n(t_s) = f_s t_s$ ), this leads to a Doppler offset between the Tx channels. This is advantageous in applications where the maximum possible Doppler shift is smaller than the unambiguously measurable Doppler range (e.g., at lower carrier frequencies). Alternatively, slow-time phases can be modulated with orthogonal codes to multiplex Tx channels. This requires Doppler-robust codes, which typically exhibit limited dynamic range in the velocity estimation.

Due to its multicarrier structure, OFDM radar allows even more freedom with respect to multiplexing for MIMO radar. OFDM subcarriers can be individually assigned to a Tx antenna, which enables the generation of various orthogonal waveforms for MIMO radar. With this approach, Tx antennas can operate simultaneously using the entire bandwidth. OFDM-specific multiplexing methods include the following:

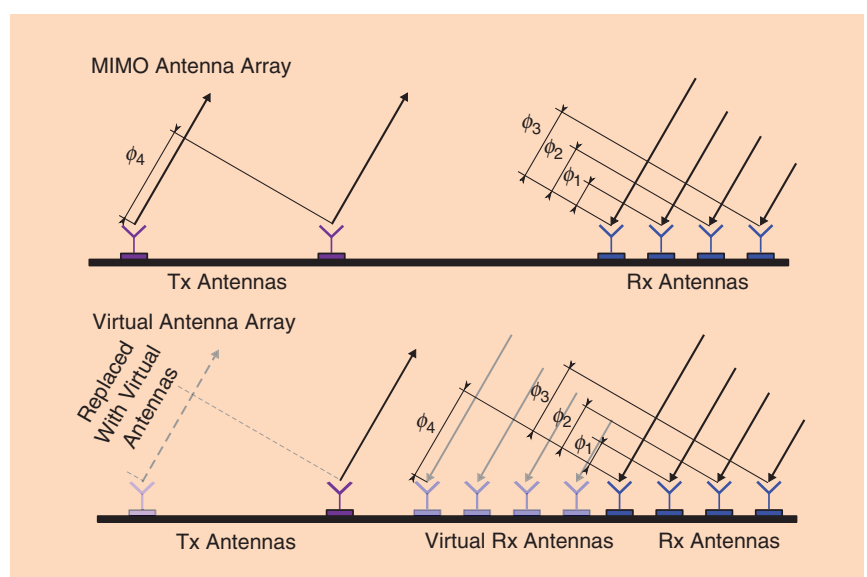


**FIGURE 4.** A diagram showing the principle of MIMO radar and virtual apertures.

■ *Equidistant subcarrier interleaving* [17]: Subcarriers of OFDM radar are interleaved equidistantly over multiple Tx antennas (every  $N_{\text{Tx}}$ th subcarrier is assigned to one of the  $N_{\text{Tx}}$  Tx antennas), such that all Tx channels use the entire bandwidth simultaneously. While maintaining the distance resolution, this reduces the unambiguously measurable distance range, as the spacing between subcarriers transmitted from one Tx antenna increases from  $\Delta f$  to  $N_{\text{Tx}}\Delta f$  (i.e., the sampling rate of distance-induced complex exponentials decreases). This method is thus less suitable for long-range applications.

■ *Nonequidistant subcarrier interleaving* [27]: To overcome the drawback of equidistant subcarrier interleaving in terms of reduced unambiguously measurable distance range, the OFDM subcarriers can be interleaved nonequidistantly. This implies a nonuniform sampling of distance-induced complex exponentials that maintains unambiguous distance range for each Tx channel. Since for nonuniform sampling, FFT-based processing leads to increased side-lobes, nonequidistant subcarrier interleaving requires more complex distance processing, e.g., based on compressed sensing. The nonequidistant subcarrier interleaving can be kept the same in slow-time (same for all OFDM symbols), or changed dynamically for each OFDM symbol, resulting in 2D nonuniform sampling patterns [28].

■ *Space–time block codes* [19]: To simultaneously use all subcarriers by all Tx antennas, OFDM subcarriers can be modulated with space–time block codes. This makes it possible to maintain distance estimation parameters for each channel. It reduces, however, the unambiguous velocity range, as consecutive OFDM symbols constituting a block of code are required for distance processing.

For PMCW radar, multiple Tx channels can be multiplexed based on orthogonal codes—in both fast- and slow-times [18]. To this end, the low cross correlation of codes (also under the condition of Doppler shift) is essential for effective separation of MIMO channels.

Evidently, both fast-chirp and digital radars enable advanced modulation-specific multiplexing schemes. As multiplexing implies sharing of available resources (e.g., time, frequency) between multiple channels, each multiplexing method leads to some specific drawbacks compared to a single Tx channel in terms of distance–velocity estimation. By a proper choice of the multiplexing method, these drawbacks are minimized, while obtaining improved DOA processing based on MIMO radar.

A further important aspect of MIMO radar to consider when choosing a multiplexing method is the coherency between the Tx channels. Maximum coherency is obtained when all Tx channels transmit simultaneously using the same bandwidth. In case of a time offset between the measurements of Tx channels, the target motion leads to Doppler-induced phase shifts between channels that add up to the DOA-induced phase progression. Analogously, different carrier frequencies of Tx channels imply a range-dependent, unknown phase shift  $\exp(j2\pi\Delta f_{c,\text{Tx}}2d/c_0)$  adding to the DOA-induced phase differences, with  $\Delta f_{c,\text{Tx}}$  denoting the carrier frequency offset of a Tx

channel from a reference frequency  $f_c$ . In case one of these phase components becomes dominant (e.g., for FDM with very large frequency offsets), the MIMO-based DOA processing becomes impractical. The coherency aspect of MIMO processing favors subcarrier interleaving schemes of OFDM radar, as they enable simultaneous transmission from all Tx channels with identical or very close carrier frequencies.

## Limits of conventional range-Doppler processing

For both fast-chirp and digital radars, the conventional automotive radar signal processing assumes that problems estimating the range (distance), velocity, and angle can be solved by processing the following three independent measurement dimensions (ignoring elevation for simplicity of discussion): 1) fast-time (single chirp, OFDM, or PMCW symbols), 2) slow-time (consecutive waveforms), and 3) spatial domain (array elements). These measurement dimensions are, however, not entirely independent. For range-Doppler processing in particular, the range of the moving target changes over consecutive waveforms, and may thus lead to a migration of the target peak between range cells over slow-time, i.e., range migration [7], [29].

Similarly, the Doppler processing of the conventional automotive radar is based on the narrowband assumption, as all frequencies in the signal are approximated by the carrier frequency. As Doppler effect is frequency dependent, each frequency in the signal undergoes a different Doppler shift for wideband systems, and thus yields a different velocity estimate. Analogous to range migration, this leads to a Doppler frequency migration. Both effects prevent the 2D Fourier transform from collecting the entire signal energy into a single range–velocity cell and thus reduce the resolution both in range and velocity [7].

Both the range and Doppler frequency migration originate from the motion of the target during the measurement. Range migration occurs when the range change during the measurement  $d_{\text{mig}} = vT_{\text{cycle}}$  exceeds one range cell (resolution)  $\Delta d = c_0/(2B)$ , i.e., for a target with the following velocity:

$$|v| \geq \frac{c_0}{2BT_{\text{cycle}}} \quad (1)$$

Consequently, the range migration normalized to a range cell is the following:

$$\zeta_{\text{RM}} = \frac{d_{\text{mig}}}{\Delta d} = \frac{2vBT_{\text{cycle}}}{c_0} \quad (2)$$

From (2), the range migration is large for a large time-bandwidth product  $BT_{\text{cycle}}$  and scales with the target velocity. The same equation describes the amount of Doppler frequency migration [7], since both effects are inherently linked. In fact, they are representations of the same phenomenon in two different dimensions: range–slow-time and frequency–Doppler-estimate, respectively. Hence, for moving targets, range and Doppler frequency migration limit the simultaneously achievable range and velocity resolution, imposing an upper bound jointly on both parameters. For a typical bandwidth of 1 GHz and measurement time of 20 ms, one cell migration occurs for velocities  $v > 7.5$  m/s. From the application perspective, the impact of

migration effects is especially adverse during driving, as the stationary targets appear moving relative to radar and thus are affected by migration-induced smearing in the radar image.

A further problem especially relevant for digital modulations, such as OFDM or PMCW, is the Doppler shift of the signal frequencies. For OFDM radar, this leads to ICI between subcarriers [17], [30], and for coded waveforms their cross- and autocorrelation characteristics deteriorate. Whereas the classical approach accounts for Doppler shift by limiting the system parametrization such that the maximum Doppler shift is still acceptable, this becomes a critical limitation for high-performance automotive radar.

## Signal processing framework for high-performance radar

As the discussion in the previous section indicates, a signal processing framework based on a more rigorous signal model is needed to fully gain the benefits from upscaling of radar parameters for increased estimation performance. This implies that the current 2D-FFT-based processing has to be replaced with a better approximation of a 2D-matched filter. An approach to achieve this for a single target (or multiple targets with the same velocity) was proposed in [31]. Next, we summarize the research in [7], [29], and [30] and present in general terms a signal processing framework capable of migration-free and Doppler-robust range–velocity processing at a feasible computational cost and for an arbitrary number of targets. We formulate it for arbitrary radar waveforms.

Consider an automotive radar transmitting a series of identical waveforms (e.g., FMCW chirps, OFDM, or PMCW symbols) for distance–velocity estimation:

$$x_{RF}(t) = x(t - \mu T_{\text{sym}}) \exp(j2\pi f_c [t - \mu T_{\text{sym}}]), \quad (3)$$

where  $x(t)$  is the waveform in  $0 < t < T_{\text{sym}}$  that repeats periodically over slow-time  $t_s = \mu T_{\text{sym}}$ ,  $\mu \in [0, N_{\text{sym}} - 1]$ , with  $N_{\text{sym}}$  being the number of waveforms (e.g., OFDM symbols) during one measurement cycle. Let us define the fast-time  $t_f = t - \mu T_{\text{sym}}$ .

Consider the radar signal in (3) reflected from a moving target at a time-dependent range

$$d(t) = d_0 + vt = d_0 + vt_f + vt_s \quad (4)$$

and let us denote the corresponding time-dependent round-trip delay:  $\tau(t) = 2d(t)/c_0 = \tau_0 + \tau_v(t_f) + \tau_v(t_s)$ , where  $\tau_0 = 2d_0/c_0$  and  $\tau_v(t) = 2vt/c_0$ .

After downconversion, the delayed signal at the receiver is as follows:

$$\begin{aligned} y(t) &= Ax_{RF}(t - \tau(t)) \exp(-j2\pi f_c t_f) \\ &= Ax(t_f - \tau(t)) \exp(-j2\pi f_c \tau(t)), \end{aligned} \quad (5)$$

where  $A$  denotes the amplitude change of the signal through propagation and reflection. By representing  $\tau(t)$  with its time-independent ( $\tau_0$ ), fast-time ( $\tau_v(t_f)$ ), and slow-time ( $\tau_v(t_s)$ ) components, we can examine the following six elements of the signal model in (5):

- 1) The waveform  $x(t)$  is delayed by  $\tau_0$  due to the initial target distance  $d_0$ . This term is commonly used for range processing.
- 2) The additional delay in fast-time  $\tau_v(t_f)$  in the argument of  $x$  denotes the delay of each time sample of the waveform, i.e., represents the Doppler-induced stretching/compression of the signal. For typical automotive applications, this term is negligible [7].
- 3) The third delay component  $\tau_v(t_s)$  in the argument of  $x$  is the range change over slow-time due to the target's motion. When ignored, this term can cause range and Doppler frequency migration.
- 4) The first exponential term  $\exp(-j2\pi f_c \tau_0)$  in (5) represents a constant phase shift for all samples and is irrelevant for the range and velocity processing.
- 5) The terms  $\exp(-j2\pi f_c \tau_v(t_f)) = \exp(j2\pi f_D t_f)$  describes the Doppler shift  $f_D = -2v_f/c_0$  of the waveform in fast-time. It has an adverse effect on the range estimation (e.g., leads to ICI in case of OFDM radar) when not taken into account.
- 6) The last term  $\exp(-j2\pi f_c \tau_v(t_s)) = \exp(j2\pi f_D t_s)$  is the Doppler-induced phase progression over slow-time. It is commonly used for Doppler processing.

The conventional radar signal processing simplifies (5) to  $Ax(t_f - \tau_0)\exp(j2\pi f_D t_s)$ . Ignoring the third and fifth terms in (5), the range and velocity estimation problems can be decoupled to fast-time and slow-time dimensions, respectively. The first term is then used for the range processing in fast-time, and the remaining sixth term for Doppler processing is used in slow-time. For high-performance automotive radar, however, neither the third nor the fifth term in (5) can be ignored, as this would lead to migration effects and reduced performance in range processing. Later, we describe a signal processing framework based on a more-precise signal model. Table 1 gives an overview of how signal processing terms in (5) are treated by the conventional Fourier-based range-Doppler processing and by the reviewed framework (the terms in the argument of  $x$  are discussed individually).

Ignoring the second and fourth terms that are irrelevant, the signal model in (5) can be rewritten in the fast-time and slow-time dimensions as follows:

$$y(t_f, t_s) = Ax(t_f - [\tau_0 + \tau_v(t_s)]) \exp(j2\pi f_D [t_f + t_s]). \quad (6)$$

The Fourier transform of (6) in fast-time leads to the following:

$$y(f, t_s) = AX(f - f_D) \exp(-j2\pi f[\tau_0 + \tau_v(t_s)]) \exp(j2\pi f_D t_s), \quad (7)$$

where  $X(f - f_D)$  is the Doppler-shifted spectrum of the radar waveform, the second exponential term is the slow-time-dependent target distance, and the last term is the Doppler shift over slow-time. The representation in (7) makes apparent that the range migration is caused by the slow-time-dependent range change  $\exp(-j2\pi f \tau_v(t_s))$ . To demonstrate that the same term is responsible for the Doppler frequency migration, we rewrite (7) as follows:

$$y(f, t_s) = AX(f - f_D) \exp(-j2\pi f \tau_0) \exp(j2\pi [f_D + \hat{f}_D(f)] t_s), \quad (8)$$

where  $\hat{f}_D = -2vf/c_0$  is the Doppler frequency migration. The representation in (8) shows that the Doppler-induced complex

**Table 1. Summary of terms in the signal model in (5).**

Term	Referred To As	Conventional Processing	Reviewed Framework
$x(t - \tau_0)$	1) Delay	For range (distance) estimation	
$x(t - \tau_v(t))$	2) Doppler scaling (fast-time)	Neglected	Neglected
$x(t - \tau_v(t_s))$	3) Migration term	Neglected	Compensated by ACMC
$\exp(-j2\pi f_c t_0)$	4) Constant phase shift		Ignored (irrelevant)
$\exp(j2\pi f_b t)$	5) Doppler shift (fast-time)	Neglected	Compensated by ACDC
$\exp(j2\pi f_D t_s)$	6) Doppler term		For velocity estimation

exponentials over the slow-time are frequency dependent for  $f \in [-B/2, B/2]$ . By compensating this frequency dependency, both the range and Doppler frequency migration can be prevented, since a single term is causing both effects.

To accomplish this, we can start from the Doppler processing and perform it for each frequency in  $f \in [-B/2, B/2]$  with a kernel that scales the frequency axis to match  $(f_b + \hat{f}_D(f))$  as opposed to the conventional Fourier transform matching to  $f_b$  [7], [30]. This operation scales proportionally the Doppler grid for each frequency, such that each frequency yields the same Doppler estimate. This results in the following migration-free Doppler spectrum in slow-time:

$$y(f, \hat{v}) = \sum_{\mu=0}^{N_{\text{sym}}-1} y(f, t_s) \exp\left(-j2\pi[f_c + f] \frac{2\hat{v}}{c_0} \mu T\right) \\ = AX(f - f_b) \exp(-j2\pi f \tau_0) \cdot D_{N_{\text{sym}}}\left(\pi[f_c + f] \frac{2[v - \hat{v}]}{c_0} T\right), \quad (9)$$

where  $D_N(x) = \exp(j[N-1]x/2) \cdot \sin(Nx/2)/\sin(x/2)$  denotes the Dirichlet kernel and represents the Doppler spectrum of the target, with maximum at the velocity cell  $\hat{v} = v$ . This operation compresses the energy of each target into the corresponding Doppler cell that is same along the frequency dimension and thus migration-free. Subsequently, the Doppler shift of the waveform can be compensated next by a frequency shift of each velocity cell by its corresponding Doppler shift. This will implicitly correct the Doppler shift for the entire radar signal, as the energy of each target is now focused in the corresponding velocity cell. For the cell  $\hat{v}$  corresponding to the target velocity  $v$ , the Dirichlet kernel in (9) becomes  $D_{N_{\text{sym}}}(0) = 1$ . Transforming  $y(f, \hat{v})$  back to the fast-time domain, we can correct the Doppler shift for the cell  $\hat{v} = v$  by the following:

$$y(t_f, \hat{v}) = Ax(t_f - \tau_0) \exp(j2\pi f_b t_f) \exp\left(j2\pi \frac{2\hat{v}}{c_0} f_c t_f\right) \\ = Ax(t_f - \tau_0). \quad (10)$$

The subsequent range processing can be conventionally performed based on a matched filter with knowledge of the waveform  $x(t_f)$ . This results in a range–velocity spectrum free of migration effects and Doppler-induced performance degradation.

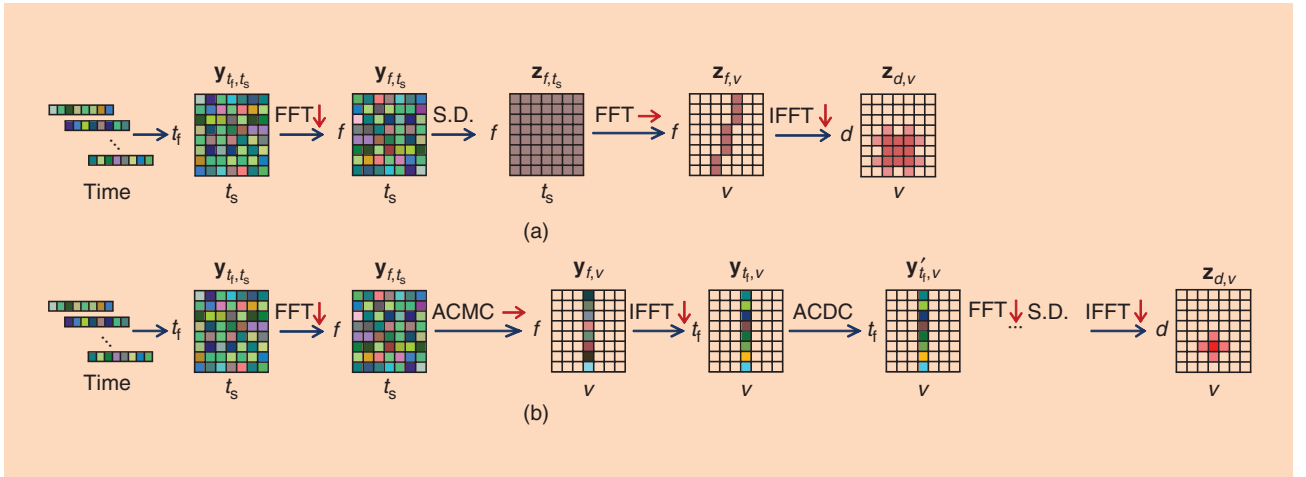
The described idea of migration compensation through scaling of the velocity axis is the basis for the all-cell migration

compensation (ACMC) for automotive radar in [7] as well as the Keystone transform in [29] for synthetic aperture radar. The linear scaling of the velocity axis can be efficiently implemented based on chirp-Z transform, which has an order of computational complexity  $O(N \log N)$  that is the same as for FFT processing. The idea of Doppler shift compensation for all cells is known as all-cell Doppler correction (ACDC) [30]. The correction step is based on elementwise multiplication

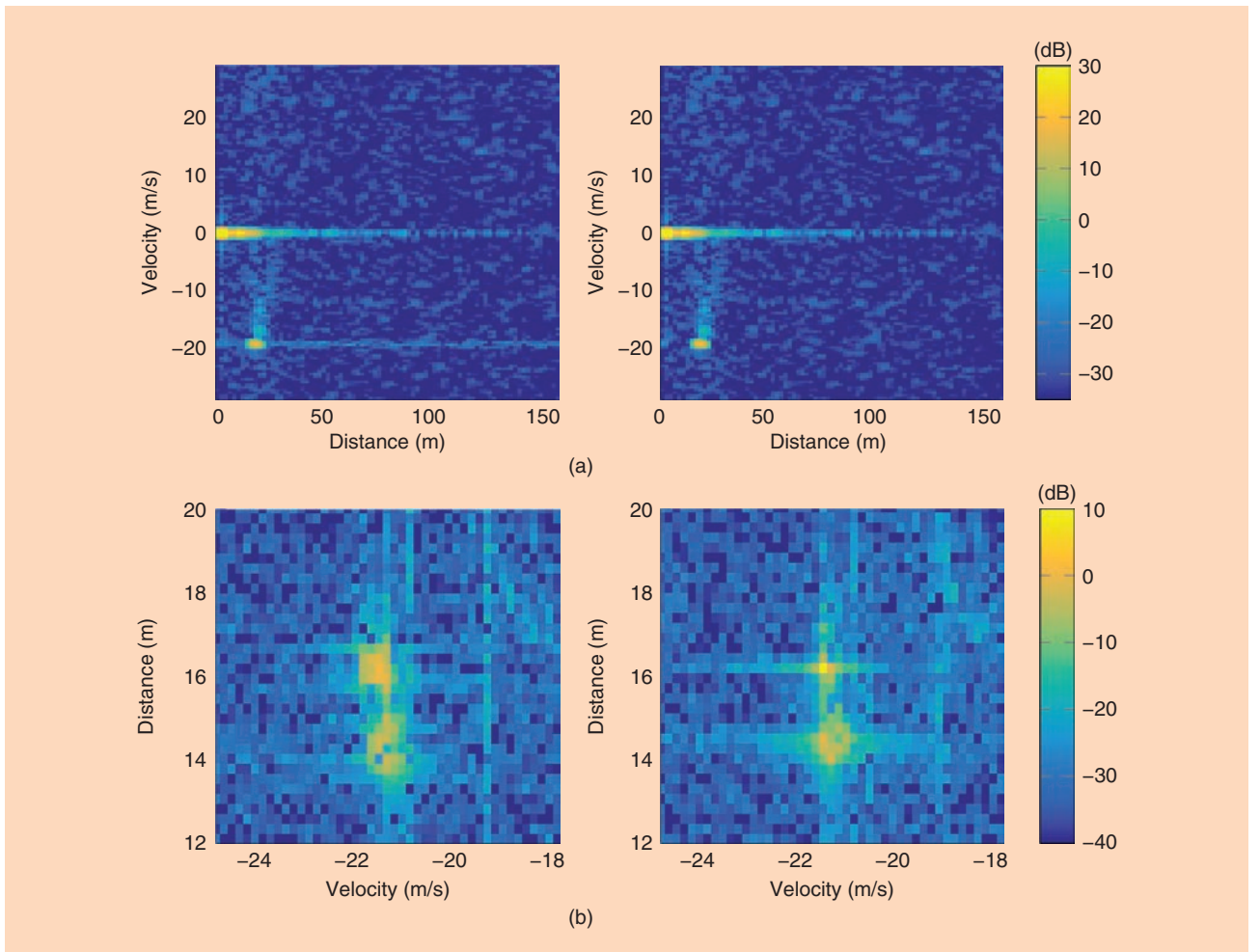
and thus its computational cost is negligible (though it might need transforms between time and frequency domains, depending on implementation). This makes the described signal processing framework feasible for real-time automotive radar implementation as well as for other multitarget applications with a sequence of identical waveforms and negligible higher-order motion terms [see (4)]. The steps of the presented framework are depicted in Figure 5 and compared to the conventional radar processing on the example of OFDM radar.

Figure 6 shows measurement results of a car driving toward an OFDM-MIMO radar prototype [7]. In Figure 6(a), OFDM subcarriers undergo a Doppler shift 0.34 times the subcarrier spacing ( $f_b/\Delta f = 0.34$ ) by reflecting from the moving car (see [30] for further details on the measurement setup). The conventional 2D-FFT processing without Doppler compensation thus results in a considerable level of ICI, constituting itself as a bright trace along the distance axis in the velocity cell of the target (Figure 6(a), left; around  $v \approx -19$  m/s). In contrast, by shifting back the Doppler frequencies for each velocity cell, ACDC prevents Doppler-induced performance degradation for the entire radar image [30]. The target energy is focused into its distance–velocity cell ( $d \approx 20$  m;  $v \approx -19$  m/s), obtaining full signal-to-noise ratio gain and preventing dynamic range reduction. Further performance analysis on ACDC is available in [7] and [30].

To study the migration effects on a real-world example, Figure 6(b) presents a measurement with a bandwidth of 625 MHz and measurement time of 39.4 ms. According to (2), for the car moving with  $v \approx -23$  m/s, conventional Fourier processing results in a range and Doppler frequency migration of more than three cells. Note that the scale of migration is equivalent to that of a system with a 1.25-GHz bandwidth and 19.7-ms measurement time, and thus is representative of automotive radar. With conventional Fourier processing, range migration leads to a smearing of the target peak of more than three cells over the range axis. The Doppler frequency migration results additionally in smearing of the same scale over the velocity axis. In Figure 6(b), left, this is particularly apparent for the corner reflector mounted on the roof of the vehicle to represent a distinct point target (smeared square around  $d \approx 16$  m and  $v \approx -23$  m/s). Figure 6(b), right, shows the same radar image when processed with ACMC. For the entire image, no migration-induced smearing of the peaks occurs. This is particularly clear for



**FIGURE 5.** An illustration comparing conventional Fourier-based processing with the reviewed migration and ICI-free signal processing framework on the example of OFDM radar [7]. (a) 2D-FFT processing. (b) ACDC- and ACMC-based processing. S.D.: spectral division.



**FIGURE 6.** Radar images of an approaching car measured with an OFDM-MIMO radar prototype. The results for 2D-FFT processing make apparent the need for both Doppler-shift and target-motion compensation. The described migration and ICI-free processing overcomes limitations of 2D-FFT. (a) ACDC (right) versus conventional 2D-FFT (left) [30]. The bright trace along the distance axis from the moving car is induced by ICI, which does not occur for ACDC. (b) ACMC (right) versus conventional 2D-FFT (left) [7]. The moving car with a corner reflector mounted on top results in a range and Doppler frequency migration of around 3.5 cells. For 2D-FFT, target reflections are smeared due to range and Doppler-frequency migration, whereas ACMC collects the signal energy into a sharp peak.

the corner reflector, the energy of which is coherently focused into a sharp peak. This illustrates that ACMC prevents the migration-induced degradation of the range and velocity resolution inherent to the conventional 2D-FFT processing. For moving targets, this allows longer coherent integration times and a higher simultaneous range and velocity resolution. Further performance analyses of ACMC are available in [7].

## Interference mitigation

As the number of automotive radar sensors on the road increases, robustness against interference becomes a more important challenge for reliable radar operation. Broadly speaking, high-end automotive radars are more susceptible to interference due to greater use of the time–frequency resources (e.g., large bandwidth, long measurement time). Considering the strict requirements on reliability of operation, interference mitigation becomes a core component of high-performance automotive radars. Generally, to avoid interference, signals of different radars must be separable at least in one dimension, e.g., time, frequency, space, or code/waveform [32]. The main methods for radar interference mitigation can be clustered into the following categories.

- *Detect and suppress at the receiver:* Interference is detected from the measurement data and suppressed via dropping the affected data and reconstructing their values (see [33] and [34] for FMCW radar and [35] and [36] for OFDM radar).
- *Detect and avoid:* When detecting interference in the measurement signal, the radar actively changes its signal to steer clear of interference in the subsequent cycles [37].
- *Interference-aware cognitive radar* [7]: The radar senses the entire operational spectrum and adaptively avoids interference via waveform adaptation [Figure 7(a)].
- *Centralized coordination* [8]: Self-driving cars are centrally coordinated to avoid radar interference [Figure 7(b)].

As these approaches range from local interference suppression at the receiver to coordinated interference avoidance, they widely vary in their sovereignty and universality. The latter class of methods requires other radars to conform to rules or cooperate, i.e., relies on actions of other radars. Methods from the first category are capable of suppressing interference of a specific form, and thus are effective only for certain interferers.

The methods based on suppression of interference at the receiver seek a representation where the interference and signal energy are maximally separable, such that the major portion of interference can be dropped without considerable loss of the radar signal. An example of such processing is mitigation of narrowband interference from OFDM radar by dropping the corrupted subcarriers [35]. Equivalently, for FMCW (fast-chirp) radar, interference from other FMCW sensors with different slopes can be filtered out from the time signal, since only a portion of the time signal is affected due to the antialiasing filter. The discarded portion of the radar signal needs to be recovered to prevent notable per-

formance degradation. For signal recovery, methods ranging from linear prediction [35] to sparse recovery [33] may be used. Similarly, digital beamforming can be used to focus interference in the angular domain toward the DOA of the interferer, thus reducing it in all other directions [34]. Alternative approaches are based on estimating the interfering signal and its subsequent subtraction (e.g., [36]). Such methods heavily rely on known characteristics of the interfering signal. These methods for interference suppression have the drawback of being specific to a certain interference type. Furthermore, since in practice perfect separation of signal from interference is often impossible, such approaches discard a portion of the radar signal. Moreover, they do not improve the overall interference situation, but only suppress it locally at the receiver, and thus typically serve as the last resort for interference mitigation.

Intuitively, a more preferable approach is interference avoidance instead of postprocessing. This requires active adaptation of the Tx signal. An approach inspired by the interference-avoidance mechanism of bats is to gradually steer clear after detecting interference in the received signal by adjusting the carrier frequency [37]. This avoids interference instead of its local suppression, and thus benefits both parties. It also does not require cooperation from the interferer. This method approaches its limits when the density of interferers makes it impractical to blindly move in frequency at a risk of interfering with another, initially unknown radar signal operating at a different frequency.

A more universal solution for adaptive interference avoidance is interference-aware cognitive radar (IACR) [7], which adopts the principles of cognitive radar [38], [39] to remedy the automotive interference problem. IACR comprises the following three main blocks [Figure 7(a)]:

- *Spectrum sensing:* This continuously analyzes the operational spectral band for interference and delivers the spectral occupancy information.
- *Spectrum interpretation:* This contains the cognitive intelligence of the system. It is responsible for applying reasoning to the information obtained via spectrum sensing by means of detection and classification of interfering signals. It also estimates various interference parameters. Based on this knowledge, prediction of the interference behavior for the next transmission cycle is performed. This serves as a basis for choosing an optimal adaptation strategy for the next measurement cycle.
- *Waveform adaptation:* This comprises possible adaptation methods along with the corresponding signal processing algorithms. It also sets in motion the chosen adaptation strategy. The goal is to avoid interference dynamically, while maintaining the radar estimation performance. Possible adaptation space is frequency, time, and waveform.

An implementation of IACR in [7] uses a smaller portion of the operational bandwidth available for automotive radar (e.g., 0.5 GHz in the frequency range 77–81 GHz) and avoids interference by adaptation of the carrier frequency and

starting time of the measurement. Based on spectrum sensing and interpretation, the carrier frequency is adapted for each measurement cycle within the entire available bandwidth to maximally mitigate interference from other radar sensors. Depending on the chosen strategy, this may imply not only cycle-to-cycle hopping of the carrier frequency, but also gradual adaptation within the measurement cycle itself. By adaptively avoiding interference from other automotive radars, IACR obtains robustness against interference in a universal, interference-agnostic manner and already in the analog domain, i.e., by avoidance instead of post-treatment. This mitigates the overall interference problem through cognitive interference avoidance, benefitting the currently deployed, nonintelligent and nonadaptive systems through cognitive interference avoidance. Thus, it represents a promising path for automotive radar to improve the interference situation. An open issue is, however, interference avoidance between multiple IACRs operating in the same environment, as each acting autonomously could potentially lead to mutual interference. To this end, sets of rules or well-defined mechanisms are needed to ensure predictable behavior.

A conceptually different approach for automotive interference mitigation is the RadarMAC architecture for centralized coordination of radar sensors on self-driving cars (Figure 7(b)). This approach requires vehicles to communicate their locations and routes to a control center, which represents the radar operation schedule of vehicles in the same environment as a graph coloring problem and determines playbooks for each self-driving car for their radars to operate interference-free. Especially suited for dense interference settings, centralized coordination is a promising approach for reducing overall interference. It requires, however, an additional reliable communication link, availability at all times, and participants obeying a central coordinator. Thus, it does not address the problem of interference with existing nonadaptive, noncooperative radar sensors operating at the same frequency band.

## Conclusions

As automated driving technology evolves, automotive radar is taking major steps toward becoming a more powerful environment sensor. This transformation involves all aspects of automotive radar, including system concept, modulation, and signal processing. In this article we summarized the major trends in the field of automotive radar especially relevant for high-performance radar systems designed for self-driving cars. One primary devel-

opment is radar operating with arbitrary digitally generated waveforms. Multicarrier modulations, such as OFDM, not only enable radar and communication to be combined in a single waveform, but also represent means for implementing new software-defined radar concepts. In the context of MIMO radar, multicarrier modulations permit the generation of a wide variety of orthogonal waveforms, enabling advantageous multiplexing schemes.

Based on a generalized signal model, we described the simplifications behind the conventional radar signal processing that no longer hold when upscaling radar parameters to increase performance. We reviewed a signal processing framework based on more rigorous modeling of radar signals that allows migration-free and Doppler-robust performance at a moderate computational cost. Finally, we surveyed automotive radar interference-mitigation methods. As automotive radar technology penetrates the market, the interference problem becomes more acute, which means that methods for suppressing interference locally at the receiver will not be sufficient. Promising paradigms for interference mitigation in adaptive, cognitive, and/or coordinated manner arise, and their role in improving the overall interference situation is becoming increasingly apparent. Although automotive radar has been known for decades, this review indicates that there is a fertile ground for research, stimulated by the development of self-driving cars.

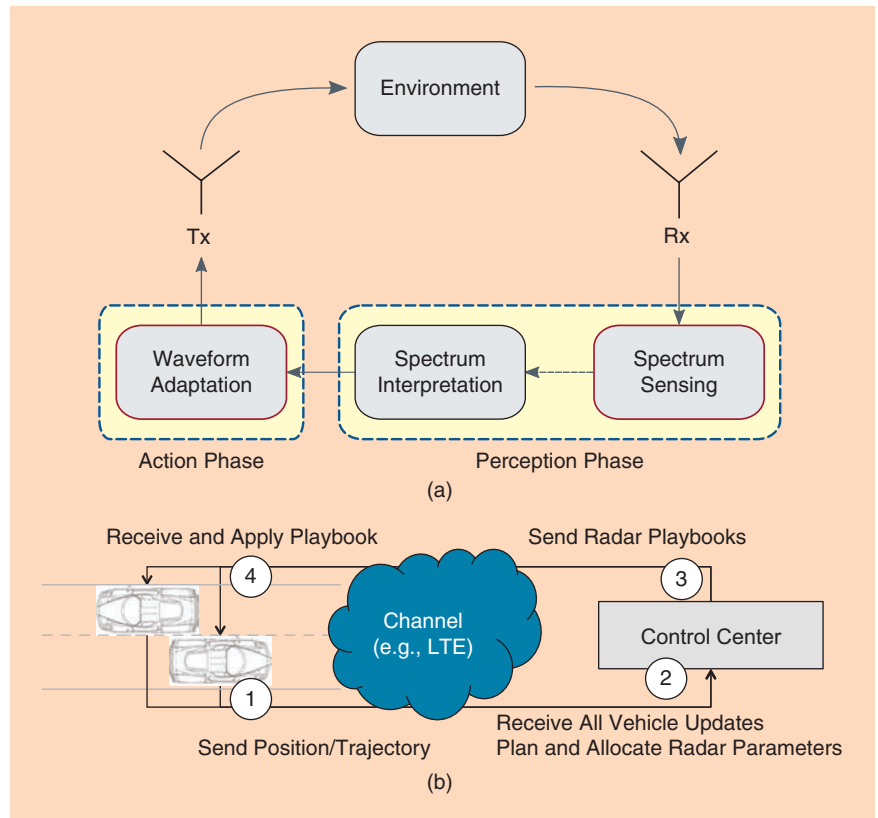


**FIGURE 7.** Diagram and illustration showing new paradigms for adaptive interference mitigation. (a) Closed-loop perception-action cycle of interference-aware cognitive radar [7]. (b) System overview of RadarMAC architecture for coordinated interference avoidance [8].

## Authors

**Gor Hakobyan** (Gor.Hakobyan@de.bosch.com) received his B.E. and M.E. degrees in radio and communication engineering from the National Polytechnic University of Armenia in 2011 and 2013, respectively, and his Dr.-Ing. degree in electrical engineering from the University of Stuttgart, Germany, in 2018. He received the Best Paper Award in the Young Scientist Contest at the 2016 International Radar Symposium. He joined the Corporate Research Division of Robert Bosch GmbH and is now a research scientist in the field of radar signal processing and system design. His current research interests include radar signal processing, compressed sensing, radar modulation schemes, and interference-mitigation techniques.

**Bin Yang** (Bin.Yang@iss.uni-stuttgart.de) received his Dipl.-Ing. and Ph.D. degrees in electrical engineering in 1986 and 1991, respectively, from the Ruhr University Bochum. He is a professor and the head of the Institute for Signal Processing and System Theory in the Faculty of Computer Science, Electrical Engineering and Information Technology at the University of Stuttgart, Germany. His research interests include algorithms and applications of signal processing and machine learning, in particular radar signal processing, energy monitoring, and medical signal processing, with an increasing focus on deep-learning methods.

## References

- [1] D. M. Grimes and T. O. Jones, "Automotive radar: A brief review," in *Proc. IEEE*, vol. 62, no. 6, pp. 804–822, June 1974.
- [2] E. Guizzo, "How Google's self-driving car works," *IEEE Spectrum*, Oct. 11, 2011. [Online]. Available: <https://spectrum.ieee.org/automaton/robotics/artificial-intelligence/how-google-self-driving-car-works>
- [3] H. H. Meinel, "Evolving automotive radar—from the very beginnings into the future," in *Proc. 8th European Conf. Antennas and Propagation (EuCAP 2014)*, Apr. 2014, pp. 3107–3114.
- [4] F. Foelster and H. Rohling, "Signal processing structure for automotive radar," *Frequenz*, vol. 60, no. 1–2, 2006. doi: 10.1515/FREQ.2006.60.1-2.20.
- [5] J. Hasch, E. Topak, R. Schnabel, T. Zwick, R. Weigel, and C. Waldschmidt, "Millimeter-wave technology for automotive radar sensors in the 77 GHz frequency band," *IEEE Trans. Microw. Theory Techn.*, vol. 60, no. 3, pp. 845–860, Mar. 2012.
- [6] S. M. Patole, M. Torlak, D. Wang, and M. Ali, "Automotive radars: A review of signal processing techniques," *IEEE Signal Process. Mag.*, vol. 34, no. 2, pp. 22–35, Mar. 2017.
- [7] G. Hakobyan, "Orthogonal frequency division multiplexing multiple-input multiple-output automotive radar with novel signal processing algorithms," Ph.D. dissertation, Univ. of Stuttgart, Germany, 2018. [Online]. Available: <http://dx.doi.org/10.18419/opus-9830>
- [8] J. Khoury, R. Ramanathan, D. McCloskey, R. Smith, and T. Campbell, "Radarmac: Mitigating radar interference in self-driving cars," in *Proc. 2016 13th Annu. IEEE Int. Conf. Sensing, Communication, and Networking (SECON)*, June 2016. doi: 10.1109/SAHCN.2016.7733011.
- [9] M. Kronauge and H. Rohling, "New chirp sequence radar waveform," *IEEE Trans. Aerosp. Electron. Syst.*, vol. 50, no. 4, pp. 2870–2877, Oct. 2014.
- [10] H. Rohling, "Radar CFAR thresholding in clutter and multiple target situations," *IEEE Trans. Aerosp. Electron. Syst.*, vol. AES-19, no. 4, pp. 608–621, July 1983.
- [11] L. Hammarstrand, L. Svensson, F. Sandblom, and J. Sorstedt, "Extended object tracking using a radar resolution model," *IEEE Trans. Aerosp. Electron. Syst.*, vol. 48, no. 3, pp. 2371–2386, July 2012.
- [12] S. A. Askeland and T. Ekman, "Tracking with a high-resolution 2D spectral estimation based automotive radar," *IEEE Trans. Intell. Transp. Syst.*, vol. 16, no. 5, pp. 2418–2423, Oct. 2015.
- [13] Z. Ji, M. Luciw, J. Weng, and S. Zeng, "Incremental online object learning in a vehicular radar-vision fusion framework," *IEEE Trans. Intell. Transp. Syst.*, vol. 12, no. 2, pp. 402–411, June 2011.
- [14] H. Krim and M. Viberg, "Two decades of array signal processing research: The parametric approach," *IEEE Signal Process. Mag.*, vol. 13, no. 4, pp. 67–94, July 1996.
- [15] F. Engels, P. Heidenreich, A. M. Zoubir, F. K. Jondral, and M. Wintermantel, "Advances in automotive radar: A framework on computationally efficient high-resolution frequency estimation," *IEEE Signal Process. Mag.*, vol. 34, no. 2, pp. 36–46, Mar. 2017.
- [16] D. Cohen and Y. C. Eldar, "Sub-Nyquist radar systems: Temporal, spectral, and spatial compression," *IEEE Signal Process. Mag.*, vol. 35, no. 6, pp. 35–58, Nov. 2018.
- [17] C. Sturm and W. Wiesbeck, "Waveform design and signal processing aspects for fusion of wireless communications and radar sensing," in *Proc. IEEE*, July 2011, vol. 99, pp. 1236–1259.
- [18] A. Bourdoux, U. Ahmad, D. Guermandi, S. Brebels, A. Dewilde, and W. V. Thilloo, "PMCW waveform and MIMO technique for a 79 GHz CMOS automotive radar," in *Proc. 2016 IEEE Radar Conf. (RadarConf)*, May 2016. doi: 10.1109/RADAR.2016.7485114.
- [19] X.-g. Xia, T. Zhang, and L. Kong, "MIMO OFDM radar IRCI free range reconstruction with sufficient cyclic prefix," *IEEE Trans. Aerosp. Electron. Syst.*, vol. 51, no. 3, pp. 2276–2293, July 2015.
- [20] B. Schweizer, C. Knill, D. Schindler, and C. Waldschmidt, "Stepped-carrier OFDM-radar processing scheme to retrieve high-resolution range-velocity profile at low sampling rate," *IEEE Trans. Microw. Theory Techn.*, vol. 66, no. 3, pp. 1610–1618, Mar. 2018.
- [21] D. Schindler, B. Schweizer, C. Knill, J. Hasch, and C. Waldschmidt, "MIMO-OFDM radar using a linear frequency modulated carrier to reduce sampling requirements," *IEEE Trans. Microw. Theory Techn.*, vol. 66, no. 7, pp. 3511–3520, July 2018.
- [22] C. Knill, B. Schweizer, S. Sparrer, F. Roos, R. F. H. Fischer, and C. Waldschmidt, "High range and Doppler resolution by application of compressed sensing using low baseband bandwidth OFDM radar," *IEEE Trans. Microw. Theory Techn.*, vol. 66, no. 7, pp. 3535–3546, July 2018.
- [23] J. Li and P. Stoica, "MIMO radar with colocated antennas," *IEEE Signal Process. Mag.*, vol. 24, no. 5, pp. 106–114, Sept. 2007.
- [24] A. Zwanetski and H. Rohling, "Continuous wave MIMO radar based on time division multiplexing," in *Proc. 2012 13th Int. Radar Symp.*, May 2012, pp. 119–121.
- [25] C. Pfeffer, R. Feger, C. Wagner, and A. Stelzer, "FMCW MIMO radar system for frequency-division multiple TX-beamforming," *IEEE Trans. Microw. Theory Techn.*, vol. 61, no. 12, pp. 4262–4274, Dec. 2013.
- [26] H. Haderer, R. Feger, C. Pfeffer, and A. Stelzer, "Millimeter-wave phase-coded CW MIMO radar using zero- and low-correlation-zone sequence sets," *IEEE Trans. Microw. Theory Techn.*, vol. 64, no. 12, pp. 4312–4323, Dec. 2016.
- [27] G. Hakobyan and B. Yang, "A novel OFDM-MIMO radar with non-equidistant subcarrier interleaving and compressed sensing," in *Proc. 17th Int. Radar Symp. (IRS)*, 2016. doi: 10.1109/IRS.2016.7497312.
- [28] G. Hakobyan and B. Yang, "A novel OFDM-MIMO radar with non-equidistant dynamic subcarrier interleaving," in *Proc. 2016 European Radar Conf. (EuRAD)*, Oct. 2016, pp. 45–48.
- [29] R. P. Perry, R. C. DiPietro, and R. L. Fante, "Coherent integration with range migration using keystone formatting," in *Proc. 2007 IEEE Radar Conf.*, Apr. 2007, pp. 863–868.
- [30] G. Hakobyan and B. Yang, "A novel intercarrier-interference free signal processing scheme for OFDM radar," *IEEE Trans. Veh. Technol.*, vol. 67, no. 6, pp. 5158–5167, June 2018.
- [31] R. F. Tigrek and P. V. Genderen, "Compensation of range migration for cyclically repetitive Doppler-sensitive waveform (OFDM)," *IEEE Trans. Aerosp. Electron. Syst.*, vol. 46, no. 4, pp. 2118–2123, Oct. 2010.
- [32] M. Kunert, "The EU project MOSARIM: A general overview of project objectives and conducted work," in *Proc. 2012 9th European Radar Conf.*, Oct. 2012, pp. 1–5.
- [33] J. Bechter, F. Roos, M. Rahman, and C. Waldschmidt, "Automotive radar interference mitigation using a sparse sampling approach," in *Proc. 2017 European Radar Conf. (EURAD)*, Oct. 2017, pp. 90–93.
- [34] J. Bechter, M. Rameez, and C. Waldschmidt, "Analytical and experimental investigations on mitigation of interference in a DBF MIMO radar," *IEEE Trans. Microw. Theory Techn.*, vol. 65, no. 5, pp. 1727–1734, May 2017.
- [35] G. Hakobyan and B. Yang, "A novel narrowband interference suppression method for OFDM radar," in *Proc. 24th European Signal Processing Conf. (EUSIPCO)*, 2016. doi: 10.1109/EUSIPCO.2016.7760645.
- [36] Y. L. Sit, B. Nuss, and T. Zwick, "On mutual interference cancellation in a MIMO OFDM multiuser radar-communication network," *IEEE Trans. Veh. Technol.*, vol. 67, no. 4, pp. 3339–3348, Apr. 2018.
- [37] J. Bechter, C. Sippel, and C. Waldschmidt, "Bats-inspired frequency hopping for mitigation of interference between automotive radars," in *Proc. 2016 IEEE MTT-S Int. Conf. Microwaves for Intelligent Mobility (ICMIM)*, May 2016. doi: 10.1109/ICMIM.2016.7533928.
- [38] S. Haykin, "Cognitive radar: A way of the future," *IEEE Signal Process. Mag.*, vol. 23, no. 1, pp. 30–40, Jan. 2006.
- [39] M. S. Greco, F. Gini, P. Stinco, and K. Bell, "Cognitive radars: On the road to reality: Progress thus far and possibilities for the future," *IEEE Signal Process. Mag.*, vol. 35, no. 4, pp. 112–125, July 2018.

Stephen Alland, Wayne Stark,  
Murtaza Ali, and Manju Hegde

# Interference in Automotive Radar Systems

*Characteristics, mitigation techniques, and current and future research*



This article examines the problem of interference in automotive radar. Different types of automotive radar as well as mechanisms and characteristics of interference and the effects of interference on radar system performance are described. The interference-to-noise ratio (INR) at the output of a detector is a measure of the susceptibility of a radar to interference. The INR is derived from different types of interfering and victim radars and depends on the location of both as well as parameters such as transmit power, antenna gain, and bandwidth. In addition, for victim radar with beamscanning, INR depends on the location of the target the victim radar is attempting to detect. Analysis is presented to show the effects of various interference scenarios on the INR. A review of the current state of the art in interference mitigation techniques previously deployed as well as areas of research currently being addressed is then provided. Finally, important future research directions are suggested.

## Vehicular sensors

Sensors for vehicular (automobiles, buses, trucks, and so on) applications are an important area of R&D. There are many different types of currently used sensors being considered for use in future vehicles, such as radars, cameras, lidars, and ultrasonics. Each of these sensors has strengths and weaknesses; good engineering judgment indicates that a combination of sensors, which complement the strengths and weaknesses of one with another, is required to maintain the integrity of safety-critical systems. For instance, radars are the best sensors for detecting range and radial velocity and have “all-weather” capability, but are weak for classification and angular resolution. Lidars, in general, have good angular resolution and range, but are limited in field of view (FOV) and have limited ability in adverse weather. Cameras have excellent color perception and classification capabilities but are limited in estimating velocity and range. Cameras also have difficulty in dark or adverse weather.

There are several different performance measures to consider when evaluating the vehicular sensors used to detect objects in the environment. A core set includes detection range, range resolution, velocity coverage, velocity resolution, FOV,

angular resolution, latency (processing delay), robustness to adverse weather, night operation, target classification, and color detection for reading signs and traffic lights. In addition, the cost of a sensor is important to consider; a vehicle might need, and thus be equipped with, multiple sensors. The cost of an individual sensor is typically affected by a number of factors: the scan type (mechanical, solid state/electronic, or digital), radio-frequency (RF) circuitry, baseband and digital chipsets, the integration level of fundamental transmit and receive components, digital processing subsystem capabilities (bandwidth, throughput, and available memory), the associated packaging and required manufacturing processes, and the number of antennas used for transmission and reception. Figure 1 shows the strengths and weaknesses of different sensor systems in relation to different performance measures [1], [2]. Note that the spider plots in the figure illustrate characteristics of radar and vision systems as deployed today in millions of production automobiles, whereas for lidar, they show the potential characteristics—lidars have not been deployed in production automobiles to date.

The considerable sensor requirements for self-driving cars described previously dictate that multiple sensor modalities will be present and that radar will be an important part of that portfolio. Radars can be used to determine location and directly measure the Doppler velocity of objects in the environment. Furthermore, with the ongoing development of RF CMOS and multiple-input, multiple-output (MIMO) radar imaging technologies at 76–77 GHz and 77–81 GHz, automotive radar cost is rapidly decreasing, while overall performance and capability of radars for point cloud imaging, edge detection, and target classification will be substantially improved in the near future.

There are multiple automotive applications for radar sensors; consequently, automotive radar is an active research field [3]–[7]. Automatic cruise control, blind-spot detection, and collision-warning systems were some of the earliest applications of vehicular radar systems. Recently, other applications, including advanced driver-assistance systems, automatic emergency braking, lane-change assist, and vulnerable user detection have been implemented. Self-driving cars will increase

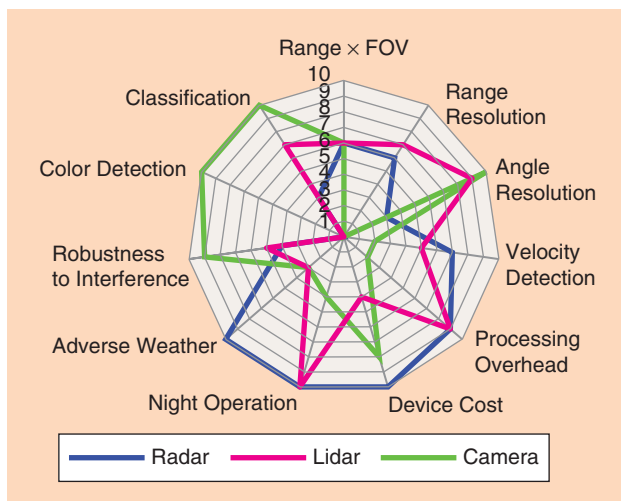


**FIGURE 1.** A comparison of automotive sensors.

the importance of systems that provide an accurate sensing of the environment. As such, it is certain that the number of sensors on vehicles will increase dramatically in the next 10 years. This makes the possibility of radar-to-radar interference in traffic much greater, as noted in [8] and [9].

The problem of radar-to-radar interference will be a significant engineering challenge that the industry will have to address. There are several signal processing techniques that mitigate interference and some of these have already been implemented in radars deployed in today's automobiles. With the increasing number of vehicles being equipped with radar and each vehicle having multiple radar sensors—several production models commercially available in the 2021–2023 time frame are investigating the possibility of deploying up to six radar systems per car—the capability of radar systems to operate in the presence of other radar systems in proximity is fast becoming a critical performance issue. As a result, interest in this area of research has increased significantly. For future radars, the ability to mitigate interference will be as critical as detection performance.

## Background

Radar systems operate by transmitting a signal; this signal is then reflected by an object or target in the environment. The radar system receiving the reflected signal compares the properties of the reflected signal to the transmitted signal [10]. A radar system with a single transmitter and receiver can estimate the range and velocity of an object in the environment; with mechanical or electronic scanning, the radar system can estimate the angle as well. A radar system with multiple receiver antennas can estimate the angle of an object via digital beamforming. With both multiple transmitter antennas and multiple receiver antennas, also known as a *MIMO system*, a radar can estimate the angle of an object via digital beamforming but with enhanced accuracy and resolution compared to more conventional (non-MIMO) radar [4], [6]. In general, radar can determine different object angles (e.g., azimuth and/or elevation) depending on the antenna scanning and/or the number and geometry of antenna-receiver channels.

Radar systems can be designed for different performance objectives. Some of the performance measures of a typical radar system include detection range, range resolution, maximum unambiguous range, velocity resolution, maximum unambiguous velocity, angular resolution, and FOV. An overview of various types of radars and estimation techniques for range, velocity, and direction in the absence of interference are given in [11]. Generally, with a fixed number of antennas, a radar with a broad FOV can be obtained at the expense of less angular resolution, while a narrow FOV can provide better angular resolution. The antenna configuration will determine the estimated target direction in the horizontal plane (azimuth), vertical plane (elevation), or in both. Multiple antennas at the transmitter and receiver can be used to beamform the signal or can be used in a MIMO configuration where different waveforms are transmitted from different antennas and the subsequent receive signals are processed to form a synthetic or virtual receive array. Early

automotive radar used mechanically scanned antennas or several fixed antennas for one-dimensional (azimuth) angle-detection capability [12], [13]. Automotive radar is now beginning to incorporate MIMO antennas configured for 2D angle-detection capability (azimuth and elevation), with future systems moving to a greater number of transmit and receive antennas to support 2D point cloud imaging.

Fundamentally, the performance of a radar system depends on the bandwidth of the signal, the time duration over which the estimation is performed, and the geometry of the transmitter and receiver antennas. A tutorial on its performance in the absence of interference is discussed in detail in [11]. This article is focused on the effect of an interfering radar on a victim radar.

### Frequency-modulated continuous wave

One type of radar, and the most common in current automotive systems, is frequency-modulated continuous-wave (FMCW) radar. In FMCW radar, the transmitted signal is a sinusoidal signal in which the frequency of the signal varies with time. The transmitted signal is

$$s_T(t) = \sqrt{2P_t} \cos(2\pi(f_c + f_m(t))t), \quad (1)$$

where  $f_c$  is the center frequency,  $P_t$  is the transmitted power, and  $f_m(t)$  is the time-varying frequency. The frequency of the transmitted signal is then  $f_T(t) = f_c + f_m(t)$ . There are different ways in which the frequency of an FMCW waveform varies. One way is via a ramp or sawtooth signal in which the frequency ramps from a minimum frequency to a maximum and then repeats. Alternatively, a signal that sweeps up in frequency (i.e., up-chirp) and then down in frequency (i.e., down-chirp) could be employed. Slopes for the up-chirp and down-chirp could vary in time as well. The time it takes for the up-chirp signal of the receiver to sweep over a bandwidth  $B$  Hz in frequency is sometimes called the *chirp duration* and is denoted by  $T_c$ . In some cases, the frequency changes in a piece-wise linear fashion, although the times for the up-chirp and down-chirp can be different.

At the receiver, the received signal is mixed with (multiplied by) the transmitted signal and filtered with a low-pass

filter of a certain bandwidth  $B_r$  to remove the double-frequency components as well as some of the noise and interference. Additional processing is done after converting from analog to digital signals. The filter bandwidth limits the unambiguous range of an FMCW radar. The transmitter and receiver block diagram for an FMCW radar is shown in Figure 2.

The transmitted signal is reflected off of a target and received. The received signal, in the case of a stationary target, is an attenuated and time-shifted version of the transmitted signal. Based on propagation of signals at the speed of light, the delay  $\tau$  is related to the range by  $R = \tau c/2$  or  $\tau = 2R/c$ . This is true for any type of radar signal, not just FMCW. The result of mixing the FMCW-transmitted signal with the received signal will be a signal with frequency proportional to the delay between the radar and the target. Filtering after mixing limits the range of targets that can be detected. The frequency of the signal after mixing and filtering is proportional to the delay between the transmitter and receiver and thus proportional to the range of the target. Suppose  $R_{\max}$  is the range of the furthest target to be detected. Then the corresponding maximum delay is  $\tau_{\max} = 2R_{\max}/c$ . The maximum frequency shift is then  $f_{\max} = 2BR_{\max}/(cT_c)$ . The minimum frequency shift is 0 corresponding to a target at distance 0. The filter must have a bandwidth at least as large as this maximum beat frequency. Equivalently, if the low-pass filter has bandwidth  $B_r$ , the largest range that can be detected is  $R_{\max} = cT_c B_r / (2B)$ . For example, if the chirp duration is 30  $\mu$ s, the sweep bandwidth is 300 MHz and the filter bandwidth is  $B_r = 15$  MHz, then the maximum range is 225 m. For automotive applications, this might be considered a long-range radar (LRR). If the sweep bandwidth is 750 MHz, the sweep time is 50  $\mu$ s and the IF bandwidth is  $B_r = 4.5$  MHz, then the maximum range is 45 m and would be considered a short-range radar (SRR). Generally, a larger bandwidth  $B$  will enable better range resolution in a radar. An SRR would typically require better range resolution than an LRR and thus, use a larger bandwidth.

### Phase-modulated continuous wave

Another type of radar is phase-modulated continuous-wave (PMCW) radar. In a PMCW radar system, the transmitted signal

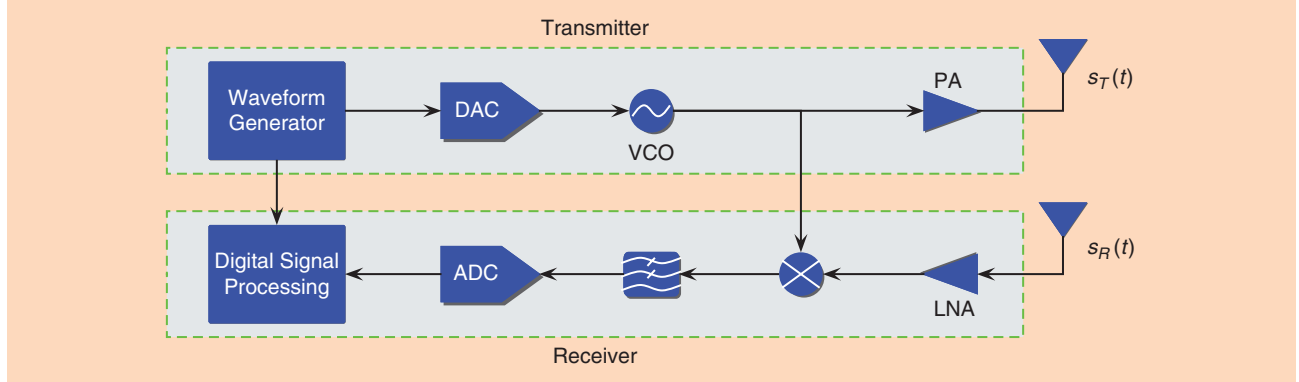


**FIGURE 2.** The block diagram of an FMCW system. DAC: digital-to-analog converter; ADC: analog-to-digital converter; VCO: voltage-controlled oscillator; PA: power amplifier; LNA: low-noise amplifier.

is a sinusoidal signal in which the phase varies with time. The transmitted signal for PMCW radar has the form

$$s_T(t) = \sqrt{2P_t} \cos(2\pi f_c t + \phi_m(t)), \quad (2)$$

where  $\phi_m(t)$  is the modulated phase waveform. The total phase of the transmitted signal is  $\phi_T(t) = 2\pi f_c t + \phi_m(t)$ . One way of generating the phases is to begin with what is known as a *spreading code*. A spreading code consists of a sequence of chips (e.g., +1, +1, -1, +1, -1, ...) with a chip duration  $T_c$ , which is mapped (e.g., +1 → 0, -1 → π) into a sequence of phases (e.g., 0, 0, π, 0, π, ...), and the phases are used to modulate the RF sinusoidal signal. The phase can be limited to either 0 or π radians (180°) or it can be arbitrary. In the event that the signal phase is only either 0 or π radians, the signal is said to be a *binary phase modulated signal*. A binary phase modulated signal can also be generated by multiplying a binary (+1 and -1) signal  $a(t)$  with a carrier. In the case of binary spreading codes, the transmitted signal can be written as

$$s_T(t) = \sqrt{2P_t} a(t) \cos(2\pi f_c t). \quad (3)$$

The spreading code  $a(t)$  could be a periodic sequence with a short period or could be a pseudorandom sequence with a very long period so that it appears to be a nearly random sequence. Codes or sequences with good autocorrelation properties are important for use in PMCW-type radar systems. There are many possible spreading codes, including Barker sequences,  $m$ -sequences (also known as *linear feedback shift register sequences*), and gold codes, all of which are binary codes. There are also nonbinary codes such as the Zadoff-Chu codes. More information about spreading codes can be found in [14]. The resulting modulated RF signal has a bandwidth that is proportional to the rate at which the phases change, called the *chip rate*, which is the inverse of the chip duration,  $T_c$ .

The receiver, as shown in Figure 3, first mixes the received signal  $s_R(t)$  down to baseband and then filters the result to remove unwanted frequency components before converting it to digital signals. The digital signals are processed with a filter matched to the transmitted signal (as part of the digital signal process unit

shown in Figure 4). A peak in the magnitude of the filter output is indicative of a target at a certain distance from the radar.

By comparing the return signal to the transmitted signal, the receiver can determine the range and velocity of objects in the environment. The digital signal processing block includes a matched filter, which correlates the received signal to all possible delays of the transmitted spreading code. For the delay that matches the delay of the reflected signal, the correlation will be high, and a target at a given distance corresponding to the delay will be detected. The wider the bandwidth, the finer the ability of the receiver to resolve two objects near each other. The matched filter will provide correlations to replicas of the transmitted spreading code of some length. The longer the length of the spreading code used to correlate, the greater the ability to detect—unambiguously—targets at a long distance.

Although there are other types of radar signals being considered for automotive applications (e.g., [15]), this article's focus is only on these two types of radars (i.e., FMCW and PMCW) and how one or more radars of one type causes interference with another radar of either the same or a different type.

## Interference in automotive radar systems

One fundamental reality for automotive radar is the potential for mutual interference due to multiple radars operating simultaneously in “close proximity” and direct line of sight [16]. Analyses and test results involving automotive radar indicate that mutual interference can be substantial unless suitable mitigation is employed.

Figure 4 shows two scenarios where in each, a vehicle with an “interfering” radar is creating interference for a “victim” radar. Consider the leftmost example scenario shown in Figure 4, with a single interfering radar at a distance  $R$  mounted on a vehicle that also acts as a target for the victim radar. In this case, the distance from the target and the distance from the interferer are identical. The signal powers received by the victim radar for the vehicle target ( $P_r$ ) and the interference ( $P_I$ ) are given by

$$P_r = \frac{P_t G^2 \lambda^2 \sigma}{(4\pi)^3 R^4}, \quad P_I = \frac{P_t G^2 \lambda^2}{(4\pi)^2 R^2}, \quad (4)$$

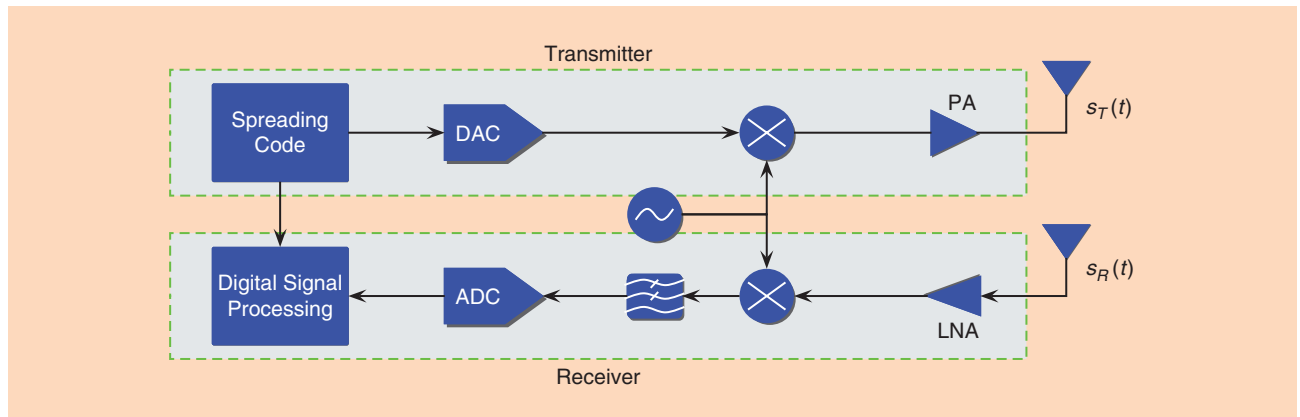


**FIGURE 3.** A block diagram of PMCW radar.

where  $P_t$  is the transmitted power of the victim radar,  $\lambda = c/f$  is the wavelength of the transmitted signal, the antenna gain in the direction of the target is  $G$ , and the radar cross section (RCS) of the target is  $\sigma$  (i.e., the effective reflection area) [17]. The RCS is often stated in units of either square meters or “units” of dBsm, which refers to dB relative to  $1 \text{ m}^2$  [i.e.,  $\sigma$  in dBsm =  $10 \log(\sigma/\text{m}^2)$ ]. The received interference power in (4) assumes that the interfering radar has the same transmitter power and antenna gain as the victim radar and is located at the same range as the target. For example, the interferer could be colocated with the target. The signal-to-interference ratio (SIR) at the victim radar receiver is then

$$\frac{P_r}{P_I} = \frac{\sigma}{4\pi R^2}, \quad \text{SIR} = G_p \frac{P_r}{P_I} = \frac{G_p \sigma}{4\pi R^2}. \quad (5)$$

Here,  $G_p$  is the processing gain of a matched filter in the victim radar, which improves the SIR. Still, the SIR can be low enough to inhibit target detection. For example, given a 10-dBsm RCS typically assumed for a small-to-midsize passenger car, and a processing gain of 50 dB, the SIR falls below 10 dB for a range greater than approximately 90 m. In practice, the RCS for a vehicle can vary substantially with the aspect angle. For example, the RCS can vary from 0 dBsm to as high as 30 dBsm at 77 GHz for midsize passenger cars, as shown in [18] for a Mazda 6. Even small changes in the aspect angle seen on a frame-to-frame basis can lead to fluctuation in the observed RCS. Hence, statistical RCS models (e.g., the well-known Swerling models) are often used to predict automotive radar performance.

In general, the parameters of the victim and interfering radar are different, and the victim radar is required to detect targets of varying range and the RCS over a defined FOV. Furthermore, automotive radar processing gain is limited by a number of factors, including the required

update time interval specified to cover the FOV (typically on the order of 50 ms).

For radar, a relevant performance metric is the INR after processing in the victim radar. In general, the INR depends on the parameters of the victim and interfering radars, signal modulation characteristics of the interfering radar, and demodulation/downconversion processing employed by the victim radar. For simplicity, consider noise-like interference spread uniformly over the passband of the victim radar. This is often the case and will result in the lowest overall INR. If the interfering radar has bandwidth  $B$ , then the power spectral density (PSD)<sub>int</sub> of the interference at the victim radar is given by

$$\text{PSD}_{\text{int}} = \left[ \frac{P_t G_T \lambda L_{TX} L_f N_{TX}}{B(4\pi R^2)} \right] \left[ \frac{G_R \lambda L_{RX} L_f N_{RX}}{4\pi} \right] (D_F)(K), \quad (6)$$

$$= \left[ \frac{P_t N_{TX} G_T L_{TX} L_f \lambda^2 G_R L_{RX} L_f N_{RX}}{B(4\pi R)^2} \right] (D_F)(K), \quad (7)$$

where  $G_T(G_R)$  is the antenna gain for the interfering (victim) radar,  $\lambda$  is the wavelength of the radar signal,  $P_t$  is the transmitted power of the interfering radar,  $N_{TX}(N_{RX})$  is the number of transmitting (receiving) antennas for the interfering (victim) radar,  $L_{TX}(L_{RX})$  is the transmit (receive) loss for the interfering (victim) radar, and  $L_f$  is the loss due to the fascia (e.g., the auto’s bumper) of both radars. The duty factor parameter  $D_F$  accounts for the fraction of time the interfering radar operates within the dwell time and band of the victim radar; hence, the value of  $D_F$  varies from 0 to 1.

The parameter  $K$  generally applies to the case of FMCW modulation for both the victim and interfering radars and is given by the inverse ratio of the interference PSD in the victim radar receiver at RF prior to downconversion versus the interference PSD at baseband after downconversion in the victim radar, i.e.,

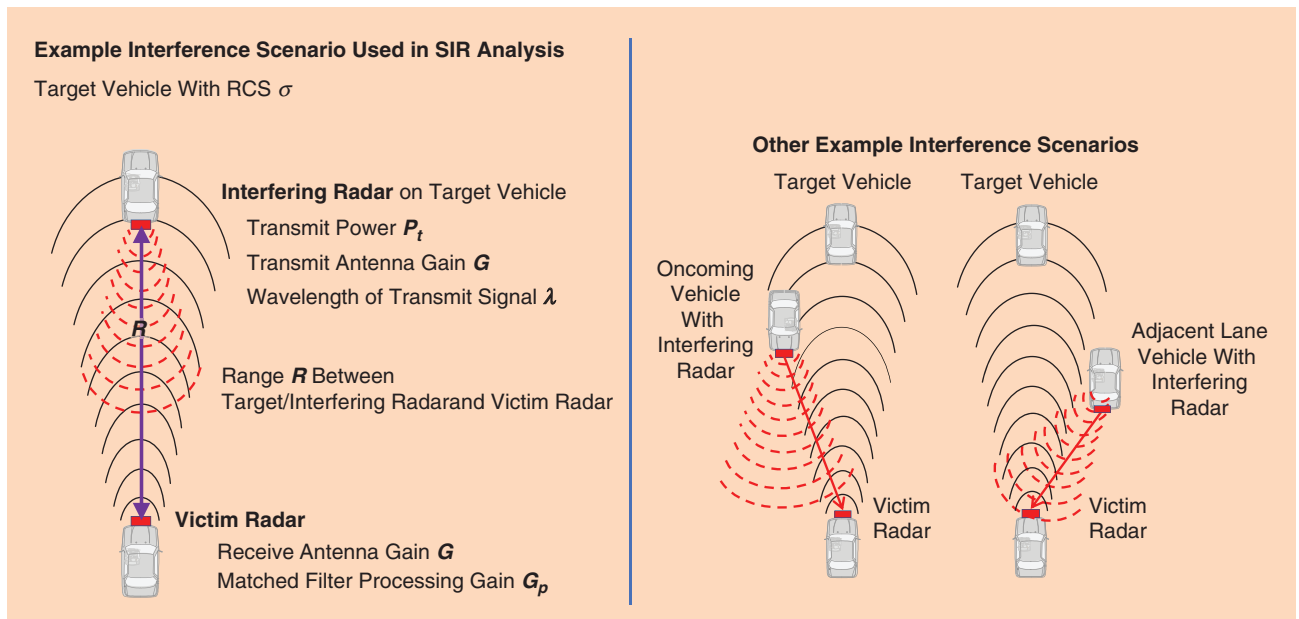


**FIGURE 4.** Example interference scenarios for automotive radar.

$$K = \frac{\text{PSD}_I^{\text{RF}}}{\text{PSD}_I^{\text{BB}}} = \frac{\Delta F_I^{\text{RF}}}{\Delta F_I^{\text{BB}}}, \quad (8)$$

where  $\text{PSD}_I^{\text{RF}}$  is the PSD of interference at RF prior to downconversion in the victim radar receiver,  $\text{PSD}_I^{\text{BB}}$  is the PSD of interference after downconversion in the victim radar receiver,  $\Delta F_I^{\text{RF}}$  is the RF sweep bandwidth of the FMCW interfering radar, and  $\Delta F_I^{\text{BB}}$  is the interference bandwidth in the FMCW victim radar receiver after downconversion to baseband. The interference bandwidth at baseband after downconversion in the victim radar receiver depends on the FMCW slopes of the interfering and victim radars (as well as their time and frequency alignment) and, for “similar” FMCW slopes, can be significantly less than the RF sweep bandwidth of the FMCW interferer. In this situation,  $K \gg 1$  as the FMCW interference is concentrated into a narrow bandwidth in the FMCW victim radar receiver, thereby increasing its PSD.

For situations with, e.g., FMCW employed by either the victim or interfering radar,  $K$  is generally equal to unity. Interference mechanisms and characteristics for both FMCW and FMCW modulations are discussed later in the “Mechanisms and Characteristics of Interference” section. In the case of FMCW modulation used by both the interferer and victim, the “Mechanisms and Characteristics of Interference” section includes equations and results for parameter  $K$  for two different examples of time and frequency alignment.

The PSD of the noise is  $\text{PSD}_{\text{noise}} = kT_0F_n$ , where  $k$  is Boltzman’s constant,  $T_0$ , is the temperature in Kelvin, and  $F_n$  is the noise factor of the receiver. Finally, the INR is

$$\text{INR} = \frac{\text{PSD}_{\text{int}}}{\text{PSD}_{\text{noise}}}. \quad (9)$$

Without mitigation, the resulting INR can be substantial depending on the range and RF bandwidth of the interfering radar.

In a dynamic on-road encounter, interference seen by a victim radar will vary depending on a number of factors, including the relative position of the interfering radar (range and cross range) and the orientation and shape of the victim and interfering radar antenna patterns, as illustrated in Figure 5. The evaluation of performance versus the geometry of victim and interferer is also addressed in [17].

Figure 5 shows contours of constant INR depending on the location of an interfering radar relative to a victim radar. The simulation is based on the theoretical equation for INR, i.e., (9). The situation depicted considers a victim radar facing an opposing interfering radar. The closer the interfering radar is to the victim radar, the larger the INR, and the worse the performance is. Parameters typical of MIMO automotive medium-range radar (MRR) were used. Both victim and interfering radars are assumed to be FMCW radars with “dissimilar fast-crossing” slopes such that  $K = 1$ . When the interfering radar is approximately 150 m downrange from the victim radar, the interference is roughly 10 dB above the thermal noise level. As

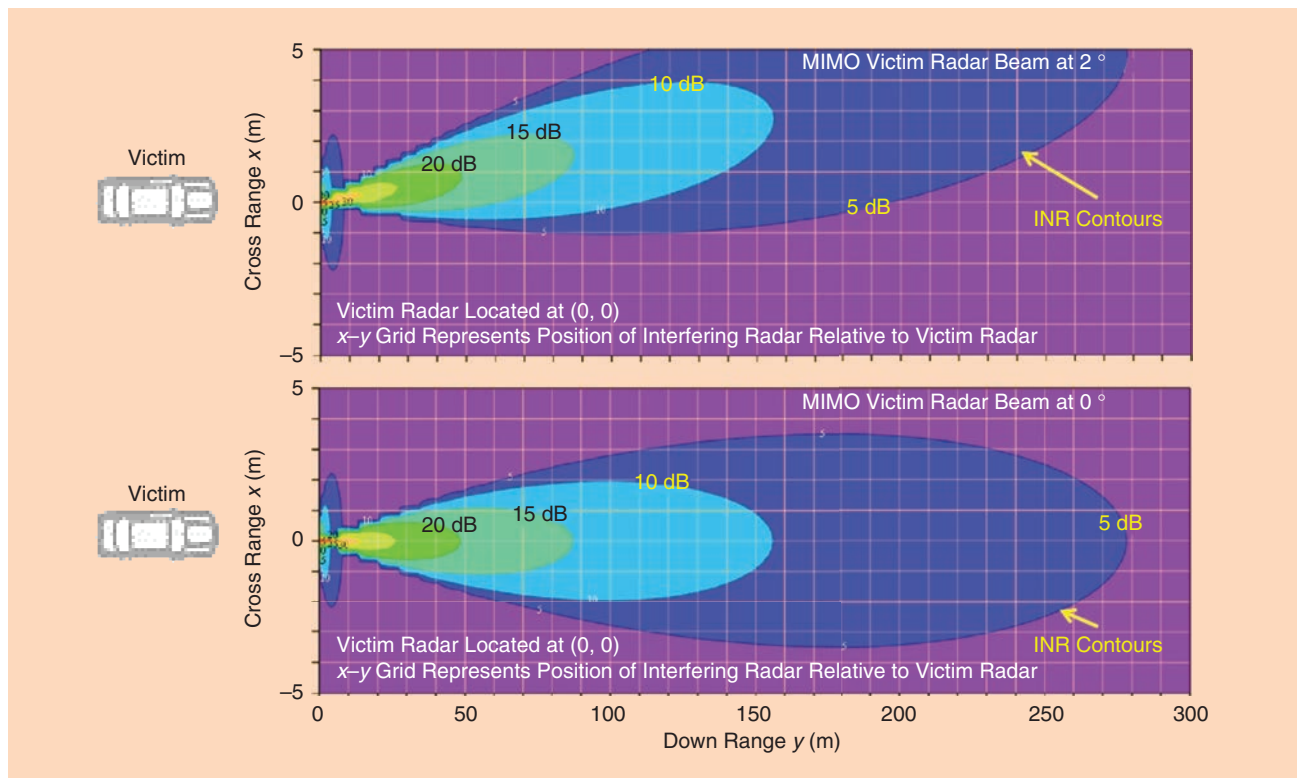


**FIGURE 5.** Example INR contours for representative MIMO automotive MRR receive beams at 0 and 2°, respectively (the x-y grid is in the position of interfering radar relative to the victim radar located at 0,0). MRR: medium-range radar.

such, without interference mitigation, the performance of the victim automotive radar may degrade considerably.

Spatial discrimination of MIMO beamforming offers mitigation of interference for beams not pointed in the direction of the interfering radar, as shown in Figure 5 for two beam positions of the MIMO victim radar, i.e., 0 and 2°, respectively. Of course, with the potential for multiple interfering radars to be spread across the FOV, the mitigation offered by beamforming may be substantially diluted.

As seen in Figure 5, the INR will increase as the interferer range decreases. Additionally, the interference level can be substantially greater for situations with interferers of higher radiated power density such as automotive LRR or traffic control radar. The MOre Safety for All by Radar Interference Mitigation (MOSARIM) project [16], [19], [20] concluded that: “For automotive radars, without any mitigation technique applied, the interference power can exceed the noise level by 20 to 50 dB. The achieved results show that for typical antenna and modulation parameters, an increase of noise in the victim receiver and thus a reduction of the usable measurement range is very likely, while the occurrence of ghost targets seems to be rather unlikely.” Note that, even in dense traffic with many interferers, the occurrence of ghost targets remains unlikely because any individual ghost target detections would, over time, be sporadic/random in nature and thereby mitigated by the tracking function in the victim radar. Mitigation can be further improved by the victim radar dither of relevant waveform timing parameters that help randomize the range and Doppler of ghost detections on a frame-to-frame basis. This technique has been implemented by a number of radar suppliers.

### Mechanisms and characteristics of interference

Here, we consider the two main modulation techniques described previously, i.e., FMCW and PMCW. Because the inter-

ference characteristics depend on which kinds of modulation the interferer and victim both have, we describe the various interference characteristics for the different types of interfering and victim radars.

#### FMCW–FMCW

Consider a victim radar and interfering radar both using FMCW modulation. Figure 6(a) shows the mechanism of interference and the resulting time-domain and frequency-domain responses. For downconversion in the receiver, FMCW radar uses a replica (coupled version) of the transmitted FMCW signal. For the situation where the interfering FMCW signal crosses the victim FMCW signal, the interference appears as a linear chirp signal after downconversion in the victim radar receiver which, assuming “dissimilar, fast-crossing” slopes, covers a wide bandwidth as it sweeps through the victim radar passband. After bandpass filtering in the victim radar, the interference signal resembles an impulse-like signal in the time domain. The resulting frequency spectrum is broadband and often well above the background noise floor [Figure 6(b)] when representative automotive MRR parameters are used (i.e., 15–20 dB above noise).

The position and width of the impulse-like interference signal in the time domain following downconversion and bandpass filtering in the victim radar depends on the relative timing and slopes of the FMCW modulation of the interfering and victim radars. The resulting frequency spectrum characteristics of the interference in the victim radar, including the PSD, depend on the relative timing and FM slopes as well. For example, with slower FM rates and/or similar FM slopes for the victim and interfering radars (i.e., “slow-crossing” slopes), the time extent of interference in the victim radar passband and the associated PSD can increase significantly.

In (8), the parameter  $K$  for FMCW-to-FMCW interference is fundamentally the ratio of the chirp bandwidth transmitted

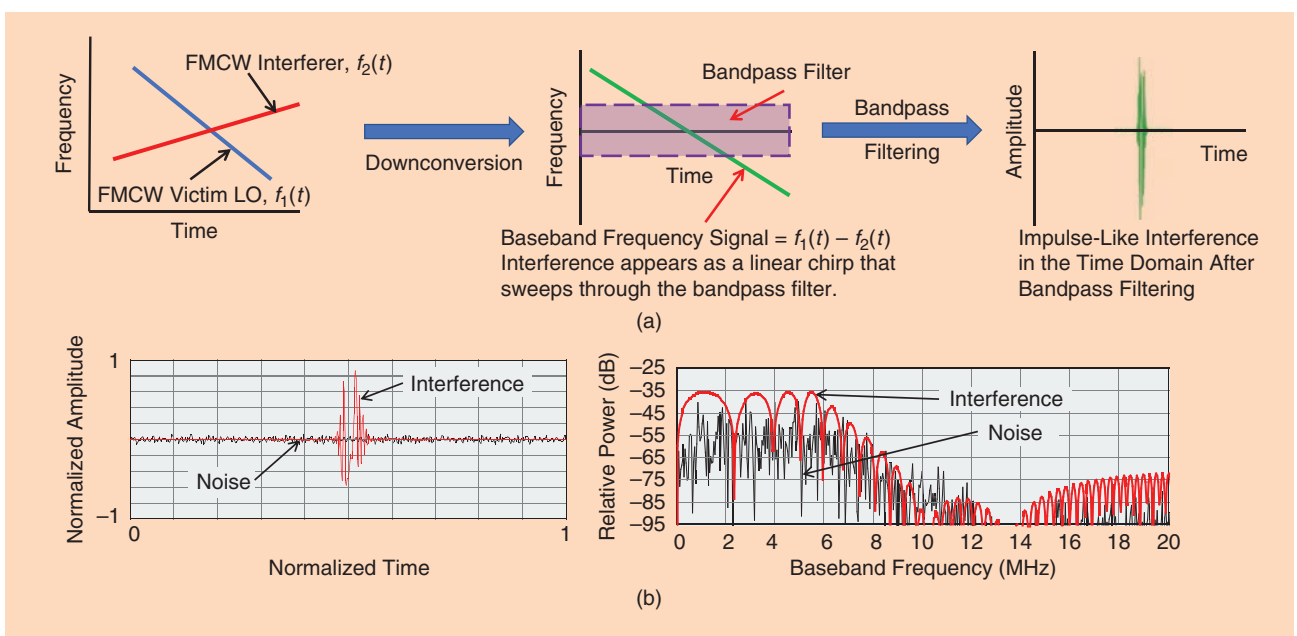


**FIGURE 6.** (a) An FMCW-to-FMCW interference mechanism and (b) its simulated time–frequency domain characteristics. LO: local oscillator.

by the interfering radar to the bandwidth of the interference chirp after downconversion in the victim radar. For FMCW, the bandwidth after downconversion in the victim radar depends on the difference in the FM sweep (i.e., modulation) rate between the interfering and victim radars. Assuming that the FM modulation rates of the interfering and victim radars produce “broadband” interference following downconversion in the victim radar, i.e., interference spread over no less than the baseband bandwidth of the victim radar,  $K$  generally ranges from a minimum value of 0.5 to a maximum value equal to the sweep bandwidth of the interfering radar divided by the baseband bandwidth of the victim radar.

The parameter  $K$  for FMCW interference in (8) depends on the FMCW sweep rates of the interfering and victim radars as well as their time and frequency alignments, as demonstrated in the following examples.

- **Case 1:** Interfering and victim radar sweeps with the same duration  $T_S$ , start time, and start frequency

$$K = \frac{\Delta F_I^{\text{RF}}}{\Delta F_I^{\text{BB}}} = \left| \frac{S_I T_S}{(S_V - S_I) T_S} \right| = \left| \frac{S_I}{(S_V - S_I)} \right|. \quad (10)$$

- **Case 2:** Interfering and victim radar sweeps with the same duration  $T_S$ , start time, and center frequency

$$K = 2 \left| \frac{S_I T_S}{(S_V - S_I) T_S} \right| = 2 \left| \frac{S_I}{(S_V - S_I)} \right|, \quad (11)$$

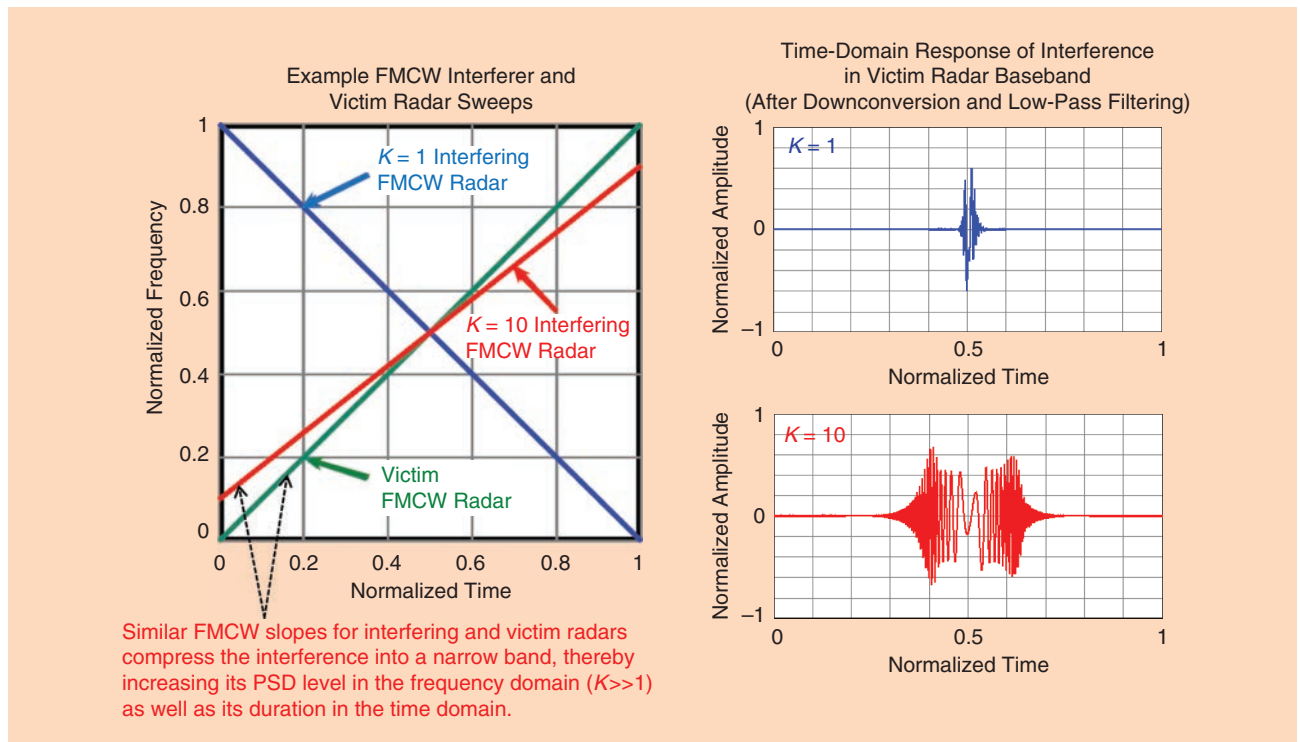
where  $S_I$  = FM sweep (modulation) rate of the interfering radar and  $S_V$  = FM sweep (modulation) rate of the victim radar.

Figure 7 shows parameter  $K$  and the corresponding interference in the time domain after downconversion and bandpass

filtering in the victim radar for a situation where the FM sweeps of the victim and interfering radar are aligned in time and have the same center frequency (i.e., case 2). Two examples are shown in Figure 7; the FM sweep of the victim radar is shown in green. One example corresponds to  $K = 1$  (i.e., the FM sweep of interfering radar (blue) with a sweep rate,  $S_I$ , equal in magnitude but opposite in sign to the sweep rate of the victim radar,  $S_V$ ); a second example corresponds to  $K = 10$  (i.e., the FM sweep of interfering radar (red) with a sweep rate similar to the sweep rate of the victim radar). Compared to a “fast” (i.e., high) crossing rate for “dissimilar” FM sweeps (e.g.,  $K = 1$ ), as the FM sweeps become more similar (e.g.,  $K = 10$ ), the crossing rate decreases, resulting in interference with a longer time duration and higher PSD after downconversion and bandpass filtering in the victim radar. All else being equal, the  $K = 10$  example results in interference with 10 times the PSD (and, correspondingly, 10 times the INR) compared to the  $K = 1$  example.

Early automotive FMCW radar typically used “slow-chirp” waveforms with one or several linear FM sweeps transmitted during a dwell or update interval and each chirp using a relatively slow sweep rate. Automotive radars using “fast-chirp” FMCW waveforms consisting of many identical linear FM chirps during a dwell, where each chirp has a relatively fast sweep rate, are becoming more prevalent. Fast-chirp FMCW radar converts the sampled time-domain data from each chirp to a 2D range-Doppler frequency spectrum, typically via a 2D fast Fourier transform (FFT) process.

The 2D frequency spectrum for a fast-chirp FMCW victim radar and slow-chirp FMCW interfering radar is shown in Figure 8 using typical automotive MRR parameters. The vertical



**FIGURE 7.** The influence of victim and interfering radar FMCW sweeps on interference in the victim radar passband.

axis has been scaled to show the INR. In Figure 6, the time-domain impulse-like interference seen by each chirp of the fast-chirp victim radar sweeps over the frequency in a linear fashion with respect to time. The corresponding interference frequency spectrum for each chirp of the victim radar (ranging frequency domain) sweeps through Doppler frequency in a linear fashion and then folds into the ambiguous Doppler interval of the victim radar. The resulting 2D range-Doppler frequency spectrum exhibits a “noise-like” response. For MRR, the simulation shows that the resulting INR is roughly 15–20 dB.

To help illustrate the parameters  $D_F$  (and  $K$ ) in (6) (i.e., the equation for determining the PSD of interference and ultimately the INR), consider the case of a fast-chirp FMCW victim radar with dwell parameters in Figure 9 and an interfering

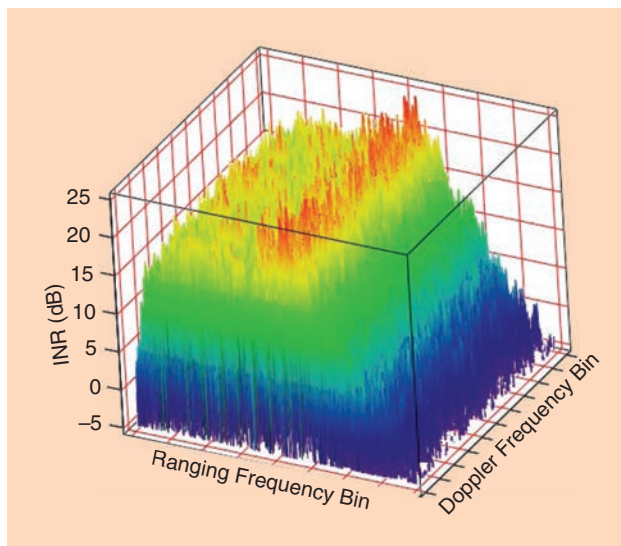


**FIGURE 8.** A 2D range-Doppler spectrum for fast-chirp FMCW victim radar with slow-chirp FMCW interfering radar.

radar with the same type of signal. This example has four 16.67-ms fast-chirp dwells in 100 ms for an overall duty factor of 67%. There are two fast-chirp dwell types, A and B, sweeping 500 and 250 MHz, respectively. Each dwell type has two complementary dwells, i.e., 1 and 2, with 512 and 450 chirps, respectively. The four-dwell sequence therefore uses four different fast-chirp sweeps.

For the dwell sequence and timing shown in this section, the probability of the victim radar encountering interference with a different chirp slope (leading to crossing FMCW slopes that produce a wideband interference spectrum) is effectively unity with the different cases and their respective  $K$  factors.

- Victim radar dwell A1—interfering radar dwell B1 ( $K = 4$ )
- Victim radar dwell A1—interfering radar dwell A2 ( $K = 16$ )
- Victim radar dwell A1—interfering radar dwell B2 ( $K = 3.5$ )
- Victim radar dwell B1—interfering radar dwell A2 ( $K = 4$ )
- Victim radar dwell B1—Interfering Radar Dwell B2 ( $K = 16$ )
- Victim radar dwell A2—interfering radar dwell B2 ( $K = 4$ ).

As previously noted,  $K = 1$  if the slopes are the same magnitude but opposite in sign. As the slopes become more similar, the crossing rate decreases and  $K$  increases. The factor  $D_F$  equals the fractional overlap of the dwells and varies from roughly 0.002 for the overlap of a single chirp (1/512), to 1 for a complete overlap. For each of the aforementioned cases, the probability of at least one chirp overlap is 33% and the probability of at least a 50% overlap ( $D_F \geq 0.5$ ) is 16.7%. Considering all of the cases, the composite probability of at least two dissimilar slopes with at least a 50% overlap is 83%.

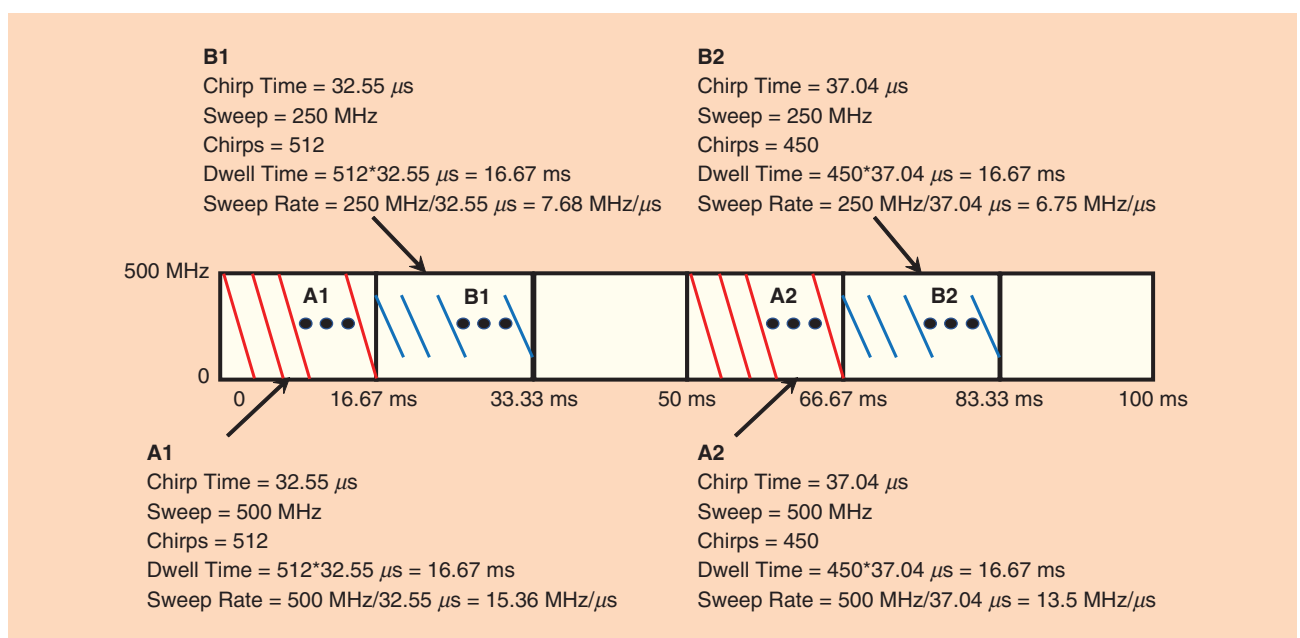


**FIGURE 9.** An example of a fast-chirp FMCW dwell sequence and its associated parameters.

The mechanism and characteristics of FMCW-to-FMCW interference in Figure 6(a) are shown for the single dwell/chirp of an interfering radar. In practice, the interference characteristics seen by an FMCW victim radar in the presence of multiple FMCW interfering radars of different types (e.g., SRR, MRR, LRR, or multimode using fast- and/or slow-chirp FMCW waveforms) can be quite complex with many impulse-like signals of different amplitudes and widths spread across the time domain.

### PMCW-PMCW

Consider a victim and interfering radar, both of which utilize PMCW modulation. Figure 10(a) and (b) shows the mechanism of interference and the resulting time-domain and frequency-domain responses. PMCW interference with random, noise-like biphasic coding using chip rate  $\Delta f_i = 1/T_c$  is assumed and appears as a spread-spectrum noise-like signal with bandwidth  $\Delta f_i = 1/T_c$  centered at carrier frequency  $f_c$ . In the example chip rate  $\Delta f_i = 1/T_c$  with bandwidth  $\Delta f_v = 1/T_c$ , the PMCW victim radar is likewise assumed to transmit a PMCW biphasic-coded noise-like signal with the same chip rate, bandwidth, and carrier (center) frequency as the interfering PMCW radar but with an independent, uncorrelated spreading code. The victim PMCW radar downconverts the received signal with a constant local oscillator frequency at the common carrier frequency (shown as  $f_1 = f_c$ ) and demodulates the received signal with a delayed copy of the PMCW biphasic code (chip rate  $\Delta f_i = 1/T_c$  and bandwidth  $\Delta f_v = 1/T_c$ , assumed to be the same as the corresponding parameters of the PMCW interfering radar in the example shown). Following downconversion, demodulation, and bandpass filtering in the victim radar, the interference appears as a noise-like signal in both time and frequency domains. The resulting frequency spectrum is broadband and often well above

the background noise floor, as illustrated in Figure 10(b) using representative parameters for automotive MRR (i.e., 15–20 dB above noise).

### PMCW-FMCW (or FMCW-PMCW)

Consider a victim radar with biphasic PMCW modulation and interfering radar with FMCW modulation or vice versa. Figure 11 illustrates the interference mechanism and the resulting time-domain and frequency-domain responses. In both situations (i.e., PMCW victim/FMCW interferer or FMCW victim/PMCW interferer), the interference is noise like in the time and frequency domains and, all else being equal, the INR is the same.

#### Comments on interference for PMCW versus FMCW modulation

Considering situations with FMCW or PMCW modulation for either the victim and/or interfering radars, the INR scales are

$$\begin{aligned} \text{INR} &\propto \frac{P_{i,v}}{B_i}, \quad \dots \quad \text{PMCW victim or PMCW interferer} \\ \text{INR} &\propto K \frac{P_{i,v}}{B_i}, \quad \dots \quad \text{FMCW victim and FMCW interferer}, \end{aligned} \quad (12)$$

where  $P_{i,v}$  is the power of the interferer received at the victim radar. Downconversion/demodulation and subsequent signal processing in the victim radar generally result in spreading of the interference in a noise-like fashion over the passband and/or detection band. The resulting INR is then given by the PSD of interference divided by the PSD of noise in the victim radar. The PSD of interference in the victim radar depends on the bandwidth of the interferer,  $B_i$  (i.e., the frequency spread of interference), and the interference power received by the victim radar,  $P_{i,v}$ , which is determined by using the “one-way”

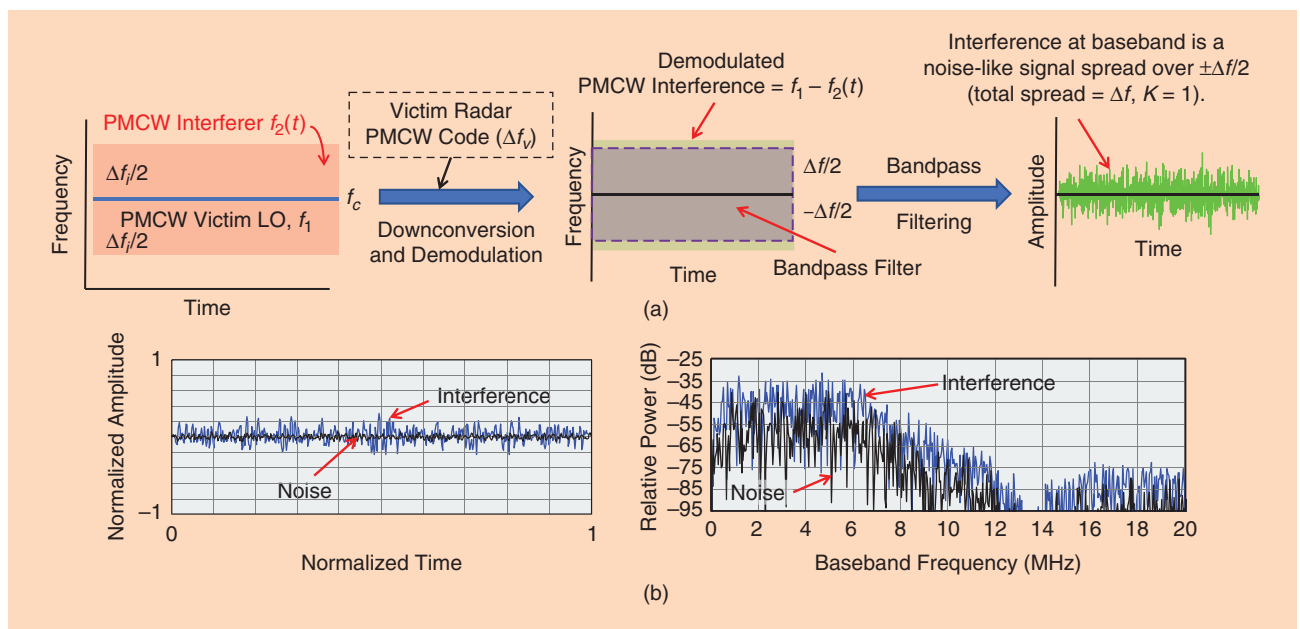


**FIGURE 10.** (a) An PMCW-to-PMCW interference mechanism with biphasic noise coding and (b) its simulated time-frequency domain characteristics.

radar equation. However, in the case of FMCW to FMCW, the frequency spread of interference after downconversion to baseband in the victim radar, and thus its PSD at baseband, depends on the relative FM sweep rates (FM slopes) of victim and interfering radars (reflected in the parameter  $K$ ). If the FMCW victim and interfering radar slopes are similar, the interference power is downconverted into a narrow frequency band increasing the PSD compared to that of dissimilar slopes ( $K > 1$ ). Hence, all else being equal, situations with phase modulation (PMCW) for either the victim or interfering radar generally results in lower INR levels.

### Interference mitigation

Interference analysis and interference mitigation techniques in radar systems have been investigated in a number of projects and reported in a number of papers. Recently, significant research has focused on a victim radar that employs FMCW modulation subject to interference from radars using FMCW modulation as well (see [17] and [21]–[24]). In this section, we focus on interference mitigation techniques.

Techniques that mitigate interference in automotive radars include transmission techniques (e.g., frequency hopping and timing jitter) and receiver techniques (e.g., time-domain excision). Generally, transmission techniques rely on ensuring that different radars transmit in such a way that the signals are nearly orthogonal to each other in some domain (e.g., polarization, time, and frequency). Most of the studies on interference in automotive radar are focused on interference mitigation at the receiver for both the interfering radar and the victim radar (e.g., the FMCW interferer and victim). The MOSARIM project [19], [20] completed a comprehensive study of interference in automotive radar systems that focused on interference mitigation. Interference mitigation techniques were grouped into six

different major domains/categories: polarization domain, time domain, frequency domain, coding domain, space domain (e.g., beamforming), and strategic approaches. Strategic approaches included detecting interference and changing waveform parameters and/or beamscanning in response, as well as detecting and excising interference with a subsequent repair of the received signal in either the time, frequency, or joint-time-frequency domains. Another strategic technique considered was the general concept of intervehicle communication that negotiates noninterfering radar parameters (e.g., time or frequency slots).

With the exception of the polarization domain, many of the techniques described in the MOSARIM project involved substantial signal processing for processing complex waveforms, adaptively nulling interference, and/or detecting and excising interference. Techniques with the highest level of signal processing complexity include digital beamforming with adaptive nulling, time-frequency transforming with detection and excision of interference, and space-time adaptive processing.

The MOSARIM project performed modeling, simulations, and tests of interference to automotive radar of the aforementioned mitigation techniques and concluded that [16]: “To assure an I/N level of 0 or  $-10$  dB, reliable mitigation techniques in the order of (a minimum of) 50 dB mitigation margin are needed.” In assessing the capability of interference mitigation, MOSARIM concluded that individual mitigation techniques are not adequate, multiple techniques will need to be applied and, as automotive radar volumes increase, it may be beneficial to include, via regulatory means, the assignment of polarization and frequency bands depending on the radar application/type (e.g., SRR, MRR, or LRR) and on-vehicle mounting location. An example of this is using different subbands in various directions (front, back, and side) and using different polarizations.

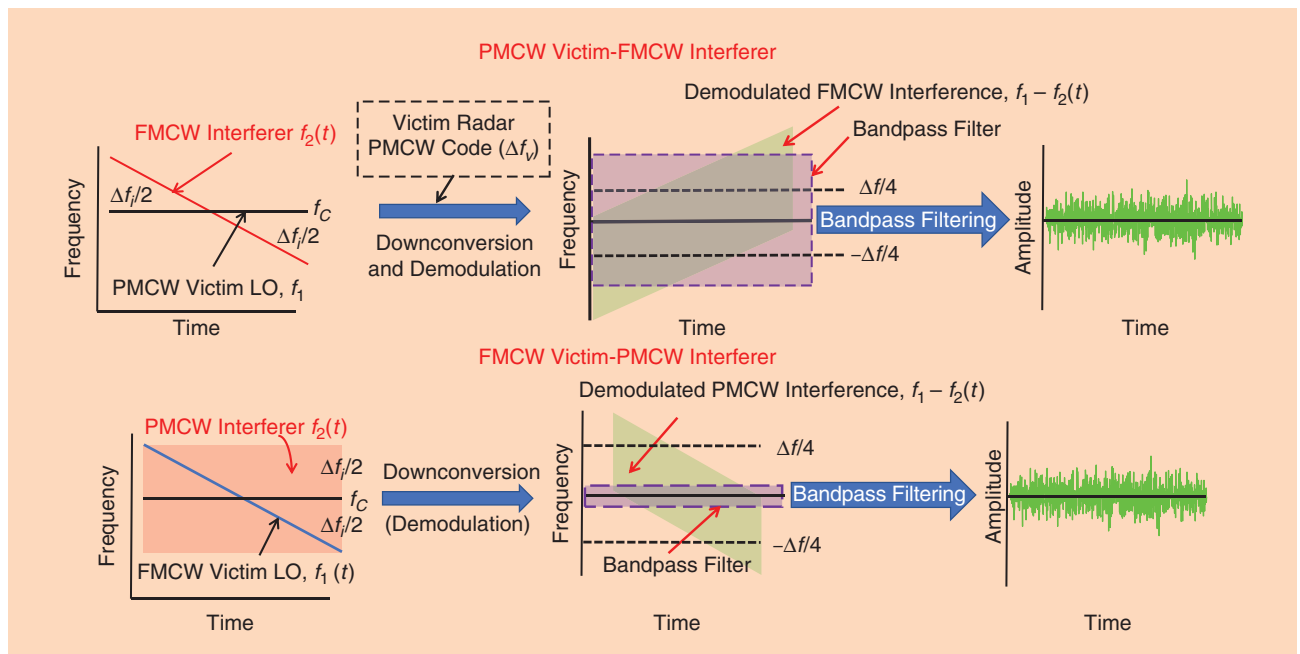


**FIGURE 11.** The mechanism of biphasic noise PMCW-to-FMCW interference.

Since the MOSARIM study concluded, research has continued on interference in automotive radar. As described in the “Mechanisms and Characteristics of Interference” section, an interfering radar with the same structure as the victim radar can create a “ghost target” if that signal, when received at the victim radar, begins a sweep within a small window of time proportional to the bandwidth of the filter. However, it is much more likely that the interfering radar creates a noise-like signal. In [17], a single FMCW interferer with a victim FMCW radar was considered. The SIR was derived as a function of the distance between the interferer and the victim radar and the distance between the target and the victim radar. Using these parameters, the region where the SIR was above some threshold (e.g., 10 dB) for a given target size was calculated. The effect of the FMCW chirp slopes on the SIR was determined. In [17], the conclusion noted that interference can cause a victim radar to “lose a target.” As an example, an FMCW radar with a processing gain (time-bandwidth product) of 50 dB and an interferer that is 10 m away will cause the SIR to drop below 10 dB when the target is 30 m away. Because FMCW radars have been the dominant type of radar used in automotive applications, there are quite a few papers that analyze the performance of an FMCW radar interferer on a victim FMCW radar.

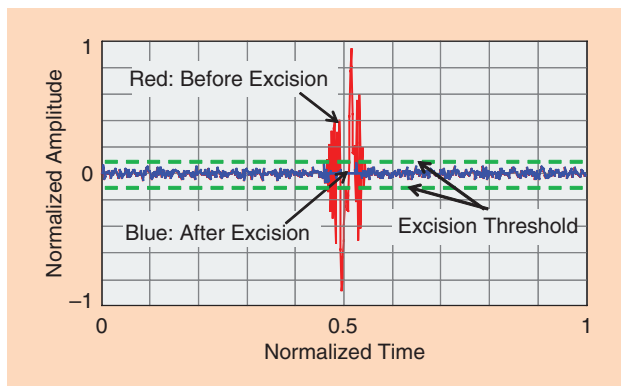


**FIGURE 12.** The simulated time-domain response before and after time-domain excision for FMCW interference (includes target + noise + interference).

Techniques that mitigate an FMCW interferer on an FMCW victim include time-domain excision of various forms [7], [21], [23], [25]–[27]. The results of a basic simulation with time-domain excision for a slow-chirp FMCW interferer and a fast-chirp FMCW victim radar are shown in Figures 12 and 13. As previously discussed, with an interferer FMCW sweep crossing a victim radar FMCW sweep, the interference appears as a linear chirp signal after downconversion in the victim radar receiver. The linear chirp interference signal sweeps through the victim radar passband and, assuming “fast-crossing” sweeps, produces an “impulse-like” signal in the time domain after bandpass filtering in the victim radar receiver. Prior to 2D range-Doppler FFT-matched filtering in a fast-chirp victim radar, the target signal is typically well below the noise level while the impulse-like interference signal is well above the noise level. Matched filtering provides substantial integration gain for a target-like constant frequency signal, while the impulse-like interference signal spreads in a noise-like fashion over the range-Doppler frequency spectrum.

Basic time-domain excision uses a threshold above the background noise level to remove interference. In other words, time-domain samples above the threshold are set to zero. Simulated results before and after time-domain excision are shown in Figure 12 for one chirp of the fast-chirp victim radar. Note that the simulated example includes target, interference, and noise. Time-domain excision is repeated for each chirp.

Simulated results for the range-Doppler frequency response of the fast-chirp victim radar are shown in Figure 13. Results correspond to the cases of target + noise (no interference) and for target + interference + noise, first without time-domain excision and then with time-domain excision. As shown, without any mitigation, the interference substantially raises the “noise” floor and masks the target. Time-domain excision is able to remove the FMCW interference while preserving the target signal; however, as expected, some signal loss and potential for artifacts occur depending on the amount and pattern of excision required.

The simulated example illustrates time-domain excision for the case of a single interferer. Overall effectiveness degrades

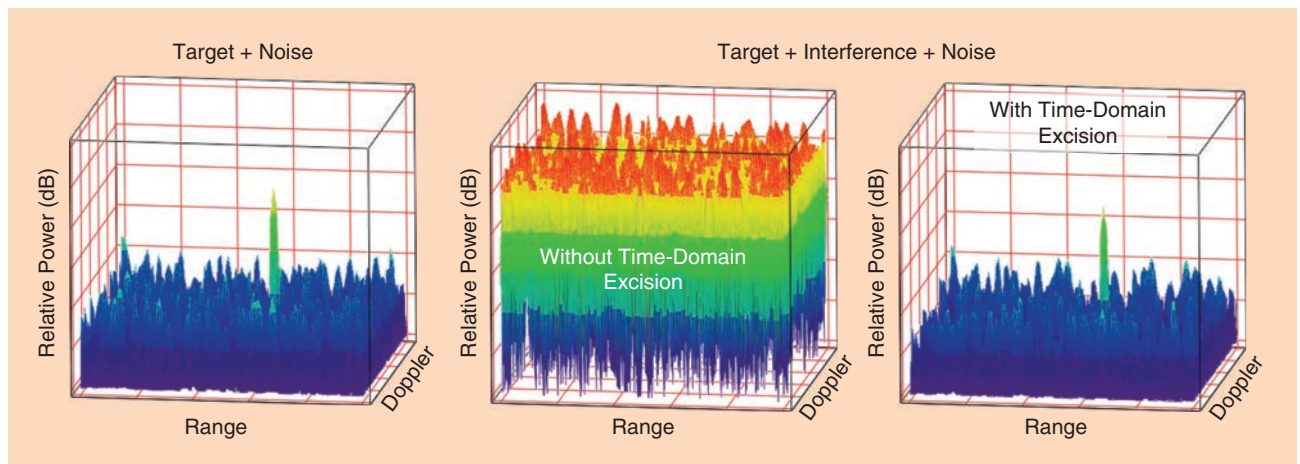


**FIGURE 13.** The fast-chirp FMCW range-Doppler frequency response without and with time-domain excision for FMCW interference.

as the number of interferers increases and the corresponding portion of the time domain to be excised becomes substantial. Although mitigation of a single FMCW interferer on an FMCW victim is fairly well understood, there is much ongoing research into other scenarios.

### Ongoing and future research

Although simple interference mitigation techniques are generally well understood—with some having been implemented in automotive radars—interference mitigation is an important and ongoing area of R&D. Typically, a radar system will have a receiver structure, as shown in Figure 14. The RF front end includes analog components such as a low-noise amplifier, mixers, and filters. The output of the RF front end is converted to digital by an analog-to-digital converter (ADC). The first process step is range processing, which is an FFT in an FMCW radar system and a matched filter in a PMCW radar system. Range processing is followed by Doppler processing, which is followed by beamforming, object detection, and tracking. Interference mitigation may be added to the block diagram, potentially at different points in the processing steps. One technique used to mitigate the effect of an interferer (either FMCW or PMCW) is isolating the part of the signal that does not have interference; this may be implemented using a time-domain notch filter in an FMCW system or a “zero-forcing” type of detector in a PMCW system (as discussed further in this section). However, these techniques also remove a portion of the desired signal and can become problematic as the number of interferers grow. Time excision would typically happen between the output of the ADC and the input of the range-matched filter.

In [23], the interference cancellation of a single FMCW interferer on an FMCW victim by identifying the interference location using techniques from image processing and then “zeroing out” those time locations with additional smoothing to avoid ringing effects, shows that without interference cancellation, the victim radar would not be able to detect a certain target due to the increase in noise level, but with interference cancellation, the radar is able to detect the target. In [25], the characteristics of an FMCW-interfering signal, which are much stronger than the desired signal reflected from the target on an FMCW victim radar, are estimated and then subtracted from the overall signal, thereby improving the receiver sensitivity. This technique would also work for multiple radars as long as the interference from one radar did not overlap in time with the interference from another radar. This interference mitigation would also occur before the range-FFT processing. In [7], interference mitigation not requiring a threshold (compared to normal time-domain excision) was considered and shown to be effective, even for

multiple interfering radars. In [24], beamforming using multiple receiving antennas was considered for eliminating a single interferer. Simulations with a CW signal as the interference source and an 800-MHz bandwidth FMCW signal for the victim radar show that the interference reduced by 40 dB. Here, four receiving antennas were used with optimal weighting to remove the interference. Measurements corresponding to the simulation show that the resulting INR was under 2 dB [24, Table 1] for a single interferer. This interference mitigation technique would be applied in the beamforming processing unit. In [27], an FMCW interferer and victim were considered, where again, the interference is detected and zeroed out. Although this does reduce the noise level because of the interferer, it also removes the desired signal over a certain time period when the frequency of the interferer falls within a certain frequency range of the victim radar. To mitigate this effect, [27] considered a technique that regenerates the desired signal during the time when the received signal was zeroed out. An iterative algorithm was used for that purpose and allowed for smaller targets to be detected than would have otherwise been detected with just the zeroing-out approach (with or without additional smoothing).

Interference in cellular communication systems has been the subject of considerable investigation. Code-division multiple access (CDMA)—the communication version of a PMCW radar—has been widely deployed in 2G and 3G cellular systems. The processing gain associated with PMCW signals, similar to the CDMA signals used for communications, allows for multiple radars to be used simultaneously.

In a PMCW–PMCW scenario, the large number of spreading codes generally ensures the interference will be a wideband, noise-like signal because each radar can use a different spreading code. There are a number of techniques that can be used in PMCW–PMCW situations to improve the interference mitigation capability. Although some of these techniques require knowing the spreading codes of other radars, there are also “blind” techniques that work without that knowledge [28]. These are the same techniques that are useful in a communications context (e.g., CDMA). These techniques do not completely eliminate interference but may drastically reduce its effect, especially in a near-far scenario similar to multiple interferers versus a victim receiver, and work best when the interference is periodic in nature, i.e., the spreading codes repeat after a certain number of chips (in much the same way an FMCW type of radar would have a repetitive signal). The interference mitigation in CDMA systems (i.e., PMCW) is based on the cyclostationary structure of the interfering signal. These interference mitigation techniques are based on estimating the correlation matrix of the received signal, then employing an “orthogonalizing matched

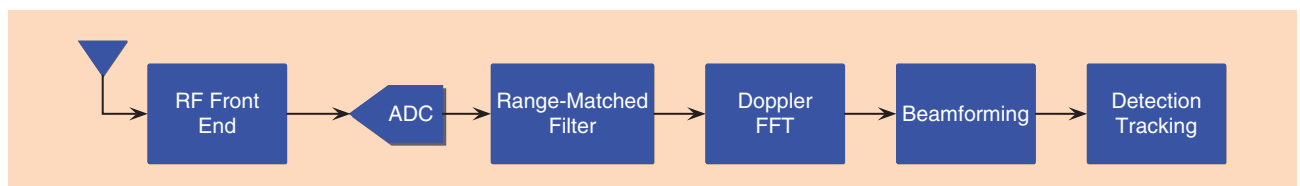


**FIGURE 14.** A generic receiver structure for radar.

filter” [29]. Note that the radar problem is easier to correct than the communication problem, because for the communication problem, there is an additional unknown (i.e., the data).

An FMCW interferer on a victim PMCW radar is very similar to a jammer in a spread-spectrum system. This type of interference, as well as effective mitigation techniques, has been well studied. An FMCW interferer signal to a PMCW victim is the same as that of a “swept-tone jammer” in spread-spectrum communication systems discussed in [30] and [31]. The performance measure in a spread-spectrum communication system is typically bit error rate, rather than the typical performance measures used in a radar system. Nevertheless, the mitigation techniques would be similar.

A PMCW interferer on a victim FMCW radar system can appear as just additional noise that might seem difficult to mitigate in the time domain. However, the PMCW signal’s spectral characteristics can be estimated and used to improve the filtering that may reject wideband color noise [32]. Certain short-term time-frequency processing techniques may be able to mitigate this interference [33]. As with other classes of interferer and victim radars, transmission techniques such as polarization or frequency separation can be applied here.

Because both FMCW and PMCW types of radar are essentially spread-spectrum types of systems, interference mitigation techniques applicable to spread-spectrum communication systems may potentially be of use in radar systems. One technique for mitigating strong interference in the presence of a weak signal is based on locally optimum Bayesian detection. For example, [34] considers a spread-spectrum signal in the presence of different types of interference and noise. Although the focus of these techniques is on communication systems, they have potential for application in radar systems as well.

Future research that addresses interference to automotive radar sensors includes joint radar/communication systems [35], decentralized multiple-access protocols, and alternative modulation techniques (and the corresponding matched-filter signal processing) that limit the potential for, and subsequent level of, interference. Further development of joint, multiple-domain-adaptive signal processing algorithms that excise/null interference within the polarization-spatial-temporal-frequency domains must be explored as well.

One aspect of interference mitigation to consider is multiple-access techniques at the transmitter. In other words, by coordinating transmission (e.g., in the time domain, frequency domain, and polarization domain), interference can be prevented from occurring. We note that this type of problem has been studied extensively in the context of communication systems, where information-theoretic formulations can be used to determine the possible rates of data transmission for different users. Of course, the radar problem is different in that data are not transmitted and targets are detected. Nevertheless, approaches to multiple access must be investigated.

## Conclusions

In general, automotive radar systems include a substantial level of inherent resistance to interference by virtue of a large time-

bandwidth product. The time-bandwidth product is the processing gain of a radar system (i.e., the time-bandwidth product is related to its ability to reject interference). Regardless, with an increasing number of radars deployed per vehicle and an increase in the number of vehicles having radars, interference levels, especially in certain situations such as rush-hour traffic, will likely be quite severe. Automotive radar manufacturers have been active in developing and implementing many of the mitigation techniques described in this article that reduce the impact of mutual interference.

Because radars are becoming pervasive and ubiquitous on automobiles and perform safety-critical functions, there is a need to optimize interference mitigation both at the transmitter and receiver by limiting the amount of interference so that victim radar performance can be affected only up to a prescribed amount. To this end, developing standards will make the engineering of interference mitigation easier and more effective.

## Authors

**Stephen Alland** (swalland@uhnder.com) received his B.S. and M.S. degrees in electrical engineering from Rensselaer Polytechnic Institute, Troy, New York, in 1976 and 1977, respectively. He is a radar consultant with more than 40 years of experience in radar systems, including 22 years in automotive radar systems. Previously, he was a technical fellow and manager for advanced radar development with Delphi Electronics and Safety in Malibu, California. From 1995 to 2014, he worked for Delphi to develop automotive radar systems. Prior to Delphi, he worked for Hughes to develop air defense radar systems, beginning in 1977. He holds 21 U.S. patents related to radar systems. His technical areas of expertise include radar system design and simulation, radar waveform design, radar signal processing, and target tracking.

**Wayne Stark** (stark@eecs.umich.edu) received his B.S., M.S., and Ph.D. degrees in electrical engineering from the University of Illinois, Urbana, in 1978, 1979, and 1982, respectively. Since 1982, he has been a faculty member in the Department of Electrical Engineering and Computer Science at the University of Michigan, Ann Arbor. He was selected by the National Science Foundation as a 1985 Presidential Young Investigator. He received the IEEE Military Communications Conference (MILCOM) Board 2002 Technical Achievement Award for sustained contributions to military communications. In 2009, he was corecipient of the IEEE MILCOM Ellersick Prize for best paper in the Unclassified Technical Program. In 2010, he received the Journal of Communications and Networks Best Paper Award. He is on the editorial board of *IEEE Journal on Selected Areas of Communications*. His research interests include the areas of coding and communication theory, spread-spectrum systems, wireless communication networks, and radar systems. He is a Fellow of the IEEE.

**Murtaza Ali** (murtaza@uhnder.com) received his B.S. degree in electrical engineering from Bangladesh University of Engineering and Technology, Dhaka, in 1989, and his

Ph.D. degree in electrical engineering from the University of Minnesota, Twin Cities, in 1995. He is currently the director of systems engineering at Uhnder, Inc. Prior to joining Uhnder, he was a Distinguished Member of Technical Staff, and manager of the Perception and Analytics Lab at Texas Instruments (TI). At TI, he led R&D teams for millimeter-wave radar, mobile WiMAX, and asymmetric digital subscriber line systems. He also represented TI in various standards organizations including Telecommunications Industry Association, the International Telecommunication Union, HomePlug, Home Phone line Networking Association, and the IEEE. His research interests include development of novel communications and signal processing systems. He holds 32 U.S. patents and has published more than 40 papers in refereed and invited forums. He is a Senior Member of the IEEE.

**Manju Hegde** (manju@uhnder.com) received his B.S. degree in electrical engineering from the Indian Institute of Technology, Bombay, and his Ph.D. degree in computer information and control engineering from the University of Michigan, Ann Arbor, in 1987 and 1979, respectively. He is the chief executive officer (CEO) of Uhnder Inc. Previously, he was the corporate vice president at Advanced Micro Devices (AMD), where he was responsible for driving and executing AMD's strategy across technology and marketing functions into the client and server computing ecosystems. He also cofounded and led AMD Ventures before joining AMD. He was vice president of Compute Unified Device Architecture technical marketing at Nvidia, where he focused on training and enabling researchers and developers to leverage the parallel architecture and performance of global processing units for general purpose applications. He was cofounder and CEO of AGEIA Technologies from its inception in 2002.

## References

- [1] B. Schoettle, "Sensor fusion: A comparison of sensing capabilities of human drivers and highly automated vehicles," Univ. of Michigan Transportation Res. Inst., Ann Arbor, Tech. Rep. SWT-2017-12, 2017.
- [2] G. Rudolph and U. Voelzke, "Three sensor types drive autonomous vehicles," *Sensors Mag.*, Nov. 2017. [Online]. Available: <https://www.sensorsmag.com/components/three-sensor-types-drive-autonomous-vehicles>
- [3] I. Bilik, O. Bialer, S. Villevale, H. Sharifi, K. Kona, M. Pan, D. Persechini, M. Musni et al., "Automotive MIMO radar for urban environments," in *Proc. IEEE Radar Conf.*, 2016, pp. 1–6. doi: 10.1109/RADAR.2016.7485215.
- [4] I. Bilik, S. Villevale, D. Brodeski, H. Ringel, O. Longman, P. Goswami, C. Y. Kumar, S. Rao et al., "Automotive multi-mode cascaded radar data processing embedded system," in *Proc. IEEE Radar Conf.*, 2018, pp. 0372–0376.
- [5] F. Engels, P. Heidenreich, A. M. Zoubir, F. K. Jondral, and M. Wintermantel, "Advances in automotive radar: A framework on computationally efficient high-resolution frequency estimation," *IEEE Signal Process. Mag.*, vol. 34, no. 2, pp. 36–46, 2017.
- [6] F. Engels, M. Wintermantel, and P. Heidenreich, "Automotive MIMO radar angle estimation in the presence of multipath," in *Proc. IEEE Radar Conf. (EURAD)*, 2017, pp. 82–85.
- [7] M. Wagner, F. Sulejmani, A. Melzer, P. Meissner, and M. Huemer, "Threshold-free interference cancellation method for automotive FMCW radar systems," in *Proc. IEEE Int. Symp. Circuits and Systems*, 2018, pp. 1–4.
- [8] H. H. Meinel and J. Dickman, "Automotive radar: From its origin to future directions," *Microw. J.*, vol. 56, no. 9, pp. 24–40, Sept. 2013.
- [9] H. H. Meinel, "Evolving automotive radar: From the very beginnings into the future," in *Proc. European Conf. Antennas and Propagation (EuCAP)*, 2014, pp. 3107–3114.
- [10] M. I. Skolnik, *Introduction to Radar*. New York: McGraw-Hill, 1962.
- [11] S. M. Patole, M. Torlak, D. Wang, and M. Ali, "Automotive radars: A review of signal processing techniques," *IEEE Signal Process. Mag.*, vol. 34, no. 2, pp. 22–35, 2017.
- [12] M. Schneider, "Automotive radar—status and trends," in *Proc. German Microwave Conf.*, 2005, pp. 144–147.
- [13] E. G. Hoare and R. Hill, "System requirements for automotive radar antennas," in *Proc. IEEE Colloq. Antennas for Automotives*, Mar. 2000, pp. 1–11.
- [14] E. Garcia, J. A. Paredes, F. J. Alvarez, M. C. Perez, and J. J. Garcia, "Spreading sequences in active sensing: A review," *Signal Process.*, vol. 106, pp. 88–105, Jan. 2015.
- [15] N. Levanon, "Multifrequency complementary phase-coded radar signal," *IEE Proc.—Radar, Sonar Navigation*, vol. 147, no. 6, pp. 276, 2000.
- [16] M. Kunert, "Final report," European Commission: MOre safety for all by radar interference mitigation (MOSARIM), Luxembourg, Tech. Rep. 248231, 2010. [Online]. Available: <https://cordis.europa.eu/project/rcn/94234/reporting/en>
- [17] T. Schipper, M. Harter, T. Mahler, O. Kern, and T. Zwick, "Discussion of the operating range of frequency modulated radars in the presence of interference," *Int. J. Microw. Wireless Technol.*, vol. 6, no. 3–4, pp. 371–378, 2014.
- [18] J. Hasch, E. Topak, R. Schnabel, T. Zwick, R. Weigel, and C. Waldschmidt, "Millimeter-wave technology for automotive radar sensors in the 77 GHz frequency band," *IEEE Trans. Microw. Theory Techn.*, vol. 60, no. 3, pp. 845–860, 2012.
- [19] M. Ahrholdt, F. Bodereau, C. Fischer, M. Goppelt, R. Pietsch, A. John, A. Ossowska, and M. Kunert, "D12.1-Study report on relevant scenarios and applications and requirements specification," European Commission: MOre Safety for All by Radar Interference Mitigation (MOSARIM), 2010. [Online]. Available: <https://cordis.europa.eu/project/rcn/94234/reporting/en>
- [20] M. Kunert, F. Bodereau, M. Goppelt, C. Fischer, A. John, T. Wixforth, A. Ossowska, T. Schipper et al., "D1.5-Study on the state-of-the-art interference mitigation techniques," Technical report, European Commission: MOre Safety for All by Radar Interference Mitigation (MOSARIM), 2010. [Online]. Available: <https://cordis.europa.eu/project/rcn/94234/reporting/en>
- [21] M. Umehira, T. Nozawa, Y. Makino, X. Wang, S. Takeda, and H. Kuroda, "A novel iterative inter-radar interference reduction scheme for densely deployed automotive FMCW radars," in *Proc. 19th Int. Radar Symp. (IRS)*, 2018, pp. 1–10. doi: 10.23919/IRS.2018.8448223.
- [22] M. Goppelt, H.-L. Blöcher, and W. Menzel, "Analytical investigation of mutual interference between automotive FMCW radar sensors," in *Proc. 6th German Microwave Conf.*, 2011, pp. 1–4.
- [23] M. Barjenbruch, D. Kellner, K. Dietmayer, J. Klappstein, and J. Dickmann, "A method for interference cancellation in automotive radar," in *Proc. IEEE MTT-S Int. Conf. Microwaves for Intelligent Mobility (ICMIM)*, 2015, pp. 1–4.
- [24] J. Bechter, K. Eid, F. Roos, and C. Waldschmidt, "Digital beamforming to mitigate automotive radar interference," in *Proc. IEEE MTT-S Int. Conf. Microwaves for Intelligent Mobility (ICMIM)*, 2016, pp. 1–4.
- [25] J. Bechter and C. Waldschmidt, "Automotive radar interference mitigation by reconstruction and cancellation of interference," in *Proc. IEEE MTT-S Int. Conf. Microwaves for Intelligent Mobility (ICMIM)*, 2015, pp. 1–4.
- [26] Z. Xu and Q. Shi, "Interference mitigation for automotive radar using orthogonal noise waveforms," *IEEE Geosci. Remote Sens. Lett.*, vol. 15, no. 1, pp. 137–141, 2018.
- [27] J. Bechter, F. Roos, M. Rahman, and C. Waldschmidt, "Automotive radar interference mitigation using a sparse sampling approach," in *Proc. European Radar Conf.*, 2017, pp. 90–93.
- [28] U. Madhow, "Blind adaptive interference suppression for direct-sequence CDMA," *Proc. IEEE*, vol. 86, no. 10, pp. 2049–2069, 1998.
- [29] K. Fukawa and H. Suzuki, "Orthogonalizing matched filter (OMF) detection for DS-CDMA mobile radio systems," in *Proc. Global Telecommunications Conf., Communications: The Global Bridge*, 1994, pp. 385–389.
- [30] G. Saulnier, P. Das, and L. Milstein, "An adaptive digital suppression filter for direct-sequence spread-spectrum communications," *IEEE J. Sel. Areas Commun.*, vol. 3, no. 5, pp. 676–686, 1985.
- [31] L. B. Milstein, "Interference rejection techniques in spread spectrum communications," *Proc. IEEE*, vol. 76, no. 6, pp. 657–671, 1988.
- [32] L. Milstein and P. Das, "An analysis of a real-time transform domain filtering digital communication system—part II: Wide-band interference rejection," *IEEE Trans. Commun.*, vol. 31, no. 1, pp. 21–27, 1983.
- [33] V. C. Chen and H. Ling, *Time-Frequency Transforms for Radar Imaging and Signal Analysis*. Norwood, MA: Artech, 2002.
- [34] S. N. Batalama, M. J. Medley, and I. N. Psaromiligkos, "Adaptive robust spread-spectrum receivers," *IEEE Trans. Commun.*, vol. 47, no. 6, pp. 905–917, 1999.
- [35] A. R. Chiriyath, B. Paul, G. M. Jacyna, and D. W. Bliss, "Inner bounds on performance of radar and communications co-existence," *IEEE Trans. Signal Process.*, vol. 64, no. 2, pp. 464–474, 2016.

Michael Gerstmair, Alexander Melzer,  
Alexander Onic, and Mario Huemer

# On the Safe Road Toward Autonomous Driving

*Phase noise monitoring in radar sensors for functional safety compliance*



The first approaches to improve vehicle safety were so-called passive safety systems, which did not directly interfere with the driving process but protected the occupants during a crash. In contrast, the first assistance system was the antilock braking system (ABS) successfully introduced in the early 1970s. This active system was developed to avoid an accident by automatically intervening in the braking behavior of the car. At about the same time, the first automotive radar prototype was presented. Since the invention of this very unwieldy radar system, organizations all around the world spent significant efforts in pushing the development of automotive radar systems forward. Today, radar sensors together with ultrasound sensors, lidar, and cameras form the backbone of advanced driver assistant systems (ADASs) as well as autonomous driving (AD), which is in the prototype stage. In particular, because of their robustness against adverse lighting and weather conditions, radar sensors are considered a key technology for modern vehicle safety and comfort systems. Along with the trend toward higher automation, more cars will be equipped with radar sensors in the near future. Because ADASs directly influence the vehicle dynamics, new regulating functional safety (FuSa) requirements, such as the ISO 26262 standard, were introduced. These requirements are mandatory to protect the road users.

Modern automotive radar systems make use of the frequency-modulated continuous wave (FMCW) principle. Despite many advantages to pulse-based radars, one of the most limiting factors of an FMCW radar is the phase noise (PN) contained in the transmit (Tx) signal, which significantly affects the sensitivity and range. To fulfill the ISO 26262 standard, it is thus of high importance to monitor the PN of a radar system throughout its whole lifecycle. In this article, we present the most common PN measurement and estimation techniques for CW signals. Further, we address the problem of estimating the PN of an FMCW signal, which is of particular relevance for automotive FMCW radars and the aforementioned monitoring to fulfill the FuSa requirements. Finally, we present state-of-the-art methods for PN estimation and monitoring in automotive FMCW radar systems.

## Introduction

The safety on our roads has been of the utmost importance since the beginning of mass motorization. The first approach to decrease the number of injuries and fatalities on the roads was the development of passive safety features such as seat belts and airbags. The aim of these passive features was to keep the vehicle's occupants protected in case of an accident. Subsequently, active systems for the prevention of accidents were invented. These safety systems proactively intervene into the driving behavior of the vehicle. The forefather of these systems was the ABS, which was followed by the traction control system and electronic stability control (ESC). With a rising degree of integration and a continuous improvement of performance and cost-efficiency, new sensors emerged for the use in ADASs, such as adaptive cruise control (ACC) or autonomous emergency braking (AEB). To fulfill the requirements of these systems, ultrasound sensors, lidars, and cameras as well as automotive radars were introduced [1]. The latter is considered a key technology for the aforementioned applications due to its unique advantage of featuring good performance even in bad weather conditions [2].

The history of ADASs as well as the designated sensor for various driver assistant systems is depicted in Figure 1. With the advent of increasingly complex safety applications, there is a growing demand of so-called imaging radar systems. Particularly for AD, these systems are required as they provide high angular resolution. In general, this is achieved by using a high number of Tx and receive (Rx) channels.

A key challenge for ADASs on the way toward AD is the necessity of safety mechanisms for the detection of systematic and random faults in both hardware and software. That trend is driven

further since the introduction of the ISO 26262 standard in 2011 [3]. Fulfilling this standard requires not only intensive verification and testing of the product functionality but also monitoring of safety-relevant parameters during operation. The latter is typically performed by built-in self-tests (BISTs). An overview of different realizations for possible integrated test solutions is provided in [4], while in [5], a built-in test architecture for radar receiver front ends is presented. These additional building blocks are increasing the complexity of ADASs and AD on the sensor and on the monolithic microwave integrated circuit (MMIC) levels.

Automotive radar applications are typically based on the FMCW principle. These radar systems are capable of simultaneously measuring the distance, velocity, and angle in elevation and azimuth of surrounding objects. One of the most limiting factors of FMCW radars in terms of range precision and detection sensitivity is signal distortions due to the PN contained in the Tx signal [6]. This signal is typically generated by a phase-locked loop (PLL), which inherently produces random fluctuations in the phase of the signal (the PN). Traditionally, the PN of a frequency-generating circuit is described by its power spectral density (PSD) measured after production under the use of expensive measurement equipment. However, the PLL may change its PN behavior with time, temperature, or supply voltage. Therefore, the estimation of the PN PSD is an important monitoring function, which requires on-chip and in-operation estimation techniques. To achieve the FuSa goals for ADASs and AD, it has to be ensured that the radar MMICs do not generate PN out of specification. This can be accomplished with proper monitoring features that are an integral part of this article. Prior to investigating this, the concept of FMCW radars is explained.

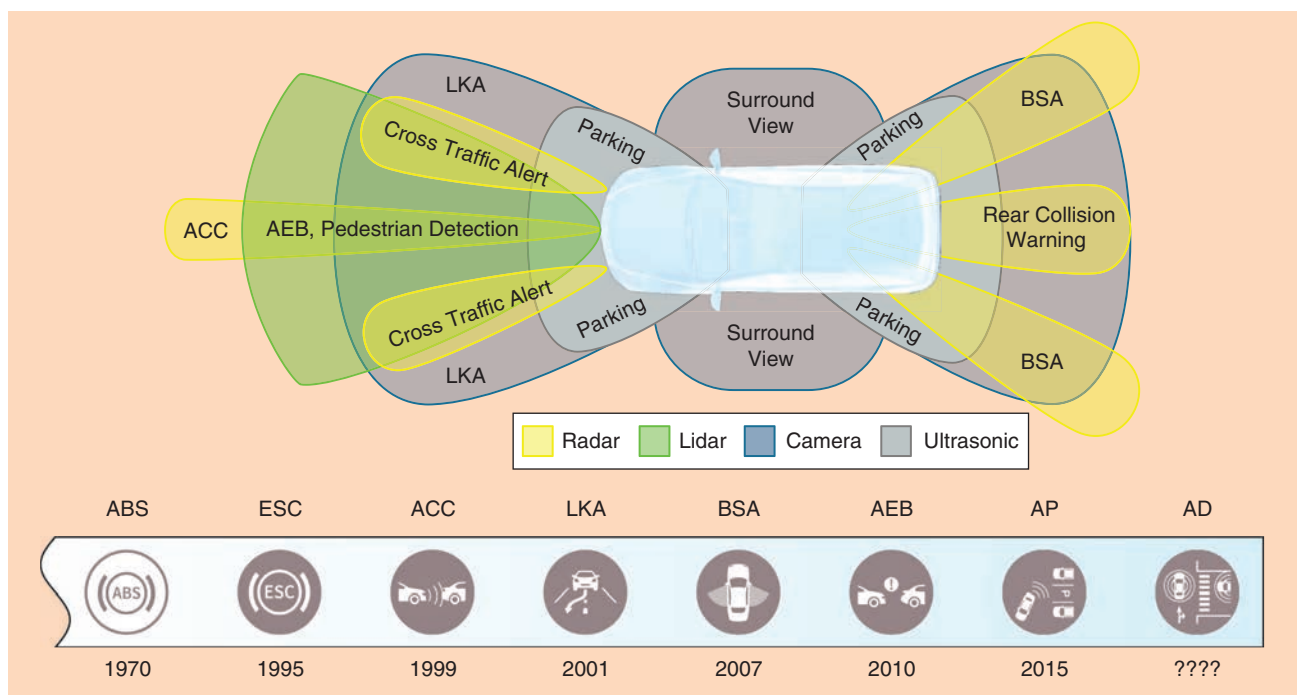


**FIGURE 1.** The history of active driver assistance systems, from the introduction of ABS in the early 1970s until future AD, and spatial coverage of ADAS sensors in a modern car. AP: autonomous parking; BSA: blind spot assist; LKA: lane keep assist.

## The FMCW radar principle

Modern automotive radar sensors typically use an FMCW modulation scheme working in frequency ranges from 76 to 81 GHz. Therefore, a frequency-generating circuit, e.g., a PLL, produces a linear frequency ramp (chirp), which is used as a Tx signal. When initially neglecting the effects of the PN and other noise sources, an ideal version of the Tx signal can be written as

$$s_{\text{Tx}}(t) = A_{\text{Tx}} \cdot \cos(2\pi f_0 t + \pi k t^2), \quad (1)$$

for  $t \in [0, T_{\text{CH}}]$ , where  $T_{\text{CH}}$  represents the time duration of one chirp-period. In (1),  $A_{\text{Tx}}$  and  $f_0$  are the amplitude and the starting frequency of the Tx signal, respectively. Further,  $k = B/T_{\text{CH}}$  is the frequency slope of the chirp, whose frequency sweep (often referred to as *sweep* or *chirp bandwidth* in radar literature) is denoted as  $B$ .

The Tx signal  $s_{\text{Tx}}(t)$  is emitted by a Tx antenna and reflected by the surrounding objects. For the sake of simplicity, the objects will be represented by simple point targets, each producing a single reflected electromagnetic wave. As illustrated in Figure 2(b), every object reflection can therefore be modeled as a damped and time-delayed version of the Tx signal. The sensed Rx signal can be calculated as the superposition of all object reflections and is thus given by

$$s_{\text{Rx}}(t) = \sum_{i=1}^N A_{\text{Tx}} \cdot \alpha_i \cdot \cos(2\pi f_0(t - \tau_i) + \pi k(t - \tau_i)^2), \quad (2)$$

where  $\alpha_i$  is a damping factor due to path and reflection losses corresponding to the signal contribution of the  $i$ th object reflection. The time delay  $\tau_i$  is typically referred to as round-trip delay time (RTDT) and represents the propagation time of the electromagnetic wave traveling from the Tx antenna to the object and back to the Rx antenna. Thus, the RTDTs  $\tau_i$  are proportional to the distances to the respective objects  $i = 1, \dots, N$  in the radar channel.

In the receiver, the Rx signal is multiplied with the instantaneous Tx [local oscillator (LO)] signal and subsequently filtered by an analog low-pass filter (LPF). The resulting signal is termed the *intermediate frequency (IF)* signal in the radar literature. A good overview of potential algorithms to process this IF signal to obtain range, relative velocity, and angle information of the surrounding objects is provided in [7]. In the sequel, we will present one possible method using the conventional 3D fast Fourier transform (FFT) approach in tutorial style.

### Range estimation

Assuming the static scenario (i.e., nonmoving objects) as depicted in Figure 2(a), the IF signal is given with

$$s_{\text{IF}}(t) = [s_{\text{Tx}}(t) * s_{\text{Rx}}(t)] * h_{\text{L}}(t) = \sum_{i=1}^N A_{\text{IF},i} \cdot \cos(2\pi f_{B,i} t + \Phi_i), \quad (3)$$

where  $*$  denotes the convolution operator and  $h_{\text{L}}(t)$  is the impulse response of the ideally assumed LPF. Further,  $A_{\text{IF},i} = (A_{\text{Tx}}^2 \cdot \alpha_i)/2$  and  $\Phi_i = 2\pi f_0 \tau_i - \pi k \tau_i^2$  are the amplitude and a constant phase term corresponding to the signal

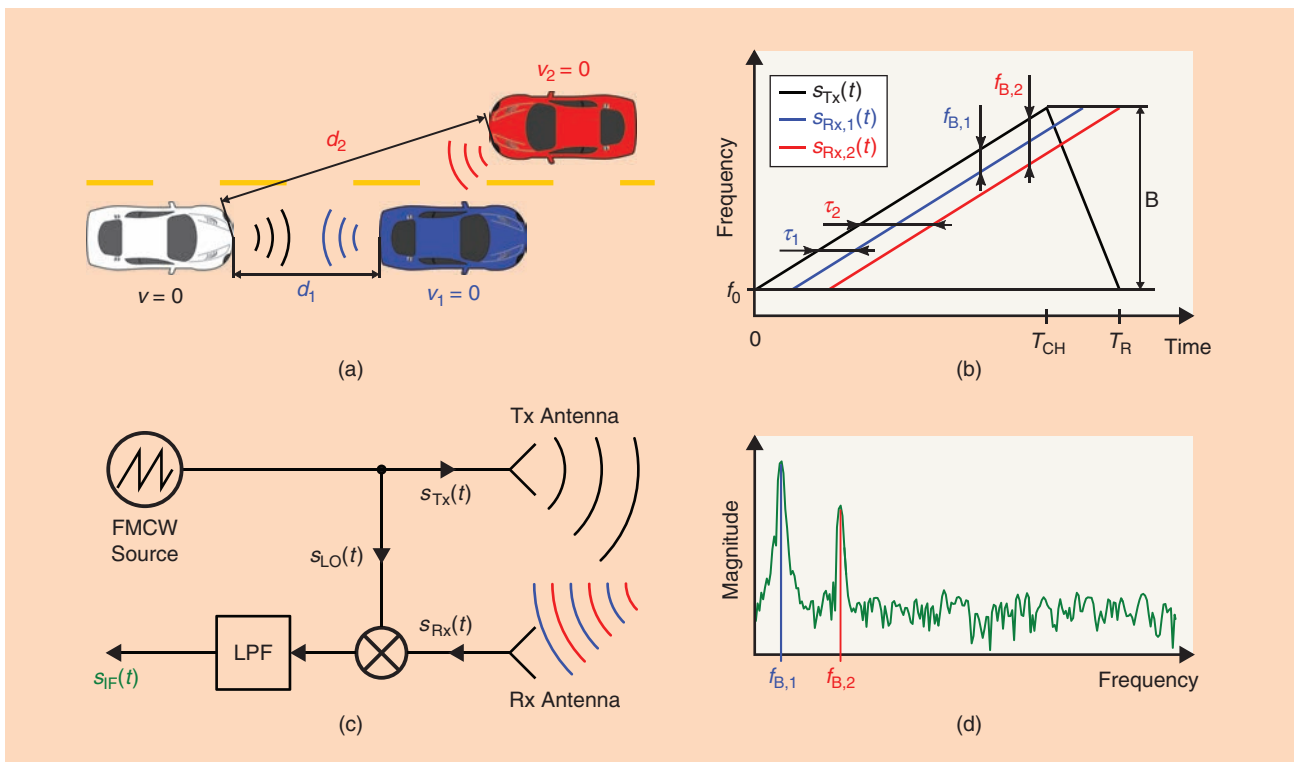


**FIGURE 2.** The FMCW radar system concept and range estimation method using an FFT approach in a static scenario (i.e., nonmoving objects). The (a) scenario, (b) time–frequency domain representation, (c) basic system model, and (d) range spectrum.

contribution of the  $i$ th object reflection, respectively. The term  $f_{B,i}$  is referred to as *beat frequency* and represents the instantaneous frequency difference between the LO and the Rx signal of each point target. As illustrated in Figure 2,  $f_{B,i}$  is proportional to the (one-way) distance  $d_i$  between the radar sensor and the  $i$ th object with

$$f_{B,i} = k \cdot \tau_i = \frac{B}{T_{CH}} \cdot \frac{2d_i}{c_0}. \quad (4)$$

According to (4) the estimation of  $f_{B,i}$  enables the range measurement, which is typically done using an FFT. An exemplary magnitude spectrum of the IF signal is depicted in Figure 2(d) showing two object reflections with the beat frequencies  $f_{B,1}$  and  $f_{B,2}$ , respectively.

### Velocity estimation

We now consider a dynamic scenario with two objects at the same distance but moving in opposite directions with relative velocities  $v_1$  and  $v_2$ , respectively. The scenario is depicted in Figure 3(a). Because the objects are located at the same distance, they share the same range bin in the magnitude spec-

trum and thus cannot be separated in the range domain. To estimate the velocity of the objects, one can take advantage of the Doppler effect. That is, the frequency of the received wave and, therefore,  $\tau_i$  slightly change over time according to the velocity of the object. To be able to measure the Doppler effect, several consecutive ramps are emitted as illustrated in the time–frequency domain representation in Figure 3(b). In a scenario with moving objects, the RTDT can be defined by

$$\tau_i(t) = \tau_{0,i} + \frac{2v_i}{c_0} t \quad (5)$$

with  $\tau_{0,i}$  representing the initial RTDT of the  $i$ th object in the radar channel. Using the time-varying RTDT (5), based on (3), and neglecting the terms providing insignificant impact on the radar measurement, the IF signal is given with

$$s_{IF}(t) = \sum_{i=1}^N A_{IF,i} \cdot \cos(2\pi(f_{B,i} + f_{D,i})t + \Phi_i), \quad (6)$$

containing the Doppler frequency  $f_{D,i} = f_0(2v_i/c_0)$ . To obtain the relative velocity, the Doppler frequencies have to be determined by estimating the phase difference between several

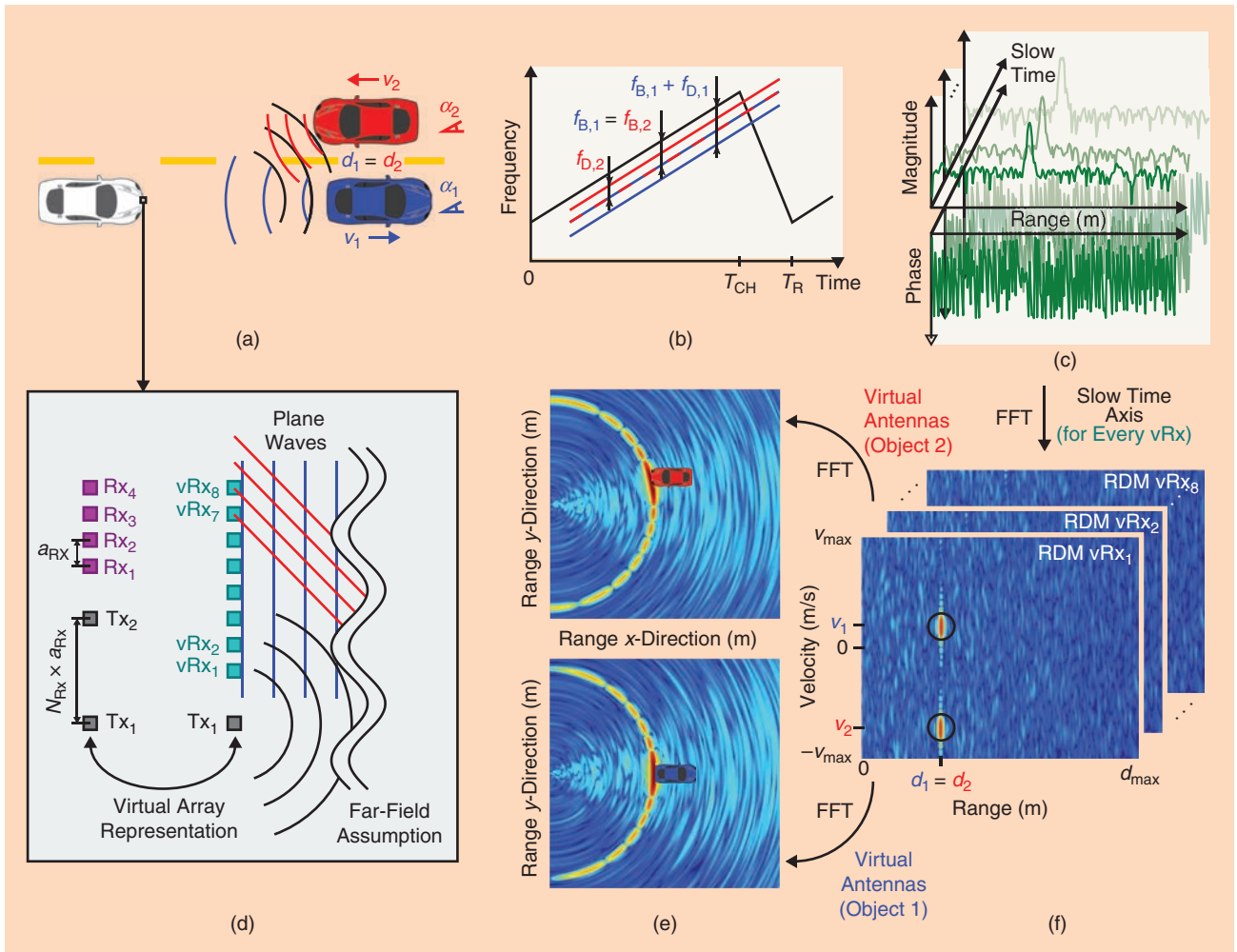


**FIGURE 3.** A schematic representation of how to build up a radar cube consisting of several RDMs using the concept of a virtual antenna array to estimate range, relative velocity, and angle of objects in the surrounding of the radar sensor. The (a) scenario, (b) time–frequency domain representation, (c) range spectra, (d) antenna setting, (e) angle estimation, and (f) radar cube. vRx: virtual Rx antenna.

consecutive ramps. One very common approach for velocity estimation in FMCW radar applications is to calculate the so-called range Doppler map (RDM) [8]. This 2D data set contains the range as well as the velocity information of all objects in the radar sensor's field of view. The RDM is obtained by stacking the complex-valued spectra of the IF signals obtained for the individual ramps into a matrix, and performing an FFT along the professed slow-time axis. The procedure as well as the resulting RDM is depicted in Figure 3(c) and (f). It can be seen that in the range spectrum, the object bins overlap, while in the RDM, they are separable in velocity.

### Angle estimation

To determine the angle of the surrounding objects, it is possible to use superresolution algorithms such as multiple signal classification (MUSIC) [9] or estimation of signal parameters via rotational invariances technique (ESPRIT) [10]. However, because of their high computational complexity, these algorithms are not widely used in automotive applications [7]. Therefore, we present an FFT-based algorithm to estimate the angle of arrival, which is commonly utilized in practice. For this purpose, multiple-input, multiple-output (MIMO) radar systems in combination with time-division multiplexing are used. These systems are composed of several Tx and Rx antennas to estimate the direction of arrival for every detected object. If the spacing between the antennas is chosen as shown in Figure 3(d) (where  $a_{Rx}$  is typically chosen as half the wavelength) with  $N_{Tx} = 2$  Tx antennas and  $N_{Rx} = 4$  Rx antennas, the MIMO radar system imitates an antenna array with one Tx antenna and  $N_{Tx} \times N_{Rx}$  equally spaced Rx antennas. This enlargement of the antenna array is referred to as *virtual array representation*, which increases the spatial resolution of the FFT-based estimation algorithms [7]. Note that this representation of the antenna array is suitable only if the far-field assumption is fulfilled.

To estimate the direction of arrival, the individual complex-valued RDMs of all of the virtual Rx (vRx) antennas are arranged in a 3D matrix, which forms the supposed radar cube. Depending on the angle of incidence, there is a certain phase difference between the sensed signals of the vRx antennas as can be seen in Figure 3(d). This phase difference may be estimated by performing an FFT across the third dimension of the radar cube for every detected object [7]. The results of these final FFTs reveal the angle of the objects in the radar channel and are often depicted as illustrated in Figure 3(e).

### Impact of PN in automotive radar systems

One of the most dominant signal distortions in an FMCW radar sensor is random fluctuations in the phase of the Tx signal (PN). It has a significant impact on the quality of the IF signal and therefore limits the performance of the radar system. The impact of PN on the spatial resolution due to a degrading signal-to-noise ratio as well as a limitation of the maximum range of the radar system is shown in [11]. In addition, according to the simulation results in [12], a deterioration of the PN characteristic may lead to a broadened object peak, which directly affects the range resolution.

To further analyze the impact of PN on the radar measurement, (1) is modified to additionally include the PN according to

$$s_{Tx}(t) = A_{Tx} \cos(2\pi f_0 t + \pi k t^2 + \varphi(t)). \quad (7)$$

On the basis of (7), the distorted IF signal can then be written as

$$s_{IF}(t) = \sum_{i=1}^N A_{IF,i} \cdot \cos(2\pi f_{B,i} t + \Phi_i + \Delta\varphi_i(t)), \quad (8)$$

where  $\Delta\varphi_i(t)$  is the alleged decorrelated PN (DPN) corresponding to the  $i$ th object reflection. It is defined as the difference between the PN contained in the instantaneous Tx signal and the PN delayed by  $\tau_i$ , and thus, it can be written as  $\Delta\varphi_i(t) = \varphi(t) - \varphi(t - \tau_i)$ . Assuming that the PN and the DPN are zero-mean wide-sense stationary ergodic processes, they can be represented by their PSDs [13]. Further applying the concept of the average PSD, it can be shown that the DPN, generated by objects close to the radar system, is raising the overall noise floor [14]. This becomes a problem especially if the radar sensor is mounted behind the vehicle's bumper. Besides the power loss, the bumper also acts as a close object reflecting a high amount of signal power back to the sensor [15]. This unwanted signal reflection in combination with the PN further limits the achievable sensitivity and accuracy of the radar system. One method to mitigate this apparent short-range (SR) leakage caused by the bumper is the integration of an artificial on-chip target (OCT), which essentially consists of a short delay line. The OCT is used to estimate the DPN of the bumper reflection. On the basis of cross correlation properties of the DPN of the OCT and the bumper reflection, almost perfect leakage cancellation is achieved [16]. This method increases the probability to detect objects with a very low radar cross section (RCS) [17]. Particularly, reflections from pedestrians, which would otherwise be covered by the noise floor, may become detectable.

The method proposed in [16] is suitable for objects at an approximately constant and close distance to the sensor, e.g., the bumper. The problem becomes somewhat different if we consider the scenario depicted in Figure 4, where the car is equipped with a radar sensor. The truck in front of the car is located at a distance of 1.5 m and has an RCS that is about a thousand times higher than the RCS of the pedestrian at a distance of 10 m [18], [19]. As shown in the simulated range spectra, the radar system with a PN PSD meeting the requirements is able to detect the hiker next to the road. If the noise figure is increased by 6 dB, the pedestrian is masked by the noise floor and is no longer visible to the radar.

In [20], the authors showed that there may be an additional distortion, affecting the ramp linearity, caused by switching in digital circuits or the transient response of the PLL. These deviations result in sinusoidal nonlinearities in the chirp signal and are referred to as *spurious oscillations* (spurs). In Figure 5, an exemplary PN PSD containing a sinusoidal nonlinearity at  $f_e = 2$  MHz is shown. This spur generates conjectural ghost targets at the frequencies  $f_{GT,1,2} = f_e \pm f_B$ , which will be interpreted as potential objects by the radar sensor.

In this section, we have shown that PN may directly cause personal injuries due to a deterioration of accuracy and detection sensitivity. Because ADASs as well as AD aim to make it less dangerous for humans to participate in traffic, it is of high importance to verify that all elements involved in the radar measurement work properly. A guideline on how the development of such functional safe products can be achieved is provided by the ISO 26262 standard, which will be the topic of the next section.

## FuSa according to ISO 26262

Statistically, an assisting system or an automated driver has to operate a vehicle in a much safer way than a human driver. Consequently, these systems need to meet very high integrity standards and demands toward FuSa. For the automotive industry, ISO 26262 enables standardized development of

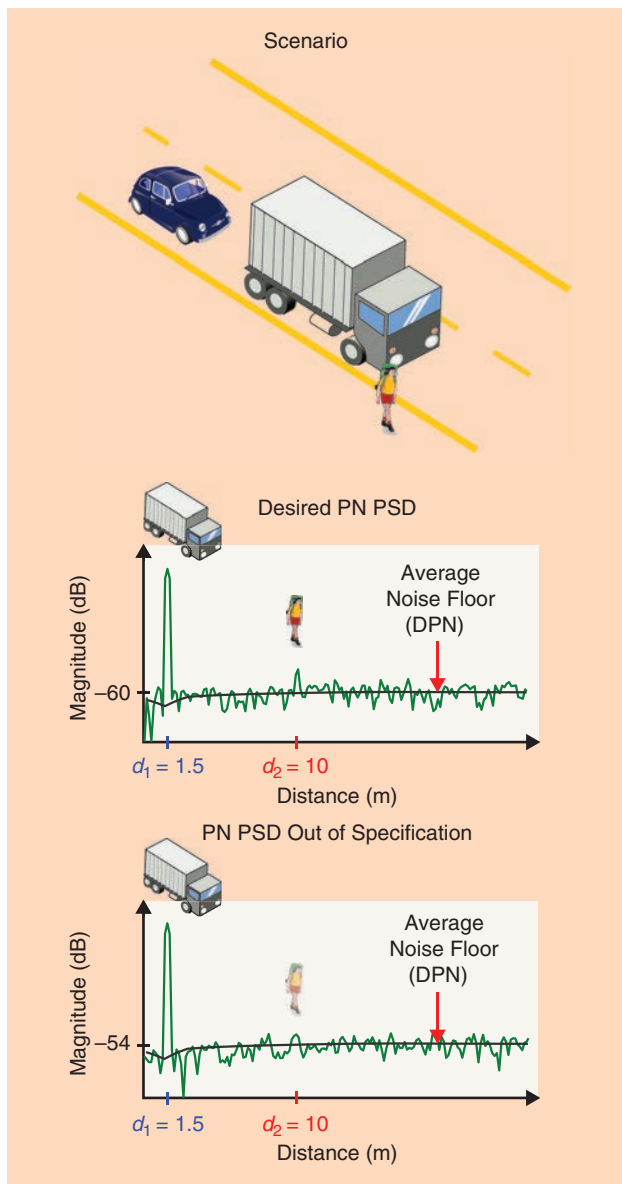


**FIGURE 4.** A scenario where the overall noise floor of a radar measurement is increased by an object close to the radar sensor, and the corresponding simulated range spectra with good and poor PN characteristic.

functional safe products [3]. In this article, we glance at some of the technical implications of the ISO 26262 standard for the development of a radar sensor only, leaving aside other activities demanded by the standard, such as planning, change management, competence management, tool qualification, audits and assessments, and also safety analyses.

To avoid unreasonable risks, ISO 26262 guides the development in an attempt to

- 1) remove hazards from random hardware faults, which are able to impair the nominal function
- 2) prevent systematic faults in hardware and software that are introduced during development
- 3) evade faulty specification of product properties.

The very high complexity of automotive systems is acknowledged by defining extensions on top of system development according to the V model and requirements engineering. Looking at the left leg of the V, a derivation and refinement process is sketched to break down the high-level goals into smaller technically feasible problems in as many steps as necessary. This could be exemplified by the chosen levels depicted in Figure 6.

The sensor function is described by requirements on the product level (radar sensor). In the elaboration of the product architecture, subparts (sensor elements) as well as the requirements to these subparts are defined. Further down the left leg of

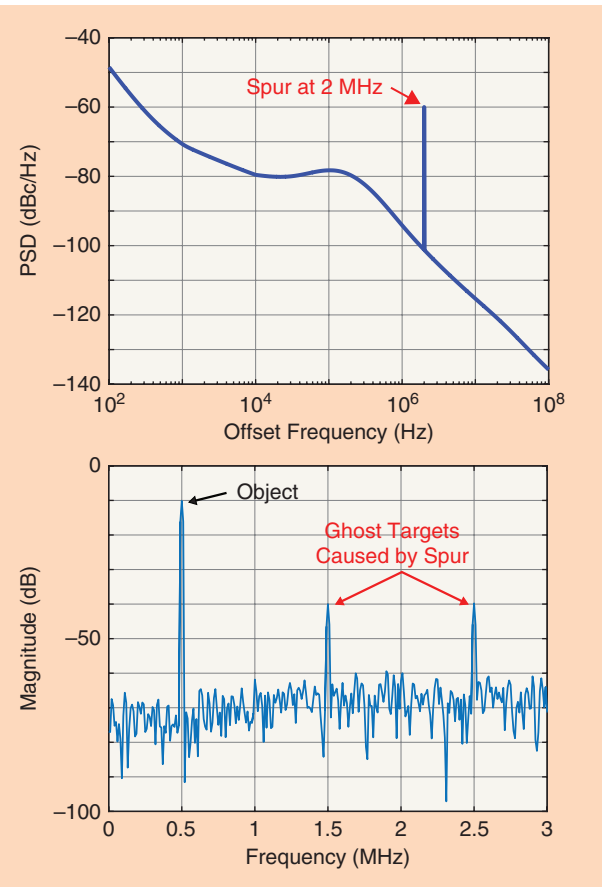


**FIGURE 5.** An exemplary PN PSD containing a sinusoidal nonlinearity at 2 MHz as well as the range spectrum with an object at  $f_b = 0.5$  MHz and two ghost targets at  $f = 2\text{ MHz} \pm f_b$ .

the V, this derivation and refinement process can be continued to sub-subparts (hardware/software) and further, if necessary.

In requirements engineering, ISO 26262 becomes directly apparent because it adds an additional safety layer, the safety requirements, alongside the usual technical requirements. The relevance of the safety requirements is affirmed by the assignment of an automotive safety integrity level (ASIL). The integrity level can be interpreted as the degree of certainty needed that the unit fulfills this requirement. With respect to requirements without an ASIL, i.e., all other regular requirements, ISO 26262 is very conservative by regarding them as systematically violated, which implies the assumption that a fulfillment cannot be relied on at all. From this, it follows directly that if a fault of those technical requirements in subparts or sub-subparts can lead to a violation of a safety requirement on the product level, their fulfillment needs to be checked and monitored by a safety mechanism. This needs to be done continuously and, especially after all final production tests, during regular operation in the field.

On the one hand, broad ASIL allocation can enhance product safety. On the other hand, an economic product development aims at having as few ASIL assignments as safely possible. This is because design and verification efforts of parts and requirements with ASIL are drastically increased to meet the higher integrity needs. Furthermore, the standard defines the inheritance of the ASIL by subparts of the product. Hence, it is reasonable to ensure the safety on higher levels to be able to develop the subparts without an ASIL.

Let us consider an emergency braking system to demonstrate the implications of ISO 26262. For an emergency braking system, it could be required with ASIL to take action if a pedestrian is directly in front of the car. Another safety requirement could be that false emergency brakings must not occur. Both of these safety requirements on the system level potentially lead to safety requirements at the product level of the radar sensor regarding a certain resolution or PN level.

As a consequence, the fulfillment of these requirements could be ensured by ASIL assignments and/or safety mechanisms for all contributing subparts and sub-subparts. However, this comes at an enormous development effort. A much more economic and elegant way is to monitor the PN PSD on the product level using

additional BIST architectures in combination with digital signal processing like the methods presented in the “PN Estimation of FMCW Signals” and “PN Estimation With FMCW Signals in Cascaded System Configuration” sections.

## PN measurement of CW signals

The characterization of a radar MMIC is usually done after production to ensure the circuit operates within its specified performance parameters. As part of this characterization, the PN PSD is measured with a spectrum analyzer in the lab. This assessment is crucial because PN is one of the most meaningful figures of merit of a PLL.

There are several methods to measure or estimate the PN PSD, each satisfying various requirements. Typically, the signal, distorted by PN, is converted to baseband to further extract either the phase or frequency information of the carrier. Thereafter, a frequency selective measuring device is used to measure the noise as a function of the offset frequency.

The common way to verify the specifications of the PLL of FMCW radar MMICs is to use the direct spectrum technique. This simple yet effective method directly measures the PN PSD of the PLL, utilizing the LO of the spectrum analyzer for down-conversion. In general, however, a direct-spectrum reading has a disadvantage [21]. A spectrum analyzer is generally not able to differentiate between amplitude noise and PN, but because the effect of amplitude noise is negligible compared to that of PN, it does not pose a problem for our application at hand [13].

As previously mentioned, the PN behavior may change due to voltage and temperature variations as well as aging. Therefore, it is necessary to estimate the PN PSD with an on-chip circuitry. This enables monitoring of the PN PSD throughout the whole lifecycle of the radar MMIC. Most state-of-the-art on-chip PN measurement techniques for CW signals use the delay line discriminator (DLD) approach [21]. In contrast to the direct spectrum technique, this method does not require a reference clock to convert the signal of interest into baseband. In Figure 7(a), the block diagram of a DLD-based measurement system is shown. To perform the PN measurement, the signal of interest is split into two paths. One signal is directly passed to the mixer, which acts as a phase detector, while the other one is sent through a delay line first. To remove the resulting sum frequency, the output of the phase detector is put through the LPF. Because of the fact that the involved signals have identical frequencies, the phase detector output is essentially a fluctuating voltage related to phase fluctuations of the PLL. Please note that the signals need to be at a 90° phase shift during the whole measurement to achieve an accurate PN value. Therefore, the authors of [22] presented an on-chip PN measurement circuit including a feedback loop to calibrate the delay line, which ensures perfect quadrature conditions and improves

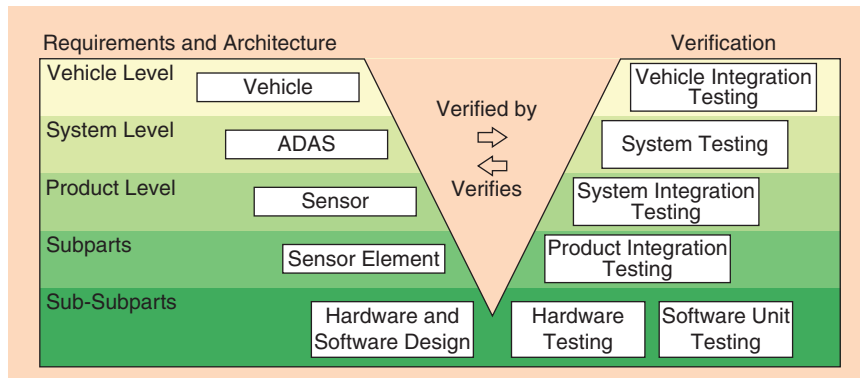


**FIGURE 6.** A system development process according to the V model.

the PN sensitivity. A different concept to enhance the PN sensitivity is to use an injection-locked-oscillator phase discriminator as proposed in [23].

Unfortunately, the techniques described previously constrain the input signal to be at a certain, fixed carrier frequency. Consequently, those methods are not suitable for automotive radar applications using linear frequency ramps. Therefore, it is necessary to develop an approach to estimate and monitor the PN PSD contained in a chirp signal, which will be the scope of the next section.

### PN estimation of FMCW signals

One of the most intuitive approaches to estimate the PN PSD from a linear FMCW signal would be to measure the PN PSD at multiple carrier frequencies covering the desired chirp bandwidth and form a simple average [24]. However, one disadvantage of this approach is that the PLL is operating in a different configuration as it is actually utilized in automotive applications. As a consequence, some disruptive effects may not occur and thus cannot be monitored.

In the following, we present two techniques to estimate the PN contained in an FMCW signal during operation [24]. The proposed methods were implemented on the hardware prototype presented in [17] and make use of the artificial OCT, which was also utilized to perform the SR leakage cancelation mentioned previously. For this application, the OCT is used as a BIST or design for testing. Similar to the DLD method presented in the “PN Measurement of CW Signals” section, the OCT is realized with a delay line. However, the DLD technique is not suitable for our problem at hand because the constant phase shift of  $90^\circ$  cannot be maintained for frequency-modulated input signals.

The system model with the artificial OCT is illustrated in Figure 7(b). Assuming the path that directly feeds the mixer has zero delay and with the Tx signal defined in (7), the OCT IF signal can be written as

$$s_{IF,O}(t) = A_{IF,O} \cdot \cos(2\pi f_{B,O} t + \Phi_O + \Delta\phi_O(t)), \quad (9)$$

with  $f_{B,O}$  denoting the beat frequency corresponding to the time delay  $\tau_O$  caused by the OCT and  $\Delta\phi_O(t)$ , the resulting DPN.

Applying the cosine sum identity and the small-angle approximation (the DPN is assumed to be sufficiently small), (9) can be rewritten as

$$\begin{aligned} s_{IF,O}(t) &\approx A_{IF,O} \cdot \cos(2\pi f_{B,O} t + \Phi_O) \\ &\quad - A_{IF,O} \cdot \sin(2\pi f_{B,O} t + \Phi_O) \Delta\phi_{O,L}(t). \end{aligned} \quad (10)$$

Note that the random phase term  $\Delta\phi_O(t)$  from (9) turned into a random amplitude  $\Delta\phi_{O,L}(t)$  due to this approximation. Because it is additionally affected by the LPF, it is referred to as *low-pass filtered DPN* and denoted with an additional subscript L in the sequel. In the following, we present the two mentioned methods based on (10), which are designated as PN estimation in the time and frequency domain, respectively.

### PN estimation in the time domain

In the first approach, the low-pass filtered DPN  $\Delta\phi_{O,L}(t)$  is extracted in time domain by rearranging (10) as

$$\Delta\phi_{O,L}(t) \approx \frac{A_{IF,O} \cdot \cos(2\pi f_{B,O} t + \Phi_O) - s_{IF,O}(t)}{A_{IF,O} \cdot \sin(2\pi f_{B,O} t + \Phi_O)}. \quad (11)$$

Because the design parameters  $A_{Tx}$ ,  $A_O$ ,  $\tau_O$ , and  $k$  are known, the amplitude of the IF signal  $A_{IF,O}$  and the beat frequency  $f_{B,O}$  as well as the constant phase term  $\Phi_O$  can be determined as shown in the section “Velocity Estimation.” To obtain the PSD  $S_{\Delta\phi_{O,L}\Delta\phi_{O,L}}(f)$  of the low-pass filtered DPN  $\Delta\phi_{O,L}(t)$ , a conventional PSD estimation is applied. In this application, we are interested in the PSD of the PN  $\varphi(t)$  contained in the Tx signal, which is directly related to the unfiltered DPN PSD via the so-called range correlation term [25]. Accordingly, the PSD of the unfiltered DPN  $\Delta\phi_O(t)$  can be calculated as

$$\underbrace{S_{\Delta\phi_O\Delta\phi_O}(f)}_{\text{DPN PSD}} = \underbrace{S_{\varphi\varphi}(f)}_{\text{PN PSD}} \underbrace{2(1 - \cos(2\pi f \tau_O))}_{\text{range correlation term}}. \quad (12)$$

Including the magnitude response of the LPF  $|H_{LPF}(f)|$  into our considerations, based on (12), we obtain an expression for the PN PSD

$$S_{\varphi\varphi}(f) = \frac{S_{\Delta\phi_{O,L}\Delta\phi_{O,L}}(f)}{2 |H_{LPF}(f)|^2 [1 - \cos(2\pi f \tau_O)]}. \quad (13)$$

Although this method can be computed efficiently using the FFT to calculate  $S_{\Delta\phi_{O,L}\Delta\phi_{O,L}}(f)$ , it is possible to bypass the extraction process by directly calculating the PN PSD in the frequency domain, as explained next.

### PN estimation in the frequency domain

For the second technique, we reconsider the approximation from (10)

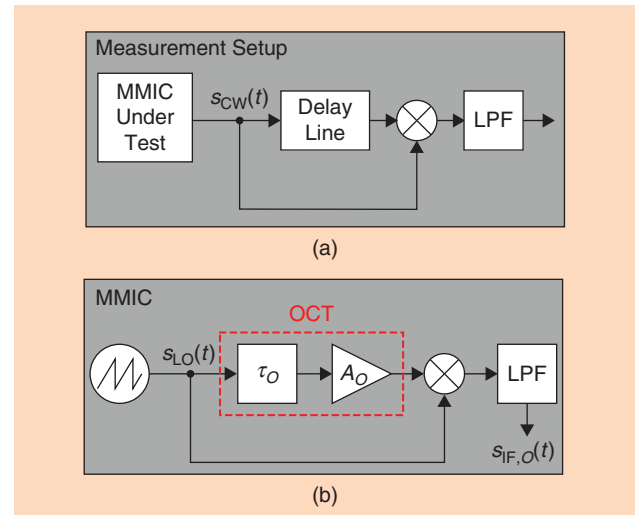


**FIGURE 7.** The system models describing the PN measurement system for (a) CW signals using a DLD approach as well as (b) estimating the PN PSD of a linear chirp utilizing the OCT.

$$s_{IF,O}(t) \approx \underbrace{A_{IF,O} \cos(2\pi f_{B,O} t + \Phi_O)}_{s_D(t)} - \underbrace{A_{IF,O} \sin(2\pi f_{B,O} t + \Phi_O) \Delta\varphi_{O,L}(t)}_{s_R(t)}, \quad (14)$$

and we split it into a deterministic signal part  $s_D(t)$  and a random signal part  $s_R(t)$  containing the low-pass filtered DPN  $\Delta\varphi_{O,L}(t)$ . In [24], it is derived in detail that the PSD of the random signal part can be evaluated as

$$S_{s_R s_R}(f, t) \approx A_{IF,O}^2 S_{\varphi\varphi}(f) |H_{LPF}(f)|^2 [1 - \cos(2\pi f \tau_O)] \gamma_R(t), \quad (15)$$

while the PSD of the deterministic part is described by

$$S_{s_D s_D}(f, t) \approx \frac{A_{IF,O}^2}{2} \delta(f) \gamma_D(t) \quad (16)$$

with  $\delta(f)$  the Dirac delta function. Further,  $\gamma_R(t)$  and  $\gamma_D(t)$  are correction terms to compensate for the nonstationarity of the signals  $s_R(t)$  and  $s_D(t)$  and, thus, the time dependency of the PSDs.

As shown in [24], the PSD of the IF signal  $s_{IF,O}(t)$  can be written as

$$S_{s_{IF,O} s_{IF,O}}(f, t) = S_{s_D s_D}(f, t) + S_{s_R s_R}(f, t). \quad (17)$$

Finally, inserting (15) into (17), the desired PN PSD can be expressed as

$$S_{\varphi\varphi}(f) \approx \frac{S_{s_{IF,O} s_{IF,O}}(f, t) - S_{s_D s_D}(f, t)}{A_{IF,O}^2 |H_{LPF}(f)|^2 [1 - \cos(2\pi f \tau_O)] \gamma_R(t)}. \quad (18)$$

In summary, to perform the PN estimation in the frequency domain, the PSD of the IF signal  $s_{IF,O}(t)$  is estimated first. Then, this estimate in combination with the known design parameters  $A_{Tx}$ ,  $A_O$ ,  $\tau_O$ , and  $k$  is used in (18) to determine the PSD of the PN contained in the Tx signal  $\varphi(t)$ . Both methods presented in this section require the integration of a delay line inside the MMIC, which is difficult to realize. Therefore, we will now present an alternative approach that enables PN estimation in cascaded radar system setups.

## PN estimation with FMCW signals in cascaded system configuration

As mentioned in the section “The FMCW Radar Principle,” the spatial resolution of an FMCW radar system is limited by the number of Tx and Rx antennas. One approach to increase the number of channels is to cascade multiple radar MMICs [26], [27]. Depending on the MMICs used, different approaches can be found to synchronize several MMICs to build up a cascaded system [28], [29]. For our novel PN PSD estimation technique, we make use of the cascaded system setup presented in [29]. In this cascaded system when operating in application mode, one master MMIC generates the LO signal and distributes it to the slave MMICs. The slave MMICs use the received LO signals both for transmission and for down-conversion of the received

radar signals. Figure 8(a) depicts an exemplary system configuration with one master MMIC and two slave MMICs acting in application mode.

In contrast, if the system is operating in our proposed PN PSD estimation mode [30], only two arbitrary MMICs are involved in the measurement simultaneously. These two MMICs are synchronized through a system clock. In this mode, both MMICs use their PLL to generate the FMCW signals  $s_1(t)$  and  $s_2(t)$ , which are defined as described in (7) using the same slope  $k$  but different starting frequencies  $f_1$  and  $f_2$ , respectively. As can be seen from Figure 8(b), the radio-frequency Tx output channel of the master MMIC is now reconfigured to be an input channel, driven by the slave MMIC. Finally, the signals  $s_1(t)$  and  $s_2(t)$  are mixed and low-pass filtered in the master MMIC.

According to the investigations previously described, the IF signal can be written (compare (10) and [30]) as

$$s_{IF,c}(t) \approx A_{IF,c} \cdot \cos(2\pi f_{B,D} t + \Phi_D) - A_{IF,c} \cdot \sin(2\pi f_{B,D} t + \Phi_D) \varphi_{D,L}(t), \quad (19)$$

where  $\Phi_D$  is a constant phase term composed of known design parameters and  $f_{B,D}$  is the frequency difference of the FMCW signals  $s_1(t)$  and  $s_2(t)$  at the mixer, which is defined by

$$f_{B,D} = f_1 - f_2 + k t_D. \quad (20)$$

The frequency component  $k t_D$  in (20) is caused by the fact that the mixing process is performed in the master, where  $t_D$  represents the difference in arrival time between the input signals of the mixer. Further, note that  $\varphi_{D,L}(t)$  does not represent the DPN but rather the low-pass filtered version of the difference of the PN time domain signals  $\varphi_1(t) - \varphi_2(t - t_D)$ . These two PN signals are uncorrelated because the signals  $s_1(t)$  and  $s_2(t)$  are generated by two different PLLs.

Assuming that  $t_D$  is known (e.g., as the result of an estimation procedure or by knowledge of the line lengths of the cascaded system), the aim of our approach is to set  $f_{B,D}$  to zero. This is achieved by properly choosing the start frequencies  $f_1$  and  $f_2$  according to (20). With this, (19) simplifies to

$$s_{IF,c}(t) \Big|_{f_{B,D}=0} \approx A_{IF,c} \cos(\Phi_D) - A_{IF,c} \sin(\Phi_D) \varphi_{D,L}(t). \quad (21)$$

As shown in [30], the PSD of  $s_{IF,c}(t)$  can be approximated with

$$S_{s_{IF,c} s_{IF,c}}(f) \approx A_{IF,c}^2 \cos^2(\Phi_D) \delta(f) + 2A_{IF,c}^2 \sin^2(\Phi_D) S_{\bar{\varphi}_L \bar{\varphi}_L}(f) \quad (22)$$

with  $S_{\bar{\varphi}_L \bar{\varphi}_L}(f)$  the mean PN PSD of the master and the slave MMIC. Finally, rearranging (22) yields this mean PN PSD

$$S_{\bar{\varphi}_L \bar{\varphi}_L}(f) = \frac{1}{2A_{IF,c}^2 \sin^2(\Phi_D)} S_{s_{IF,c} s_{IF,c}}(f) - \frac{\cos^2(\Phi_D)}{2 \sin^2(\Phi_D)} \delta(f). \quad (23)$$

This approach can be used to detect if one (or both) involved MMICs generate PN out of specification. To identify the erroneous MMIC, the cascaded system has to be composed of

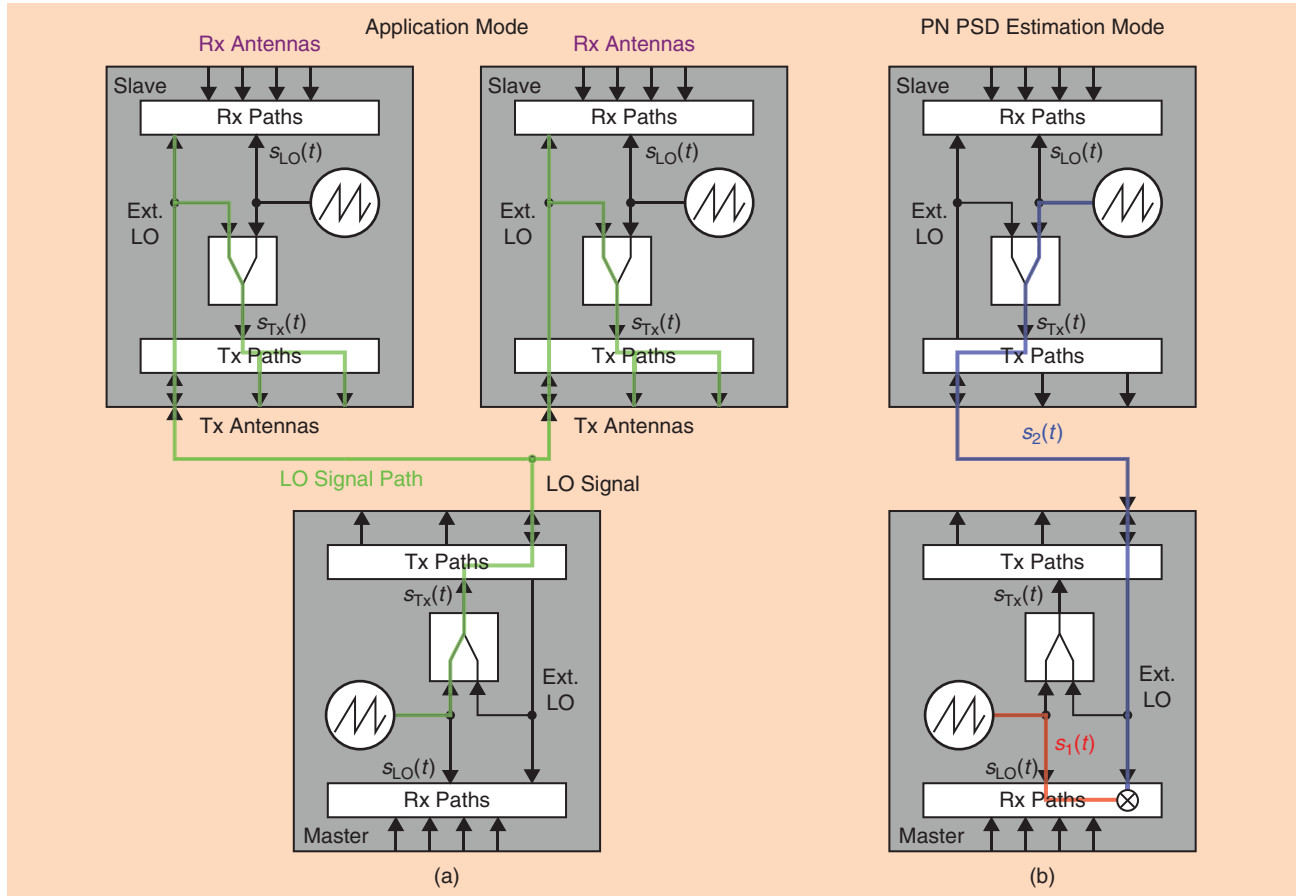


**FIGURE 8.** The cascaded MMIC setup in application mode as well as in PN PSD estimation mode. (a) The exemplary system configuration with one master MMIC and two slave MMICs acting in application mode. (b) The system configuration for the PN PSD estimation mode with two arbitrary MMICs. Ext.: external.

at least three MMICs. Then the estimation process has to be repeated for every possible MMIC combination.

In contrast to the methods presented in the “PN Measurement of CW Signals” section, our novel approach enables PN monitoring using FMCW signals. As an advantage over the methods mentioned in the section “PN Estimation of FMCW Signals,” no delay line integration is required, but instead, it requires an underlying cascaded radar MMIC system. Further, the radar MMICs used have to support specific functionalities required for the PN PSD estimation mode.

## Conclusions

In this article, we illustrated the basics of FMCW radar signal processing, providing the most important formulas as well as supplementary examples. We demonstrated how to extract the range, relative velocity, and angle information from the measured IF signal, and we gave an insight into a common state-of-the-art radar signal processing technique in tutorial style. Further, we showed the impact of PN on radar measurement accuracy and pointed out the relevance of PN monitoring to verify that the PLL generates PN within its specifications. Because PN is the main figure of merit for a PLL, such monitoring functions are indispensable in terms of FuSa for ADAS and future AD. Finally, as the core of this article, state-of-the-art methods to

estimate the PSD of the PN contained in an FMCW signal in compliance to the ISO 26262 standard were presented.

## Acknowledgments

We thank Infineon Technologies for supporting this article and allowing for its publication. We also express our sincere gratitude to Oliver Lang and Lukas Heschl for the interesting discussions regarding radar signal processing and PN measurement techniques, and we thank Carl Böck from the Institute of Signal Processing at the Johannes Kepler University Linz for his contributions.

## Authors

**Michael Gerstmair** (michael.gerstmair@infineon.com) received his B.S. degree in telematics from Graz University of Technology, Austria, in 2013 and his Dipl.-Ing. in information electronics in 2016 from Johannes Kepler University Linz, Austria. Since July 2016, he has been a Ph.D. student at Danube Integrated Circuits Engineering GmbH & Co KG (Infineon Technologies) in cooperation with the Institute of Signal Processing, Johannes Kepler University Linz. His research interests include radio-frequency impairments in highly integrated radar front ends as well as radar signal processing. He is a Student Member of the IEEE.

**Alexander Melzer** (alexander.melzer@infineon.com) received his Dipl.-Ing. degree from Graz University of Technology, Austria, in

2012 and his Ph.D. degree in radar signal processing from Johannes Kepler University Linz, Austria, in cooperation with Infineon Technologies. Since 2017, he has been a product architect for future automotive radar transceiver monolithic microwave integrated circuits at Infineon Technologies. From 2013 to 2014, he was with Maxim Integrated Austria. He received the German Informationstechnische Gesellschaft im Verband der Elektrotechnik Elektronik Informationstechnik e.V. Award in 2016. He has published several conference and journal papers and holds various patents in the area of phase noise estimation and leakage cancellation in radar transceivers. He is a Member of the IEEE.

**Alexander Onic** (onic@ieee.org) received his Dipl.-Ing. degree in electrical engineering from Friedrich-Alexander-Universität Erlangen-Nürnberg, Germany, in 2007 and his Ph.D. degree from Alpen-Adria-Universität Klagenfurt, Austria, in 2013. He is a product architect for next-generation 77-GHz automotive radar monolithic microwave integrated circuits at Danube Integrated Circuits Engineering GmbH & Co KG (Infineon Technologies) in Linz, Austria. He is certified as an ISO 26262 functional safety engineer by Technischer Überwachungsverein SÜD. His research interests include sensor technologies for autonomous driving as well as signal processing, communication engineering, and estimation theory, which are supplemented by research cooperation with Johannes Kepler University Linz, Austria, on mixed signal processing topics. He is a Member of the IEEE.

**Mario Huemer** (mario.huemer@jku.at) received the Dipl.-Ing. degree in mechatronics and the Dr. techn. (Ph.D.) degree from Johannes Kepler University Linz, Austria, in 1996 and 1999, respectively, where he is a full professor and the head of the Institute of Signal Processing. He currently serves as an associate editor of *IEEE Signal Processing Letters*. He received dissertation awards from the German Society of Information Technology and the Austrian Society for Information and Communication Technology, the Austrian Cardinal Innitzer Award in natural sciences, and the German Informationstechnische Gesellschaft im Verband der Elektrotechnik Elektronik Informationstechnik e.V. Award. His research interests are adaptive and statistical signal processing, signal processing architectures and implementations, as well as mixed signal processing with applications in communications, radio-frequency and baseband integrated circuits, battery and power management for mobile devices, and sensor signal processing. He is a Senior Member of the IEEE.

## References

- [1] R. Adomat, G.-O. Geduld, M. Schamberger, and P. Rieth, "Advanced driver assistance systems for increased comfort and safety—Current developments and an outlook to the future on the road," in *Advanced Microsystems for Automotive Applications*, J. Valldorf and W. Gessner, Eds. Berlin: Springer, 2003, pp. 431–446. doi: [https://doi.org/10.1007/978-3-540-76988-0\\_34](https://doi.org/10.1007/978-3-540-76988-0_34).
- [2] J. Dickmann, N. Appenrodt, J. Klappstein, H. L. Bloecher, M. Muntzinger, A. Sailer, M. Hahn, and C. Brenk, "Making Bertha see even more: Radar contribution," *IEEE Access*, vol. 3, pp. 1233–1247, Aug. 2015.
- [3] *Road Vehicles - Functional Safety, Part 1-10*, ISO 26262, Nov. 2011.
- [4] D. Kissinger, B. Laemmle, L. Maurer, and R. Weigel, "Integrated test for silicon front ends," *IEEE Microw. Mag.*, vol. 11, no. 3, pp. 87–94, May 2010.
- [5] D. Kissinger, R. Agethen, and R. Weigel, "A versatile built-in test architecture for integrated millimeter-wave radar receiver front-ends," in *Proc. IEEE Int. Instrumentation and Measurement Technology Conf. (I2MTC 2012)*, May 2012, pp. 254–258.
- [6] F. Herzl, D. Kissinger, and H. J. Ng, "Analysis of ranging precision in an FMCW radar measurement using a phase-locked loop," in *IEEE Trans. Circuits Syst. I, Reg. Papers*, vol. 65, no. 2, pp. 783–792, Feb. 2018.
- [7] S. M. Patole, M. Torlak, D. Wang, and M. Ali, "Automotive radars: A review of signal processing techniques," *IEEE Signal Process. Mag.*, vol. 34, no. 2, pp. 22–35, Mar. 2017.
- [8] F. Ali and M. Vossiek, "Detection of weak moving targets based on 2-D range-Doppler FMCW radar Fourier processing," in *German Microwave Conf. Dig. Papers*, Mar. 2010, pp. 214–217.
- [9] R. Schmidt, "Multiple emitter location and signal parameter estimation," *IEEE Trans. Antennas Propag.*, vol. 34, no. 3, pp. 276–280, Mar. 1986.
- [10] R. Roy and T. Kailath, "ESPRIT-estimation of signal parameters via rotational invariance techniques," *IEEE Trans. Acoust., Speech, Signal Process.*, vol. 37, no. 7, pp. 984–995, July 1989.
- [11] D. Dhar, P. T. M. van Zeijl, D. Milosevic, H. Gao, and A. H. M. van Roermund, "Modeling and analysis of the effects of PLL phase noise on FMCW radar performance," in *Proc. IEEE Int. Symp. Circuits and Systems (ISCAS 2017)*, May 2017. doi: 10.1109/ISCAS.2017.8050525.
- [12] M. Dudek, I. Nasr, D. Kissinger, R. Weigel, and G. Fischer, "The impact of phase noise parameters on target signal detection in FMCW-radar system simulations for automotive applications," in *Proc. IEEE Int. Conf. Radar (CIE 2011)*, vol. 1, Oct. 2011, pp. 494–497.
- [13] A. Chorti and M. Brookes, "A spectral model for RF oscillators with power-law phase noise," *IEEE Trans. Circuits Syst. I, Reg. Papers*, vol. 53, no. 9, pp. 1989–1999, Sept. 2006.
- [14] M. Gerstmair, A. Melzer, A. Onic, R. Stuhlberger, and M. Huemer, "Highly efficient environment for FMCW radar phase noise simulations in IF domain," *IEEE Trans. Circuits Syst. II, Exp. Briefs*, vol. 65, no. 5, pp. 582–586, May 2018.
- [15] R. Schnabel, D. Mittelstraß, T. Binzer, C. Waldschmidt, and R. Weigel, "Reflection, refraction, and self-jamming," *IEEE Microw. Mag.*, vol. 13, no. 3, pp. 107–117, Apr. 2012.
- [16] A. Melzer, A. Onic, F. Starzer, and M. Huemer, "Short-range leakage cancellation in FMCW radar transceivers using an artificial on-chip target," *IEEE J. Sel. Topics Signal Process.*, vol. 9, no. 8, pp. 1650–1660, Dec. 2015.
- [17] A. Melzer, F. Starzer, H. Jäger, and M. Huemer, "Real-time mitigation of short-range leakage in automotive FMCW radar transceivers," *IEEE Trans. Circuits Syst. II, Exp. Briefs*, vol. 64, no. 7, pp. 847–851, July 2017.
- [18] M. Richards, *Fundamentals of Radar Signal Processing*, 2nd ed. New York: McGraw-Hill Education, 2014.
- [19] N. Yamada, Y. Tanaka, and K. Nishikawa, "Radar cross section for pedestrian in 76 GHz band," in *Proc. European Microwave Conf. (EuMC 2005)*, vol. 2, Oct. 2005. doi: 10.1109/EUMC.2005.1610101.
- [20] S. Ayhan, S. Scherr, A. Bhutani, B. Fischbach, M. Pauli, and T. Zwick, "Impact of frequency ramp nonlinearity, phase noise, and SNR on FMCW radar accuracy," *IEEE Trans. Microw. Theory Techn.*, vol. 64, no. 10, pp. 3290–3301, Oct. 2016.
- [21] H. Gheidi and A. Banai, "Phase-noise measurement of microwave oscillators using phase-shifterless delay-line discriminator," *IEEE Trans. Microw. Theory Techn.*, vol. 58, no. 2, pp. 468–477, Feb. 2010.
- [22] W. Khalil, B. Bakkaloglu, and S. Kiaei, "A self-calibrated on-chip phase-noise measurement circuit with -75 dBc single-tone sensitivity at 100 kHz offset," *IEEE J. Solid-State Circuits*, vol. 42, no. 12, pp. 2758–2765, Dec. 2007.
- [23] Y.-J. Chen and T.-S. Chu, "An injection-locked-oscillator phase discriminator for RF built-in self test on local oscillator phase noise," in *Proc. IEEE MTT-S Int. Microwave Symp.*, June 2014. doi: 10.1109/MWSYM.2014.6848248.
- [24] A. Melzer, A. Onic, and M. Huemer, "Online phase-noise estimation in FMCW radar transceivers using an artificial on-chip target," in *IEEE Trans. Microw. Theory Techn.*, vol. 64, no. 12, pp. 4789–4800, Dec. 2016.
- [25] M. C. Budge and M. P. Burt, "Range correlation effects in radars," in *Proc. Rec. IEEE Nat. Radar Conf. (RadarConf'93)*, Apr. 1993, pp. 212–216.
- [26] C. Pfeffer, R. Feger, C. Wagner, and A. Stelzer, "A multimode-beamforming 77-GHz FMCW radar system," in *Proc. IEEE MTT-S Int. Microwave Symp. Dig. (MTT 2013)*, June 2013. doi: 10.1109/MWSYM.2013.6697554.
- [27] H. J. Ng, M. Kucharski, W. Ahmad, and D. Kissinger, "Multi-purpose fully differential 61- and 122-GHz radar transceivers for scalable MIMO sensor platforms," *IEEE J. Solid-State Circuits*, vol. 52, no. 9, pp. 2242–2255, Sept. 2017.
- [28] I. Bilik, S. Villeval, D. Brodeski, H. Ringel, O. Longman, P. Goswami, C. Y. B. Kumar, S. Rao, et al., "Automotive multi-mode cascaded radar data processing embedded system," in *Proc. IEEE Radar Conf. (RadarConf'18)*, Apr. 2018, pp. 372–376.
- [29] A. Och, C. Pfeffer, J. Schratenecker, S. Schuster, and R. Weigel, "A scalable 77 GHz massive MIMO FMCW radar by cascading fully-integrated transceivers," in *Proc. Asia-Pacific Microwave Conf. (APMC 2018)*, Nov. 2018, pp. 1235–1237.
- [30] M. Gerstmair, A. Melzer, A. Onic, and M. Huemer, "Phase noise power spectral density estimation in cascaded automotive radar transceiver MMICs," in *Proc. 2018 52nd Asilomar Conf. Signals, Systems, and Computers*, Oct. 2018, pp. 1131–134. doi: 10.1109/ACSSC.2018.8645074.

Sergio Saponara, Maria Sabrina Greco, and Fulvio Gini

# Radar-on-Chip/in-Package in Autonomous Driving Vehicles and Intelligent Transport Systems

*Opportunities and challenges*



This article addresses the signal processing challenges for the design of a radar-on-chip/in-package in the autonomous-driving era, taking into account recent integration trends and technology capabilities. Radar signal processing platform specifications are discussed, and the radar sensor is compared with other competing sensors, such as lidars, ultrasonics, and video cameras, that aim at detecting still or moving objects and measuring their motion parameters. This survey first focuses on signal processing techniques for a low-cost and power-efficient radar sensor, which operates in real time while ensuring the automotive coverage-range needs. The main signal processing techniques for velocity-range estimation, direction estimation, waveform design, and beamforming are analyzed with particular emphasis on the radar physical layer codesign. The future evolution of embedded computing platforms and advanced signal processing techniques are explored, such as multiple-input, multiple-output (MIMO) and cognitive radars, along with adaptive waveforms for solving interference and spectrum scarcity issues.

## Introduction

Intelligent transportation systems for surveillance and assisted/autonomous driving require robust sensing platforms that are tolerant of bad light and weather conditions [1], [2]. This is a topic of high economic and societal impact because, every year, 1.25 million people die worldwide due to accidents. Moreover, each year, 90 million vehicles are sold, and, hence, a market of more than hundreds of billions of U.S. dollars (USD) is potentially available for the adoption of radar as a ubiquitous mobility sensor. In that respect, due to the emerging scenario of autonomous vehicles [3], [4], with alliances among traditional original equipment manufacturers or tier 1 companies, (e.g., BMW, Volkswagen-Audi, Toyota, Fiat Chrysler Automobiles, Daimler, General Motors, Ford, Bosch, Denso, Continental, Valeo, Magneti Marelli, and others), and new companies investing in vehicular technologies (including Intel, Google's Waymo, Uber, and Tesla), the interest in low-cost, compact, and energy-efficient radar signal processing techniques is further increasing.

In recent years, the design of ubiquitous radars, available with low cost and low power in a large-volume market as a system-in-package solution (SiP), has become feasible [5]–[9]. This is mainly due to the recent advances in 1) in-package antenna-array design, 2) integration as a system-on-chip (SoC) of multichannel radiofrequency (RF) transceivers and high-performance analog-to-digital converters (ADC), and 3) embedded high-performance computing (HPC) and memory platforms that enable advanced signal processing techniques to be implemented in real time and with low power cost.

Intelligent transport systems (ITSs) involve two main uses of radars (Figure 1):

- surveillance, for which radar sensors are embedded in the infrastructure to increase the safety of railroad crossing,

urban crossing, and parking areas [10] or for traffic-flow analysis [11]

- vehicles' perception, for which radar sensors are mounted on vehicles to enable high levels of autonomy in assisted/autonomous driving [5].

Many signal processing review works have been proposed in the literature for automotive radar, but most of them survey basic signal processing techniques [2]–[4], [12], considering the scenario of a car moving in a multitarget scenario and equipped with pulsed or frequency-modulated continuous-wave (FMCW) radar. Such articles are missing the analysis of implementation technology capabilities and trends and of advanced techniques, such as cognitive radar signal processing. Indeed, when vehicles and ITSs are moving from assisted



**FIGURE 1.** A scenario with multiple vehicles, all equipped with multiple remote sensors and connected with V2V/V2I links [51].

to autonomous driving, the application scenario will be that shown in Figure 1, which corresponds to the last three of six levels in the Society of Automotive Engineers (SAE) classification of assisted/autonomous driving [5], moving from L0 (full human and manual control of all aspects of driving) to L5 (full autonomous driving), with L1, L2, L3, and L4 being intermediate levels of assisted or autonomous driving. Such a scenario foresees multiple vehicles, all equipped with multiple onboard remote sensors (radars, cameras, ultrasonics, and lidars), connected to each other and with the infrastructure with vehicle-to-vehicle (V2V)/vehicle-to-infrastructure (V2I) communication technologies.

The needs for real-time and low-latency perception and decision making, a continuous adaption to the sensed environment, and overcoming mutual-interference and spectrum scarcity issues require cognitive radar signal processing solutions. Cognitive radar signal processing has been recently discussed in [13] and [14] (and the references therein) but without any mention of the cost, power, and time budgets necessary for real implementation in vehicles. Moreover, mixing active and passive radar signal processing technologies can help reduce spectrum scarcity and electromagnetic (EM) interference. Several opportunities to solve these issues come from the recent advances in SoC and SiP integration capabilities, which are reviewed here.

This article considers both the scenarios of embedded signal processing for inexpensive and power-efficient radar sensor nodes and scenarios needing HPC for cognitive and multisensor perception systems with active and passive technologies. Therefore, this article is a companion to [15] and [16], published in this same special issue, which focus more on the many new signal processing techniques for automotive radars. The intent of this article is to review already implemented and new radar signal processing algorithms in light of existing and prospective technology solutions and capabilities.

## **Mobility sensor and radar-on-chip/in-package specifications**

As shown in Figure 1, the current sensing technologies competing with radars to detect the presence of a target and measure its distance, motion direction, and speed are mainly lidars and video cameras. Ultrasonic technology, because of its maturity and low cost, is adopted as well, but it is limited to use in an array of multiple devices for the short-range (<1 m) detection of vehicle-surrounding obstacles in low-speed urban scenarios.

Lidar is an active sensor, which allows measurements of distance with high resolution and speed. However, lidars are heavy and costly. For instance, the LMS 291 in [17] has a weight of 4.5 kg and a power consumption of 20 W from a 24-V dc supply. The HDL-32E has a lower weight [18], 1.3 kg, and lower power consumption, 12 W. The cost of today's commercially available lidars [17], [18] for autonomous driving ranges from a few thousand to tens of thousands of USD. The cost of a lidar sensor is one of the main bottlenecks for the widespread adoption of this technology in vehicles, and, as discussed in [5], there are several initia-

tives in industry to reduce it. For example, microelectromechanical systems and micromirror technology can be used to reduce the cost of 3D scanning lidars, but this technology is still in its infancy.

Arrays of video cameras and/or ultrasonic sensors and/or infrared sensors have been proposed in [19] for obstacle detection. These allow the low-cost and low-power recognition and classification of targets, as a consequence of the evolution of CMOS camera-on-chip technology. However, the detection range and measurements of distance and speed with video cameras is typically limited to tens of meters. Therefore, applications are limited to parking assistance for cars or obstacle detection at low speed in crowded urban traffic. Moreover, camera sensors operating in the visible spectrum are not robust in the case of bad weather or lighting conditions. By adding thermal cameras, operating in the long-wave infrared (LWIR) spectrum range (wavelengths from 7 to 14  $\mu\text{m}$ ), thus creating a multicamera, multispectral system, the detection and measurement activities become more robust to bad operating conditions (e.g., sun glares, low light, and fog). However, the maximum covered range is still limited to tens of meters, and the increased robustness is paid in terms of increased cost (thousands of euros for multispectral video measuring systems, including an LWIR camera, although with a limited  $640 \times 480$ -pixel resolution).

Radar are less sensitive to weather conditions, allowing for the safe detection of obstacles during heavy rain, snow, and hail and in the presence of dense fog, strong sun glare, and environmental noises and vibrations. Radar sensing is also preferable to nonimaging technologies, such as induction loops and photoelectric or RF interruption beam sensors, due to its relatively small size and easier installation, use, and maintenance.

Low-cost and low-power radars have recently been proposed, such as the 60-GHz radar in [20], for proximity detection, as have low-power ultrawideband (UWB) radar sensors for measuring vital signs in [21], which can be useful for driver health and attention status in assisted-driving systems. However, in these cases, the covered range is limited to a few meters, and, therefore, the sensors are not suited for land or maritime transport surveillance applications or for autonomous driving in extraurban or highway scenarios.

For transport surveillance radar, when monitoring a railroad crossing or road crossing or when parking, the needed detection range is on the order of hundreds of meters. Extending the requirement to maritime applications, such as monitoring harbor ingress/egress traffic [22], the range distance to be covered is greater than 1 km. The use for transport applications leads to strict requirements in terms of both harsh operating conditions and functional safety. A safety integrity level of 4 is often required, with an acceptable fault rate of less than 10 failures in time (FIT)—where 1 FIT equals a maximum of one failure for each  $10^9$  h of operation—and a fault-diagnosis rate higher than 99%.

Many low-cost and low-power radars have been proposed in the recent literature by academia and industry. For example,

STARS Railway Systems [23], a new joint venture company of Ingegneria Dei Sistemi and Intecs, proposed radar-based solutions for the automatic detection of objects that have fallen on railway tracks in high-risk zones (e.g., near overpasses, tunnels, and areas prone to landslides) or for the prevention of train collisions with obstacles on the track at level crossings. A network of multiple X-band FMCW radars is used, each exploiting a microwave commercial off-the-shelf board for the front end and field-programmable gate array (FPGA)-based radar signal processing [24].

For perception use in autonomous vehicles (automotive and drone/robotics applications), electronics companies like Bosch, Denso, and Continental, to name just a few, have proposed several types of short-range and low-range millimeter-wave (mm-wave) radars (operating at 22–24 GHz in [25], 77–79 GHz in [26], 80 GHz in [27], or 90 GHz or above in [28]). However, there is a tradeoff between the field of view (FoV) and distance, with the maximum detection range limited to 250 m at a very narrow FoV or fewer than 10 m for a large FoV. Moreover, the detection accuracy in distance, angle, and speed is still not enough for fully autonomous driving, where accuracy to the centimeter is required. Although estimation algorithms, such as ESPRIT, MUSIC, or RELAX, are available in the literature [29], [30], their cost-effective and real-time implementation in automotive radar has yet to be achieved. Problems, such as interference with other V2V/V2I RF signals [31]–[33], privacy/security, low EM emissions, and data fusion with other sensors, still must be solved.

To improve the resolution and signal-to-noise ratio (SNR) performance, MIMO schemes may be applied in automotive radar [22], [24], [34]–[37]. In a MIMO radar, a critical design issue is the optimal placement of transmitting and receiving arrays. For example, the series-production radar in [36] has two transmitting antennas with 5.32-cm spacing and six receiving antennas with 8.9-mm spacing. The physical position of the transceivers directly affects the properties of the virtual array. The radar system in [37] for urban environments has up to 16 transmitting antennas, working

simultaneously, and 16 receiving antennas, each one with a dedicated ADC and processing channel using a commercial gallium arsenide (GaAs)-based monolithic microwave integrated circuit (MMIC) with 77-GHz carrier and 2-GHz bandwidth. In the literature, research on genetic algorithms to search for the optimal antenna placement has been reported (e.g., see [38]). An integrated silicon germanium (SiGe) time-division-multiplexing MIMO radar sensor for the 76–81-GHz frequency band was presented in [39] with dielectric lens antennas (four arrays of patch antennas integrated on the board).

Increasing the integration capability will enable new opportunities for radar signal processing. As discussed in [7]–[9], radar integration technology has moved from using costly GaAs discrete MMIC [e.g., the 2G long-range radar (LRR2) from Bosch] to silicon-integrated mm-wave circuits with SiGe bipolar CMOS in 3G and 4G. This gave the technology the ability to increase the complexity of the embedded radar techniques; increase the number of in-package antennas (from four to six); and increase the accuracy level, from an LRR2 accuracy of 50 cm to better than 10 cm in LRR4 (the fourth-generation LRR).

The latest commercial generation from Bosch, LRR4, is a monostatic multimodal radar that has six fixed antennas. The four central antennas can be properly fed to create a focused beam pattern with an opening angle of  $\pm 6^\circ$  (narrow FoV for detection ranges up to 250 m with a transmitted power of up to 10 dBm), with minimal interference from traffic in adjacent lanes. In the near range, the LRR4's outer two antennas expand the FoV to  $\pm 20^\circ$  at a distance of up to 5 m to detect vehicles entering or leaving the vehicle's lane. Table 1 summarizes, with reference to recent vehicular radars proposed in the market, the performance and specifications of low-power automotive radar in terms of maximum distance; FoV at azimuth and elevation; accuracy (best case) achieved in terms of range, speed, and angle; object separability; and physical characteristics like size, weight, and power consumption.

**Table 1. The specifications of automotive radar, all at 76–77 GHz.**

Radar Type	Maximum Range	Azimuth FoV	Elevation FoV	Best Accuracy (Range, Speed, Angle)	Object Separability (Range, Speed, Angle)	Weight, Size, Power
ARS408 Continental	250 m	$\pm 9^\circ$ at 250 $\pm 450^\circ$ at 100 m $\pm 600^\circ$ at 20 m	14° at 250 m 20° at 20 m	$\pm 0.1/0.4$ m near/far $\pm 0.03$ m/s $\pm 0.1^\circ$	$\pm 0.1$ m/s near, $\pm 0.12$ m/s far	330 g 13.8 × 9.1 × 3 cm 6.6 W
LRR4 Bosch	250 m	$\pm 60^\circ$ at 250 m $\pm 100^\circ$ at 100 m $\pm 150^\circ$ at 30 m $\pm 200^\circ$ at 5 m	$\pm 4.5^\circ$ at 200 m	0.12 m 0.11 m/s $\pm 0.3^\circ$	0.72 m 0.4 m/s $\pm 4^\circ$ Maximum 24 targets	<240 g 7.8 × 8.1 × 6.2 cm <sup>3</sup> 4.5 W
MRR Bosch	160 m	$\pm 60^\circ$ at 160 m $\pm 100^\circ$ at 60 m	$\pm 25^\circ$ at 36 m $\pm 42^\circ$ at 12 m	0.12 m 0.11 m/s $\pm 0.3^\circ$	0.72 m 0.66 m/s $\pm 7^\circ$	<190 g 7 × 6 × 3 cm <sup>3</sup> 4.5 W
MRRear Bosch	80 m	$\pm 50^\circ$ at 70 m $\pm 750^\circ$ at close (1 m)	None	0.12 m 0.14 m/s $\pm 0.8^\circ$	Maximum 32 targets	

MRR: midrange radar.

However, advanced digital radar signal processing, requiring nanoscale CMOS technology, is still implemented outside these radar-on-chip transceivers, and only local raw-data-processing algorithms are implemented in the radar node, in a separate CPU. More complex radar-data-processing algorithms remain out of scope in current designs. With reference to the SAE classification of six assisted or autonomous driving levels from L0 to L5, discussed in the “Introduction” section, the available automotive radar technology nodes are suited only for L3, that is, assisted driving, where human intervention is still needed. Moving to advanced autonomous solutions at L4 (vehicles that are “designed to perform all safety-critical driving functions and monitor roadway conditions for an entire trip” [5], although in some defined scenarios) or even L5 (fully autonomous in every scenario) require much more complex signal processing capabilities, possibly exploiting machine-learning techniques [40]. The challenges to face include

- radar image understanding and object tracking (obstacles, pedestrians, bikers, and vehicles) [41] at very low missed-detection/false-alarm rates
- radar data fusion with other mobility sensors
- low-latency reaction time, which implies real-time implementation of signal processing
- crowded environments with interference from radar sources of neighboring vehicles and V2I/V2V RF signals
- green radar to minimize the overall EM emissions of all radars mounted onboard all vehicles, on account of precise/adaptive beamforming, including waveform design and/or passive radars [42]
- correct identification/authentication of the proper radar trace and security against hacking or privacy violation.

## Embedded signal processing for low-cost, low-power, and real-time radar sensors

### Radar SoC parameters

New opportunities to embed radar signal processing techniques in inexpensive, low-power, and real-time SoCs arise owing to the technology evolution to pure CMOS or 45-nm or 28-nm nodes, as in last single-chip radar released in [7]–[9]. For example, the SoC in [7] integrates for a cost less than €50 and has a power consumption of 2 W for the entire mm-wave RF and analog and digital baseband signal processing chain. It integrates two transmitters and four receivers as well as two customer-programmable processors: a 600-MHz C674x digital signal processor (DSP) and a 200-MHz ARM Cortex-R4F microcontroller with 1.5 megabytes of on-chip random-access memory (RAM). Half of the on-chip memory is devoted to radar data-cube processing and half to cache memories for the two processors. The SoC allows for 12.5 dBm of transmitter (Tx) power and 14 (or 15)-dB receiver noise figure, with  $-95$  (or  $-93$ )-dBc/Hz phase noise at 1-MHz offset, in the 76–77- GHz (or 77–81-GHz) band. Being AECQ100 and ASIL-B qualified, operating in the  $-40$ – $125$  °C temperature range, the SoC in [7] is ready for automotive use. The computational capability of the SoC allows for a 256-cell constant false alarm rate (CFAR) based on cell averaging (CFAR-CA) implemented in  $1.55\ \mu s$  and 16-bit 256 (512) points fast Fourier transform (FFT) in  $1.55$  ( $3.61$ )  $\mu s$ .

Thanks to the embedded DSP, the SoC implements MUSIC and ESPRIT technologies for high-resolution angle estimation. Hardware-based security accelerators are embedded, such as the true random-number generator, Advanced Encryption Standard, and secure hash algorithm to address radar-hacking and privacy-violation issues. Figure 2 reports an example of SoC

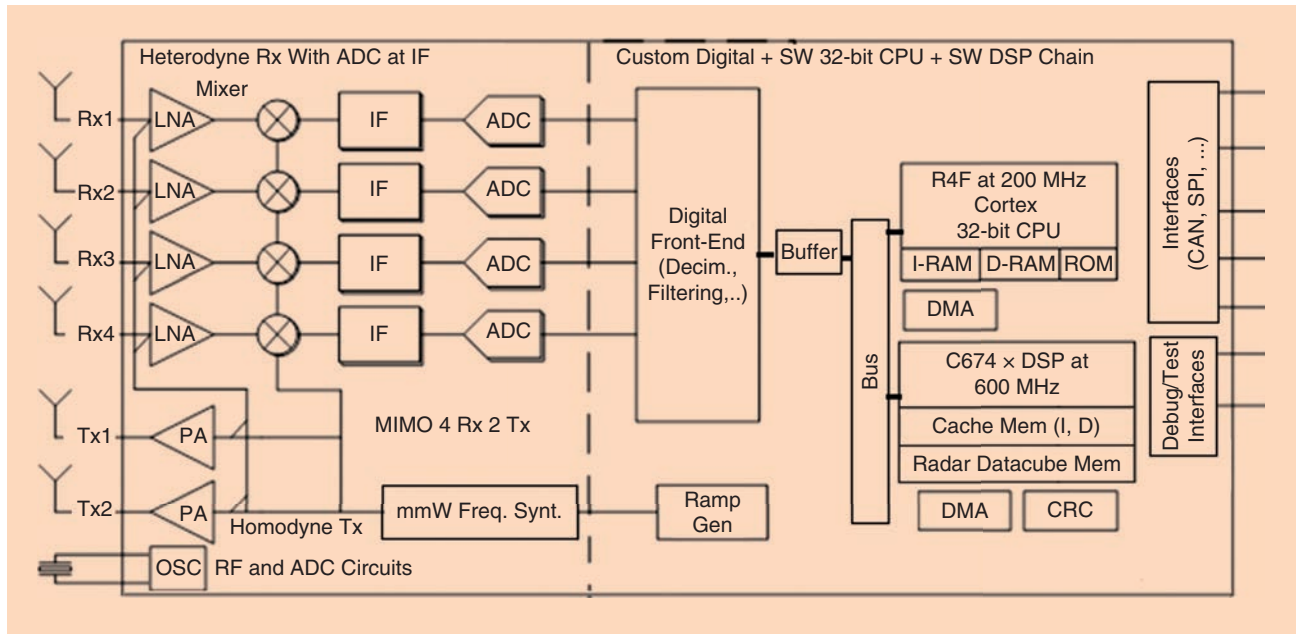


**FIGURE 2.** A radar SoC architecture (76–81 GHz, FMCW, MIMO four receive/two transmit). freq.: frequency; IF: intermediate frequency; mem: memory; Rx: receiver; Tx: transmitter; PA: power amplifier; OSC: oscillator; IF: intermediate frequency; synt.: synthesis; decim.: decimation; SW: software; DMA: direct memory access; CRC: cyclic redundant code; CAN: controller area network; SPI: serial peripheral interface; I: instruction; D: data; gen: generation.

radar architecture with such characteristics, considering for the RF part a heterodyne receiver with a high-speed ADC working at the intermediate frequency and a homodyne transmitter. The radar SoC architecture in Figure 2 is just one possibility, because there are many different architectures from various chip makers. The SoC radar in [7] can be configured for an unambiguous-detection range of 80 m and a maximum unambiguous speed of 90 km/h with 35-cm distance resolution and 0.3-m/s velocity resolution. Such performance is achieved due to FMCW-based range-velocity estimation with a 3D FFT calculation of 128 FMCW ramps  $\times$  four channels  $\times$  256 points, 425-MHz FMCW sweep bandwidth, 128 chirps (51- $\mu$ s chirp duration and 7.5- $\mu$ s reset time). The horizontal-and vertical-elevation FoVs are 120° and 10°, respectively. The same SoC can be reconfigured for a lower range of 20 m, but with higher resolution of 8.7 cm, by using a 1.725-GHz sweep bandwidth. By moving from a CMOS of 45 nm in [7] to 28 nm in [8], the memory and computational capability will double, thus enabling more complex radar algorithms to be implemented. Next, we review the signal processing chain of the SoC in Table 2.

### Range- and velocity-estimation algorithm

All radars in Tables 1 and 2 operate in the 77-GHz band and adopt FMCW pulses to provide simultaneous range-velocity estimations in multitarget traffic scenarios. Continuous-wave (CW) radars are not able to provide a measure of the target distance, only of the velocity. Because of frequency modulation, FWCW radars are able to provide measures of both range and velocity. The target velocity can be estimated by exploiting the Doppler effect. With  $v_D$  as the differential velocity between the vehicle of interest and the target (e.g., another car, a pedestrian, a biker, and so on) along the radar-illumination direction, the reflected waves will be delayed by time  $t_d = 2(R \pm v_D t)/c$ . The time-dependent delay causes a frequency shift in the received wave known as the Doppler shift,  $f_d = \pm 2v_D/\lambda$ , which is inversely proportional to wavelength  $\lambda$ , and its sign is positive or negative,

depending on whether the target is approaching or receding from the radar [2].

The FMCW radar transmits periodic wideband FM pulses (chirps), the frequency of which increases linearly during the pulse (see Figure 3). A single FMCW pulse  $p(t)$  can be written as

$$p(t) = e^{i2\pi(f_c + 0.5Kt)t}, 0 < t < T_{\text{chirp}}, \quad (1)$$

where  $f_c$  is the carrier frequency,  $T_{\text{chirp}}$  (51  $\mu$ s in Table 2) is the chirp length, and  $K = B/T_{\text{chirp}}$  is the sweep rate, with  $B$  as the sweep bandwidth ( $K = 8.3 \text{ MHz}/\mu\text{s}$ ,  $B = 425 \text{ MHz}$  in Table 2). The signal received after reflection with a target is mixed (output of the receiver mixer in Figure 2), with the transmitted signal to produce a low-frequency beat signal, whose frequency is linearly dependent on the range of the target. This operation is repeated for  $P$  consecutive pulses. Consecutive reflected pulses give a 2D waveform arranged across two time indices, where the slow time index  $p$  corresponds to the pulse number and the fast time index  $n$  assumes that for each pulse. The corresponding continuous beat signal is sampled with frequency  $f_s$  to collect  $N$  samples within the duration time  $T$  (58.5  $\mu$ s in Table 2). The latter includes the chirp time  $T_{\text{chirp}}$  and the rest time  $T_{\text{rest}}$  (7.5  $\mu$ s in Table 2).

Figure 3 represents the ideal case of  $T_{\text{rest}} = 0$  and, therefore,  $T = T_{\text{chirp}}$ . Assuming single target and neglecting reflected signal distortions, (2) shows the FMCW radar receiver signal  $x(n, p)$  as a function of time indices  $n$  and  $p$ , where  $\omega(n, p)$  is additive white Gaussian noise:

$$x(n, p) \sim \exp \left\{ i2\pi \left[ \left( \frac{2KR}{c} + f_d \right) \frac{n}{f_s} + f_d p T + \frac{2f_c R}{c} \right] \right\} + \omega(n, p). \quad (2)$$

Discrete Fourier transform across fast time  $n$  can be applied to obtain the beat frequency  $f_b$ , which includes the information about both the target range (which is related to the time delay  $t_d$  in Figure 3 between the transmitted chirp and received signal) and

**Table 2. Hardware and signal processing parameters of an SoC radar with the architecture shown in Figure 2.**

Hardware Parameters (mm-wave Front-End and Baseband Digital Processing)								
Power	Cost	Tech.	RF, IF	Tx Power	Rx NF	Phase Noise	DSP	MCU
2.14 W	<€50	SoC 45 nm	76–81 GHz, 5 MHz	12 dBm	15 dB	-95 dBc/Hz	600 MHz C674X	200 MHz ARM CortexRF4
Signal Processing Parameters (FMCW)								
Sweep Band $B$	Chirps $P$	Frame Time	$T_{\text{chirp}}/T_{\text{rest}}$	Rx/Tx Channels	Detection	Angle Estimation	ADC	Range FFT
0.425 (1.725) GHz	128	7.5 ms	51/7.5 $\mu$ s	4/2	CFAR-CA	MUSIC/ESPRIT	6.25 million samples/s	256
Radar System Parameters								
Range	HFoV	VFoV			Maximum Speed		Speed Resolution	Range Resolution
80 (20) m	1,200° (1,600° at 10 m)	100° (300° at 10 m)			90 (30) km/h*		1 km/h	35 (8.7) cm

\*The value within parentheses for speed corresponds to the values within parentheses for range, HFoV, and VFoV. HFoV: horizontal FoV; VFoV: vertical FoV; NF: noise figure; Tech: technology; IF: intermediate frequency; MCU: microcontroller unit.

the target velocity (which is related to the Doppler frequency shift  $f_d$ ). Therefore, applying a 2D FFT algorithm, a range-Doppler map can be produced [2]. In the range-Doppler map, the peaks along the rows reveal the distance of a target, and the peaks along the columns reveal the speed of the target. For this, a peak-detection algorithm has to be used. To identify valid targets in the presence of clutter, the threshold for the target detection should be properly chosen. If the amplitude of the spectrum at an estimated range is greater than some threshold, the target is said to be detected. Thus, the threshold should depend on the noise or, in other words, on the clutter in the given system. As clutter increases, a higher threshold may be chosen. A simple CFAR-CA uses a sliding window to derive the local clutter level by averaging the multiple-range bin samples. CFAR-CA is the technique used both in the SoC radar of Table 2 and by our

single-board radar in [10]. To further increase the detection accuracy, more sophisticated CFAR algorithms can be used, such as the ordered-statistic or trimmed-mean CFAR [2].

Moreover, to improve performance, the CFAR algorithm could be followed by a binary integrator (e.g., with an  $M$ -out-of- $N$  decision rule) as in Figure 4, which shows the digital baseband signal processing chain implemented at the University of Pisa, Italy, for parking and road-crossing surveillance as described in [10].

Figure 5 shows an example of a range-Doppler map obtained with such an FMCW radar. The range-Doppler image in Figure 5 was obtained with 0-dBm (1-mW) transmitted power,  $P = 256$  FMCW ramps, and 2,048 samples/ramp, that is, by using a  $256 \times 2,048$  2D FFT,  $B = 500$ -MHz sweep bandwidth, and 12-bit ADC. Three different targets have been detected in this

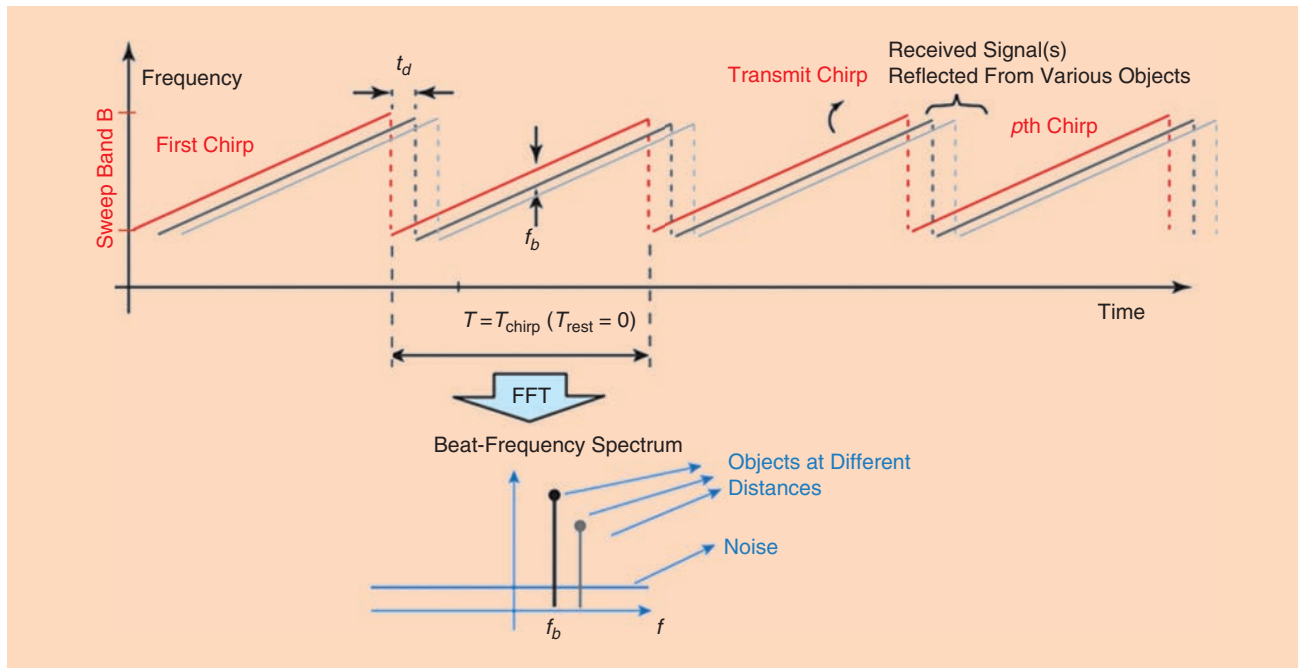


**FIGURE 3.** FMCW range-velocity estimation and waveforms.

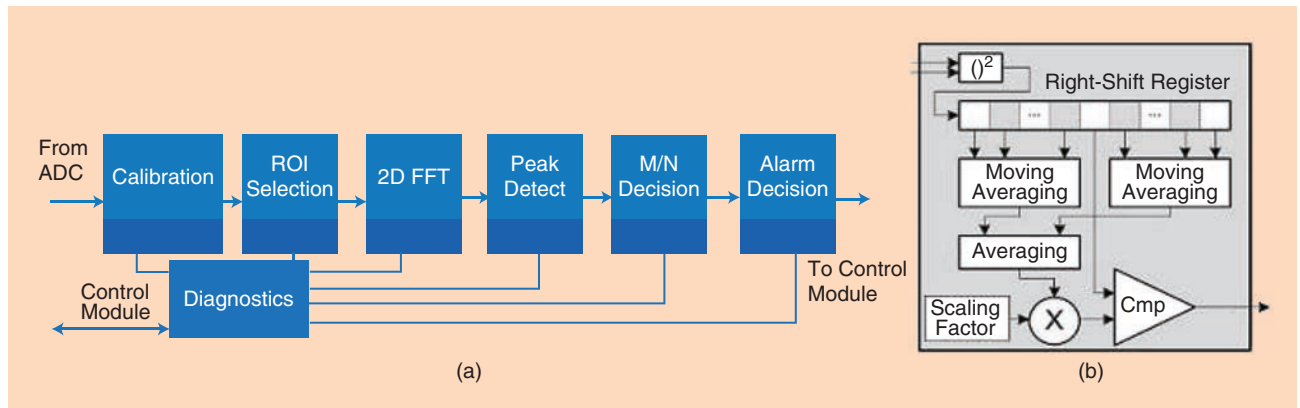


**FIGURE 4.** (a) The baseband digital signal processing architecture of an FMCW radar for range-speed estimation. (b) The details of CA-CFAR peak detection. ROI: region of interest; CMP: comparator; M/N:  $M$  out of  $N$ .

specific scene for a parking surveillance application: target A at a distance of 81 m and with a relative speed of 21 km/h; target B at a distance of 44 m and with a relative speed of 5.5 km/h; and target C, almost still, at a distance of 77 m. The detected targets do not appear like a point in the range-Doppler map but, rather, like an oval. This is due to the physical size of the targets and also the resolution limits in distance and speed of the implemented FMCW radar sensor. Indeed, the limited sweep bandwidth  $B$  determines the limit of the distance resolution  $dR = c/2B$ , that is, 30 cm at  $B = 500$  MHz. The speed resolution limit mainly depends on  $\lambda/(2PT)$  and is 1 km/h at 77 GHz in the example case of  $\lambda = 4$  mm,  $P = 128$ , and  $T = 58 \mu\text{s}$ , as in Table 2.

A convenient alternative to the chirp waveform is the double chirp or triangular chirp (Figure 6). The positive slope of

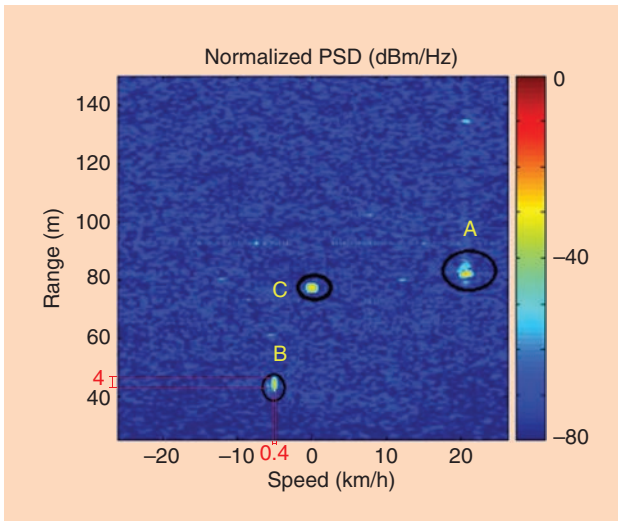


**FIGURE 5.** An example of a range-Doppler map obtained with an FMCW radar sensor (256 chirps, 2,048 samples/chirp, 0-dBm transmission, 500-MHz sweep bandwidth) with three targets (A, B, and C). PSD: power spectral density.

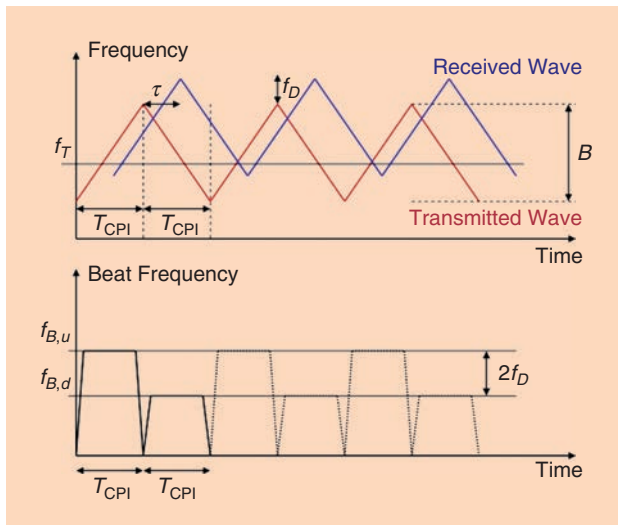


**FIGURE 6.** A triangular chirp [3].

the signal indicates an up-chirp signal, and the negative slope indicates a down-chirp signal with the same sweep bandwidth  $B$ . In the first interval  $T_{\text{CPI}}$ , the up-chirp is transmitted, followed in the second  $T_{\text{CPI}}$  by a down-chirp.

The advantage of this waveform compared with the single chirp is that, in this case, for every triangular pulse, the radar has two beat frequencies,  $f_{B,u}$  and  $f_{B,d}$ , as shown in the bottom part of Figure 6, both related to the range and Doppler frequency of the target. Therefore, the radar can estimate both range and Doppler frequency at the same time [3]. A triangular pulse provides an unambiguous estimate of these target parameters only when a single target is present. In a multiple-targets scenario, the triangular chirp provides an up and down beat-frequency equation for each target and, for two targets, four different ambiguous solutions. In this case, alternative waveforms as stepped-frequency (SF) CWs, orthogonal frequency-division multiplexing (OFDM), and frequency-shift keying (FSK) have been proposed as explained in [43].

#### Direction-of-arrival estimation

To implement a direction-of-arrival (DOA) estimation, which is essential in the perception process, a multiantenna receiver array is needed. In a realistic traffic scenario, several targets are surrounding the radar that collects direct and multipath reflections from them. In such cases, to spatially resolve equidistant targets and deliver comprehensive representation of the traffic scene, the angular location of the targets should be estimated. In vehicular radars, the location of a target is often described in terms of a spherical coordinate system, which includes the range, azimuth angle, and elevation angle. The single antenna radar discussed previously allows for a range-velocity estimation, but it lacks the information in terms of angular locations of the targets. The latter can be achieved by comparing the received signals of multiple receiver channels placed at a predetermined distances.

Consider an antenna array located in plane  $xy$ , and let  $l$  be the abscissa corresponding to each receiver antenna position, for example, four elements in the uniform linear array (ULA) in Figure 7, at distance  $d$  each (often in the literature  $d = \lambda/2$ ; therefore, the total length of the ULA in Figure 7 would be  $L = 2\lambda$ ). Let  $(R_q, \theta_q)$  be the position of the  $q$ th target in spherical coordinates, moving with relative velocity  $v_q$  to the radar. With the help of far-field approximation for the  $q$ th target, the round-trip time delay between a transmitter located at the origin and the receiver positioned at coordinate  $l$  is given by  $\tau_{lq} = (2(R_q + v_q t) + ld \sin(\theta_q))/c$ . Hence, a 3D FMCW radar signal can be obtained that, in the case of  $Q$  targets, can be expressed as in (3), where  $\alpha_q$  is a complex scalar whose magnitude represents the  $q$ th target the attenuation due to antenna gain, path loss, and the radar cross section (RCS) of the target. The delay term  $\tau_{lq}$  creates uniform phase progression across antenna elements, which permits the estimation of the angle by FFT in the spatial domain. Thus, the 2D location (range and angle) and speed of targets can be jointly estimated by 3D FFT. The relevant cube of data of

range, FMCW ramps, and multiple receiving channels is shown in Figure 7(b).

$$x(l, n, p) \sim \sum_{q=0}^{Q-1} \alpha_q \exp \left\{ i 2 \pi \left[ \left( \frac{2 K R_q}{c} + f_{dq} \right) \frac{n}{f_s} + \frac{f_c l d \sin(\theta_q)}{c} + f_{dq} p T + \frac{2 f_c R_q}{c} \right] \right\} + \omega(l, n, p). \quad (3)$$

The FMCW 3D FFT radar with CFAR-CA peak detection that we have proposed has been implemented at the University of Pisa at the board level with separate chips for mm-wave transceivers, analog front-end, and ADC and baseband digital signal processing (while that in Table 2 is integrated at the single-chip level). The digital signal processing is implemented in a Zynq XA7Z020 device. It is a pure digital FPGaC integrating Dual-Core ARM 32-bit Cortex-A9-based application processor unit with 2.5 Dhystone million instructions per second/MHz computational capability, clocked at 200 MHz, plus NEON hardware instruction set extension (128-bit, single-instruction, multiple-data architecture), plus FPGA resources, plus a large set of peripherals. The peripherals include external synchronous dynamic RAM, nonvolatile memory controllers, two controller area network interfaces, and 1 megabyte of on-chip RAM memory. The 3D FFT FMCW computing unit occupies approximately 94% of available Zynq XA7Z020 resources in terms of flip-flops, memory blocks, and DSP blocks (mainly with multiply and add capabilities) and 46% of available look-up tables for custom combinatorial logic.

### Adaptive beamwidth

In contrast to what has been analyzed in survey articles [2], rather than a fixed specification for the beamforming, the last generation of vehicular radars in Tables 1 and 2 supports multiple antennas and adaptive beamforming. As an example, in Table 1, the azimuth FoV in long-range radars is adapted from a minimum of  $\pm 9^\circ$  to a maximum of  $\pm 60^\circ$  when the range varies from 250 m to 20 m, whereas, in medium range radars, it is adapted from a minimum of  $\pm 5^\circ$  to a maximum of  $\pm 75^\circ$  when the range varies from 70 to 1 m. In commercial devices, the adaptive beamformer is often obtained by a proper mix of the antennas in the array. For example, in the LRR4 sensor from Bosch, four central antennas are properly fed to create a focused beam pattern with an azimuth FoV of  $\pm 6^\circ$  at maximum distance of 250 m, whereas two outer antennas are used to achieve an extended FoV of  $\pm 20^\circ$  at a target distance of less than 5 m.

A narrowband beamforming array usually characterizes mm-wave automotive radars. Indeed, the fractional bandwidth of mm-wave radar signals is within 5% (e.g., 1–4-GHz bandwidth at approximately 80 GHz in Tables 1 and 2). Moreover, the time delay  $\tau_{\max}$  between the first and last elements of the antenna array is usually so small that the signals received by the opposite ends of the array are still correlated with each other. Indeed, in the example case of a ULA of  $M$  elements with  $\lambda/2$  spacing,  $\tau_{\max} = ((M - 1) \cdot \lambda)/2c$ , which corresponds to a delay in the range of  $10^{-11}$ – $10^{-10}$  ps when considering the typical parameters of on-chip/in-package radars in Tables 1 and 2.

A special mention has to be made of the elevation antenna FoV. As a result, the radar sensing system may achieve a wide

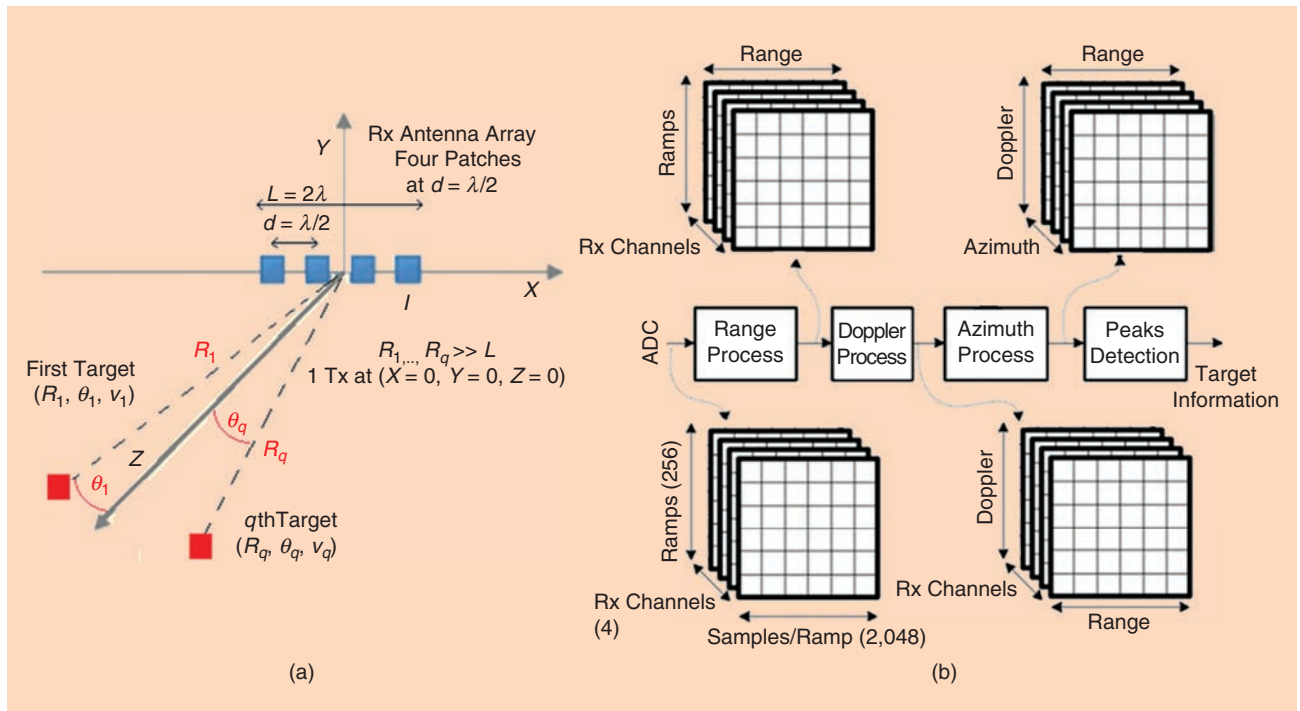


**FIGURE 7.** The range-velocity-angle estimation with a 3D FFT through (a) a multichannel receiver array (e.g., ULA with four channels at  $d = \lambda/2$ ) and (b) the corresponding radar data cube.

opening angle at close range, so a pedestrian stepping out into the road from behind a parked car is detected at an early stage. An independent mode for height measurement using an elevation antenna enables the system to reliably classify objects and brake safely, even when the object is stationary.

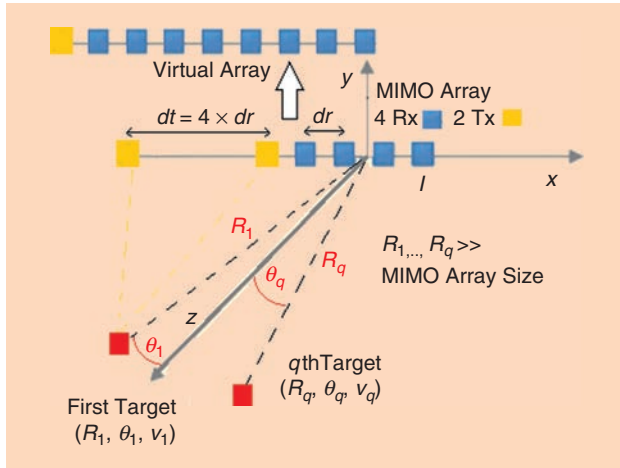


**FIGURE 8.** A colocated MIMO radar with two Tx and four Rx antenna elements. A 1D virtual array.

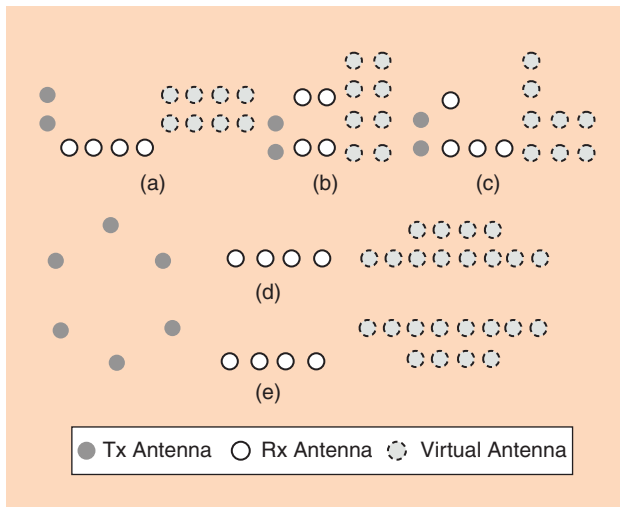


**FIGURE 9.** Examples of a 2D virtual antenna array with (a)–(c) two Tx and four Rx elements and (d) and (e) three Tx/four Rx elements.

When designing an antenna for on-chip/in-package radar applications (whose detailed discussion is beyond the scope of this article), achieving a wide FoV is often a contrasting requirement versus other key performance parameters, such as high gain and compact size. One option to achieve the required azimuth and elevation FoV is to exploit an antenna array by placing the antennas so that the operation in MIMO mode (see further discussion in the “MIMO Radar” section) synthesizes a 2D virtual array, thus enabling angle estimation along both the azimuth and elevation.

Such a technique is already exploited by the latest commercial generation of mm-wave radar sensors from Texas Instruments (TI) [44] for automotive and industrial applications. For example, the radar-on-chip sensor in Table 2 sustains two transmitting and four receiving antennas; other state-of-the-art devices [44] with the same architecture support three transmitting and four receiving antennas. As detailed in the “MIMO Radar” section and Figure 8, if the two (or three) transmitting antennas and the four receiving antennas are placed on the same azimuth plane (i.e., at the same height), a virtual array of eight (or 12) receiving antennas is obtained on the azimuth plane. Instead, if the antennas are placed so that one or more antennas are at a different height versus the other elements, then a virtual array also along the elevation is obtained. See Figure 9 for more details.

### Waveform design

The adaptability and selection of the radar waveform is a key issue in embedded automotive radar because this affects the performance in terms of range resolution; velocity resolution; angular direction; and SNR; the probability of target detection; and, in the case of FMCW radars, the number of targets that can be resolved without ambiguity (ghost targets) [43]. In general, the radar waveforms can be characterized whether or not they are CW, pulsed and frequency, or phase modulated. Modulated radar waveforms include, for example, FMCW, SFCW, OFDM, and FSK. Each waveform type has a certain advantage in processing, implementation, and performance, as shown in Table 3.

In vehicular radars, the most common are the linear frequency-modulated CWs (chirps). In unmodulated CW radar, a conjugate mixing of a high-frequency transmitted and received signal produces the output signal at the Doppler frequency

**Table 3. The main waveforms that can be selected in a single-chip CW radar.**

Waveform	Transmit Signal	Detection by	Range, Doppler Resolution	Notes
Pulsed CW	$\text{rect}(t/T_p) \cdot e^{j2\pi f_c t}$	Correlation	$\Delta R = c \frac{T_p}{2}, \Delta f_d = \frac{1}{T_p}$	$\Delta R$ depends on $1/\Delta f_d$ .
FMCW	$e^{j2\pi(f_c+Kt)t}, K = B/2T$	Conjugate mix	$\Delta R = \frac{c}{2B}, \Delta f_d = \frac{1}{PT}$	$P$ = number of ramps, each with duration $T$ .
SFCW	$e^{j2\pi f_n t}, f_n = f_c + (n-1)\Delta f$	Inverse FFT	$\Delta R = \frac{c}{2B}, \Delta f_d = \frac{1}{PT}$	$\Delta f$ sets $R_{\max}$ , $P$ = number of ramps each with duration $T$ .
OFDM	$\sum_{n=0}^{N-1} l(n) \cdot e^{j2\pi(f_c+n\Delta f)t}$	Channel estimation in frequency domain	$\Delta R = \frac{c}{N\Delta f}, \Delta f_d = \frac{1}{PT_N}$	$N$ = number of carriers, $P$ = number of OFDM blocks of duration $T_N$ . $l(t)$ is an arbitrary sequence.

of the target. The resolution of the frequency measurement is inversely proportional to the time duration of the signal capture. The continuous nature of the waveform precludes a round-trip delay measurement, which is necessary for a range estimation of the target. As discussed, FMCW, also known as *linear frequency modulation* or *chirp*, is used for simultaneous range and velocity estimation. The range resolution is inversely proportional to the bandwidth of the FMCW signal and is independent of pulsedwidth. For example, short-range FMCW radars use UWB waveforms to measure small distances with higher resolution. The Doppler resolution is a function of the pulsedwidth and the number of pulses used for the estimation.

In contrast to FMCW waveforms, the frequencies of FSK and SFCW vary in a discrete manner [2]. In this case, the range profile of the target and the data collected at discrete frequencies form the inverse Fourier transform relationship. Also, hybrid waveform types can be employed to achieve an additive performance. The FSK waveform can be combined with the multislope FMCW waveform to overcome ghost targets in radar processing [14]. Similarly, alternate pulses of CW and FMCW are used to accurately estimate the range and Doppler [9].

OFDM is another multifrequency waveform that offers unique features of the joint implementation of automotive radar and vehicle-to-vehicle communications [11], [12]. For radar operation, the orthogonality between OFDM subcarriers is ensured by choosing carrier spacing more than the maximum Doppler shift, and the cyclic prefix duration is selected greater than the longest round-trip delay. The range profile is estimated through a frequency-domain channel estimation.

## Advanced radar signal processing

### Embedded HPC for high-end signal processing

The “Embedded Signal Processing Toward Low-Cost, Low-Power, and Real-Time Radar Sensors” section discussed the scenario to achieve low-cost, low-power, and small-size radar sensors to be mounted onboard a vehicle (multiple sensors covering short/medium range and medium/long range and positioned in different places to achieve 360° of coverage). From a signal processing point of view, a multiantenna FMCW-based technique for range-speed-angle estimation, with adaptive beamforming and a diverse waveform selection, has been discussed, and single-chip and single-board implementations have been reviewed. This scenario does not consider the case of all vehicles being equipped with multiple remote sensors and being interconnected with V2V/V2I technologies when issues of spectrum occupation and interference will arise. This is why advanced signal processing techniques may be needed. MIMO radar to further improve resolution is discussed in the “MIMO Radar” section, and cognitive radar to achieve a full adaptability to the environment is reviewed in the “Cognitive Radar” section.

Although the signal processing capability integrated in the SoC radar of Figure 2 is on the order of few giga operations

per second (GOPS), emerging automotive HPC processors are promising to increase this value by one order of magnitude at least. For example, the recently (March 2018) launched Renesas-H3 integrates 16-nm technology in a PowerVR GX6650 graphics processing unit (GPU) with 192 arithmetic logic unit cores for 3D graphics (more than 100 GOPS) plus eight 64-bit ARM cores (4-Cortex-A57 and 4-Cortex-A53) and one 32-bit Cortex-R7 (main controller) offering an extra 40 GOPS. The announced new embedded HPC designs from Intel and Nvidia are further increasing these numbers. EyeQ5 SoC from Mobileye (now Intel) is targeting 24,000 GOPS at 10 W. The Xavier artificial intelligence car’s computer from Nvidia is targeting 30,000 GOPS with a power consumption of 30 W (thanks to eight ARM 64-bit cores plus a 512-core Volta GPU, a video processing unit supporting 8K video decode and encode, and high dynamic range as well as a computer vision accelerator).

### MIMO radar

MIMO radar systems employ multiple transmitters, receivers, and waveforms, and MIMO radars can be classified as widely separated or colocated. In widely separated MIMO radars, transmit–receive antennas capture different aspects of the RCS of a target, whereas, in colocated MIMO radar, the RCS observed by each antenna element is indistinguishable. Due to size requirements, automotive radar typically uses colocated MIMO radars, which are compact. For proper transmitter spacing, the colocated MIMO radar can emulate a larger-aperture phased-array radar, that is, a virtual array. For MIMO radar processing, consider  $L_T$  and  $L_R$  as the numbers of transmit and receive antenna elements, respectively ( $L_T = 2$  and  $L_R = 4$  for the SoC radar in Figure 2 and for the example in Figure 8). Suppose that  $d_T$  and  $d_R$  represent the corresponding transmit (yellow dots in Figure 8) and receive (blue dots in Figure 8) antenna spacings. Also, assume that the transmit and receive antenna positions, in Cartesian coordinates, are given by  $l_T$  and  $l_R$ . Hence, the 2D FMCW mixer output signal across fast time and aperture is given by (4). If  $d_T = L_R \times d_R$ , then MIMO radar imitates a regular 1D array radar with single transmit and  $L_R \cdot L_T$  receive antenna elements (virtual array representation [2]). Hence, the spatial resolution of FFT-based target imaging can be improved by the factor of  $L_T$ .

$$x(l_T, l_R, n) \sim \sum_{q=0}^{Q-1} \alpha_q \exp \left\{ i2\pi \left[ \frac{2KR_q}{c} \frac{n}{f_s} + \frac{f_c(l_T d_T + l_R d_R) \sin(\theta_q)}{c} \right. \right. \\ \left. \left. + \frac{2f_c R_q}{c} \right] \right\} + \omega(l_T, l_R, n). \quad (4)$$

As previously discussed in the “Adaptive Beamwidth” section, the transmit and receive antenna elements can be also placed so that the operation in MIMO mode synthesizes a 2D virtual array (see example in Figure 9) instead of the 1D virtual array (as in Figure 8). For example, the commercial TI AWR1443 and IWR1443 radar sensors in [44] for automotive and industrial uses exploit the 2D array configuration in Figure 9(d) to reach an elevation FoV of 30°.

One of the challenging aspects of MIMO radar is the selection of waveforms. The waveforms can be made

orthogonal in the frequency, time, or code domains. Consequently, the matched filter design at the receiver varies, which is necessary to separate reflected waveforms originating from different transmitters. From the basic FMCW radar signal given in the “Embedded Signal Processing Toward Low-Cost, Low-Power, and Real-Time Radar Sensors” section, various orthogonal waveforms can be constructed, as reported in Table 4. More details on vehicular MIMO radars are provided [15].

### Cognitive radars

Fundamental for automotive radars are the problems of mutual interference due to multiple radars operating closely and simultaneously and of interference with communication systems working in the same mm-wave bandwidth, particularly when 5G systems will be fully operating. A detailed analysis of these interferences is provided in [45]. This issue of spectrum crowding can be partially addressed by traditional modes of operation, such as spatial signal processing and beamforming [46]. However, more likely, future automotive radar systems will be able to anticipate the behavior of other emitters in the operational environment and adapt their transmissions in a cognitive fashion based on the spectrum availability. As cognitive radio systems devoted to communications, cognitive radar systems should then perform the spectrum sensing function, which has the goal of obtaining necessary observations about the radio frequency channel, such as the presence of other users and the appearance of spectrum opportunities (free channels), where it is possible to transmit without interfering.

Spectrum sensing can be performed via two different architectures: single radio and dual radio. In the single-radio architecture, only a specific time slot of the signal at the radar receiver is allocated for spectrum sensing. In the dual-radio sensing architecture, one radio chain is dedicated to the radar operations, and the other chain is dedicated to spectrum sensing. A single antenna would be sufficient for both chains [13] and would make it easy to realize the cognitive system in an SoC. As detailed in [46], there are multiple techniques for performing the spectrum sensing, as already implemented in cognitive radios. The open literature mainly focuses on energy-detector, feature-detector, and matched-filter techniques. In general, based on the knowledge acquired by analyzing

the environment through the sensing block, the automotive radar should be able to change its carrier on the fly (for OFDM radars), transmit subband, and chirp slope or waveform shape, code, pulse repetition interval, and so on, not only to reduce the cross-interference between coexisting radars and/or communication systems but also to improve the range and frequency resolution and the SNR. Thus, the cognition is limited not only to the reduction of the interference, but it can be beneficial as well for the radar detection and tracking performance, as shown, for instance, in [47] and [48].

### Passive radars

To mitigate the spectrum crowding problem at mm-wave bands, another advanced radar signal processing technique to be exploited in the future is the use of passive radars [49], [50]. They are bistatic radars that make use of emissions from a noncooperative transmitter of opportunity, such as broadcast, communications, or radionavigation transmitters rather than a dedicated, cooperative radar transmitter. In large ground-based radars, emissions from FM radio stations, digital audio broadcasting and digital video broadcasting, and 3G and 4G cellular signals are used for target detections purposes. Although in active radar sensors the time of transmission and the transmitted waveform are exactly known, and this allows the target range, speed, and DoA to be estimated, a passive radar is missing such information directly, even with embedded systems, as discussed in previous sections. To overcome this issue, a dedicated receiver channel acting as a reference channel can be used to monitor each noncooperative transmitter being exploited and dynamically sample the transmitted waveform. Different from active radars, the detection range in passive radars is also a function of the deployment geometry, because the distance of the passive receiver from the noncooperative transmitter determines the level of external noise against which the targets must be detected. In addition, passive radar accuracy is a strong function of the deployment geometry and the number of receivers and transmitters being used.

Unlike other applications, such as early warning, harbor protection, and so on, for which the research has already produced many prototypes, for automotive applications, the passive radar technology is still seen as immature, and the reliance on third-party illuminators and the complexity of

**Table 4. MIMO radar waveform design.**

Type	Pulse Expression	Notes
Beat frequency division	$\exp\left\{i2\pi\left[(f_c - \Delta f_b)t + 0.5Kt^2 + 0.5\left(\frac{\Delta f_b^2}{K}\right)\right]\right\}$	The value $\Delta f_b$ is the frequency offset introduced for waveform orthogonalization. The last term in the exponential corresponds to the residual video phase compensation, which is necessary for coherent receiver processing.
Modulation constant division	$\exp\{i2\pi[f_c + 0.5(K + \Delta K)t]t\}$	The modulation constant, or chirp rate offset, is given by $\Delta K$ , which is obtained by varying the pulse period. The bandwidth at each transmitter remains the same to maintain the range resolution. The reset time between the pulses ensures synchronization at the receiver.
Code division	$\exp\{i2\pi[f_c + 0.5Kt]t + 0.5\beta(t)\}$	The value $\beta(t)$ corresponds to the binary phase-shift keying (BPSK) signal with a low update rate that assumes values $\pm 1$ . The bandwidth of the BPSK signal is kept smaller to ensure proper operation of the FMCW radar.

deployment contrast with the need for a high functional safety level in autonomous driving.

A promising evolution of the passive radar concept, also exploiting the deployment of the emerging 5G technology, for automotive use was recently presented in [49]. These works introduce the principle of cooperative passive coherent location (CPCL), which is seen as an integrated radar service of future mobile radio networks such as 5G. Whereas passive radar technology does not consider any cooperation between radar illuminators and radar sensors, the CPCL concept assumes that all radar nodes belong to the same network. This way, CPCL will turn the mobile radio networks into a distributed MIMO radar network, which opens a wide scope of cooperation between sensor nodes, including cooperative bi-/multistatic target scene illumination, radar data networking, and radar sensor fusion. Such technology is applicable to several applications involving networking nodes, such as intelligent transport systems and logistics. Besides 5G, V2V and V2I links may also be used to sustain the CPCL concept.

## Conclusions and future trends

Radar-on-chip/in-package has seen a huge development in the last 20 years, since 1999 when Mercedes mounted the first commercial vehicular radar on its top-class cars. Thanks to the technology improvements in SoCs and SiPs, embedded HPC, and new investments, radar is becoming a more ubiquitous sensor, available at a low cost and at low power in a large-volume market. When it appeared for the first time on the market, the radar-on-chip was able to perform very simple signal processing with a single antenna and at a high cost. Today, modern radar systems are able to perform much more complex signal processing algorithms, with multiple antennas and orthogonal waveforms, as in MIMO radars, with increased range and frequency resolutions, and they can be connected in network with other radars and other sensors for safer driving or intelligent transportation systems. Moreover, the evolution has not yet reached a steady state. It is easy to foresee that, in the future, new on-chip radars will be cognitive, able to adapt their bandwidth and transmit waveforms based on the environment and the target features, and less sensitive to interference, with improved detection and tracking capabilities. To mitigate the spectrum-crowding problem at mm-wave bands, another option to be exploited in the future is the use of passive radars. By making use of emissions from a noncooperative transmitter of opportunity, this technology promises to be green, reducing power consumption and EM interference emission. Although it is still not mature, and its reliance on third-party illuminators and on the scene deployment contrast with the need in autonomous driving for high functional safety levels in every condition, new sources of opportunity will come from 5G communications systems and the V2V and V2I signals. To this end, new sensing schemes are emerging, whereby multiple passive MIMO radar nodes can cooperate to create a reliable and ubiquitous radar service that may be adaptive, reconfigurable, and cognitive.

## Authors

**Sergio Saponara** (sergio.saponara@unipi.it) received his M.S. and Ph.D. degrees in electronic engineering, cum laude, from the University of Pisa, Italy, in 1999 and 2003, respectively. He is a full professor of electronics at the University of Pisa, Italy, and chief technical officer and cofounder of IngemiArs. He coauthored more than 300 scientific publications and 18 patents. He was a Marie Curie research fellow at Interuniversity Microelectronics Center (Leuven, Belgium). He is an IEEE Distinguished Lecturer and cofounder of the Internet of Things (IoT) special interest group of the IEEE Circuits and Systems and Signal Processing Societies. He is the associate editor of many IEEE, Institution of Engineering and Technology, Springer Nature, and MDPI journals. He has contributed to the organizing committees of roughly 150 IEEE and SPIE conferences. He is responsible for the summer school “Enabling Technologies for IoT” and CrossLab “Industrial IoT” and of many national, European Union and industrial projects. He is a Senior Member of the IEEE.

**Maria Sabrina Greco** (m.greco@iet.unipi.it) received her M.S. degree in electronic engineering in 1993 and her Ph.D. degree in information engineering in 1998. She is a full professor in the Department of Information Engineering, University of Pisa, Italy. She is a corecipient of the 2001 and 2012 IEEE Aerospace and Electronic Systems Society’s (AEES’s) Barry Carlton Award for Best Paper and a recipient of the IEEE AEES 2008 Fred Nathanson Young Engineer of the Year Award. She has been general chair, technical program chair, and organizing committee member of many international conferences. She is an associate editor of *IET Radar, Sonar & Navigation* and Springer’s *Journal of Advances in Signal Processing*, a senior editorial board member of *IEEE Journal of Selected Topics in Signal Processing*, and a senior area editor of *IEEE Transactions on Signal Processing*. Her general interests are in the areas of statistical signal processing, estimation, and detection theory. She is a Fellow of the IEEE.

**Fulvio Gini** (fulvio.gini@unipi.it) received his Dr.-Ing. and Ph.D. degrees in electronic engineering from the University of Pisa, Italy, in 1990 and 1995, respectively. Currently, he is a full professor in the Department of Information Engineering at the University of Pisa. He has received several awards, including the 2001 and 2012 IEEE Aerospace and Electronic Systems (AES) Society’s Barry Carlton Award for Best Paper published in *IEEE Transactions on Aerospace and Electronic Systems*, the 2003 IEEE Achievement Award, and the 2003 IEEE AES Society Fred Nathanson Young Engineer of the Year Award. He has authored 11 book chapters, approximately 130 journal articles, and 170 conference papers. He is a Fellow of the IEEE.

## References

- [1] A. Mukhtar, L. Xia, and T. Boon Tang, “Vehicle detection techniques for collision avoidance systems: A review,” *IEEE Trans. Intell. Transp. Syst.*, vol. 16, no. 5, pp. 2318–2338, 2015.
- [2] S. Patole, M. Torlak, D. Wang, and M. Ali, “Automotive radars: A review of signal processing techniques,” *IEEE Signal Process. Mag.*, vol. 34, no. 2, pp. 22–35, 2017. doi: 10.1109/MSP.2016.2628914.

- [3] S. Saponara, E. Ragonese, M. Greco, B. Neri, and G. Palmisano, *Highly Integrated Low-Power Radars*. Norwood, MA: Artech House, 2014.
- [4] R. Hult, R. Campos, E. Steinmetz, L. Hammarstrand, P. Falcone, and H. Wymeersch, "Coordination of cooperative autonomous vehicles: Toward safer and more efficient road transportation," *IEEE Signal Process. Mag.*, vol. 34, no. 1, pp. 74–84, 2017.
- [5] F. Pieri, C. Zambelli, A. Nannini, P. Olivo, and S. Saponara, "Consumer electronics is redesigning our cars? Challenges of integrated technologies for sensing, computing and storage," *IEEE Consum. Electron. Mag.*, vol. 7, no. 4, pp. 8–17, 2018.
- [6] I. Gresham, N. Jain, T. Budka, A. Alexanian, N. Kinayman, B. Ziegner, S. Brown, and P. Staeker, "A compact manufacturable 76–77 GHz radar module for commercial ACC applications," *IEEE Trans. Microw. Theory Techn.*, vol. 49, no. 1, pp. 44–58, 2001. doi: 10.1109/22.899961.
- [7] J. Singh, B. Ginsburg, S. Rao, and K. Ramasubramanian, "AWR1642 mmWave sensor: 76–81-GHz radar-on-chip for short-range radar applications," Texas Instruments, Dallas, TX, Doc. SPYY006, 2017.
- [8] D. Guermandi et al., "A 79-GHz 2x2 MIMO PMCW radar SoC in 28-nm CMOS," *IEEE J. Solid-State Circuits*, vol. 52, no. 10, pp. 2613–2626, Oct. 2017. doi: 10.1109/JSSC.2017.2723499.
- [9] K. Ramasubramanian and B. Ginsburg, "AWR1243 sensor: Highly integrated 76–81-GHz radar front-end for emerging ADAS applications," Texas Instruments, Dallas, TX, Doc. SPYY003, 2017.
- [10] S. Saponara and B. Neri, "Radar sensor signal acquisition and multidimensional FFT processing for surveillance applications in transport systems," *IEEE Trans. Instrum. Meas.*, vol. 66, no. 4, pp. 604–615, 2017.
- [11] A. A. Lopez et al. "Coherent signal processing for traffic flow measuring radar sensor," *IEEE Sensors J.*, vol. 18, no. 12, pp. 4803–4813, 2018.
- [12] F. Engels, P. Heidenreich, A. M. Zoubir, F. K. Jondral, and M. Wintermantel, "Advances in automotive radar: A framework on computationally efficient high-resolution frequency estimation," *IEEE Signal Process. Mag.*, vol. 34, no. 2, pp. 36–46, Mar. 2017.
- [13] M. Greco, F. Gini, P. Stinco, and K. Bell, "Cognitive radars: On the road to reality: Progress thus far and possibilities for the future," *IEEE Signal Process. Mag.*, vol. 35, no. 4, pp. 112–125, July 2018. doi: 10.1109/MSP.2018.2822847.
- [14] Special Issue on Machine Learning for Cognition in Radio Communications and Radar, *IEEE J. Sel. Top. Signal Process.*, vol. 12, no. 1, Feb. 2018.
- [15] A. Sayin, S. Pooni, E. Hoare, and M. Antoniou, "MIMO array for short-range, high-resolution automotive sensing," *IET Radar, Sonar, Navigation*, vol. 12, no. 10, pp. 1165–1171, 2018. doi:10.1049/iet-rsn.2018.5031.
- [16] G. Hakobyan, "High-performance automotive radar: A review of signal processing algorithms and modulation schemes," *IEEE Signal Process. Mag.*, vol. 36, no. 5, pp. 32–44, Sept. 2019.
- [17] Y. Li, Y. Ruichek, and C. Cappelle, "Optimal extrinsic calibration between a stereoscopic system and a lidar," *IEEE Trans. Instrum. Meas.*, vol. 62, no. 8, pp. 2258–2269, 2013.
- [18] Velodyne Lidar HDL32, "High-definition real-time 3D LIDAR," Velodyne Lidar, San Jose, CA, Doc. 97-0038 rev. F, pp. 1–2, 2016.
- [19] Z. Xiong, Y. Zhang, F. Wu, and W. Zeng, "Computational depth sensing: Toward high-performance commodity depth cameras," *IEEE Signal Process. Mag.*, vol. 34, no. 3, pp. 55–68, 2017.
- [20] Y. Zhu, "60 GHz mobile imaging radar," in *Proc. ACM HotMobile'15*, Santa Fe, NM, 2015, pp. 65–80.
- [21] E. Piuzzi, "Complex radar cross section measurements of the human body for breath-activity monitoring applications," *IEEE Trans. Instrum. Meas.*, vol. 64, no. 8, 2015, pp. 2247–2258.
- [22] Y. Huang, P. V. Brennan, D. Patrick, I. Weller, P. Roberts, and K. Hughes, "FMCW based MIMO imaging radar for maritime navigation," *Progress Electromagnetic Res.*, vol. 115, pp. 327–342, 2011. doi: 10.2528/PIER11021509.
- [23] STARS Railway Systems, "Sirio-OD: Automatic detection of obstacles on the track." Accessed on: 2019. [Online]. Available: [http://www.starsrailway.com/download/Brochure\\_Sirio\\_OD.pdf](http://www.starsrailway.com/download/Brochure_Sirio_OD.pdf)
- [24] W. Wang, D. Liang, Z. Wang, H. Yu, and Q. Liu, "Design and implementation of a FPGA and DSP Based MIMO Radar imaging system," *Appl. Wireless Commun.*, vol. 24, no. 2, pp. 518–526, 2015. doi: 10.13164/re.2015.0518.
- [25] S. Scherr, "An efficient frequency and phase estimation algorithm with CRB performance for FMCW radar applications," *IEEE Trans. Instrum. Meas.*, vol. 64, no. 7, pp. 1868–1875, 2015.
- [26] J. Hasch, E. Topak, R. Schnabel, T. Zwick, R. Weigel, and C. Waldschmidt, "Millimeter-wave technology for automotive radar sensors in the 77 GHz frequency band," *IEEE Trans. Microw. Theory Techn.*, vol. 60, no. 3, pp. 845–860, 2012. doi: 10.1109/TMTT.2011.2178427.
- [27] C. Baer, "Contactless detection of state parameter fluctuations of gaseous media based on an mm-wave FMCW radar," *IEEE Trans. Instrum. Meas.*, vol. 64, no. 4, pp. 865–872, 2015. doi: 10.1109/TIM.2014.2374696.
- [28] G. Rubio-Cidre, A. Badolato, L. Úbeda-Medina, J. Grajal, B. Mencia-Oliva, and B.-P. Dorta-Naranjo, "DDS-based signal-generation architecture comparison for an imaging radar at 300 GHz," *IEEE Trans. Instrum. Meas.*, vol. 64, n. 11, pp. 3085–3098, 2015. doi: 10.1109/TIM.2015.2440557.
- [29] S. Kim, D. Oh, and J. Lee, "Joint DFT-ESPRIT estimation for TOA and DOA in vehicle FMCW radars," *IEEE Antennas Wireless Propag. Lett.*, vol. 14, pp. 1710–1713, Apr. 2015.
- [30] A. Laribi, "A new height-estimation method using FMCW radar Doppler beam sharpening," in *Proc. EUSIPCO*, 2018. doi: 10.23919/EUSIPCO.2017.8081546.
- [31] P. Kumari, J. Choi, N. González-Prelcic, and R. W. Heath, "IEEE 802.11ad-based radar: An approach to joint vehicular communication-radar system," *IEEE Trans. Veh. Technol.*, vol. 67, no. 4, pp. 3012–3027, 2018.
- [32] M. Mehrnoush, "Coexistence of WLAN network with radar: Detection and interference mitigation," *IEEE Trans. Cogn. Commun. Netw.*, vol. 3, no. 4, pp. 655–667, 2017.
- [33] P. Papadimitratos, A. La Fortelle, K. Evensen, R. Brignolo, and S. Cosenza, "Vehicular communication systems: Enabling technologies applications and future outlook on intelligent transportation," *IEEE Commun. Mag.*, vol. 47, no. 11, pp. 84–95, 2009. doi: 10.1109/MCOM.2009.5307471.
- [34] S. Lutz, K. Baur, and T. Walter, "77 GHz lens-based multistatic MIMO radar with colocated antennas for automotive applications," in *Proc. 2012 IEEE/MTT-S Int. Microwave Symp.*, 17–22 June 2012, pp. 1–3. doi: 10.1109/MWSYM.2012.6259526.
- [35] J. D. Wit, W. Van Rossum, and A. D. Jong, "Orthogonal waveforms for FMCW MIMO radar," in *Proc. IEEE Radar Conf.*, 2011, pp. 686–691.
- [36] F. Engels, M. Wintermantel, and P. Heidenreich, "Automotive MIMO radar angle estimation in the presence of multipath," in *Proc. IEEE Radar Conf.*, 2017. doi: 10.23919/EURAD.2017.8249152.
- [37] I. Bilik, "Automotive MIMO radar for urban environments," in *Proc. IEEE Radar Conf.*, 2016, pp. 1–6.
- [38] C. Vasanelli, R. Batra, and C. Waldschmidt, "Optimization of a MIMO radar antenna system for automotive applications," in *Proc. IEEE EUCAP*, 2017, pp. 1113–1117.
- [39] S. Lutz, and T. Walter, "Lens-based 77 GHZ MIMO radar for angular estimation in multitarget environments," *Intern. J. Microw. Wireless Technol.*, 2014, vol. 6, no. 3/4, pp. 397–404. doi: 10.1017/S1759078714000506.
- [40] W. Li, S. Fortunati, M. S. Greco, and F. Gini, "Waveform optimization for multi-target detection with a reinforcement learning approach," in *Proc. 2018 Asilomar Conf. Signals, Systems, and Computers*, Oct. 2018.
- [41] D. M. Gavrila, "Sensor-based pedestrian protection," *IEEE Intell. Syst.*, vol. 16, no. 6, pp. 77–81, 2001. doi: 10.1109/5254.972097.
- [42] P. Samczynski, K. Kulpa, M. Malanowski, P. Krysik, and Ł. Maślikowski, "A concept of GSM-based passive radar for vehicle traffic monitoring, microwaves," in *Proc. Radar Remote Sensing Symp.*, Kiev, Ukraine, 2011, pp. 271–274.
- [43] H. Rohling and M. Kronauge, "Continuous waveforms for automotive radar systems," in *Waveform Design and Diversity for Advanced Radar Systems* (IET Radar, Sonar and Navigation Series), vol. 22, F. Gini, A. De Maio, and L. Patton, Eds. Stevenage, U.K.: Institution of Engineering and Technology, 2012.
- [44] S. Rao, A. Ahmad, J. C. Roh, and S. Bharadwa, "77GHz single chip radar sensor enables automotive body and chassis applications," Texas Instruments, Dallas, TX, TI Application Note n. SPRY315, Dec. 2017.
- [45] S. Alland, W. Stark, M. Ali, and M. Hegde, "Automotive radar systems: Optimizing transmitter and receiver interference mitigation," *IEEE Signal Process. Mag.*, vol. 36, no. 5, Sept. 2019.
- [46] J. Lundén, V. Koivunen, and H. V. Poor, "Spectrum exploration and exploitation for cognitive radio: Recent advances," *IEEE Signal Process. Mag.*, vol. 32, no. 3, 2015, pp. 123 – 140. doi: 10.1109/MSP.2014.2338894.
- [47] G. E. Smith, Z. Cammenga, A. Mitchell, K. L. Bell, J. T. Johnson, M. Rangaswamy, and C. J. Baker, "Experiments with cognitive radar," *IEEE Aerosp. Electron. Syst. Mag.*, vol. 31, no. 12, pp. 34–46, Dec. 2016. doi: 10.1109/MAES.2016.150215.
- [48] S. Haykin, Y. Hue, and P. Setoodeh, "Cognitive radar: Step toward bridging the gap between neuroscience and engineering," *Proc. IEEE*, vol. 100, no. 11, pp. 3102–3130, 2012. doi: 10.1109/JPROC.2012.2203089.
- [49] R. S. Thomä et al., Cooperative passive coherent location: A promising 5G service to support road safety, Dec. 2018. [Online]. Available: <https://arxiv.org/pdf/1802.04041>
- [50] L. Zheng and X. Wang, "Super-resolution delay-Doppler estimation for OFDM passive radar," *IEEE Trans. Signal Process.*, vol. 65, no. 9, pp. 2197–2210, May 2017.
- [51] S. Lamagna, "Building the next-generation car with intel IoT," IoT@Intel, Nov. 23, 2015. [Online]. Available: <https://blogs.intel.com/iot/2015/11/23/building-the-next-generation-car-with-intel-iot/>

Le Zheng, Marco Lops, Yonina C. Eldar,  
and Xiaodong Wang

# Radar and Communication Coexistence: An Overview

*A review of recent methods*



Increased amounts of bandwidth are required to guarantee both high-quality/high-rate wireless services (4G and 5G) and reliable sensing capabilities, such as for automotive radar, air traffic control, earth geophysical monitoring, and security applications. Therefore, coexistence between radar and communication systems using overlapping bandwidths has come to be a primary investigation field in recent years. Various signal processing techniques, such as interference mitigation, precoding or spatial separation, and waveform design, allow both radar and communications to share the spectrum.

This article reviews recent work on coexistence between radar and communication systems, including signal models, waveform design, and signal processing techniques. Our goal is to survey contributions in this area to provide a primary starting point for new researchers interested in these problems.

## Introduction

The use of radar has been widened to numerous civilian applications, including traffic control, remote sensing, car cruise control, and collision avoidance. On a parallel track, the quest for ever-increasing rates in wireless communications has pushed the carrier frequencies toward bands traditionally assigned to radar systems. This, along with the need to limit electromagnetic pollution, has resulted in the scenario of coexisting radar and communication systems [1], [2]. Emerging technologies in this field rely on such concepts as passive sensing, waveform diversity, codesign, and the so-called bioinspired strategies, wherein each part of a given architecture is seen as a subsystem whose design choices must be negotiated with the other constituent subsystems. To this last philosophy belongs the class of cognitive systems, which are, in turn, intimately linked to the concept of Bayesian learning as a means to facilitate and sometimes enable individual decision making [1], [3], [4].

In recent years, vibrant industrial and academic interest has grown regarding the convergence of sensing and communication functions. This has been affirmed by the announcement of the Shared Spectrum Access for Radar and Communication program by the U.S. Defense Advanced Research Projects

Agency [5] and the demands of sensing and communication for self-driving cars [6]. As a result, a number of studies have been conducted, based on a variety of scenarios, degrees of cooperation between the coexisting systems, and design strategies.

The goal of this article is to review the existing results in this context and define a taxonomy of the different philosophies proposed so far. Three major architectures for coexistence can be defined as follows:

- 1) coexistence in spectral overlap
- 2) coexistence via cognition
- 3) functional coexistence.

Category 1 includes architectures wherein both radar and communication systems are equipped with active transmitters using the same frequency spectrum. Here, the major problem is to eliminate or mitigate mutual interference while guaranteeing satisfactory performance for both functions. Different degrees of cooperation between the active systems have been so far considered. For example, in [7] and [8], the inherent resilience to interference of properly designed coherent multiple-input, multiple-output (MIMO) radars is exploited, and attention is paid only to the performance of the radar system. A similar radar-centric philosophy is adopted in [9] and [10], wherein coexisting communication users are safeguarded by limiting the amount of interference produced by the radar on given subbandwidths. In a symmetrical fashion, uncooperative, communication-centric approaches have been suggested in a number of more recent studies, wherein countermeasures against the radar-induced interference are taken either at the communication receiver [11] or, in the presence of some prior information, directly at the transmitter [12], [13].

Cooperation between the active systems, possibly operating in full spectral overlap, to negotiate the respective transmit policies and adjust the corresponding detection/demodulation strategies is the idea underlying codesign, first introduced in [3] and further developed in [14]–[19]. In this approach, which we define as *holistic*, the coexisting systems are seen as constituent parts of a whole, so that the degrees of freedom under the designer's control are both the waveforms transmitted by the sensing systems and the codebooks employed by the communication systems. These are jointly optimized so as to guarantee that both the communication and the radar performance are satisfactory. Codesign allows taking into account in the transceiver design such effects as reverberation produced by the radar due to clutter or targets moving in close proximity to the communication receiver, range ambiguities, and (random) Doppler frequencies. It is important to underline that these schemes are heavily knowledge based and rely on information exchange between the constituent systems. This presupposes, on the one hand, the presence of a fusion center accessible to both systems and, on the other, the accessibility of a common database, wherein the basic channel parameters are made available.

In dynamic scenarios, codesign may greatly benefit from cognitive paradigms. Here, the channel state is learned through suitable algorithms, which is conducive to the philosophy of coexistence via channel sensing put forth in [4] and, more generally, to category 2 of the previously discussed classification.

In fact, category 2 comprises systems wherein spectral overlap between the communication and radar transmitters is avoided through cognition, so that the corresponding channels are interference free. Starting from the idea (proposed in [14] and borrowed from cognitive radio networks) of using pilot signals to estimate the channels and share the channel information between the subsystems, new approaches have been recently proposed wherein the radar and/or the communication system is able to learn the environment without transmitting pilots or avoiding the need for coordination [20]–[23]. In [4], for example, the SpeCX system combines sub-Nyquist multiband sensing with sub-Nyquist radar [24] to enable the radar to sense the communication channel at very low rates.

Category 3 comprises architectures in which there is only one active transmitter, whereby coexistence is functional but no interference is produced and no real resource negotiation takes place. Dual-function radar communication systems rely on combining radar and communication transmitters in the same hardware platform, which is designed to guarantee the performances of both systems. The information is embedded [25]–[28] in the radar signal, and a MIMO radar transmitter uses a combination of beamforming and waveform diversity to direct information bits toward multiple communication receivers without affecting the performance of the sensing function and while guaranteeing satisfactory bit error rate performance.

Opportunistic sensing systems instead consist of a receiver colocated with the communication transmitter and a dedicated software chain aimed at processing the received signal. The receiver can avail itself of some side information, such as timing and transmitted data. This architecture has been proposed and theoretically assessed with reference to the 802.11ad format used in conjunction with a sensing system in an automotive environment [29], [30]. Passive radar systems also can be thought of as belonging to category 3 because they exploit other transmissions (communications or broadcast) rather than having their own dedicated radar transmitter [1], [31].

## Coexistence in spectral overlap

### System model

In the discussion hereinafter, we unify the single-input, single-output and MIMO settings, as they are amenable to similar approaches. Thus, to keep the discussion as general as possible, we consider a scenario wherein a MIMO radar with  $M_T$  transmit and  $M_R$  receive antennas (typically, but not necessarily, colocated) should coexist with a MIMO communication system equipped with  $N_T$  transmit and  $N_R$  receive antennas, respectively, as illustrated in Figure 1.

The MIMO radar transmits  $M_T$  signals, where the signal sent from the  $i$ th transmit element is characterized by a fast-time code  $\mathbf{c}_i = [c_i(0), \dots, c_i(P_r - 1)] \in \mathbb{C}^{P_r}$ . The continuous-time waveform at the  $i$ th transmit element is then given by

$$\tilde{c}_i(t) = \sum_{p=0}^{P_r-1} c_i(p) \psi(t - pT_r). \quad (1)$$

Here,  $\psi(\cdot)$  is a Nyquist waveform of bandwidth  $B = 1/T_r$ , i.e., such that its autocorrelation  $R_\psi(\cdot)$  satisfies the condition  $R_\psi(kT_r) = \delta(k)$ , with  $\delta(\cdot)$  denoting the Kronecker delta and  $1/T_r$  the fast-time coding rate. (Nyquist waveforms with bandwidth  $B = 1/T_r$  are strictly band limited and therefore not time limited. In practice, they are generated by the truncation of an ideal waveform, whereby the discretization may incur some degree of aliasing; however, by allowing some excess bandwidth, this effect can be kept under control. A detailed discussion can be found in [32].) The product of the bandwidth and the effective duration of these coded pulses is typically much larger than one. Therefore, these signals are sometimes referred to as *sophisticated waveforms*, as opposed to conventional unsophisticated signals whose bandwidth is on the order of the inverse of their duration.

In the architecture of Figure 1, every radiating element is allowed to transmit a train of  $N$  coded pulses of the form of (1), spaced apart by the pulse repetition time  $T$  and amplitude modulated by a slow-time code  $\mathbf{g}_i = [g_i(0), g_i(1), \dots, g_i(N-1)]^T \in \mathbb{C}^N$ . Thus, the  $i$ th element transmits the signal

$$s_i(t) = \sum_{n=0}^{N-1} g_i(n) \tilde{c}_i(t - nT). \quad (2)$$

Some special cases of the radar signal model (2) are as follows:

- **Case 1:** In this instance, a single-antenna transmitter uses a single signal with fast-time code  $\mathbf{c} = [c(0), \dots, c(P_r - 1)]^T$ , corresponding to  $N = M_T = 1$ .
- **Case 2:** Here, a single-antenna transmitter employs an amplitude-modulated train of pulses, corresponding to  $M_T = 1$ ,  $P_r = 1$ . The train is uniquely determined by the slow-time code  $\mathbf{g} = [g(0), \dots, g(N-1)]^T \in \mathbb{C}^N$ . The usual pulsed radar corresponds to an all-one slow-time code.
- **Case 3:** In this scenario, there is a multiantenna transmitter, wherein each antenna transmits a single sophisticated signal. As a consequence,  $N = 1$ ,  $s_i(t) = c_i(t)$ , and the  $P_r \times M_T$

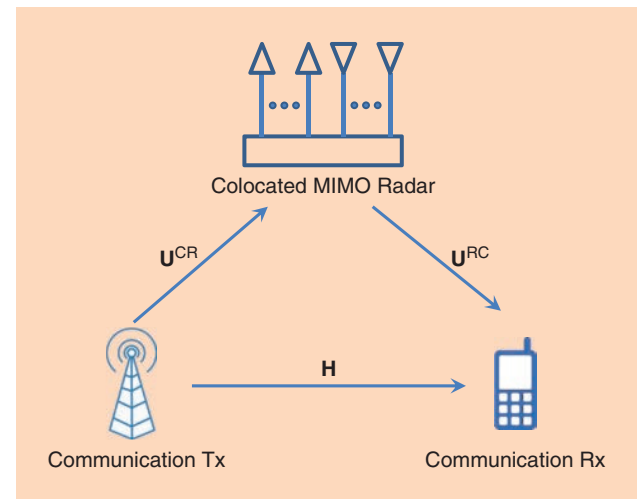


**FIGURE 1.** A MIMO communication system sharing spectrum with a MIMO radar system. Tx: transmitter; Rx: receiver.

space-time code matrix  $\mathbf{C} = [\mathbf{c}_1, \dots, \mathbf{c}_{M_T}]$  is the degree of freedom to be employed at the transmitter side [33].

- **Case 4:** Here, there exists a multiantenna transmitter wherein each antenna transmits a train of unsophisticated signals, amplitude modulated by the slow-time code. In this case,  $P_r = 1$ , and the  $N \times M_T$  space-time code matrix  $\mathbf{G} = [\mathbf{g}_1, \dots, \mathbf{g}_{M_T}]$  is the degree of freedom at the transmitter side [17].

Radar use radio waves to determine the range, angle, or velocity of objects. The operation of a typical MIMO radar receive chain is summarized in “The Stages of Multiple-Input, Multiple-Output Radar Processing.” For a given signal-to-noise ratio (SNR), the radar range resolution is dictated by the transmit bandwidth, i.e.,  $1/T_r$  in (1). The velocity resolution is determined by the duration of coherent integration, i.e.,  $NT$  in (2). In cases 1 and 3, no Doppler processing is undertaken, mainly because typical single-pulse durations are too short to allow the measuring of the Doppler shift induced by targets in moderate radial motion. In cases 2 and 4, moving objects that generate steering vectors

## The Stages of Multiple-Input, Multiple-Output Radar Processing

Classic colocated multiple-input, multiple-output (MIMO) radar processing traditionally includes the following stages.

- **Sampling:** At each radar receiver  $1 \leq j \leq M_R$ , the signal  $r_j(t)$  is projected onto the orthonormal system  $\{\psi(t - mT_r)\}_{m=0}^{P_r-1}$  and sampled at its Nyquist rate  $B = 1/T_r$ , creating the samples  $r_j(m)$ ,  $0 \leq m \leq P_r - 1$ .
- **Matched filter:** The sampled signal is convolved with the transmitted radar codes  $\mathbf{c}_i$ ,  $1 \leq i \leq M_T$ . The time resolution attained in this step is  $1/B$ .
- **Beamforming:** The correlations between the observation vectors from the previous step and the steering vectors corresponding to each azimuth on the grid defined by the array aperture are computed.

- **Doppler detection:** The correlations between the resulting vectors and Doppler vectors, with Doppler frequencies lying on the grid defined by the number of pulses, are computed. The Doppler resolution is  $1/NT$ .
- **Peak detection:** This is a heuristic detection process, in which knowledge of the number of targets, the targets’ powers, clutter location, and so on may help in discovering the targets’ positions. For example, if we know there are  $\kappa$  targets, then we can choose the  $\kappa$ -strongest points in the map. Alternatively, constant false alarm rate detectors determine a power threshold, above which a peak is considered to originate from a target so that a required false alarm probability is achieved.

and Doppler shifts up to  $1/T$  can be unambiguously measured. Likewise, pulse trains with pulse repetition time  $T$  generate range ambiguities whereby scatterers located at distances corresponding to delays that are integer multiples of  $T$  contribute to the same range cell.

The signal model for the communication system is simpler, in that we just have to distinguish between the case of single and multiple transmit antennas. In particular, we assume that the communication system operates on the same frequency band as the radar, occupying a fraction  $B/L$  of its dedicated bandwidth. Setting  $T_c = L/B$ , the signal radiated by the  $i$ th transmit element is written as

$$x_i(t) = \sum_{p=-\infty}^{\infty} v_i(p) \psi_L(t - pT_c), \quad (3)$$

where  $v_i(p)$  is the data sequence to be transmitted, and  $\psi_L(\cdot)$  satisfies the Nyquist criterion with respect to  $T_c = LT_r$ . The situation of full spectral overlap corresponds to  $L = 1$ . We note that there may be a multiplicity of narrow-band communication systems, each occupying a fraction of the radar bandwidth.

Assume that the radar and the communication receivers are equipped with  $M_R$  and  $N_R$  receive antennas, respectively. The signal at the  $j$ th antenna of the radar receiver can be cast in the form

$$r_j(t) = \sum_{i=1}^{M_T} a_{i,j} s_i(t - \tau_{i,j}) + \sum_{i=1}^{N_T} (u_{i,j}^{\text{CR}} * x_i)(t) + \sum_{i=1}^{M_T} (a_{i,j}^{\text{I}} * s_i)(t) + n_{R,j}(t), \quad (4)$$

where  $a_{i,j}$  is the target complex backscattering coefficient, including the path loss and the phase shift due to the target angle and position with respect to the transmit and receive antennas;  $u_{i,j}^{\text{CR}}(t)$  is the response of the channel from the communication transmitter to the radar receiver;  $\tau_{i,j}$  is the delay of the target from the  $i$ th transmitter to the  $j$ th receiver;  $a_{i,j}^{\text{I}}(t)$  is the response of the clutter;  $*$  is the convolution operation; and  $n_{R,j}(t)$  denotes the noise at the  $j$ th receiver antenna. Likewise, the signal received at the  $j$ th antenna of the communication receiver is given by

$$y_j(t) = \sum_{i=1}^{N_T} (h_{i,j} * x_i)(t) + \sum_{i=1}^{M_T} (u_{i,j}^{\text{RC}} * s_i)(t) + n_{C,j}(t), \quad (5)$$

where  $h_{i,j}(t)$  is the channel response from the  $i$ th communication transmitter to the  $j$ th communication receiver;  $u_{i,j}^{\text{RC}}(t)$  is the response of the interfering channel from the radar transmitter to the communication receiver; and  $n_{C,j}(t)$  denotes the noise of the  $j$ th communication receiver antenna.

In (4), the transmitted signal  $s_i(t)$  is known, and  $u_{i,j}^{\text{CR}}(t)$  can be estimated via pilot training. On the other hand,  $x_i(t)$  and  $a_{i,j}^{\text{I}}(t)$  are unknown at the radar receiver. The radar needs to detect the presence of the target, i.e.,  $a_{i,j} = 0$  for  $\mathcal{H}_0$  and  $a_{i,j} \neq 0$  for  $\mathcal{H}_1$ , and estimate the parameters  $\tau_{i,j}$  and  $a_{i,j}^{\text{I}}(t)$ . For the communication system given by (5),  $h_{i,j}(t)$  can be esti-

mated via pilot training. In coordinated architectures, where the radar transmits pilots and communicates with the communication receiver,  $u_{i,j}^{\text{RC}}$  and  $s_i(t)$  are known at the communication receiver, while, in uncoordinated scenarios,  $u_{i,j}^{\text{RC}}$  and  $s_i(t)$  are both unknown.

Based on the models (4) and (5), different coexistence scenarios can be analyzed. In the section “Uncoordinated Design: Radar Centric” a radar-centric approach wherein a single-antenna radar transmits a single sophisticated signal with fast-time code, i.e., case 1, is discussed. The section “Uncoordinated Design: Communication Centric” reviews some communication-centric approaches, assuming different degrees of prior knowledge as to the radar interference (i.e., cases 2 and 3). The section “Coordinated Design” focuses on the coordinated design of the radar waveforms and the communication codebooks, assuming the most general scenario (i.e., cases 3 and 4) of multiple transmit and receive antennas for both systems, with either slow-time or fast-time coding.

### Uncoordinated design: Radar centric

We begin by discussing a radar-centric approach in which the radar function is considered primary while unlicensed users are allowed to transmit in partial spectral overlap on the same bandwidth. Following [9] and [10], we assume  $N_I$  interferers of the form (3). Their presence is acknowledged by limiting the amount of interference the radar produces on the shared bandwidths. The focus is on the design of the radar system, assumed to employ a single coded pulse according to case 1 in the previous section, designed so as to guarantee the maximum possible signal-to-interference-plus-noise ratio (SINR) at the radar receiver.

Assume that the radar receiver is equipped with a single antenna and the interference is dominated by the direct path between the radar and the communication. The subscript  $j$  can thus be removed from the variables in (4). Therefore,  $r_j(t)$  becomes  $r(t)$ , and  $u_i^{\text{CR}}(t) = \delta(t - \tau_i^{\text{RC}})$ , with  $\tau_i^{\text{RC}}$  dictated by the distance between the  $i$ th communication transmitter and the radar receiver. Such a model holds for narrow-band systems, where the flat-fading assumption is valid [14], and can be extended to more sophisticated situations by using different forms of channel responses [34]. For simplicity, we assume there is only one target and let the target delay be  $\tau = 0$ .

Plugging (2) into (4) and projecting the equation onto the orthonormal system  $\{\psi(t - mT_r)\}_{m=0}^{P_r-1}$  leads to

$$\begin{aligned} r(m) &= \langle r(t), \psi(t - mT_r) \rangle \\ &= \left\langle a \sum_{p=0}^{P_r-1} c_i(p) \psi(t - pT_r), \psi(t - mT_r) \right\rangle \\ &\quad + \sum_{k=1}^{N_T} u_k \underbrace{\langle x(t - \tau_k^{\text{CR}}), \psi(t - mT_r) \rangle}_{x_k(m)} \\ &\quad + \underbrace{\left\langle \sum_{i=1}^{M_T} (a_i^{\text{I}} * s_i)(t), \psi(t - mT_r) \right\rangle}_{n_i(m)} \\ &\quad + \underbrace{\langle n_R(t), \psi(t - mT_r) \rangle}_{n_R(m)} \end{aligned} \quad (6)$$

with  $a$  the target complex backscattering coefficient, including the path loss, and  $u_k$  the coefficient of the interfering channel for user  $k$ . Denoting  $\mathbf{r} = [r(0), r(1), \dots, r(P_r - 1)]^T$ , we have

$$\mathbf{r} = a\mathbf{c} + \sum_{k=1}^{N_I} u_k \mathbf{x}_k + \mathbf{n}_I + \mathbf{n}_R \in \mathbb{C}^{P_r} \quad (7)$$

with  $\mathbf{x}_k = [x_k(0), x_k(1), \dots, x_k(P_r - 1)]^T$  the  $k$ th communication user occupying the bandwidth,  $\mathbf{n}_I = [n_I(0), n_I(1), \dots, n_I(P_r - 1)]^T \in \mathbb{C}^{P_r}$  the clutter, and  $\mathbf{n}_R = [n_R(0), n_R(1), \dots, n_R(P_r - 1)]^T \in \mathbb{C}^{P_r}$  the noise term.

Equation (7) describes the model for the signal in the radar receiver. Next, we discuss the interference from the radar to the communication users, i.e., the second term in (5). As to the communication users coexisting with the radar of interest, we suppose that each of them is operating over a frequency band  $[f_1^k, f_2^k]$ , where  $f_1^k$  and  $f_2^k$  denote the lower and upper normalized frequencies for the  $k$ th system, respectively. Following (2) and (3) in [9], the interfering energy produced on the  $k$ th communication user is given by  $\mathbf{c}^H \mathbf{R}_k \mathbf{c}$ , where

$$\mathbf{R}_k(m, n) = \begin{cases} f_2^k - f_1^k, & \text{if } m = n \\ \frac{e^{j2\pi f_2^k(m-n)} - e^{j2\pi f_1^k(m-n)}}{j2\pi(m-n)}, & \text{if } m \neq n \end{cases}, \quad (m, n) \in \{1, 2, \dots, P_r\}^2. \quad (8)$$

The covariance matrix  $\mathbf{M}$  of the exogenous interference, i.e., of the signal-independent component of the overall interference  $\sum_{k=1}^{N_I} u_k \mathbf{x}_k + \mathbf{n}_R$ , is assumed to be known or perfectly estimated.

The objective thus becomes to design the radar code  $\mathbf{c}$  so as to maximize the SINR at the radar receiver while ensuring that the interference produced on the coexisting communication users is smaller than a constrained value. Additional constraints to be enforced are an energy constraint on the radar code  $\mathbf{c}$  and its closeness to some reference code  $\mathbf{c}_0$  with prescribed correlation properties [9], [10]. The latter is also referred to as a *similarity constraint*. The design then reduces to solving the following constrained maximization problem:

$$\begin{aligned} \max_{\mathbf{c} \in \mathbb{C}^{N \times 1}} \text{SINR} &= a^2 \mathbf{c}^H \mathbf{M}^{-1} \mathbf{c} \\ \text{s.t. } &\sum_{k=1}^{N_R} \omega_k \mathbf{c}^H \mathbf{R}_k \mathbf{c} \leq E_1, \\ &(1 - \eta)\rho \leq \mathbf{c}^H \mathbf{c} \leq \rho, \\ &\|\mathbf{c} - \mathbf{c}_0\|_2 \leq \epsilon. \end{aligned} \quad (9)$$

In this equation, the terms  $\mathbf{c}^H \mathbf{R}_k \mathbf{c}$  represent the interference produced onto the  $k$ th communication receiver,  $k = 1, 2, \dots, N_R$ ;  $E_1$  is the maximum interference that can be tolerated by the coexisting communication networks;  $\omega_k \geq 0$  for  $k = 1, 2, \dots, N_R$  are weights that can be assigned to the coexisting wireless users, based, for instance, on their distance from the radar and their tactical importance;  $0 \leq \eta \leq 1$  is a design parameter that introduces some tolerance on the nominal interference level; and  $\rho$  is the transmit energy of the radar. With relaxation, the optimization problem (9) can be transformed into

a convex optimization amenable to semidefinite programming, which entails polynomial computational complexity [10].

The scenario leading to problem (9) holds true only when the clutter is either absent or has a rank one covariance matrix, i.e., is modeled as a specular image of the transmitted signal reflected toward the receiver by a point-like scatterer. Conversely, if more complex channel models are considered and the clutter covariance has a rank larger than one (i.e., the point-like model does not carry over to reverberation), then constrained maximization of the SINR results in a fractional nonconvex problem [16].

### Uncoordinated design: Communication centric

The approach of optimizing radar waveforms, although theoretically well established, is not always applicable, mainly because government and military agencies are unwilling to make major changes in their radar deployments, which may impose huge costs. Thus, coexisting communication systems must be equipped with proper countermeasures to guarantee the required quality of service (QoS) when the radar systems do not modify their transmission policy. Attention is thus shifted back to the communication transceiver, which explains the name *communication-centric* design. The approaches so far available in the literature focus either on the receiver [11], when prior information on the radar signals is not available, or on the transmitter [13], when the structure of the radar transmitted waveform is known.

Assume first the scenario considered in [11], wherein a multiplicity of radars may be potentially active in full spectral overlap with a communication system. Each radar is allowed to transmit a sophisticated waveform, but no prior knowledge is available as to the number of active systems, their distance from the communication receiver, or the channel gains. The scenario is thus akin to the one outlined in case 3 in the “System Model” section, wherein  $M_T$  now plays the role of the maximum number of potentially active emitters. The antennas of such a multiple input system are widely spaced, so that the delays with which their signals arrive at the communication receiver are all different and unknown.

As to the communication signal, the scenario assumed in [11] is fairly general. The transmitted symbols are assumed to undergo suitable precoding, where the choice of the precoding matrix dictates the type of system, ranging from code-division multiple access (CDMA) to orthogonal frequency-division multiplexing (OFDM). In particular, suppose the communication and radar systems have the same bandwidth, i.e.,  $L = 1$ ,  $T_c = T_r$ , and  $\psi_L(t) = \psi(t)$ . The signal transmitted by the communication system in the interval  $[0, P_r T_r]$  is assumed to have the form

$$x(t) = \sum_{p=0}^{P_r-1} v(p) \psi(t - pT_r).$$

In this equation,  $\mathbf{v} = [v(0), \dots, v(P_r - 1)]^T \in \mathbb{C}^{P_r}$  is tied to a generic  $P$ -dimensional data vector  $\mathbf{b}_0 = [b_0(0), \dots, b_0(P - 1)]^T$  to be transmitted as  $\mathbf{v} = \mathbf{A}\mathbf{b}_0$ , with  $\mathbf{A} \in \mathbb{C}^{P_r \times P}$  a suitable matrix. Relevant special cases of this model are the OFDM transmission

format (wherein  $P_r = P$  and  $\mathbf{A}$  take on the form of an inverse discrete Fourier transform matrix) and a CDMA system with  $P$  active users (wherein  $\mathbf{A}$  contains the users' signatures) [11]. Here, to keep the discussion simple, we confine our attention to the case of direct transmission of the constellation points in full spectral overlap, so that  $P = P_r$ ,  $\mathbf{b}_0 = \mathbf{b} \in \mathbb{C}^{P_r}$ , and  $\mathbf{A} = \mathbf{I}_{P_r}$  ( $\mathbf{I}_{P_r}$  denotes the identity matrix of order  $P_r$ ).

Suppose a single antenna communication receiver and a single-tap model for both communication and interference channels. It is also assumed that the typically high-power radar transmitter is not saturating the front end of the communication receiver. The communication signal in (5) can thus be rewritten as

$$y(t) = h \sum_{p=0}^{P_r-1} b(p) \psi(t - pT_r) + \sum_{m=1}^{M_T} \sum_{p=0}^{P_r-1} u_m c_m(p) \psi(t - pT_r - \tau_m) + n_c(t). \quad (10)$$

Here, a flat-fading channel is assumed for the communication network, where  $h$  is the channel coefficient, and  $\tau_m$  and  $u_m$  denote the unknown delay and complex coupling coefficient for the  $m$ th radar, respectively. When  $u_m = 0$ , the  $m$ th transmitter is idle. We also assume that, in each frame,  $P_r$  symbols are transmitted and that the frame synchronization between the radar and communication is guaranteed, i.e., the communication system is made aware of the beginning of the radar train pulse. This is low-rate information that can be shared once and for all and regularly updated to account for possible timing drifts.

The communication receiver has to accomplish jointly the two tasks of interference estimation/removal and data demodulation. For interference removal, we need to estimate  $\tau_m$  and  $u_m c_m(p)$  so as to subtract the second term from (10). Obviously, data demodulation and interference estimation are inherently

coupled. In [11], an iterative procedure is proposed for joint data demodulation and interference estimation, and a direct demodulation function  $\hat{\mathbf{b}}^{(0)} = \Psi(\{y(t)\}_{0 \leq t \leq P_r T_r})$  is used as the initial step.

In a general uncoordinated scenario, the communication receiver may not know the exact form of the interfering radar signals but rely only on the coarse information of the family to which they belong. A viable means to account for this uncertainty is to assume that  $\mathbf{c}_m$  lives in a low-dimensional subspace of  $\mathbb{C}^{P_r}$ , spanned by the columns of a known  $P_r \times K$  matrix  $\Phi = [\phi_0, \phi_1, \dots, \phi_{P_r-1}]^T \in \mathbb{C}^{P_r \times K}$ , with  $K \ll P_r$ , i.e.,  $\mathbf{c}_m = \Phi \boldsymbol{\alpha}_m$  for some unknown  $\boldsymbol{\alpha}_m \in \mathbb{C}^K$ , tied to the corresponding minimal and maximum distances of all of the potential radar transmitters from the receiver.

Following [11], the signal  $z^{(0)}(t) = y(t) - h \sum_{p=0}^{P_r-1} \hat{b}^{(0)}(p) \psi(t - pT_r)$  contains the superposition of the residual communication signal (due to demodulation errors), the residual radar interference, and noise. To understand the joint interference removal and symbol demodulation algorithm proposed in [11], let us refer to the first iteration:

$$z^{(1)}(t) = h \sum_{p=0}^{P_r-1} \frac{(b(p) - \hat{b}^{(0)}(p)) \psi(t - pT_r)}{\beta^{(0)}(p)} + \underbrace{\sum_{m=1}^{M_T} \sum_{p=0}^{P_r-1} \phi_m^T \mathbf{u}_m \boldsymbol{\alpha}_m \psi(t - pT_r - \tau_m) + n_c(t)}_{X(t)}, \quad (11)$$

where  $\tau_m$  for  $m = 1, 2, \dots, M_T$  are the desired unknown delays. In (11), the quantities  $\phi_m$  and  $h$  are known, while the objects of interest to be estimated are  $\tau_m$ ,  $\beta^{(0)}(p)$ , and  $\mathbf{u}_m \boldsymbol{\alpha}_m$ .

Define  $\beta^{(0)} = [\beta^{(0)}(0), \beta^{(0)}(1), \dots, \beta^{(0)}(P_r-1)]^T$ . Notice that building up iterations may rely on two types of sparsity:  $X(t)$  in (11) is a combination of at most  $M_T$  components with unknown modulation  $\mathbf{u}_m \boldsymbol{\alpha}_m$ , and  $M_T \ll P_r$ ; and  $\|\beta^{(0)}\|_0$  has to be as small as possible. The problem can be solved by using the recently developed mathematical theory of continuous sparse recovery for superresolution and, in particular, by employing atomic-norm minimization techniques [11]. Figure 2 illustrates the achievable results in terms of the symbol error rate for atomic norm-based and compressed sensing- (CS)-based methods, and it allows assessing the loss due to the lack of prior knowledge as to the delays of the radar systems.

A fairly different scenario is the one considered in [13], where it is assumed that the radar transmits a pulse train, possibly amplitude modulated (according to the transmit format of case 2 in the “System Model” section). Perfect channel state information concerning the attenuation and delay of the radar signal in its travel to the communication receiver is assumed. Thus, the interference generated by the radar onto the communication system is intermittent and presents a large peak-to-average-power ratio because it consists of pulses with large amplitudes.

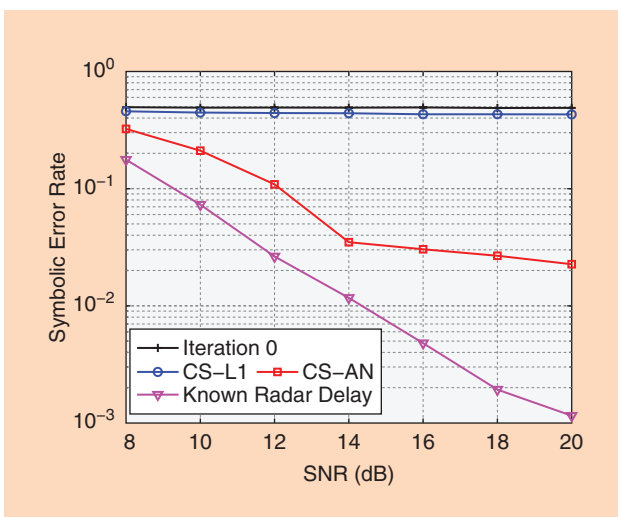


**FIGURE 2.** A comparison of the algorithm symbolic error rates. L1:  $\ell_1$  norm; AN: atomic norm. (From [11].)

If the radar transmit code is a phase-only one (or if, more realistically, the pulse complex amplitudes vary significantly only in the phase), then a narrow-band communication system experiences an interference that is approximately a constant-envelope additive signal. Specifically, the interference is  $(u_{i,j}^{\text{RC}} * s_i)(t) = \sqrt{I} e^{j\theta(t)}$ ,  $t \in \Xi$ , where  $\theta(t)$  is the interference phase, assumed uniform in  $[0, 2\pi]$ ;  $I = |ug|^2$  denotes the average power of the radar interference, assumed known; and  $\Xi$  designates the time intervals where the communication system is interfered. The communication transmitter, in turn, randomly selects the symbols to be transmitted from the set  $\mathcal{B} = \{\tilde{b}_1, \tilde{b}_2, \dots, \tilde{b}_Q\}$  of unit-energy and equally likely points. Exploiting the statistical independence between these symbols and  $\theta(t)$ , the optimal decoding regions can be obtained, and the constellation  $\mathcal{B}$  can be designed to maximize the transmission rate and/or minimize the error rate.

### Coordinated design

The major drawback of the previous approaches is that they rely on a simplified scenario wherein several important phenomena are not accounted for.

- The radar system, especially when operating in search mode, generates reverberation from the surrounding environment, so-called clutter, which impairs not only its own performance but that of the communication system.
- The scattering centers creating clutter could have radial motion with respect to both the radar and the communication receivers, thus generating Doppler shifts that should be accounted for if slow-time coding is considered.

Cooperation between the active systems, possibly operating in full spectral overlap, to negotiate the respective transmit policies and adjust the corresponding detection/demodulation strategies is the idea underlying codesign, first introduced in [3] and further developed in [14], [16], and [17]. It is generally assumed that the radar and the communication system may exchange information. The availability of large databases accurately mapping the scattering characteristics of large areas has allowed the development of cognitive systems (see, e.g., [35] and [36]). Joint design of the radar waveforms and the communication system codebook thus appears as a natural means to allow coexistence by preserving the performance of both.

Consider an  $N_T \times N_R$  communication system coexisting in full spectral overlap with an  $M_T \times M_R$  MIMO radar with closely spaced antennas and colocated transmitter and receiver. We denote by  $\mathbf{D}$  the space–time code matrix of the radar. If fast-time coding is adopted, then  $\mathbf{D} = \mathbf{C}$ , with  $\mathbf{C}$  defined in case 3. If, instead, slow-time coding is undertaken, then  $\mathbf{D} = \mathbf{G}$ , and case 4 occurs. Denote by  $\mathbf{V}$  the signal matrix of the communication system, composed of the  $N_T$  spatial codewords emitted in successive epochs. Specifically,  $\mathbf{V} = [\mathbf{v}(0), \mathbf{v}(1), \dots, \mathbf{v}(P_r - 1)] \in \mathbb{C}^{N_T \times P_r}$ , where  $\mathbf{v}(p) = [v_1(p), v_2(p), \dots, v_{N_T}(p)]^T$  is the spatial codeword transmitted at epoch  $p$ . Projecting the received signal (4) and (5) onto the orthonormal system  $\{\psi(t - mT_r)\}_{m=0}^{P_r-1}$  leads to

$$\mathbf{R} = \mathbf{AD} + \mathbf{U}^{\text{CR}} \mathbf{V} + \mathbf{A}^{\text{I}} \mathbf{D} + \mathbf{N}_R, \quad (12)$$

$$\mathbf{Y} = \mathbf{HV} + \mathbf{U}^{\text{RC}} \mathbf{D} + \mathbf{N}_C, \quad (13)$$

where  $\mathbf{A} \in \mathbb{C}^{M_R \times M_T}$  is the response of the target to be detected,  $\mathbf{A}^{\text{I}} \in \mathbb{C}^{M_R \times M_T}$  is the response of the clutters,  $\mathbf{N}_R$  is the noise at the radar receiver,  $\mathbf{N}_C$  is the noise at the communication receiver,  $\mathbf{U}^{\text{CR}} \in \mathbb{C}^{M_R \times N_T}$  is the interfering channel from the communication transmitter to the radar receiver,  $\mathbf{U}^{\text{RC}} \in \mathbb{C}^{N_R \times M_T}$  is the interfering channel from the communication transmitter to the radar receiver, and  $\mathbf{H} \in \mathbb{C}^{N_R \times N_T}$  is the channel matrix from the communication transmitter to the radar receiver. In (13), the MIMO communication system is assumed to have perfect channel state information, i.e., knowledge of  $\mathbf{V}$ , to be periodically shared with the radar system through a dedicated channel.

In (12), the purpose of the MIMO radar is to detect the presence of a target ( $\mathbf{A} = \mathbf{0}$  for  $\mathcal{H}_0$  and  $\mathbf{A} \neq \mathbf{0}$  for  $\mathcal{H}_1$ ) and estimate the matrix  $\mathbf{A}$  related to the target parameters, such as angle and velocity. An important additional degree of freedom is the space–time filter that can be applied to the radar signal  $\mathbf{R}$  in (12). Let  $\tilde{\mathbf{r}} = \text{vec}(\mathbf{R}) = [\mathbf{r}(0)^T, \mathbf{r}(1)^T, \dots, \mathbf{r}(P_r - 1)^T]^T$  with  $\mathbf{r}(p)$  the  $(p + 1)$ th column of  $\mathbf{R}$ . The filtered signal becomes

$$\bar{\mathbf{r}} = \tilde{\mathbf{w}}^T \tilde{\mathbf{r}} \quad (14)$$

with  $\tilde{\mathbf{w}} \in \mathbb{C}^{M_R P_r \times 1}$ . We recall here that the receive filter is of fundamental importance in coherent MIMO radar because time filtering regulates the transmit beamwidth, while space filtering controls the receive beampattern.

A possible criterion to exploit transmitter coordination for a coherent MIMO radar coexisting with a communication system is to force the radar waveforms  $\mathbf{D}$  to live in the null space of the interference channel  $\mathbf{U}^{\text{RC}}$  via a spatial approach [18]. The MIMO structure indeed provides the degrees of freedom to suitably design the space–time code matrix determining the probing signal. To illustrate further, assume that the case 3 model in the “System Model” section is in force, and that the fast-time space–time code matrix  $\mathbf{C}$  is to be designed. To this end, we regroup the signals transmitted by the MIMO radar in the vectors  $\mathbf{c}(p) = [c_1(p), c_2(p), \dots, c_{M_T}(p)]^T$ , encapsulating the spatial codeword transmitted for the  $p$ th subpulse.

Consider the situation in which  $\bar{N}$  communication receivers exist, and let the interference channels of the communication receivers be  $\{\mathbf{U}^{(1)}, \mathbf{U}^{(2)}, \dots, \mathbf{U}^{(\bar{N})}\}$ . In [15], where the idea is fully developed, these abstract communication receivers are actually clusters of base stations. The interference that would be produced onto the  $n$ th communication receiver is  $\mathbf{U}^{(n)} \mathbf{c}(p)$ . At the MIMO radar, the channel state information can be estimated using a blind null-space learning algorithm [37].

Our goal here is to assure zero interference to one of the communication receivers with minimum degradation in the radar performance. Suppose we want no interference at the  $n$ th communication receiver. The communication signal can be projected onto the null space of the channel  $\mathbf{U}^{(n)}$ . The null space  $\mathcal{N}(\mathbf{U}^{(n)}) = \{\mathbf{c} \in \mathbb{C}^{M_T} : \mathbf{U}^{(n)} \mathbf{c} = \mathbf{0}\}$  can then be calculated

using the singular value decomposition. Specifically, letting  $\mathbf{U}^{(n)} = \mathbf{Y}_1 \Sigma \mathbf{Y}_2^H$ , the right singular vectors corresponding to vanishing singular values are collected in  $\tilde{\mathbf{Y}}_2$  for the formation of the projection matrix  $\mathbf{P}_{\tilde{\mathbf{Y}}_2}^{(n)} = \tilde{\mathbf{Y}}_2 (\tilde{\mathbf{Y}}_2^H \tilde{\mathbf{Y}}_2)^{-1} \tilde{\mathbf{Y}}_2^H$ . The transmitted radar signal is thus the projection of  $\mathbf{c}(p)$  onto the null space, i.e.,

$$\tilde{\mathbf{c}}(p) = \mathbf{P}_{\tilde{\mathbf{Y}}_2}^{(n)} \mathbf{c}(p). \quad (15)$$

The precoder  $\mathbf{P}_{\tilde{\mathbf{Y}}_2}^{(n)}$  inevitably introduces correlation among the signals emitted by the different transmit elements, thus generating some performance loss for target direction estimation. Note that the radar waveform is orthogonal to one communication channel but not to all. The MIMO radar selects the best interference channel, defined as

$$\mathbf{U}_{\text{Best}} = \mathbf{U}^{(i_{\max})}, \text{ with } i_{\max} = \arg \max_{1 \leq i \leq N} \dim[\mathcal{N}(\mathbf{U}^{(i)})], \quad (16)$$

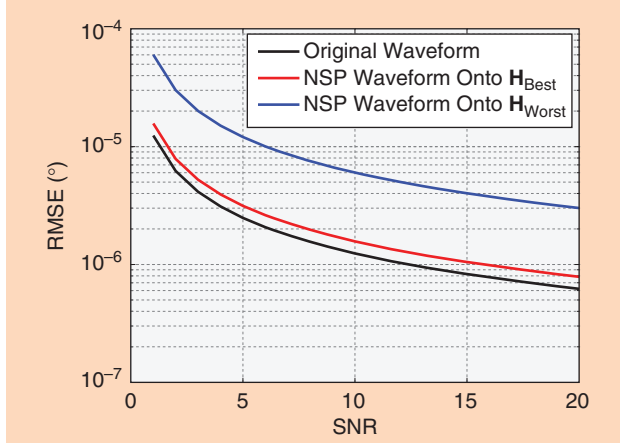


**FIGURE 3.** The Cramer–Rao bound on the target direction RMSE as a function of the SNR, when  $\mathbf{U}_{\text{Best}}$  and  $\mathbf{U}_{\text{Worst}}$  (marked as  $\mathbf{H}_{\text{Best}}$  and  $\mathbf{H}_{\text{Worst}}$ , respectively) channels are selected. NSP: null-space projection. (From [18].)

and avoids the worst channel, defined as

$$\mathbf{U}_{\text{Worst}} = \mathbf{U}^{(i_{\min})}, \text{ with } i_{\min} = \arg \min_{1 \leq i \leq N} \dim[\mathcal{N}(\mathbf{U}^{(i)})]. \quad (17)$$

In general, in the fully cooperative scenario outlined in [15], the radar can take a snapshot of the interference situation for each cluster and broadcast it to allow proper users assignment protocols. Users may then be assigned to less- or more-interfered base stations based on priority order.

In Figure 3, we compare the root-mean-square error (RMSE) of the target direction estimation under different radar waveforms. Note that the estimation performance using the null-space projection (NSP) waveform onto  $\mathbf{U}_{\text{Best}}$  is closer to the performance of the original radar waveform, in the RMSE sense. Thus, by an appropriate selection of the interference channel, the degradation in the radar performance due to the waveform's NSP can be reduced.

A MIMO radar may operate without creating interference at any of the communication receivers if the number of radar transmit antennas is greater than the sum of the requested degrees of freedom of all of the communication receivers [38]. Cooperation between all of the base stations and radar allows forming the interference matrix  $\bar{\mathbf{U}} = [\mathbf{U}^{(1)T}, \mathbf{U}^{(2)T}, \dots, \mathbf{U}^{(N)T}]^T \in \mathbb{C}^{NN_R \times MT}$ . Applying the previous strategy yields  $\tilde{\mathbf{c}}(p) \in \mathcal{N}(\bar{\mathbf{U}})$ . Other alternative strategies may rely on forcing the radar waveform to be designed according to a minimum mean square error criterion (rather than the aforementioned zero-forcing strategy).

More general approaches to the coordinated design of radar and communication are based on optimization methods (illustrated in Figure 4). We assume that the radar uses a  $P_r \times M_T$  space–time code matrix  $\mathbf{C}$ . The extension to slow-time coding can be undertaken by changing the time scale, considering the Doppler effect in the signal model of (12) and (13), and solving for the slow-time space–time matrix  $\mathbf{G}$ .

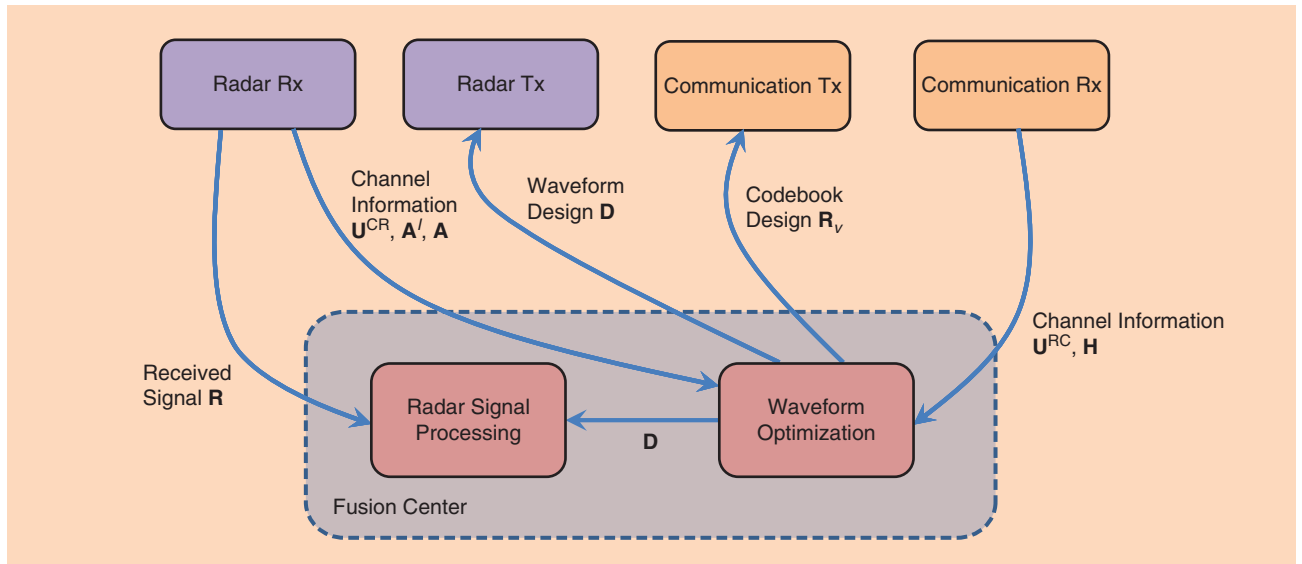


**FIGURE 4.** The schematic structure of a coordinated design of radar and communication waveforms based on optimization.

[16]. The space–time filter  $\tilde{\mathbf{w}}$  in (14) can also be optimized to improve radar performance.

Assume that the SINR is the figure of merit of interest to the radar, and let  $\mathbf{Q}$  be the figure of merit chosen for the communication system. They depend on  $\mathbf{D}$ , on the symbol matrix  $\mathbf{V}$  (or on some statistical feature thereof, if random coding is undertaken), and on a number of channel parameters tied to the reverberation that we combine in an unspecified array  $\mathbf{Z}$ . A suitable figure of merit guaranteeing the performance of the communication system is the mutual information between the input symbol stream and the observations [3], [16]. In particular, the mutual information averaged over  $P_r$  time slots, assuming Gaussian interference, is

$$C = \frac{1}{P_r} \sum_{p=0}^{P_r-1} \log_2 \det(\mathbf{I}_{N_R L} + \mathbf{R}_{\text{Cin}}^{-1} \mathbf{H} \mathbf{R}_v(p) \mathbf{H}^H), \quad (18)$$

where  $\mathbf{R}_v(p) = \mathbb{E}[\mathbf{v}(p)\mathbf{v}(p)^H]$  is the covariance matrix of the communication codebook, and  $\mathbf{R}_{\text{Cin}} \in \mathbb{C}^{N_R \times N_R}$  is the covariance of interference plus noise, assumed to be either known or perfectly estimated. The transceivers are designed to guarantee a prescribed QoS to both systems.

A possible optimization problem can be formulated as

$$\begin{aligned} \mathcal{P} = & \max_{D, \{\mathbf{R}_v(p)\}, \tilde{\mathbf{w}}} \text{SINR}(\mathbf{D}, \{\mathbf{R}_v(p)\}, \mathbf{Z}, \tilde{\mathbf{w}}), \\ & \text{s.t. } \mathbf{Q}(\mathbf{D}, \{\mathbf{R}_v(p)\}, \mathbf{Z}) \geq Q_0, \quad \text{QoS of Comm. Syst.} \\ & g_i(\mathbf{D}) \leq 0, i = 1, \dots, I_R, \quad \text{Rad. Wav. Constr.} \\ & f_i(\{\mathbf{R}_v(p)\}) \leq 0, i = 1, \dots, I_T, \quad \text{Comm. Codes. Constr.} \end{aligned} \quad (19)$$

where  $\text{SINR}(\cdot)$  is the SINR at the output of the radar receiver, and  $g_i(\cdot)$  and  $f_i(\cdot)$  are a set of constraints forced on the radar and communication transmitted signals, respectively. [Note that the expansions of the abbreviations in (19) are as follows: QoS of Comm. Syst.: QoS of communication system; Rad. Wav. Const.: radar waveform constraint; and Comm. Codes. Constr.: communication codes constraint.] The problem in (19) is typically nonconvex. Alternating maximization techniques have been proposed and implemented in [14] and [16] through decompositions into subproblems that are either convex or solvable through fractional programming methods. In [16], for example, (19) has been reformulated for slow-time coding, explicitly accounting for Doppler shifts of both the target to be detected and the environmental reverberation.

## Coexistence via cognition

### Environment-sensing techniques

The idea of knowledge-based design is central for spectrum-sharing systems [4], [7], [14], [17]–[19], [38]. The communication and/or the radar system undertakes suitable environment-sensing phases to determine the transmit policies. Inspired by cooperative methods in cognitive radio networks, [14] uses pilot signals to estimate the channels and feed back the channel information between the subsystems, possibly assigning to one of them a functional prior-

ity, as, e.g., in [39] and [40], where the radar is considered primary. These approaches rely on a centralized architecture, namely, a strict coordination between the active players, to allow coexistence.

More recently, approaches wherein the radar and/or the communication system is able to learn the environment without transmitting pilots or avoiding the need for coordination have been proposed. These advanced approaches are discussed in the following two scenarios:

- 1) *Environment sensing at the communication receiver*: A communication system shares its spectrum with an ensemble of potential interferers, i.e., a set of radar/sensing systems. The interfering waveforms from the radars lie in the subspace of a known dictionary and impinge on the communication receiver with unknown, possibly time-varying delays and coupling coefficients.
- 2) *Environment sensing at the radar receiver*: A sparse target scene is assumed, allowing the reduction of the radar sampling rate without sacrificing delay and Doppler resolution. The Xampling framework can be adopted, where the system architecture is designed for sampling and processing of analog inputs at rates far below Nyquist, whose underlying structure can be modeled as a union of subspaces [24].

The former situation has been described in the section “Uncoordinated Design: Communication Centric.” The communication receiver must be made adaptive to jointly accomplish the two tasks of interference estimation/removal and data demodulation. For the latter situation, the SpeCX system (shown in Figure 5) was proposed in [4]; it combines sub-Nyquist multiband sensing with sub-Nyquist radar to enable the radar to sense the communication channel at very low rates. Compared to other works, SpeCX presents a complete solution that shows the recovery of both the radar and communication signal with minimal information known about the spectrum.

More specifically, a sub-Nyquist cognitive radio is first implemented to sense the communication channel and determine which bands are occupied. This can be done using the modulated wideband converter (MWC), a sub-Nyquist communication receiver developed specifically for this task, which is capable of detecting sparse signals at very low rates [20]–[23]. Once the empty bands in the spectrum are identified, a cognitive radar receiver is employed that transmits a wideband signal that consists of several narrow-band signals in the vacant frequency bands [41].

Using the radar Xampling paradigm, it can be shown that high-resolution delay and Doppler can be performed from such a multiband, wideband radar signal by combining the methods of sub-Nyquist sampling and compressed beamforming [22], [42], [43]. This allows the detection of targets with high resolution while using a transmit signal that consists of several narrow bands spread over a wide frequency regime. The advantage of such a system is that the total bandwidth occupied is small while still allowing for high resolution. This enables the transmission of an adaptive radar signal that can coexist

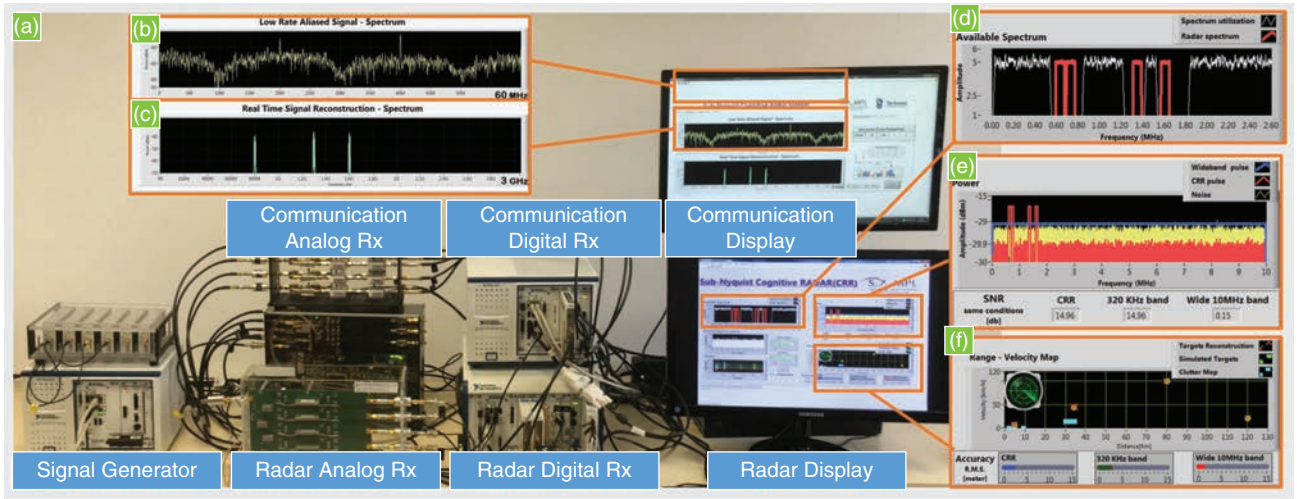


**FIGURE 5.** (a) A SpeCX prototype. The system consists of a signal generator, a cognitive radio receiver based on the MWC, a communication digital receiver, and a cognitive radar. The SpeCX communication system display shows (b) low-rate samples acquired from one MWC channel at a rate of 120 MHz and (c) a digital reconstruction of the entire spectrum from sub-Nyquist samples. The SpeCX radar display shows (d) the coexisting communication and cognitive radar, (e) the cognitive radar spectrum compared with the full-band radar, and (f) the range–velocity display of the detected and true locations of the targets. (From [4].)

with a standard communication channel and also leads to low-rate, low-power receivers.

### Knowledge-based design

In this subsection, we survey knowledge-based radar transmission designs based on environment sensing. For example, in some settings, the radar interference can be eliminated by forcing the radar waveforms to live in the null space of the interference channel between the radar transmitters and the communication receiver [18]. This idea has been well studied in the cognitive radio research community and has been applied to spectrum-sharing systems. Typical approaches include exploiting the spatial degrees of freedom granted by a MIMO radar [7], [18], [19], [38] and adaptive transmit/receive strategies to test the occupancy of the frequency bands [4].

In [4] and [22], the bands selected by the radar are chosen to optimize the radar probability of detection. More specifically,

after the communication signal support is identified, denoted as  $\mathcal{F}_c$ , the communication receiver provides a spectral map of occupied bands to the radar. Equipped with the detected spectral map and known radio environment map, denoted as  $\mathcal{F}_r$ , the objective of the radar is to identify an appropriate transmit frequency set that does not overlap with the union of  $\mathcal{F}_c$  and  $\mathcal{F}_r$  and maximizes the probability of correct detection. This probability increases with the SINR when the probability of false alarm is fixed. Therefore, it is proposed to maximize the SINR or minimize the spectral power in the undesired parts of the spectrum. This is achieved by using a structured sparsity framework [44]. Additional requirements of transmit energy constraints, range sidelobe levels, and a minimum separation between the bands can also be imposed. Once the optimal radar support is identified, a suitable waveform code may be designed over it.

There is another approach to waveform design. Rather than creating a waveform that avoids interference, one can base a design on spectral notching that minimizes the transmit energy in specific frequency bands while maintaining desirable envelope and sidelobe characteristics [45]. A waveform designed to avoid transmitting in specific bands, a spectrally disjoint waveform, must be characterized using other metrics because interference is not driving the design, and, thus, no such SINR can be calculated. Such metrics include average power levels in the undesired frequency bands, peak sidelobe levels, and integrated sidelobe levels.

### Functional coexistence

#### Embedding data into radar waveforms

A fairly natural evolution of radar and communication coexistence is to use radar to perform communication, also known as *dual-function radar communication* [46]. This approach is illustrated in Figure 6, wherein radar and communication

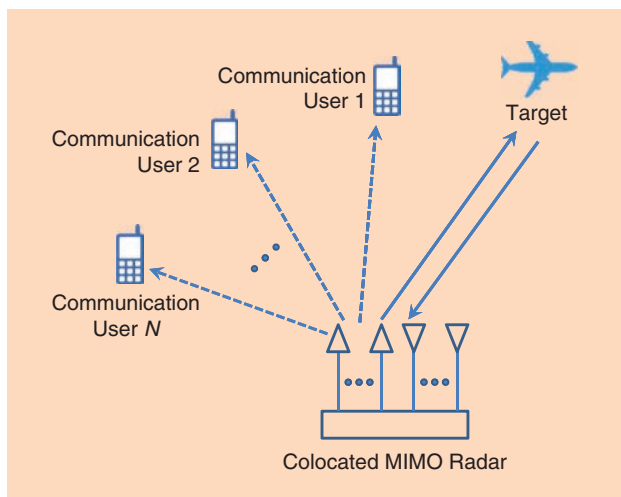


**FIGURE 6.** Dual-function radar communications.

systems are combined in the same hardware platform, usually with the same waveform or transmitter, which should be designed so as to guarantee the performance of both systems. In these architectures, as echoed by the name itself, coexistence is basically functional, and no spectrum overlap or resource negotiation takes place. This philosophy relies on the strategy of information embedding. Consider a joint radar communication platform equipped with  $M_T$  transmit antennas arranged as a uniform linear array. The radar receiver employs an array of  $M_R$  receive antennas with an arbitrary linear configuration. Without loss of generality, a single-element communication receiver is assumed to be located in the direction  $\theta_c$ , which is known to the transmitter.

Let  $\mathbf{s}(t) = [s_1(t), s_2(t), \dots, s_{M_T}(t)]^T \in \mathbb{C}^{M_T \times 1}$  be the baseband equivalent of the signal transmitted by a MIMO radar. Suppose a target is located at  $\theta$  with delay  $\tau$ . The received signal is then given by

$$\mathbf{r}(t) = \gamma \mathbf{a}_r(\theta) \mathbf{a}_r(\theta)^T \mathbf{s}(t - \tau) + \mathbf{n}_R(t), \quad (20)$$

where  $\mathbf{a}_t(\theta)$  and  $\mathbf{a}_r(\theta)$  are the steering vectors of the transmit and receive array, and  $\gamma$  is the coefficient accounting for both target reflection and propagation loss. The radar needs to detect the presence of the target, i.e.,  $\gamma = 0$  for  $\mathcal{H}_0$  and  $\gamma \neq 0$  for  $\mathcal{H}_1$ , and estimate the parameters  $\theta$  and  $\tau$ . Assuming a single-antenna communication receiver and considering a sophisticated single-pulse MIMO radar, the baseband signal at the output of the communication receiver can be expressed as

$$\begin{aligned} y(t) &= u \mathbf{a}_t(\theta_c)^T \mathbf{s}(t) + n_C(t) \\ &= u \mathbf{a}_t(\theta_c)^T \sum_i \tilde{\mathbf{s}}_i(t) + n_C(t), \end{aligned} \quad (21)$$

where  $u$  is the channel coefficient of the received signal encapsulating the propagation environment between the transmit array and the communication receiver, and  $\tilde{\mathbf{s}}_i(t)$  is the transmitted radar signal in the  $i$ th subpulse.

The fine structure of the transmitted signal  $\mathbf{s}(t)$  dictates the information-embedding method. Proposed strategies include the following.

■ *Waveform diversity-based information embedding [47]:* Here,  $N_b$  bits of information per pulse are embedded by selecting the radar waveform on a pulse-to-pulse basis from a set of  $K = 2^{N_b}$  waveforms [46]. Assume that the  $k$ th communication symbol is embedded in the  $i$ th pulse. Then the corresponding transmit signal vector can be expressed as

$$\tilde{\mathbf{s}}_i(t) = \sqrt{P_t} \mathbf{1}_{M_T} \psi_k(t - iT_r), \quad (22)$$

where  $P_t$  is the transmitting power,  $\mathbf{1}_{M_T}$  is the  $M_T \times 1$  vector of 1, and  $\psi_k(t)$  for  $k = 1, 2, \dots, K$  are orthogonal waveforms.

### A fairly natural evolution of radar and communication coexistence is to use radar to perform communication, also known as dual-function radar communication.

■ *Phase modulation-based information embedding [48]–[50]:* Information is embedded by controlling the phase of the signal. Assume that the  $k$ th communication symbol  $b(k)$  is transmitted through the phase information of the constant-envelope vector  $\mathbf{v} = [v(0), v(1), \dots, v(P_r - 1)]^T$ . Suppose the symbol  $\mathbf{v}$  is, in turn, embedded in a

single antenna radar waveform. The total transmit signal is then given by

$$\mathbf{s}(t) = \sum_{p=0}^{P_r-1} v(p) c(p) \psi(t - pT_r), \quad (23)$$

where the radar phase modulation  $c(p)$  enables direct control of the degree of range sidelobe modulation (RSM). RSM occurs because of the changing waveform structure during the coherent processing interval [51] by trading off bit error rate and/or data throughput. When not properly addressed, RSM translates to residual clutter in the range/Doppler response and hence degraded target visibility [2], [52]. Receive filter design to mitigate RSM is addressed for this type of information embedding in [48] and [52]. Design methods focus on the realization of a common filter response and exploit the inherent commonality among the radar/communication waveforms. It is worth noting that phase modulation will also inevitably lead to spectrum alteration of the radar waveform, which may result in energy leakage outside the assigned bandwidth [53].

■ *Sidelobe amplitude modulated-based communications [54]–[56]:* To embed the  $k$ th communication symbol  $b(k)$  during the  $i$ th pulse, the beamforming weight vector  $\mathbf{c}_k$  should be associated with that symbol. The amplitude modulated-based method models the transmit signal during the  $i$ th pulse as

$$\tilde{\mathbf{s}}_i(t) = \sqrt{P_t} \mathbf{c}_k \psi(t - iT_r). \quad (24)$$

The design of  $\mathbf{c}_k$  is formulated as the following optimization problem [26]:

$$\begin{aligned} \min_{\mathbf{c}_k} \max_{\theta} |G(\theta) - |\mathbf{c}_k^H \mathbf{a}_t(\theta)||, \theta \in \Theta, \\ \text{s.t. } |\mathbf{c}_k^H \mathbf{a}_t(\theta)| \leq \epsilon, \theta \in \bar{\Theta}, \mathbf{c}_k^H \mathbf{a}_t(\theta_c) = \Delta_k, \end{aligned} \quad (25)$$

where  $G(\theta)$  is the desired transmit beampattern,  $\Theta$  is the spatial sector the radar keeps under surveillance,  $\bar{\Theta}$  is the sidelobe region for communication,  $\epsilon$  is a positive number of users' choice for controlling the sidelobe levels, and  $\Delta_k$  is the  $k$ th sidelobe level toward the communication direction  $\theta_c$ . Several other variations of the sidelobe-modulating approach are discussed in [57] and [58].

■ *Multiwaveform amplitude shift keying-based information embedding [26]:* This method uses multiple waveforms and two transmit beamforming weight vectors  $\mathbf{c}_H$  and  $\mathbf{c}_L$ . The method requires  $N_b$  orthogonal waveforms to embed  $N_b$  bits per radar pulse. Then,  $N_b$  waveforms are transmitted

simultaneously, where the total transmit energy  $P_t$  is divided equally among the  $N_b$  waveforms. Every transmitted waveform is used to deliver one information bit, and the waveform  $\psi_k(t)$ ,  $k = 1, 2, \dots, N_b$ , is radiated either via  $\mathbf{c}_H$  for  $b_i(k) = 0$  or  $\mathbf{c}_L$  for  $b_i(k) = 1$  [46]. The transmit signal is then

$$\tilde{\mathbf{s}}_i(t) = \sqrt{\frac{P_t}{N_b}} \sum_{k=1}^{N_b} ((1 - b_i(k)) \mathbf{c}_H + b_i(k) \mathbf{c}_L) \psi_k(t - iT_r). \quad (26)$$

### Radar employing communication waveforms

Another evolution of functional coexistence is to exploit the waveforms transmitted by a communication network to perform sensing (radar) functions. Without loss of generality, we assume a single-element communication transmitter (or a phased array with an extremely directional beampattern). The baseband signal at the communication transmitter is given by (3), with  $x_i(t)$  and  $v_i(p)$  replaced by  $x(t)$  and  $v(p)$ , respectively.

Suppose the radar is equipped with  $M_R$  antennas and the communication transmitter is located at angle  $\theta_c$ . There are a number of scattering centers (targets), the  $i$ th of which is with path delay  $\tau_i$ , Doppler shift  $\nu_i$ , and angle  $\theta_i$ . Let  $\gamma_i$  be the coefficient accounting for both the target reflection and propagation loss of the  $i$ th target. The response from the communication transmitter to the radar receiver in (4) can be rewritten as

$$u_j^{\text{CR}}(t) = ua_{r,j}(\theta_c)\delta(t - \tau_c) + \sum_i \gamma_i a_{r,j}(\theta_i) e^{j2\pi\nu_i t} \delta(t - \tau_i),$$

where  $a_{r,j}(\theta)$  is the angle response of the  $j$ th radar receiver,  $u$  is the coefficient of the direct path between the communication transmitter and radar receiver, and  $\tau_c$  is the delay of the direct path. As no radar transmitter is used, the baseband equivalent signal at the radar receiver can be obtained from (4), with  $\sum_{i=1}^{M_T} a_{i,j} s_i(t - \tau_{i,j})$  and  $\sum_{i=1}^{M_T} (a_{i,j}^T * s_i)(t)$  removed:

$$\mathbf{r}(t) = u \mathbf{a}_r(\theta_c) x(t - \tau_c) + \sum_i \gamma_i e^{j2\pi\nu_i t} \mathbf{a}_r(\theta_i) x(t - \tau_i) + \mathbf{n}_R(t), \quad (27)$$

where  $\mathbf{a}_r(\theta) = [a_{r,1}(\theta), a_{r,2}(\theta), \dots, a_{r,M_R}(\theta)]^T \in \mathbb{C}^{M_R}$  is the receive steering vector.

One option for using a communication waveform  $x(t)$  for sensing is the opportunistic radar based on the 802.11ad standard proposed in [29] and [30]. The adoption of the 802.11ad standard for 5G wireless systems and the exploitation of millimeter waves (mm-waves) in the 28-GHz and 60-GHz bandwidths [59] immediately raised interest in utilizing some key characteristics of the proposed standard for sensing applications. Indeed, mm-waves suffer from heavy atmospheric attenuation, resonance in the oxygen molecule, absorption by rain, and almost complete shadowing by obstacles, thus requiring line-of-sight paths between transmitter and receiver. This, in turn, is achievable thanks to extremely

directional beampatterns and frequent scanning procedures during which the surrounding space is swept in search of nodes willing to establish directional links.

As a consequence, the so-called sector level sweep phase of the beamforming training protocol provides signals of opportunity that can be exploited for short-range obstacle detection, typically in automotive applications [29]. In such a phase, the transmitted signal consists of a preamble, containing concatenated complementary Golay codes, and a payload, containing data. The proposed architectures rely on the presence of a receiver, colocated with the wireless transmitter and accessing some key information, such as the timing, as well as part, if not all, of the transmitted signal. With reference to (27),  $\tau_c = 0$  and  $u = 0$  because there is no direct path, and  $x(t)$  is either partially known, because the preamble has a fixed structure, or completely known, if the transmitted data are communicated to the radar receiver.

Suppose there is one target in each sector. We denote by  $\gamma$  its unique complex scattering coefficient. A number of receiving structures have been proposed for target detection and localization in the range/Doppler domain in [29] and [30], mostly based on the generalized likelihood ratio test (GLRT) [60] and assuming different degrees of prior knowledge and cooperation between the radar receiver and the communication transmitter.

- 1) *GLRT-1*: Everything but the triplet  $(\gamma, \nu, \tau)$  in (27) is known.
- 2) *GLRT-1, simplified version (simpl.)*: The receiver is as in GLRT-1 but processes only the preamble.
- 3) *GLRT-2, Swerling (SW)-I*: This is like GLRT-1, but  $\gamma$  is a nuisance parameter, modeled as complex Gaussian.
- 4) *GLRT-3*: The payload data are not available to the radar receiver.
- 5) *GLRT-4 SW-I*: This is as in GLRT-3 but with  $\gamma$  a nuisance parameter.
- 6) *Preamble detector*: This is the preamble detector of [29].

We underline here that the GLRT strategy is aimed at solving composite hypotheses tests, namely, those wherein the densities under the two alternatives contain unknown parameters. In practice, these parameters are replaced by the corresponding maximum-likelihood estimates, performed with the same set of data used to make the final decision. Consequently, the GLRT considers, as a by-product, an estimate of the unknown parameters. Figures 7 and 8 represent examples of what can be achieved with such opportunistic structures in terms of both detection and localization of an obstacle in short-range applications.

Notwithstanding the encouraging results so far available, a number of problems still remain before claims can be made on the feasibility of such structures. The channel models underlying the results of Figures 7 and 8 are very simple, assuming that either a single object is present or that it absorbs all of the radiation, thus shielding other obstacles. Moreover, because the range resolution is on the order of decimeters, most objects are typically range spread, a situation not accounted for so far in the open literature.

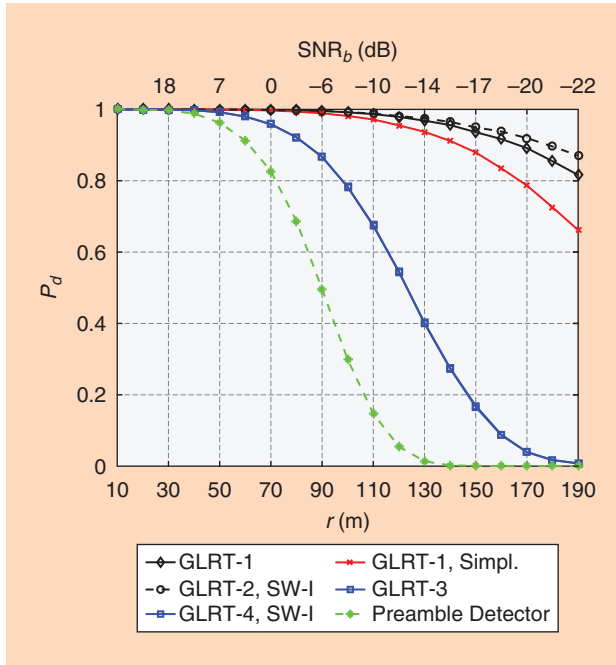


**FIGURE 7.** The detection probability as a function of the target range and the SNR per bit. The false alarm probability is set at  $P_{fa} = 10^{-4}$ . (Used with permission from [30].)

Passive radar is another option that exploits other transmissions (communications, broadcast, or radio navigation) rather than having its own dedicated radar transmitter [1], [31]. It is generally necessary to have a reference channel (RC) dedicated to acquiring the direct path signal as the reference waveform for matched filtering and for there to be surveillance channels (SCs) from which the target reflections are acquired. For a communication transmitter with a known position,  $\theta_c$  in (27) can be obtained [61]. The signal in the RC is given by

$$z_{RC}(t) = \mathbf{a}_r(\theta_c)^H \mathbf{z}(t) = ux(t - \tau_c) + n_{RC}(t), \quad (28)$$

where  $n_{RC}(t) = \mathbf{a}_r(\theta_c)^H (\sum_i \gamma_i \mathbf{a}_r(\theta_i)x(t - \tau_i) + \mathbf{n}_R(t))$ .

The SC signal is obtained via beamforming on direction  $\tilde{\theta}$ :

$$\begin{aligned} z_{SC}(t) &= \mathbf{a}_r(\tilde{\theta})^H \mathbf{z}(t) \\ &= u\zeta_c x(t - \tau_c) + \sum_i \gamma_i e^{j2\pi\nu_i t} \zeta_i x(t - \tau_i) + n_{SC}(t), \end{aligned} \quad (29)$$

where  $\zeta_c = \mathbf{a}_r(\tilde{\theta})^H \mathbf{a}_r(\theta_c)$ ,  $\zeta_i = \mathbf{a}_r(\tilde{\theta})^H \mathbf{a}_r(\theta_i)$ , and  $n_{SC}(t) = \mathbf{a}_r(\tilde{\theta})^H \mathbf{n}_R(t)$ . To detect the target at delay  $\tau$  and Doppler  $\nu$ , the signal is match-filtered via [62]

$$r(\tau) = \int z_{SC}(t) e^{-j2\pi\nu t} z_{RC}^*(t - \tau + \tau_c) dt. \quad (30)$$

The surveillance signal  $z_{SC}(t)$  contains the signal from the direct path, which causes strong interference. Another issue is that the RC is not very clean in many practical cases, and the performance of the radar is significantly degraded when there is a great deal of interference, clutter, and noise.

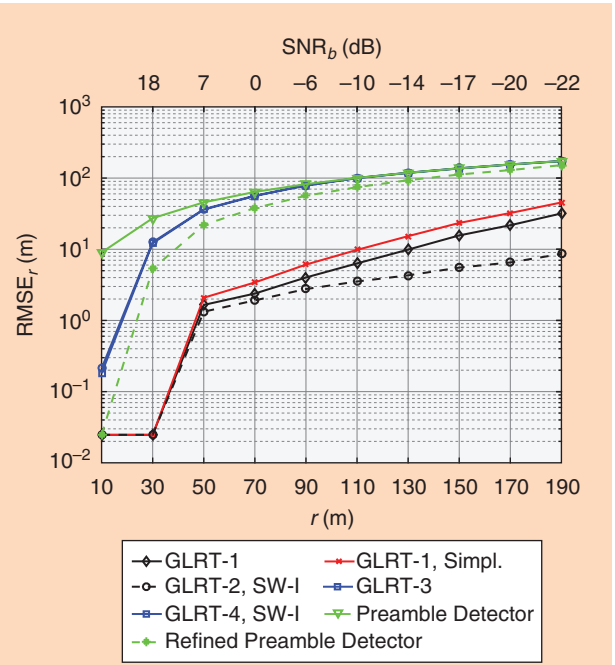


**FIGURE 8.** The ranging accuracy as a function of the target range and the SNR per bit. (Used with permission from [30].)

To improve the performance of passive radar, one can make use of the structural information of the underlying communication signal. In particular, because the type of modulation is typically known, we can first estimate the data symbols by demodulation. As demodulation provides better accuracy than directly using the signal in the RC, detection and estimation performance of such radar systems may improve [61], [62]. It is worth noting that passive radar operation is generally inferior to active radar operation because of nonoptimal waveforms, spatial beampatterns, and transmit power [2]. Some recent works proposed what they called *commensal radar* [63], [64], in which the communication signal is designed with the double purpose of transferring information and improving target localization (through a careful autocorrelation function shaping) for a coexisting passive sensing system.

## Conclusions

We reviewed some of the main ideas and techniques to allow the coexistence of sensing and communication functions in sharing the same frequency spectrum. The strategies so far proposed are grouped into three major categories. The first allows spectral overlap between the signal transmitted by the radar and communication systems, while the other two avoid mutual interference either by cognitively assigning disjoint subbands to the different services or allowing just one transmitter to be active and guaranteeing functional coexistence.

For each of these categories, the basic ideas are outlined, discussing advantages and disadvantages and offering some examples to illustrate their performance. In the future, hardware prototypes should be built and deployed to be tested

on real data. This would permit assessing their performance under real-world conditions, including different types of noise, clutter, and interference.

## Authors

**Le Zheng** (le.2.zheng@aptiv.com) received his B.S. degree in communication engineering from Northwestern Polytechnical University, Xi'an, China, in 2009 and his Ph.D. degree in target detection and recognition from the Beijing Institute of Technology, China, in 2015. From 2015 to 2018, he was a postdoctoral researcher in the Electrical Engineering Department of Columbia University, New York. He now works at Aptiv (formerly Delphi), Los Angeles, as a principal radar systems engineer. His research interests lie in the areas of automotive radar, statistical signal processing, wireless communication, and high-performance hardware for signal processing. He is a Member of the IEEE.

**Marco Lops** (lops@unina.it) received his laurea and Ph.D. degrees in electronic engineering from the Federico II University of Naples, Italy, where he was an assistant professor (1989–1991) and an associate professor (1991–2000) and where he is now a professor in the Department of Electrical Engineering and Information Technologies. From 2000 to 2018, he was a professor at the University of Cassino and Southern Lazio, Italy, and, in 2009–2011, he was also with ENSEEIHT, Toulouse, France, first as a full professor and then as a visiting professor. In the fall of 2008, he was a visiting professor at the University of Minnesota, Minneapolis and St. Paul, and, in the spring of 2009, at Columbia University, New York. He was selected to serve as a Distinguished Lecturer for the IEEE Signal Processing Society during 2018–2020. His research interests are in detection and estimation, with an emphasis on communications and radar signal processing. He is a Fellow of the IEEE.

**Yonina C. Eldar** (yonina@ee.technion.ac.il) is a professor in the Department of Electrical Engineering at the Technion–Israel Institute of Technology, Haifa, where she holds the Edwards chair in engineering. She is also an adjunct professor at Duke University, Durham, North Carolina, and a research affiliate with the Research Laboratory of Electronics at the Massachusetts Institute of Technology, Cambridge, and she was a visiting professor at Stanford University, California. She is a member of the Israel Academy of Sciences and Humanities and a Fellow of the IEEE and the European Association for Signal Processing. She has received many awards for excellence in research and teaching, including the IEEE Signal Processing Society Technical Achievement Award, the IEEE/Aerospace and Electronic Systems Society Fred Nathanson Memorial Radar Award, the IEEE Kiyo Tomiyasu Award, the Michael Bruno Memorial Award from the Rothschild Foundation, the Weizmann Prize for Exact Sciences, and the Wolf Foundation Krill Prize for Excellence in Scientific Research. She is the editor-in-chief of *Foundations and Trends in Signal Processing* and serves the IEEE on several technical and award committees.

**Xiaodong Wang** (wangx@ee.columbia.edu) received his B.S. degree in electrical engineering and applied mathematics from Shanghai Jiao Tong University, China, and his Ph.D. degree in electrical engineering from Princeton University, New Jersey. He is a professor of electrical engineering at Columbia University, New York. He has published extensively in the areas of computing, signal processing, and communications. Among his writings is the book *Wireless Communication Systems: Advanced Techniques for Signal Reception* (Prentice Hall, 2003). His current research interests include wireless communications, statistical signal processing, and genomic signal processing. He received the 1999 National Science Foundation CAREER Award, the 2001 IEEE Communications Society and Information Theory Society Joint Paper Award, and the 2011 IEEE Communication Society Award for Outstanding Paper on New Communication Topics. He has served as an associate editor of *IEEE Transactions on Communications*, *IEEE Transactions on Wireless Communications*, *IEEE Transactions on Signal Processing*, and *IEEE Transactions on Information Theory*. He is listed as an ISI Highly Cited Researcher and is a Fellow of the IEEE.

## References

- [1] H. Griffiths, L. Cohen, S. Watts, E. Mokole, C. Baker, M. Wicks, and S. Blunt, "Radar spectrum engineering and management: Technical and regulatory issues," *Proc. IEEE*, vol. 103, no. 1, pp. 85–102, 2015.
- [2] S. Blunt and E. Perrins, *Radar and Communication Spectrum Sharing* (Electromagnetics and Radar). Raleigh, NC: Scitech Publishing, 2018.
- [3] B. Li, A. P. Petropulu, and W. Trappe, "Optimum co-design for spectrum sharing between matrix completion based MIMO radars and a MIMO communication system," *IEEE Trans. Signal Process.*, vol. 64, no. 17, pp. 4562–4575, 2016.
- [4] D. Cohen, K. V. Mishra, and Y. C. Eldar, "Spectrum sharing radar: Coexistence via Xampling," *IEEE Trans. Aerosp. Electron. Syst.*, vol. 54, no. 3, pp. 1279–1296, 2018.
- [5] J. B. Evans, "Shared spectrum access for radar and communications (SSPARC)," Defense Advanced Res. Projects Agency, Arlington, VA, press release, 2016. [Online]. Available: <http://www.darpa.mil/program/shared-spectrum-access-for-radar-and-communications>
- [6] S. M. Patole, M. Torlak, D. Wang, and M. Ali, "Automotive radars: A review of signal processing techniques," *IEEE Signal Process. Mag.*, vol. 34, no. 2, pp. 22–35, 2017.
- [7] H. Deng and B. Himed, "Interference mitigation processing for spectrum-sharing between radar and wireless communications systems," *IEEE Trans. Aerosp. Electron. Syst.*, vol. 49, no. 3, pp. 1911–1919, 2013.
- [8] F. H. Sanders, R. L. Sole, J. E. Carroll, G. S. Secrest, and T. L. Allmon, "Analysis and resolution of RF interference to radars operating in the band 2700–2900 MHz from broadband communication transmitters," U.S. Dept. Commerce, Nat. Telecommun. Inform. Admin., NTIA Report 13-490, 2012.
- [9] A. Aubry, A. De Maio, M. Piezzo, and A. Farina, "Radar waveform design in a spectrally crowded environment via nonconvex quadratic optimization," *IEEE Trans. Aerosp. Electron. Syst.*, vol. 50, no. 2, pp. 1138–1152, 2014.
- [10] A. Aubry, A. De Maio, Y. Huang, M. Piezzo, and A. Farina, "A new radar waveform design algorithm with improved feasibility for spectral coexistence," *IEEE Trans. Aerosp. Electron. Syst.*, vol. 51, no. 2, pp. 1029–1038, 2015.
- [11] L. Zheng, M. Lops, and X. Wang, "Adaptive interference removal for uncoordinated radar/communication coexistence," *IEEE J. Sel. Topics Signal Process.*, vol. 12, no. 1, pp. 45–60, 2018.
- [12] F. Liu, C. Masouros, A. Li, T. Ratnarajah, and J. Zhou, "MIMO radar and cellular coexistence: A power-efficient approach enabled by interference exploitation," *IEEE Trans. Signal Process.*, vol. 66, no. 14, pp. 3681–3695, 2018.
- [13] N. Nartasilpa, A. Salim, D. Tuninetti, and N. Devroye, "Communications system performance and design in the presence of radar interference," *IEEE Trans. Commun.*, vol. 66, no. 9, pp. 4170–4185, 2018.
- [14] B. Li and A. P. Petropulu, "Joint transmit designs for coexistence of MIMO wireless communications and sparse sensing radars in clutter," *IEEE Trans. Aerosp. Electron. Syst.*, vol. 53, no. 6, pp. 2846–2864, 2017.

- [15] J. Mahal, A. Khawar, A. Abdelhadi, and C. Clancy, "Spectral coexistence of MIMO radar and MIMO cellular systems," *IEEE Trans. Aerosp. Electron. Syst.*, vol. 53, no. 2, pp. 655–668, 2017.
- [16] J. Qian, M. Lops, L. Zheng, X. Wang, and Z. He, "Joint system design for co-existence of MIMO radar and MIMO communication," *IEEE Trans. Signal Process.*, vol. 66, no. 13, pp. 3504–3519, 2018.
- [17] L. Zheng, M. Lops, X. Wang, and E. Grossi, "Joint design of overlaid communication systems and pulsed radars," *IEEE Trans. Signal Process.*, vol. 66, no. 1, pp. 139–154, 2018.
- [18] A. Khawar, A. Abdel-Hadi, and T. C. Clancy, "Spectrum sharing between S-band radar and LTE cellular system: A spatial approach," in *Proc. IEEE Int. Symp. Dynamic Spectrum Access Networks (DYSNAP)*, 2014, pp. 7–14.
- [19] A. Puglielli, A. Townley, G. LaCaille, V. Milovanović, P. Lu, K. Trotskovsky, A. Whitcombe, N. Narevsky et al., "Design of energy-and cost-efficient massive MIMO arrays," *Proc. IEEE*, vol. 104, no. 3, pp. 586–606, 2016.
- [20] M. Mishali, Y. C. Eldar, O. Dounaevsky, and E. Shoshan, "Xampling: Analog to digital at sub-Nyquist rates," *IET Circuits, Devices, Syst.*, vol. 5, no. 1, pp. 8–20, 2011.
- [21] M. Mishali and Y. C. Eldar, "From theory to practice: Sub-Nyquist sampling of sparse wideband analog signals," *IEEE J. Sel. Topics Signal Process.*, vol. 4, no. 2, pp. 375–391, 2010.
- [22] Y. C. Eldar, *Sampling Theory: Beyond Bandlimited Systems*. Cambridge, United Kingdom: Cambridge Univ. Press, 2015.
- [23] D. Cohen, S. Tsiper, and Y. C. Eldar, "Analog-to-digital cognitive radio: Sampling, detection, and hardware," *IEEE Signal Process. Mag.*, vol. 35, no. 1, pp. 137–166, 2018.
- [24] D. Cohen and Y. C. Eldar, "Sub-Nyquist radar systems: Temporal, spectral, and spatial compression," *IEEE Signal Process. Mag.*, vol. 35, no. 6, pp. 35–58, 2018.
- [25] S. D. Blunt, P. Yathan, and J. Stiles, "Intrapulse radar-embedded communications," *IEEE Trans. Aerosp. Electron. Syst.*, vol. 46, no. 3, pp. 1185–1200, 2010.
- [26] A. Hassanien, M. G. Amin, Y. D. Zhang, and F. Ahmad, "Dual-function radar-communications: Information embedding using sidelobe control and waveform diversity," *IEEE Trans. Signal Process.*, vol. 64, no. 8, pp. 2168–2181, 2016.
- [27] Z. Geng, R. Xu, H. Deng, and B. Himed, "Fusion of radar sensing and wireless communications by embedding communication signals into the radar transmit waveform," *IET Radar, Sonar, Navigation*, vol. 12, no. 6, 2018. doi: 10.1049/iet-sn.2017.0405.
- [28] F. Liu, L. Zhou, C. Masouros, A. Li, W. Luo, and A. Petropulu, "Toward dual-functional radar-communication systems: Optimal waveform design," *IEEE Trans. Signal Process.*, vol. 66, no. 16, pp. 4264–4279, 2018.
- [29] P. Kumari, N. Gonzalez-Prelcic, and R. W. Heath, "Investigating the IEEE 802.11ad standard for millimeter wave automotive radar," in *Proc. IEEE 82nd Vehicular Technology Conf. (VTC Fall)*, 2015, pp. 1–5. doi: 10.1109/VTCFall.2015.7390996.
- [30] E. Grossi, M. Lops, L. Venturino, and A. Zappone, "Opportunistic radar in 802.11ad networks," *IEEE Trans. Signal Process.*, vol. 66, no. 9, pp. 2441–2454, 2018.
- [31] H. Griffiths, "Passive bistatic radar and waveform diversity," Defence Acad. U.K., Shrivenham, U.K., Tech. Rep. ADA567763, 2009.
- [32] S. D. Blunt and E. L. Mokole, "Overview of radar waveform diversity," *IEEE Aerosp. Electron. Syst. Mag.*, vol. 31, no. 11, pp. 2–42, 2016.
- [33] A. De Maio and M. Lops, "Design principles of MIMO radar detectors," *IEEE Trans. Aerosp. Electron. Syst.*, vol. 43, no. 3, pp. 886–898, 2007.
- [34] A. Aubry, A. DeMaio, A. Farina, and M. Wicks, "Knowledge-aided (potentially cognitive) transmit signal and receive filter design in signal-dependent clutter," *IEEE Trans. Aerosp. Electron. Syst.*, vol. 49, no. 1, pp. 93–117, 2013.
- [35] M. Piezzo, A. De Maio, A. Aubry, and A. Farina, "Cognitive radar waveform design for spectral coexistence," in *Proc. IEEE Radar Conf.*, 2013. doi: 10.1109/RADAR.2013.6586024.
- [36] A. Aubry, A. De Maio, M. Piezzo, M. Naghsh, M. Soltanianian, and S. Petre, "Cognitive radar waveform design for spectral coexistence in signal-dependent interference," in *Proc. IEEE Radar Conf.*, 2014, pp. 474–478.
- [37] Y. Noam and A. J. Goldsmith, "Blind null-space learning for MIMO underlay cognitive radio with primary user interference adaptation," *IEEE Trans. Wireless Commun.*, vol. 12, no. 4, pp. 1722–1734, 2013.
- [38] A. Babaei, W. H. Tranter, and T. Bose, "A practical precoding approach for radar/communications spectrum sharing," in *Proc. 8th Int. Conf. Cognitive Radio Oriented Wireless Networks (CROWNCOM)*, 2013, pp. 13–18.
- [39] R. Zhang and Y.-C. Liang, "Exploiting multi-antennas for opportunistic spectrum sharing in cognitive radio networks," *IEEE J. Sel. Topics Signal Process.*, vol. 2, no. 1, pp. 88–102, 2008.
- [40] R. Zhang, Y.-C. Liang, and S. Cui, "Dynamic resource allocation in cognitive radio networks," *IEEE Signal Process. Mag.*, vol. 27, no. 3, pp. 102–114, 2010.
- [41] D. Cohen, A. Dikopolskay, R. Ifraimov, and Y. C. Eldar, "Towards sub-Nyquist cognitive radar," in *Proc. IEEE Radar Conf.*, 2016, pp. 1–4. doi: 10.1109/RADAR.2016.7485122.
- [42] O. Bar-Ilan and Y. C. Eldar, "Sub-Nyquist radar via Doppler focusing," *IEEE Trans. Signal Process.*, vol. 62, no. 7, pp. 1796–1811, 2014.
- [43] E. Baransky, G. Itzhak, N. Wagner, I. Shmuel, E. Shoshan, and Y. Eldar, "Sub-Nyquist radar prototype: Hardware and algorithm," *IEEE Trans. Aerosp. Electron. Syst.*, vol. 50, no. 2, pp. 809–822, 2014.
- [44] J. Huang, T. Zhang, and D. Metaxas, "Learning with structured sparsity," *J. Mach. Learning Res.*, vol. 12, pp. 3371–3412, Nov. 2011.
- [45] S. W. Frost and B. Rigling, "Sidelobe predictions for spectrally-disjoint radar waveforms," in *Proc. IEEE Radar Conf.*, 2012, pp. 247–252.
- [46] A. Hassanien, M. G. Amin, Y. D. Zhang, and F. Ahmad, "Signaling strategies for dual-function radar communications: An overview," *IEEE Trans. Aerosp. Electron. Syst. Mag.*, vol. 31, no. 10, pp. 36–45, 2016.
- [47] S. D. Blunt, M. R. Cook, and J. Stiles, "Embedding information into radar emissions via waveform implementation," in *Proc. IEEE Int. Waveform Diversity and Design Conf. (WDD)*, 2010, pp. 195–199.
- [48] C. Sahin, J. Jakabosky, P. M. McCormick, J. G. Metcalf, and S. D. Blunt, "A novel approach for embedding communication symbols into physical radar waveforms," in *Proc. IEEE Radar Conf.*, 2017, pp. 1498–1503.
- [49] C. Sahin, J. G. Metcalf, A. Kordik, T. Kendo, and T. Corigliano, "Experimental validation of phase-attached radar/communication (PARC) waveforms: Radar performance," in *Proc. 2018 Int. Conf. Radar (RADAR)*, 2018. doi: 10.1109/RADAR.2018.8557302.
- [50] M. J. Nowak, Z. Zhang, L. LoMonte, M. Wicks, and Z. Wu, "Mixed-modulated linear frequency modulated radar-communications," *IET Radar, Sonar, Navigation*, vol. 11, no. 2, pp. 313–320, 2016.
- [51] J. Tian, W. Cui, and S. Wu, "A novel method for parameter estimation of space moving targets," *IEEE Geosci. Remote Sens. Lett.*, vol. 11, no. 2, pp. 389–393, 2014.
- [52] C. Sahin, J. G. Metcalf, and S. D. Blunt, "Filter design to address range sidelobe modulation in transmit-encoded radar-embedded communications," in *Proc. IEEE Radar Conf.*, 2017, pp. 1509–1514.
- [53] X. Chen, Z. Liu, Y. Liu, and Z. Wang, "Energy leakage analysis of the radar and communication integrated waveform," *IET Signal Process.*, vol. 12, no. 3, pp. 375–382, 2018.
- [54] J. Euziere, R. Guinvarc'h, M. Lesturgie, B. Uguen, and R. Gillard, "Dual function radar communication time-modulated array," in *Proc. IEEE Radar Conf.*, 2014. doi: 10.1109/RADAR.2014.7060416.
- [55] P. M. McCormick, S. D. Blunt, and J. G. Metcalf, "Simultaneous radar and communications emissions from a common aperture, Part I: Theory," in *Proc. IEEE Radar Conf.*, 2017, pp. 1685–1690.
- [56] P. M. McCormick, B. Ravenscroft, S. D. Blunt, A. J. Duly, and J. G. Metcalf, "Simultaneous radar and communication emissions from a common aperture, Part II: Experimentation," in *Proc. IEEE Radar Conf.*, 2017, pp. 1697–1702.
- [57] A. Hassanien, M. G. Amin, Y. D. Zhang, and F. Ahmad, "Efficient sidelobe ASK based dual-function radar-communications," in *Proc. SPIE Defense + Security*, May 26, 2016. doi: 10.1117/12.2227252.
- [58] A. Hassanien, M. G. Amin, Y. D. Zhang, and F. Ahmad, "Phase-modulation based dual-function radar-communications," *IET Radar, Sonar, Navigation*, vol. 10, no. 8, pp. 1411–1421, 2016.
- [59] T. S. Rappaport, S. Sun, R. Mayzus, H. Zhao, Y. Azar, K. Wang, G. N. Wong, G. N. Schulz et al., "Millimeter wave mobile communications for 5G cellular: It will work!" *IEEE Access*, vol. 1, pp. 335–349, May 2013.
- [60] S. M. Kay, *Detection Theory (Fundamentals of Statistical Signal Processing Series, Volume II)*. Englewood Cliffs, NJ: Prentice Hall, 1993.
- [61] L. Zheng and X. Wang, "Super-resolution delay-Doppler estimation for OFDM passive radar," *IEEE Trans. Signal Process.*, vol. 65, no. 9, pp. 2197–2210, 2017.
- [62] C. R. Berger, B. Demissie, J. Heckenbach, P. Willett, and S. Zhou, "Signal processing for passive radar using OFDM waveforms," *IEEE J. Sel. Topics Signal Process.*, vol. 4, no. 1, pp. 226–238, 2010.
- [63] H. Griffiths, I. Darwazeh, and M. Inggs, "Waveform design for commensal radar," in *Proc. IEEE Radar Conf.*, 2015, pp. 1456–1460.
- [64] B. Ravenscroft, P. M. McCormick, S. D. Blunt, J. Jakabosky, and J. G. Metcalf, "Tandem-hopped OFDM communications in spectral gaps of FM noise radar," in *Proc. IEEE Radar Conf.*, 2017, pp. 1262–1267.

Kumar Vijay Mishra, M.R. Bhavani Shankar, Visa Koivunen,  
Björn Ottersten, and Sergiy A. Vorobyov

# Toward Millimeter-Wave Joint Radar Communications

A signal processing perspective



**S**ynergistic design of communications and radar systems with common spectral and hardware resources is heralding a new era of efficiently utilizing a limited radio-frequency (RF) spectrum. Such a joint radar communications (JRC) model has advantages of low cost, compact size, less power consumption, spectrum sharing, improved performance, and safety due to enhanced information sharing. Today, millimeter-wave (mm-wave) communications have emerged as the preferred technology for short distance wireless links because they provide transmission bandwidth that is several gigahertz wide. This band is also promising for short-range radar applications, which benefit from the high-range resolution arising from large transmit signal bandwidths. Signal processing techniques are critical to the implementation of mm-wave JRC systems. Major challenges are joint waveform design and performance criteria that would optimally trade off between communications and radar functionalities. Novel multiple-input, multiple-output (MIMO) signal processing techniques are required because mm-wave JRC systems employ large antenna arrays. There are opportunities to exploit recent advances in cognition, compressed sensing, and machine learning to reduce required resources and dynamically allocate them with low overheads. This article provides a signal processing perspective of mm-wave JRC systems with an emphasis on waveform design.

## Spectrum sharing at mm-wave

In recent years, sensing systems (e.g., radar, lidar, or sonar) that share the spectrum with wireless communications (RF, optical, or acoustical) and continue to operate without any significant performance losses have captured significant research attention [1], [2]. The interest in spectrum-sharing systems is mostly because the spectrum required by the wireless media is a scarce resource, whereas the performances of communications and remote sensing systems improve from utilizing a wider spectrum. In this article, we focus on RF spectrum sharing between radar and communications.

Several portions of frequency bands—from very high frequency to terahertz—are allocated exclusively for different

radar applications [3]. Although a large fraction of these bands remains underutilized, radars must maintain constant access to these bands for target sensing and detection as well as to obtain more spectrum to accomplish missions such as secondary surveillance, multifunction integrated RF operations, communications-enabled autonomous driving, and cognitive capabilities. Conversely, the wireless industry's demand for spectrum continues to increase, providing new services and accommodating a massive amount of users with high data-rate requirements. The present spectrum is used very inefficiently due to its highly fragmented allocation.

Emerging wireless systems such as commercial LTE communications technology, 5G, Wi-Fi, the Internet of Things (IoT), and Citizens Broadband Radio Services have long caused spectral interference to legacy military, weather, astronomy, and aircraft surveillance radars [1], [3]. Similarly, radar signals in adjacent bands leak into spectrums allocated for communications and deteriorate the service quality. Therefore, it is essential and beneficial for radar and communications to develop strategies that simultaneously and opportunistically operate in the same spectral bands in a mutually beneficial manner.

The spectral overlap of centimeter-wave (cm-wave) radars with a number of wireless systems at the 3.5-GHz frequency band led to the 2012 U.S. President's Council of Advisors on Science and Technology report on spectrum sharing [4], and the changes in regulations for this band became a driver for the spectrum-sharing research programs of multiple agencies [3]. Today, it is the higher end of the RF spectrum, i.e., the mm-wave, formally defined by the frequency range of 30–300 GHz, which requires concerted efforts for spectrum management because its technologies are in an early developmental stage. Increasingly, mm-wave systems [5] are the preferred technology for near-field communications because they provide transmission bandwidth that is several gigahertz wide; however, this bandwidth is currently unlicensed. This enables applications that require very large data rates, such as 5G wireless backhaul, uncompressed high-definition video, in-room gaming, intra-large-vehicle communications, intervehicular communications, indoor positioning systems, and IoT-enabled wearable technologies [6].

The amount of novel sensing systems in the mm-wave band has also grown. Although these devices typically have short ranges because of heavy attenuation by physical barriers, weather, and atmospheric absorption, they provide high range resolution resulting from the wide bandwidth. Typical mm-wave radar applications include autonomous vehicles [7], gesture recognition [8], cloud observation [9], RF identification [10], indoor localization [11], and health monitoring [12]. In the following sections, we explain the distinct features and JRC challenges of mm-wave channels.

## The mm-wave channel

Compared to cm-wave, the channel environment for mm-wave is characterized by unique challenges that motivate the ensuing specific design constraints.

### Strong attenuation

Compared to sub-6-GHz transmissions envisaged in 5G, mm-wave signals encounter a more complex propagation environment characterized by higher scattering, severe penetration losses, and lower diffraction. These losses result in mm-wave communication links that are near line of sight (LOS) with fewer non-LOS (NLOS) clusters and smaller coverage areas. Similarly, lower diffraction results in poorer coverage around corners. High attenuation also implies that mm-wave radars are useful only at short ranges and, as a result, multipath is a less-severe problem.

### High path loss and large arrays

Quite naturally, mm-wave signals suffer from higher path loss (PL) for fixed transmitter (Tx) and receiver (Rx) gains. According to the Friis transmission formula, compensating for these losses while keeping the same effective antenna aperture (or increasing the gain) imposes constraints on the transceiver hardware. Because the received power is contingent on the beams of the Tx and Rx being oriented toward each other, the same aperture is accomplished by using steerable antenna arrays whose elements are spaced by at most half the wavelength ( $\lambda/2$ ) of the transmitted signal to prevent undesirable grating lobes. This interelement spacing varies between 0.5 and 5 mm for mm-wave carriers. Such narrow spacings impact the choice of RF and intermediate frequency (IF) elements because they should fit in a limited amount of space, which makes precise mounting difficult to accomplish, e.g., in vehicular platforms.

### Wide bandwidths

The unlicensed, wide mm-wave bandwidth enables higher data rates for communications as well as range resolution in radar. In automotive radar, this ensures the detection of distinct, informative micromotions of targets such as pedestrians and cyclists [13]. Mm-wave Rx sampling at the Nyquist rate requires expensive, high-rate analog-to-digital converters (ADCs). Large bandwidths also imply that using low-complexity algorithms in Tx and Rx processing is critical [7]. Furthermore, mm-wave channels are sparse in both time and angular dimensions—a property that is exploited for its low-complexity, low-rate reconstruction by using techniques such as compressed sensing [11], [14]. It is crucial to consider whether relevant narrow-band assumptions hold in an mm-wave application; otherwise, the signal bandwidth is very broad with respect to the center frequency, and the steering vectors become frequency dependent.

### Power consumption

The power consumption of an ADC increases linearly with the sampling frequency. At baseband, each full-resolution ADC consumes 15–795 mW at 36-MHz–1.8-GHz bandwidths. In addition, the power consumed by other RF elements such as power amplifiers and data interface circuits, in conjunction with the narrow spacing between antenna elements, renders it infeasible to utilize a separate RF–IF chain for each element. Thus, a feasible multiantenna Tx/Rx structure and its beamformers should

be analog or hybrid (wherein the potential array gain is exploited without using a dedicated RF chain per antenna and phase shifter) [15] because fully digital beamforming is infeasible.

### Short coherence times

Mm-wave environments such as indoor and vehicular communications are highly variable with typical channel-coherence times in the range of nanoseconds [5]. The reliability and coverage of dynamic mm-wave vehicular links are severely affected by the use of narrow beams. The intermittent blockage necessitates frequent beam realignment to maintain high data rates. Additionally, mm-wave radar requires a wide Doppler range to detect fast vehicles and slow pedestrians [13]. Short coherence times impact the use of feedback and waveform adaptation in many JRC designs, where the channel knowledge may be invalid or outdated when transmit waveform optimization occurs.

### Communications channel

Consider a Tx that employs an antenna array or a single directional antenna with carrier frequency  $f$  and Tx/Rx antenna gain  $G_{Tx}$  ( $G_{Rx}$ ). The LOS communications channel with a delay spread comprising  $L_c - 1$  delay taps is  $h_c(t, f) = G_c \sum_{l=0}^{L_c-1} \alpha_l e^{-j2\pi\tau_l f} e^{j2\pi\nu_l t}$ , where  $G_c$  is the large-scale communications channel gain at the reception, and  $\alpha_l$  is the PL coefficient of the  $l$ th path with time delay  $\tau_l$  and Doppler shift  $\nu_l$ . The free-space attenuation model yields  $G_c = (G_{Tx} G_{Rx} \lambda^2) / ((4\pi)^2 \rho_c^\gamma)$ , where  $\gamma$  is the PL exponent. Furthermore,  $\gamma \approx 2$  for mm-wave LOS in outdoor urban [5] and rural scenarios [16].

### Radar channel

The doubly selective (i.e., time- and frequency-selective) mm-wave radar channel is modeled after Tx/Rx beamforming using virtual representations obtained by uniform sampling in range dimensions [17]. Assume  $L$  uniformly sampled range bins and that the  $\ell$ th range bin consists of a few  $K_\ell$  virtual scattering centers. Each  $\ell$ ,  $k$ th virtual scattering center is characterized by its distance  $\rho_\ell$ , delay  $\tau_\ell$ , velocity  $v_{\ell,k}$ , Doppler shift  $\nu_{\ell,k} = 2v_{\ell,k}/\lambda$ , large-scale channel gain  $G_{\ell,k}$ , and small-scale fading gain  $\beta_{\ell,k}$ . Then, the multitarget radar channel model is  $h_r(t, f) = \sum_{\ell=0}^{L-1} \sum_{k=0}^{K_\ell-1} G_{\ell,k} \beta_{\ell,k} e^{-j2\pi\tau_\ell f} e^{-j2\pi\nu_{\ell,k} t}$ . The large-scale channel gain corresponding to the  $\ell$ ,  $k$ th virtual target scattering center is  $G_{\ell,k} = ((\lambda^2 \sigma_{\ell,k}) / (64\pi^3 \rho_\ell^4))$ , where  $\sigma_{\ell,k}$  is the corresponding scatterer's radar cross section (RCS). The small-scale gain is assumed to be the superposition of a complex Gaussian component and a fixed LOS component leading to Rician fading. Similarly, the corresponding frequency-selective models can also include Rician fading. They capture, as a special case, the spiky model used in prior works on mm-wave communications/radar. In this case, the corresponding radar target models are approximated by the Swerling III/IV scatterers [18].

Furthermore, clustered channel models can be used to incorporate correlations and extended target scenarios, although they remain unexamined in detail. For instance, the conventional mm-

wave automotive target model assumes a single, nonfluctuating (i.e., a constant RCS) scatterer based on the Swerling 0 model. This greatly simplifies the development and analysis of receive processing algorithms and tracking filters [7]. However, when the target is located within the close range of a high-resolution radar, the received signal is composed of multiple reflections from different parts of the same object. This extended target model is more appropriate for mm-wave applications and may also include a correlated RCS [13].

It is typical to assume a frequency-selective Rayleigh fading model for both communications and radar channels during the dwell time comprising  $N_{CPI}$  coherent processing intervals (CPIs). In radar terminology, this corresponds to the Swerling I/II target models. In each CPI with  $M$  frames, the channel amplitude of each tap is considered to be constant, i.e., a block fading model is assumed. Moreover, constant velocity and quasi-stationarity conditions are imposed on the target model.

### Channel-sharing topologies

Existing mm-wave JRC systems could be classified by the joint use of the channel [1], [23] (Figure 1). In the spectral coexistence approach, radar and communications operate as separate entities and focus on devising strategies that adjust transmit parameters and mitigate the interference adaptively for the other [3]. To this end, some amount of information exchange between the two systems, i.e., spectral cooperation, may only be allowed with minimal changes to the standardization, system hardware, and processing. In spectral co-design [1], [7], new, joint RF sensing and communications techniques are developed where a single unit is employed for both purposes while also accessing the spectrum in an opportunistic manner. New, fully adaptive, software-defined systems are attempting to integrate these systems into the same platform to minimize circuitry and maximize flexibility. Here, each Tx and Rx may have multiple antennas in a phased-array or MIMO configuration.

### JRC at mm-wave: Coexistence

Interference management is central to the spectral coexistence of different radio systems. This typically requires sensing the state of the shared spectrum and adjusting Tx and Rx parameters so that the impact of interference is sufficiently reduced and individual system performance is enhanced. In the next section, we present figures of the merit-qualifying system performance and then discuss methodologies for mm-wave coexistence.

### Communications performance criteria

Because the goal of communications systems is the error-free transfer of data at a high rate for a given bandwidth, commonly used performance criteria include quality-of-service (QoS) indicators such as spectral efficiency, mutual information (MI), channel capacity, pairwise error probability, bit/symbol error rates (BERs/SERs), and signal-to-interference-and-noise ratio (SINR). Given a communications signal model, the achievable spectral efficiency can be

used as a universal communications performance criterion. In practice, the achievable spectral efficiency  $r$  is an upper bound, while the effective spectral efficiency  $r_{\text{eff}}$  depends on the implemented Rx [e.g., minimum mean-square error (MMSE)] [24], decision feedback [25], or time-domain equalizer [26]) and is a fraction of the achievable spectral efficiency. The effective communications rate is then the product of the signal bandwidth  $W$  and  $r_{\text{eff}}$ .

### Radar performance criteria

By virtue of their use in both detection and estimation, radar systems lend themselves to a plethora of performance criteria depending on the particular task. Target-detection performance is characterized by probabilities of correct detection, misdetection, and false alarm. In parameter-estimation tasks, MSE, or variance in comparison to the Cramér–Rao lower bound (CRLB), is commonly considered. The CRLB defines the lower bound for estimation error variance for unbiased estimators. There are also several radar design parameters such as

range/Doppler/angular resolution/coverage as well as the number of targets a radar can simultaneously resolve. In particular, the radar's ability to discriminate in both range and velocity is completely characterized by the ambiguity function (AF) of its transmit waveform; it is obtained by correlating the waveform with its Doppler-shifted and delayed replicas.

### Interference mitigation

The mm-wave radar and communications Tx and Rx can use all of their degrees of freedom (DoF), e.g., different antennas, frequency, coding, transmission slots, power, or polarization to mitigate or avoid mutual interference. Interference may also be caused by the leakage of signals from adjacent channels as a result of reusing identical frequencies in different locations. In general, the higher the frequency in mm-wave bands, the weaker the multipath effects. The Txs can adjust their parameters so that the level of interference is reduced at the Rx. To this end, awareness about the dynamic state of the radio spectrum and interference experienced in different locations, subbands, and

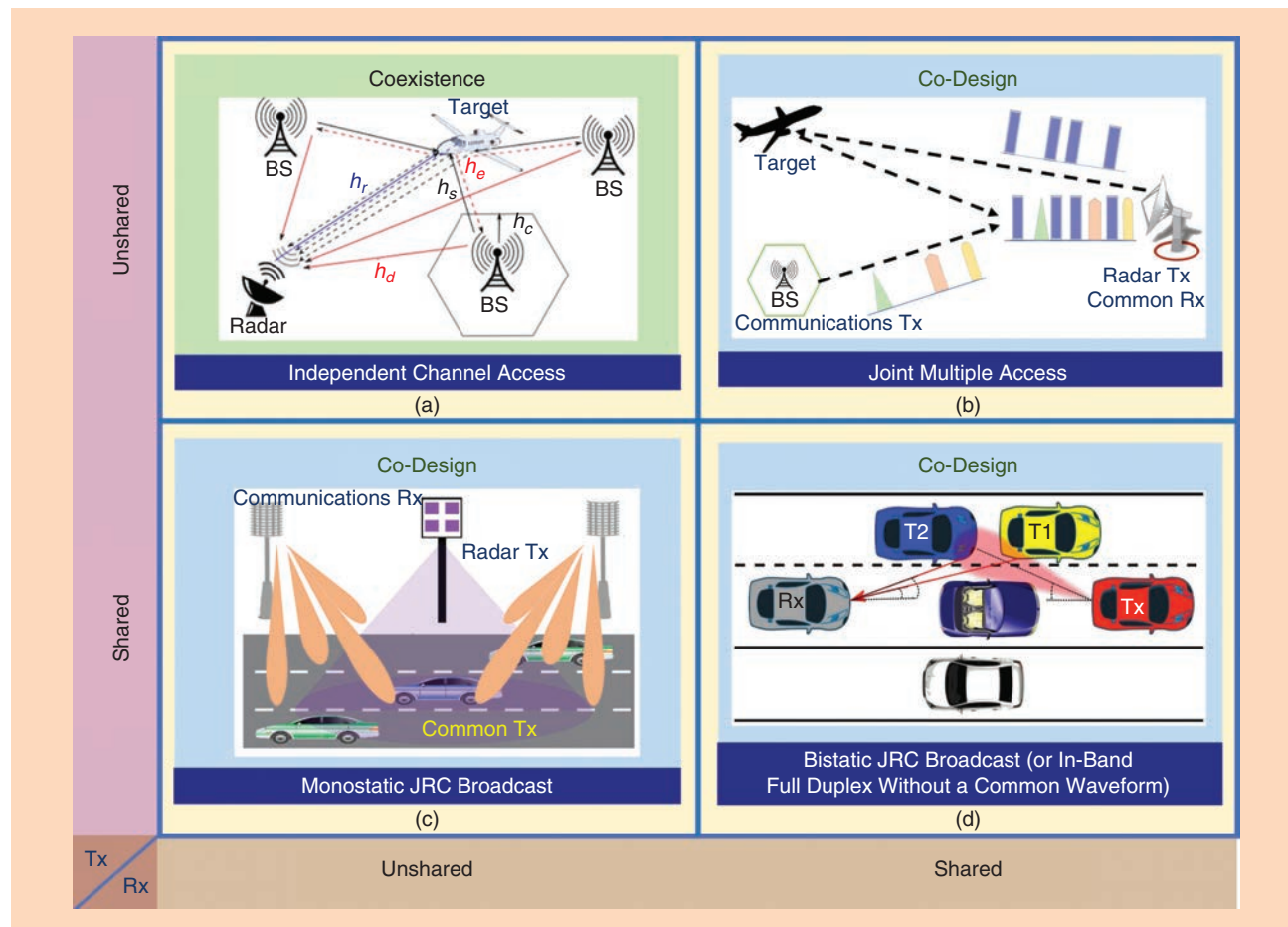


**FIGURE 1.** (a) The spectral coexistence system where radar and communications subsystems are independently located and access the associated radio channels such as radar target channel  $h_r$ , communications channel  $h_c$ , radar-to-communications interference  $h_s$ , and communications-to-radar interference  $h_d$  [19]. (b) The co-design system where only Rx are shared. In this joint multiple-access channel, the radar operates in monostatic mode, and both systems transmit different waveforms that are orthogonal in spectrum, code, or time [20]. (c) In a Tx-shared co-design, the monostatic radar functions as a communications Tx, emitting a common JRC waveform [21]. (d) A bistatic broadcast co-design with a common Tx, Rx, and joint waveform [7]. The joint waveform transmitted by the Tx vehicle bounces off targets (e.g., T1 and T2) and is received by the Rx vehicle. A variant is the in-band, full-duplex system with different waveforms but common Txs and Rxs [22]. BS: base station.

time instances is desired. This may be in the form of feedback provided by the Rx to the Tx about the channel response and SINR. Both the Tx and Rx can be optimized such that the SINR is maximized at the Rx for both subsystems.

### Rx techniques

Interference mitigation may be performed only at the Rx that renders the channel state information (CSI) exchange optional. Typically, this requires multiple antennas at the Rx, a common feature at the mm-wave, and processing of the received signals in the spatial and/or temporal domains. These techniques employ the receive-array covariance matrix  $\Sigma$  (or its estimate  $\hat{\Sigma}$ ) in certain interference-canceling Rx structures. Here, the received signal space spanned by eigenvectors of  $\Sigma$  is divided into two orthogonal subspaces of signal and interference plus noise. The received signal is then projected onto a subspace orthogonal to the interference-and-noise subspace to enable processing of practically interference-free signals. If the interference impinges the Rx from angles different than that of the desired signal, Rx beamforming is commonly used [23]. The beampattern design ensures high gains toward the desired signals and steers nulls toward the interference. Common solutions include minimum-variance distortion-less response, linearly constrained minimum variance, and diagonal loading [27].

Advanced interference cancellation Rx estimate CSI, use feedback about channel response, or sense other properties of the state of the radio spectrum. These estimates are later used to cancel interference contribution from the overall received signal. The coherence time of the channels should be sufficiently long enough so that the feedback or channel estimates are not outdated during the interference cancellation process. These techniques either require knowledge of modulation schemes employed by coexisting radio systems or are applied to digital modulation methods only. A prime example of this is the successive interference cancellation method, which decodes and subtracts the strongest signal first from the overall received signals and then repeats the same procedure by extracting the next-weakest signal from the residual signal and so on [1]. In the absence of CSI, nontraditional radar interference models are used for robust communications signal decoders [28].

### Tx techniques

Adapting Txs and optimizing transmit waveforms may be used to minimize the impact of interferences in coexistence systems. In a radar communications coexistence scenario, e.g., the optimization objective could be maximizing the SINR at each Rx while providing the desired data rate for each communications user and target Neyman–Pearson detector performance for radar users. Designing a precoder for each Tx and/or decoders for each Rx achieves this goal by steering the interferences to different spaces than the desired signals.

One such example design in the context of MIMO communications and MIMO radar is the switched small singular-value space projection method [29] in which the

interference is steered to space spanned by singular vectors corresponding to zero or negligible singular values. This method requires information exchange between the radar subsystem and communications base stations. Another example of a precoder/decoder design for interference management in radar communications coexistence is via interference alignment (IA) [30] where IA coordinates coexisting multiple Txs such that their mutual interference aligns at the Rx and occupies only a portion of the signal space. The interference-free signal space is then used for radar and communications purposes.

### JRC at mm-wave: Co-Design

Central to facilitating the co-design of radar and communications systems are waveform design and their optimization exploiting available DoF (e.g., spatial, temporal, and spectral polarization). The optimization is based on the system performance criteria and availability of CSI, awareness about the target scene, and the levels of unintentional or intentional interference at the Rx.

### JRC performance criteria

In co-design, JRC waveforms are modeled to simultaneously improve the functionalities of both subsystems with a quantifiable tradeoff. In [31], a radar round-trip delay-estimation rate is developed and coupled with the communications information rate. This radar estimation, however, is not drawn from the same class of distributions as that of communications data symbols; therefore, it provides only an approximate representation of the radar performance. However, the potential invalidity of some assumptions limits the extension of this to the estimation of other target parameters.

The mm-wave designs for single- and multiple-target scenarios in [32] and [33] suggest an interesting JRC performance criterion, which attempts to parallel the radar CRLB performance with a new, effective communications symbol MMSE criteria as a function of effective maximum-achievable communications spectral efficiency,  $r_{\text{eff}}$ . The MMSE communications criteria presented in this section is analogous to the MSE distortion in the rate distortion theory. Let  $\text{MMSE}_c$  be the MMSE of a communications system with spectral efficiency  $r$ . Then,  $\text{MMSE}_c$  and  $r$  are related to each other through the equation  $(1/N)\text{Tr}[\log_2 \text{MMSE}_c] = -r$ , where  $N$  is the code length. Therefore, the effective communications distortion MSE (DMSE) that satisfies  $(1/N)\text{Tr}[\log_2 \text{DMSE}_{\text{eff}}] = -r_{\text{eff}} = -\delta \cdot r$  can be defined as  $\text{DMSE}_{\text{eff}} \triangleq \text{MMSE}_c^\delta$ , where  $\delta$  is a constant fraction of communications symbols transmitted in a CPI with the channel capacity  $C$ . The performance tradeoff between communications and radar is quantified in terms of a weighted combination of the scalar quantities  $(1/N)\text{Tr}[\log_2 \text{DMSE}_{\text{eff}}]$  and  $(1/Q)\text{Tr}[\log_2 \text{CRLB}]$ , respectively, where the log scale is used to achieve proportional fairness between the communications distortion and radar CRLB values, and  $Q$  is the number of detected targets. Pareto-optimal solutions that assign weights to different design goals have also been explored [34].

MI is also a popular waveform-optimization criterion. At the radar Rx, depending on whether the communications signal reflected off the target is treated as useful energy or interference or is ignored altogether, a different MI-based criterion results. Although MI maximization enhances the characterizing capacity of a radar system, it does not maximize the probability of detection. The optimal radar signals for target characterization and detection tasks are generally different [3], [19].

### Radar-centric waveform design

In this section, we first consider the appropriate radar-centric waveforms. These range from conventional signals to emerging multicarrier waveforms.

Conventional continuous-wave and modulated waveforms A simple continuous-wave (CW) radar provides information about only Doppler velocity. To extract range information, either the frequency/phase of the CW signal is modulated or very short-duration pulses are transmitted. In practice, the well-known frequency-modulated CW (FMCW) and phase-modulated CW (PMCW) radars are used. A typical FMCW radar transmits one or multiple chirp signals wherein the frequency increases or decreases linearly in time, and the chirps reflected off the targets are captured at the Rx. A chirp bandwidth of a few gigahertz may be used to provide a range resolution of a few centimeters, e.g., a 4-GHz chirp achieves a range resolution of 3.75 cm. For PMCW radar, binary pseudorandom sequences with desirable autocorrelation/cross-correlation properties are typically used. The PMCW signal is easier to implement in hardware, and its AF has lower sidelobes than that of FMCW [7].

A general, bistatic uniform linear array (ULA) PMCW-JRC system [7] follows the topology shown in Figure 1(d). The Tx sends  $M$  repetitions of the PMCW code of length  $L$  from each of its  $N_t$  transmit antennas. The Doppler shift and flight time for the paths are assumed to be fixed over the CPI. The reflections from  $Q$  targets that impinge on  $N_r$  receive antennas. Let  $t_c$  represent chip time (the time needed for transmitting one element of one PMCW code sequence, i.e., fast time). The Doppler shifts and flight time for every path are assumed to be fixed over a coherent transmission time  $Mt_b$ , where  $t_b = Lt_c$  is the time taken to transmit one block of code, i.e., slow time. The transmit waveform takes the form

$$x_i(t) = \sum_{m=0}^{M-1} \sum_{l=0}^{L-1} a_m e^{j\zeta_l} s(t - lt_c - mt_b) e^{j2\pi f_c t} e^{j(i-1)kds\sin\beta}, \quad (1)$$

where  $i \in [1, N_t]$  and  $a_m = e^{j\phi_m}$  denote differential phase-shift keying (DPSK) symbols over slow time (time for sending one code sequence). The DPSK modulation is robust to constant phase shifts. Furthermore,  $s(t)$  is the elementary baseband pulse shape,  $\zeta_l \in \{0, \pi\}$  is the binary phase code,  $e^{j(n-1)kds\beta}$  is the beamsteering weight for the  $n$ th antenna,  $k = 2\pi/\lambda$  is

wavenumber, and  $\beta$  is the angle between the radiating beam perpendicular to the ULA (for simplicity, we consider only azimuth and ignore common elevation angles). The Tx steers the beam in multiple transmissions from  $[-\pi/2, \pi/2]$ , each time with angle  $\beta$ . As shown in Figure 2, the communications and radar waveform for PMCW-JRC are combined in analog hardware.

Let  $\Delta V_q^{(1)}$  be the radial-relative velocity between the Tx and  $q$ th path, where the superscript in  $(\cdot)^{(1)}$  in the formula at the beginning of this paragraph refers to the Tx-target path, and the corresponding Doppler shift is  $f_{D_q}^{(1)} = (\Delta V_q^{(1)} / c) f_c$ , where  $c = 3 \times 10^8$  m/s is the speed of light. The signal that impinges on the  $q$ th scatterer is

$$z_{q,n}(t) = \sum_{m=0}^{M-1} \sum_{l=0}^{L-1} h_{q,n}^{(1)} a_m e^{j\zeta_l} s(t - lt_c - mt_b - \tau_q^{(1)}) e^{j2\pi f_c t - j2\pi f_{D_q}^{(1)} t - j2\pi f_c \tau_q^{(1)}}, \quad (2)$$

where  $\tau_q^{(1)}$  and  $h_{q,n}^{(1)}$  are  $q$ th point scatterer time delay and propagation loss for each path, respectively. We exploit the standard narrow-band assumption to express the received signal as a phase-Doppler-shifted version of the transmit signal. Assume  $\tau_q = \tau_q^{(1)} + \tau_q^{(2)}$  to be the total flight time corresponding to a bistatic range  $R_q = ct_q$ , where the superscript in  $(\cdot)^{(2)}$  in the formula presented earlier in this paragraph denotes variable dependency on the target-Rx path. Assume  $f_{D_q} = f_{D_q}^{(1)} + f_{D_q}^{(2)}$  to be the bistatic Doppler shift and  $\psi_q$  to be the angle between the  $q$ th scatterer and perpendicular line to receive the ULA. After Tx/Rx beamforming and frequency synchronization, the received signal at antenna  $p$ , obtained as a superposition of these reflections, takes the form shown in (3)

$$\begin{aligned} \tilde{y}_p(t) &= \sum_{q=1}^Q \sum_{n=1}^{N_t} h_{q,p}^{(2)} z_{q,n}(t - \tau_q^{(2)}) e^{j2\pi f_{D_q}^{(2)} t} + \tilde{N}_p(t) \\ &= \sum_{q=1}^Q \sum_{n=1}^{N_t} \sum_{m=1}^M \sum_{l=0}^{L-1} h_{q,p}^{(2)} h_{q,n}^{(1)} a_m e^{j\zeta_l} \\ &\quad \times s(t - lt_c - mt_b - \tau_q^{(1)} - \tau_q^{(2)}) e^{j2\pi(f_c - f_{D_q}^{(1)} - f_{D_q}^{(2)})t} \\ &\quad \times e^{j\eta_q} e^{-jkds\sin(\psi_q)(p-1)} + \tilde{N}_p(t). \end{aligned} \quad (3)$$

In (3),  $e^{j\eta_q} = e^{-j2\pi(f_c(\tau_q^{(1)} + \tau_q^{(2)}) + f_{D_q}^{(1)}\tau_q^{(2)})}$  is a static phase shift,  $h_{q,p}^{(2)}$  accumulates the effect of the  $q$ th Tx-target-Rx point scatterer as well as the PL and RCS of the target, and  $\tilde{N}_p(t)$  is complex circularly symmetric white Gaussian noise with variance  $\sigma^2$ . An extended target is modeled as a cluster of points. This, combined with the superposition of reflections from the independent scatterer, renders the model in (3) applicable for extended targets. After downconversion to baseband and ignoring RCS dependency on Tx and Rx antennas, i.e.,  $\sum_{n=1}^{N_t} h_{q,n}^{(1)} h_{q,p}^{(2)} e^{j\eta_q} = \sum_{n=1}^{N_t} d_{q,p,n} = N_t d_q = d_q$ , the received signal is

$$\begin{aligned} y_p(t) &= \sum_{q=1}^Q \sum_{m=1}^M \sum_{l=0}^{L-1} d_q a_m e^{-j2\pi f_{D_q} t} c_q^{p-1} e^{j\zeta_l} s(t - lt_c - mt_b - \tau_q) \\ &\quad + N_p(t), p \in [1, N_r], \end{aligned} \quad (4)$$

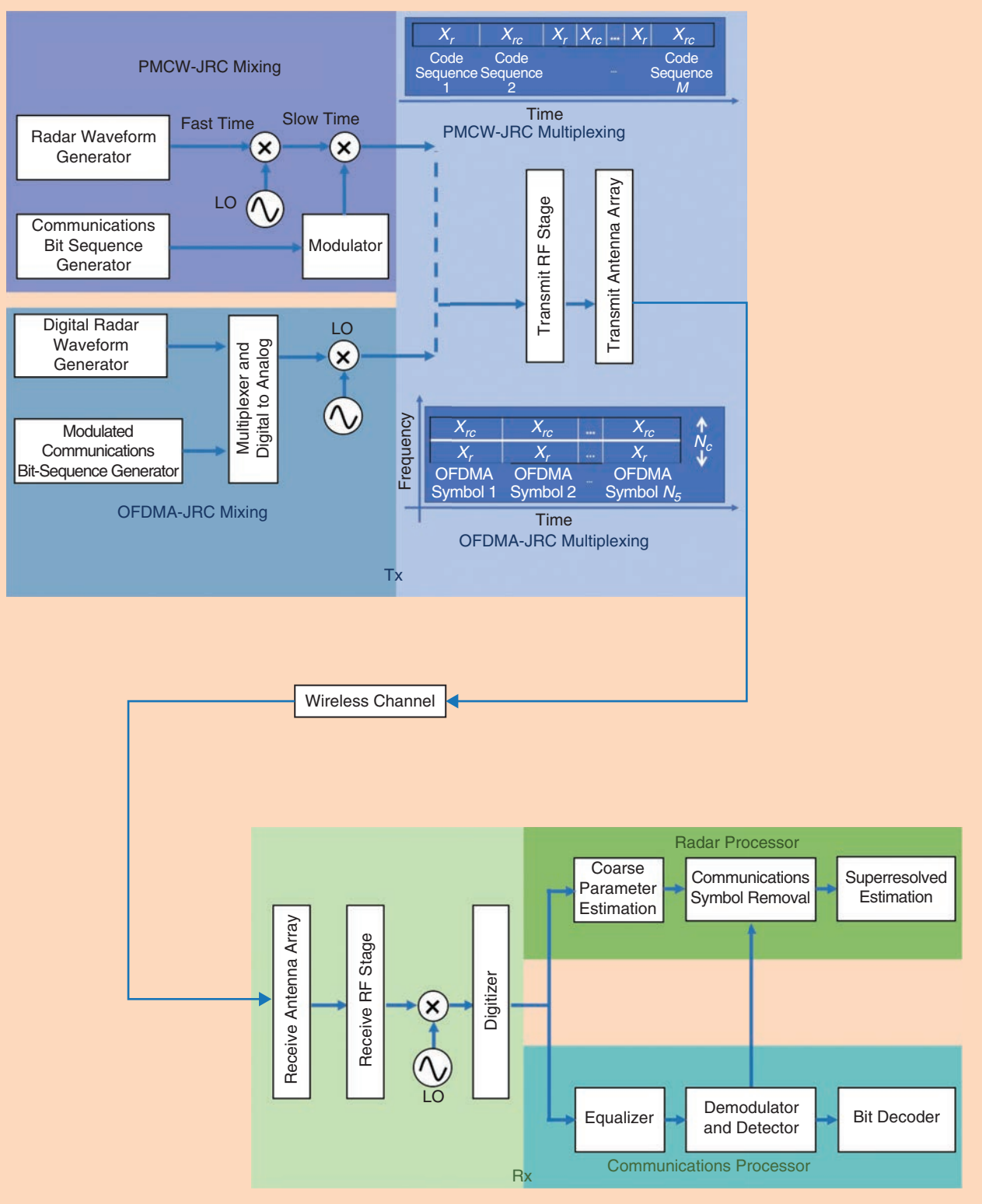


**FIGURE 2.** A simplified block diagram that shows the major steps of transmit and receive processing for a general mm-wave JRC system. In case of PMCW-JRC, the radar and communications waveforms are combined in the analog hardware before the RF stage. On the other hand, the information bits from these two subsystems are mixed digitally in OFDMA-JRC. The multiplexing of radar-only and radar-communications frames for both PMCW- and OFDMA-JRC are depicted in the transmit portion. The receive processing for both systems is largely similar. OFDMA: orthogonal frequency-division multiplexing access; LO: local oscillator.

where  $c_q = e^{-jkd\sin(\psi_q)}$ . Collecting the Nyquist time samples for antenna  $p$  and rearranging them accordingly to slow/fast time, we form the matrix

$$\begin{aligned} \mathbf{Y}_p^{\text{PMCW-JRC}} &= \sum_{q=1}^Q c_q^{p-1} d_q \text{Diag}\{\mathbf{a}\} [(\mathbf{b}_q^T \odot s^T \mathbf{P}_{k_q}) \otimes e_q] + N_p \\ &\in \mathbb{C}^{M \times L}, \end{aligned} \quad (5)$$

where vectors  $\mathbf{e}_q = [e^{j2\pi f_{D_q} m L t_c}]_{m=1}^M$  and  $\mathbf{b}_q = [e^{j2\pi f_{D_q} l t_c}]_{l=1}^L$  collect Doppler samples in slow and fast time, respectively,  $s = [e^{j\zeta_l}]_{l=0}^L$  contains  $L$  chips of code sequence, and  $\mathbf{P}_{k_q}$  is a cyclic permutation matrix for a shift of  $k_q$

$$\mathbf{P}_{k_q} = \begin{bmatrix} \mathbf{0}_{K_q \times L-K_q} & \mathbf{I}_{K_q \times K_q} \\ \mathbf{I}_{L-K_q \times L-K_q} & \mathbf{0}_{L-K_q \times K_q} \end{bmatrix} \in \mathbb{C}^{L \times L}, \quad (6)$$

where  $k_q \in \{0, \dots, L-1\}$  is determined by the range of the  $q$ th scatterer. If there is no delay between the Tx and Rx for all of the paths, then  $k_q = 0$  for all  $q$  and  $\mathbf{P}_{k_q}$  becomes identity matrix.

In a PMCW-JRC system, the communications symbols and Doppler parameters are coupled, thus leading to a nonidentifiable model. This is resolved by a multiplexing strategy through which unknown parameters in the received signal are uniquely identified. The PMCW-JRC system adopts time-division multiplexing between radar-only ( $X_r$ ) and JRC ( $X_{rc}$ ) frames, which are transmitted for  $\mu$  and  $(1-\mu)\%$  of the CPI, respectively. The value of  $\mu$  depends on the amount of prior knowledge about the target scene. For instance, when the scene is stationary, such as driving a straight path on a highway, we may not need full sensing capacity and may scale up the allocated time appropriately for communications. A coarse estimate of radar target parameters (e.g., range, angle, and Doppler) is obtained from  $\mathbf{Y}_p^{\text{PMCW-JRC}}$  of radar-only frames  $X_r$ , while communications symbols are extracted from the received signal samples of the  $X_{rc}$  frame. After extracting communications symbols from  $X_{rc}$ , the residual signal is exploited to further improve the radar target estimates using low-complexity JRC superresolution algorithms [7].

### Multicarrier waveforms

Multicarrier waveform radars provide additional DoF to deal with dense spectral use and demanding mm-wave target scenarios such as drones, low-observable objects, and many moving vehicles in automotive scenarios. Different DoF can be used in an agile manner to achieve optimal performance depending on the radar task, nature of the targets, and state of the radio spectrum. A general drawback of multicarrier radar waveforms is their time-varying envelope, leading to an increased peak-to-average-power ratio (PAPR) or peak-to-mean-envelope-power ratio, which makes it difficult to use the amplifiers efficiently when high-transmit powers are needed. However, in mm-wave radars, the transmit powers tend to be small, and surveillance ranges are short. The PAPR reduction is achieved by not allocating all of the subcarriers or by using an appropriate coding/

waveform design. Hence, the PAPR issue in mm-wave may be less severe.

Multicarrier complementary phase-coded (MCPC) waveforms [35], wherein each subcarrier is modulated by a pseudorandom code sequence of a specific length, is also a viable mm-wave JRC candidate. The MCPC design exploits DoF in spectral and code domain. In a sense, it is related to orthogonal frequency-division multiplexing (OFDM) because after each subcarrier is modulated by a code in the time domain, the subcarriers remain orthogonal without intercarrier interference. If the subcarriers are uncoded, the waveform is exactly OFDM. The intercarrier spacing in MCPC must accommodate spreading the signals in frequency due to phase codes such as Barker, P3, or P4 polyphase codes [18]. This is achieved by choosing the intercarrier spacing to be the inverse of chip duration. In OFDM, intercarrier spacing is smaller. A generalized multicarrier radar (GMR) waveform devised in [36] and [37] subsumes most of the widely used radar waveforms, such as pseudorandom frequency hopping, MCPC, OFDM, and linear-step approximations of linear FM signals (as special cases). A matrix model of TxS and RxS is developed for GMR and allows for the defining of waveforms and codes, spreading in the time and frequency domains, power allocations, and active subcarriers using a compact notation. Different waveforms are obtained by choosing the dimensions of the matrix model and filling the entries appropriately. This approach allows for relaxing the perfect orthogonality requirement, which may lead to a better resolution of target delays and Doppler velocities at the mm-wave.

### Spatial DoF and multiple waveforms

A few different solutions use the same waveform for both subsystems but make use of radar's spatial DoF for communications symbols. For instance, in [38], the radar array beampattern sidelobes are modulated by communications messages along the user directions. In [39], the communications symbols are represented by a different pairing of antennas and waveforms in an MIMO configuration. Spatial DoF are also useful for adaptively canceling specific users. A joint beamforming method is suggested in [40] for dual-function radar communications, which comprise MIMO radar and communications systems, assuming full-duplex transmission. The downlink communications signal is embedded into the transmit radar waveform, and uplink communications takes place when the radar is in listening mode. This necessitates accurate synchronization among the subsystems. The technique utilizes spatial diversity by enforcing the spatial signature of the uplink signals to be orthogonal to the spatial steering vectors associated with the radar target returns. The Rx beamformer employs adaptive and nonadaptive strategies to separate the desired communications signal from echoes of targets, clutter, and noise even if they impinge the array from the same direction. Other solution paths consist of finding spatial filters that mitigate in-band MIMO communications interference through optimization of the sidelobe and cross-correlation levels in

MIMO radar systems [41], [42], by exploiting coarray processing with multiple waveforms [43] and designing precoders/decoders through IA [44].

However, for mm-wave JRC systems, full-resolution ADCs at the baseband signal result in an unacceptably high power consumption. This makes it infeasible to utilize an RF chain for each antenna element, implying that the prevailing MIMO systems that employ fully digital beamforming are not practical for mm-wave systems. Thus, the benefits of using multiple waveforms for spatial mitigation in mm-wave JRC systems are yet to be carefully evaluated. Currently, a single data stream model that supports analog beamforming with frequency-flat Tx/Rx beamsteering vectors is more common [17]. The use of large antenna arrays in mm-wave suggests that one feasible JRC approach may be to simply partition the arrays for radar and communications functionalities [14].

### Communications-centric waveform design

The most popular communications signal for mm-wave JRC is OFDM because it provides a stable performance in multipath fading and relatively simple synchronization [22]. Also, frequency division in duplexing has an added advantage; unlike time-division duplexing, the former employs different bands for uplink and downlink so that the impact on the interference in radar systems is less severe. Some solutions [7], [22] also employ the related OFDM access (OFDMA) waveform for a JRC system. Although OFDM users are allocated only on time domain, OFDMA users can be differentiated using time and frequency. The latter, therefore, provides DoF in both temporal and spectral domains. Although OFDM-JRC offers high dynamic range and efficient Rx processing implementation based on fast Fourier transform (FFT), it requires additional processing to suppress high sidelobes in Rx processing and to reduce the PAPR. Moreover, the OFDM cyclic prefix (CP) used to transform frequency-selective channels to multiple frequency-flat channels, leading to a simplified equalizer, may be a nuisance in the radar context. The CP may adversely affect the radar's ability to resolve ambiguities in radar ranging. Its length depends on the number of channels, particularly the maximum excess delay that the radar signal may experience (i.e., the time difference between the first- and last-received component of the signal). For radar applications, the CP duration should be equal to or longer than the total maximum signal travel time between the radar platform and target. Other communications waveforms proposed for mm-wave automotive JRC include spread spectrum, noise OFDM, and multiple encoded waveforms [7].

### OFDMA-JRC

Consider the same bistatic scenario in Figure 1(d) that was previously analyzed for the PMCW-JRC system. The OFDMA-JRC Tx (Figure 2) sends  $N_s$  OFDM symbols from  $N_t$  transmit antennas and reflections from  $Q$  targets impinge on  $N_r$  receive antennas. Assume that  $\beta$  is the angle of depar-

ture. The Doppler shift and flight time for the paths are assumed to be fixed over a CPI, i.e.,  $N_s T_{\text{sym}}$ , where  $T_{\text{sym}}$  is the duration of one OFDM symbol, and  $a_{n,m}$  are multiplexed communications/radar DPSK on the  $n$ th carrier of the  $m$ th OFDM symbol. Let  $N_c$  be the number of subcarriers and  $\Delta f$  be the subcarriers spacing, then the joint transmit waveform in baseband neglecting the CP is

$$x_i(t) = \sum_{m=0}^{N_s-1} \sum_{n=0}^{N_c-1} a_{n,m} e^{j2\pi f_n t} e^{jk \sin(\beta)(i-1)\frac{\lambda}{2}} s(t - mT_{\text{sym}}), \quad (7)$$

where  $s(t)$  is a rectangular pulse of the width  $T_{\text{sym}}$ ,  $i \in [1, N_t]$ ,  $n$  and  $m$  are frequency and time indices, respectively, and  $f_n = n\Delta f = n/T_{\text{sym}}$  [7]. The received signal at the  $p$ th Rx over a CPI is seen in (8)

$$\tilde{y}_p(t) = \sum_{m=0}^{N_s-1} \sum_{q=1}^Q \sum_{n=0}^{N_c-1} \sum_{i=1}^{N_t} d_{q,i,p} a_{n,m} e^{j2\pi f_n(t-\tau_q)} e^{j2\pi f_{D,q} t} e^{jk \sin(\psi_q)(p-1)\frac{\lambda}{2}} s(t - mT_{\text{sym}} - \tau_q) + \tilde{N}_p(t). \quad (8)$$

In (8),  $\tilde{N}_p(t)$  is the additive noise on antenna  $p$ . Similar to PMCW-JRC,  $d_{q,i,p}$  denotes the PL, the phase shift caused by carrier frequency, and the RCS of the target;  $d_{q,i,p}$  is independent of the subcarrier index due to a narrow-band assumption. Similarly, the Doppler is assumed to be identical for all of the subcarriers given a small intercarrier spacing. For notational convenience, we omit the noise in the following equation. We sample (8) at intervals  $t_s = 1/N_c \Delta f$  as

$$\tilde{y}_p[t_s] = \sum_{m=0}^{N_s-1} \sum_{q=1}^Q \sum_{n=0}^{N_c-1} d_q s_{n,m} e^{j2\pi \frac{nl}{N_c}} s(lt_s - mT_{\text{sym}} - \tau_q), \quad (9)$$

where,  $l \in [1, L]$ ,  $n \in [1, N_c]$ ,  $L \leq N_c$ ,  $d_q = \sum_{i=1}^{N_t} d_{q,i,p}$  as before, and  $\tilde{s}_{n,m} = a_{n,m} e^{-j2\pi n \Delta f (R_q/c)} e^{j2\pi m T_{\text{sym}} f_{D,q}} e^{j\pi \sin(\psi_q)(p-1)} \tilde{s}_{n,m}$  contains information about range, Doppler, angle of arrival, and communications. We assume that the number of inverse FFT (IFFT) points  $N_c$  is equal to the number of fast-time samples  $L$  in each OFDM symbol. The received signal samples can be viewed as a radar data cube in spatial, spectral, and temporal domains with  $N_t$  antennas,  $N_c$  subcarriers, and  $N_s$  OFDM symbols. Let us stack the entire DPSK symbols into a matrix  $\mathbf{A} \in \mathbb{C}^{N_c \times N_s}$  and let  $\mathbf{a}_m = [\mathbf{A}]_m$  be the communications symbols over all of the subcarriers at  $m$ th OFDM symbol time. For a given OFDM symbol, i.e.,  $m$ , collecting signals from all of the subcarriers across different antennas leads to the following slow-time slice of the data cube:

$$\mathbf{Y}_m^{\text{OFDMA-JRC}} = \mathbf{F}_{N_c} \text{Diag}(\mathbf{a}_m) \Xi \left( \frac{-\Delta f R_q}{c} \right) \text{Diag}(\mathbf{d}) \mathbf{C} \in \mathbb{C}^{N_c \times N_r}, \quad (10)$$

where  $m \in [1, N_s]$ ,  $\Xi((-\Delta f R_q)/c) = [e^{-j2\pi n \Delta f (R_q/c)}]_{n=1,q=1}^{N_c,Q} \in \mathbb{C}^{N_c \times Q}$ ,  $\mathbf{C} = [e^{jk \sin(\psi_q)(p-1)(\lambda/2)}]_{q=1,p=1}^{Q,N_r} \in \mathbb{C}^{Q \times N_r}$ , and  $\mathbf{d} = [d_1 \dots d_Q]$ . Additionally,  $\mathbf{F}_{N_c} = [e^{j2\pi (nl/N_c)}]_{l=0,n=0}^{N_c-1, N_c-1}$  denotes the  $N_c$ -point IFFT matrix. To estimate Doppler shifts, we consider a subcarrier slice of data cube (9)

$$\mathbf{Z}_n^{\text{OFDMA-JRC}} = \text{Diag}(\mathbf{a}_n)(f_{D_q} T_{\text{sym}}) \text{Diag}(\mathbf{d}) \mathbf{C} \in \mathbb{C}^{N_s \times N_r}, \quad (11)$$

where  $\mathbf{a}_n = [\mathbf{A}]_n \in \mathbb{C}^{N_s}$  are the DPSK symbols over slow time, i.e.,  $\Xi(f_{D_q} T_{\text{sym}}) = [e^{j2\pi m T_{\text{sym}} f_{D_q}}]_{m=1,q=1}^{N_s,Q}$ .

As in PMCW-JRC, the receive processing of OFDMA-JRC is affected by the coupling of communications symbols with a radar parameter (i.e., the range in case of OFDMA-JRC). To ensure that range estimation does not suffer from using all of the subcarriers, FDM is employed (2) such that  $\mu\%$  of the OFDMA subcarriers are allocated to radar (with known  $a_{n,m}$  on these subcarriers) and the rest to JRC. The rest of the OFDMA-JRC receive processing is similar to PMCW-JRC (Figure 2) [7].

### Comparison of PMCW- and OFDMA-JRC

Despite the fact that OFDMA encodes radar and communications simultaneously in the entire time and space, PMCW does so in the entire frequency and space; hence, their DoF and design spaces are in different domains. Although it turns out that the receive system models of both waveforms are mathematically identical after matched filtering and retrieve all of the JRC parameters using similar superresolution algorithms [7], [45], their individual performances mimic their respective communications and radar-centric properties. For example, the AF of the bistatic PMCW-JRC inherits the low sidelobes from its parent stand-alone PMCW radar waveform, as shown in a comparison with the AF of OFDMA-JRC in Figure 3, given the same bandwidth. On the other hand, PMCW-JRC is more sensitive to the number of users while the orthogonality of waveforms in OFDMA-JRC makes the latter robust to interchannel interference. Finally, in a networked vehicle scenario, it requires less-complex infrastructure and processing to apply PMCW with predefined or stored sequences rather than using OFDMA to adaptively

allocate bands to each user [7], [22]. A comparison of estimation errors in the coupled parameter—range for OFDMA-JRC and Doppler for PMCW-JRC—using JRC superresolution recovery [7] is shown in Figure 4 for  $\mu = 50\%$ .

### Joint coding

Recently, existing mm-wave communications protocols that are embedded with codes that exhibit favorable radar AFs are garnering much attention for JRC. In particular, the 60-GHz IEEE 802.11ad standard wireless protocol has been employed with time-division multiplexing of radar-only and radar-communications frames. In general, these designs have temporal DoF (for a monostatic radar case). The IEEE 802.11ad single-carrier physical layer (SCPHY) frame consists of a short training field (STF), a channel-estimation field (CEF), a header, and a data and beamforming training field. The STF and CEF form the SCPHY preamble. The CEF contains two 512-point sequences, i.e.,  $G_{512}[n]$  and  $G_{v512}[n]$ , each containing a Golay complementary pair with a length of 256,  $\{G_{au256}, G_{bu256}\}$  and  $\{G_{av256}, G_{bv256}\}$ , respectively. A Golay pair has two sequences, i.e.,  $G_a$  and  $G_b$ , each of the same length  $N$  with entries  $\pm 1$ , such that the sum of their aperiodic autocorrelation functions has a peak of  $2N$  and zero sidelobes:

$$G_a[n] * G_a[-n] + G_b[n] * G_b[-n] = 2N\delta[n], \quad (12)$$

where  $*$  denotes linear convolution. This property is useful for channel estimation and target detection.

By exploiting the preamble of a single SCPHY frame for radar, the existing mm-wave 802.11ad waveform simultaneously achieves a cm-level range resolution and a gigabyte/s data rate [17]. The limited-velocity-estimation performance of this waveform can be improved by using multiple fixed-length frames in which preambles are reserved for radar [17].

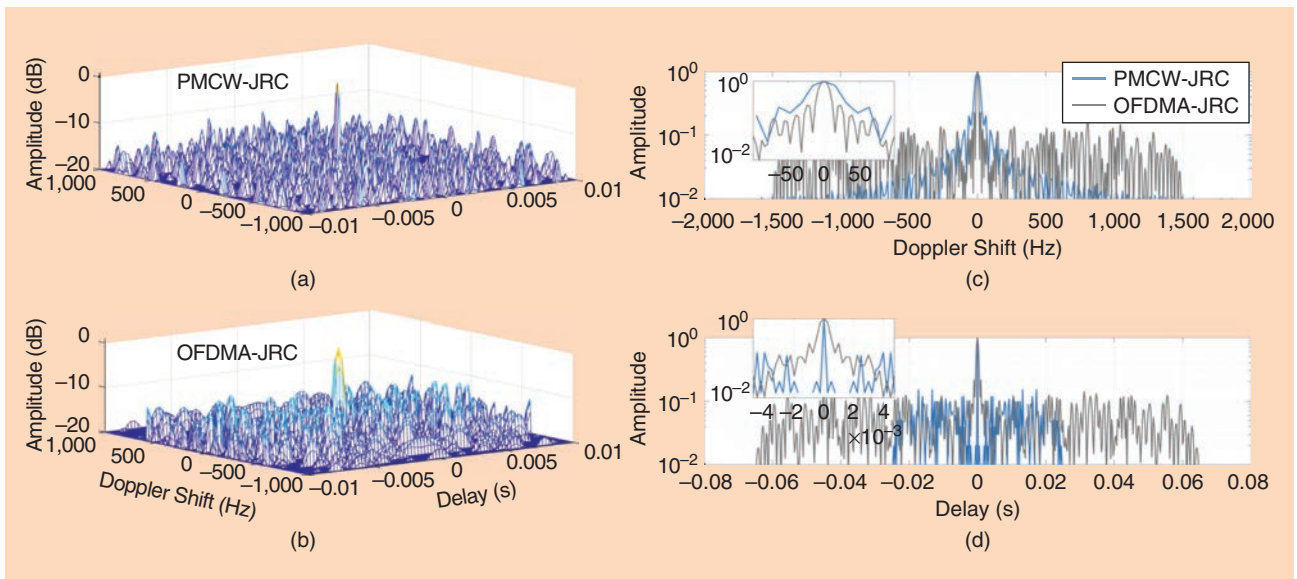


**FIGURE 3.** The AFs of bistatic mm-wave JRC using (a) OFDMA and (b) PMCW signals with (c) Doppler and (d) delay cuts [7].

Although this increases the radar integration duration leading to a more-accurate velocity estimation, the total preamble duration is also prolonged, causing a significant degradation in the communications data rate [33]. A joint coding scheme based on the use of sparsity-based techniques in the time domain can minimize this tradeoff between communications and radar [32]. Here, the frame lengths are varied such that their preambles (exploited as radar pulses) are placed in non-uniformly. These nonuniformly pulses in a CPI are then used to construct a virtual block of several pulses, which increase the radar pulse-integration time and enable an enhanced-velocity-estimation performance. If the channel is sparse, the same performance can be achieved in the frequency domain by using sub-Nyquist processing [11]. In [13], the wide bandwidth of the mm-wave is exploited using a Doppler-resilient 802.11ad link to obtain very-high-resolution profiles in range and Doppler with the ability to distinguish among various automotive targets. Figure 5 shows distinct, detailed movements of each wheel of a car and the body parts of a pedestrian as detected by an 802.11ad-based Doppler-resilient short-range radar.

### Carrier exploitation

Selecting active subcarriers and controlling their power levels or PAPR in an adaptive manner is also useful for interference management. To achieve high range resolution, radar systems require wide transmit bandwidths. On the other hand, communications systems often allocate the resource blocks from a certain number of subcarriers to each user based on a channel-quality indicator that satisfies their rate and system QoS requirements. Through feedback from the RxS, spectrum sensing, databases, or other sources, the TxS of both systems can have information about the occupancy of different subcarriers, instantaneous or desired SINR levels, channel gains, and power constraints imposed by other coexisting subsystems. This awareness can be exploited by adaptively optimizing the

power allocation among different subcarriers. An example of optimizing subcarrier power ( $P_k$ ) allocations and imposing minimum-desired rate constraints on wireless communications users and maximum power constraint  $P_T$  for the radar is as follows:

$$\begin{aligned} & \underset{P_k, \eta}{\text{maximize}} \quad p_D \\ & \text{subject to } p_{\text{FA}} \leq \alpha, \\ & \log(1 + \text{SINR}_k) \geq t_k, \forall k, \\ & \sum_{k=0}^{N-1} P_k \leq P_T, \end{aligned} \quad (13)$$

where  $\eta$  is the detection threshold for a likelihood ratio test using the Neyman–Pearson detection strategy with false alarm constraint  $\alpha$ . Two example power allocations from the radar perspective are depicted in Figure 6. A water-filling solution [Figure 6(a)] obtained by maximizing MI between the received data and target and channel responses allocates radar power to those parts of the spectrum where the signal experiences the least attenuation and interference level is low. The second approach [Figure 6(b)] takes into account the channel gains and required SINR values at the communications subsystems, while maximizing the radar performance in the Neyman–Pearson sense for target-detection tasks.

### Cognition and learning in mm-wave JRC

More-recent enabling architectures and technologies for mm-wave JRC where the system can sense, learn, and adapt to changes in the channel are discussed in the following sections.

### Cognitive systems

Cognitive radars and radios sense the spectrum and exchange information to build and learn their channel states. This typically involves channel estimation and feedback on

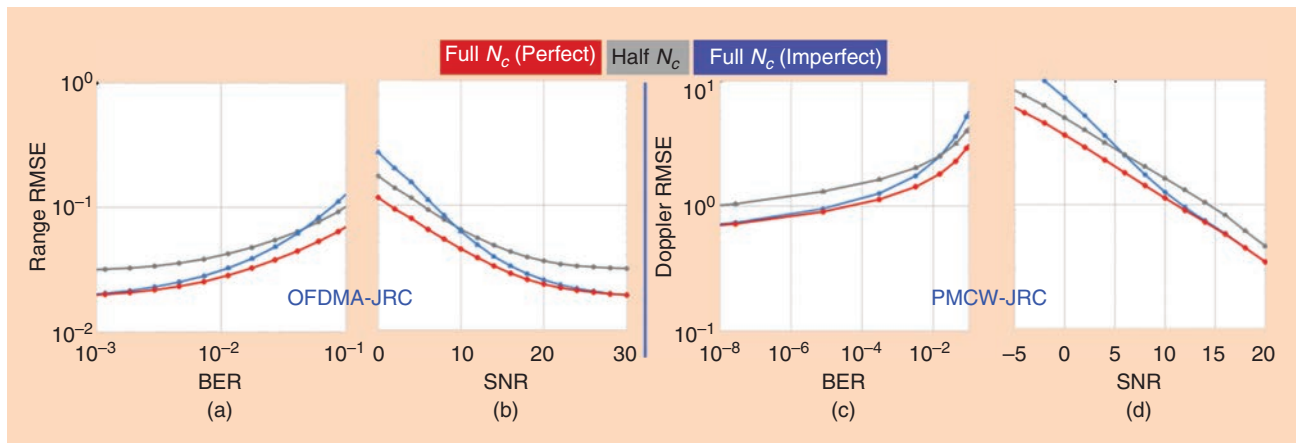
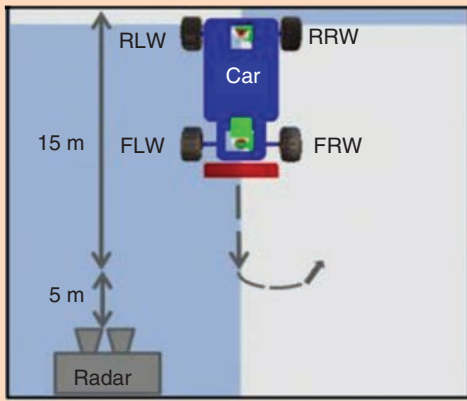
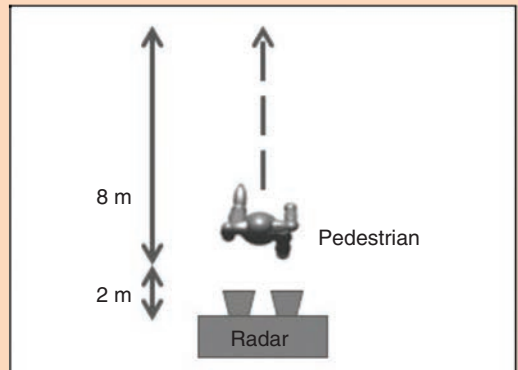


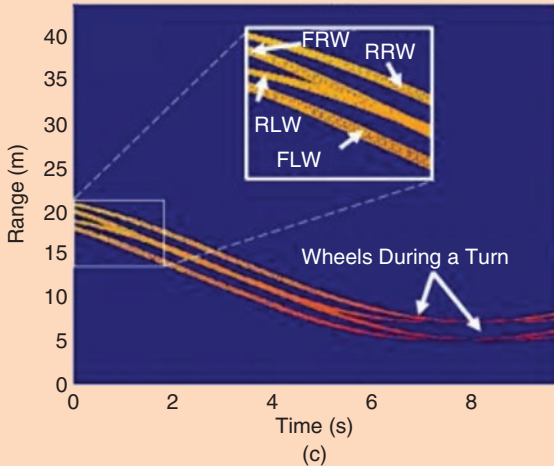
**FIGURE 4.** The root-mean-square error (RMSE) of the estimated range of a single target using OFDMA-JRC with respect to (a) signal-to-noise ratio (SNR) and (b) BER using half, i.e., ( $\mu = 50\%$ ), or all of the subcarriers ( $full N_c$ ) with perfect and imperfect recovery of communications symbols. The RMSE in the Doppler estimate of a single target for PMCW-JRC using all and half-frames with respect to (c) SNR and (d) BER. In both cases, JRC superresolution algorithms [7] have been employed.



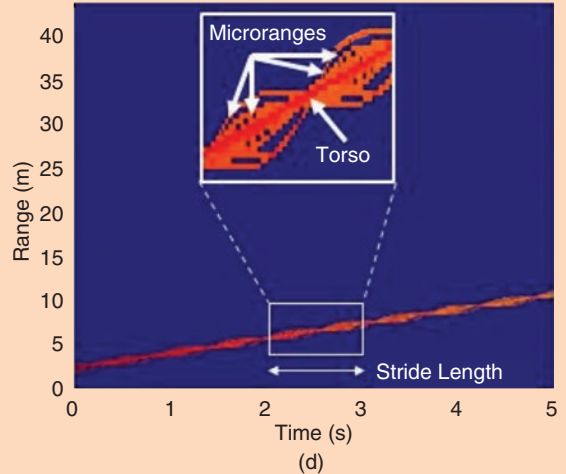
(a)



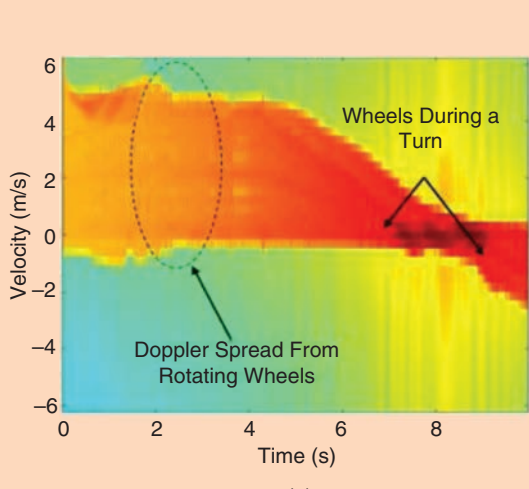
(b)



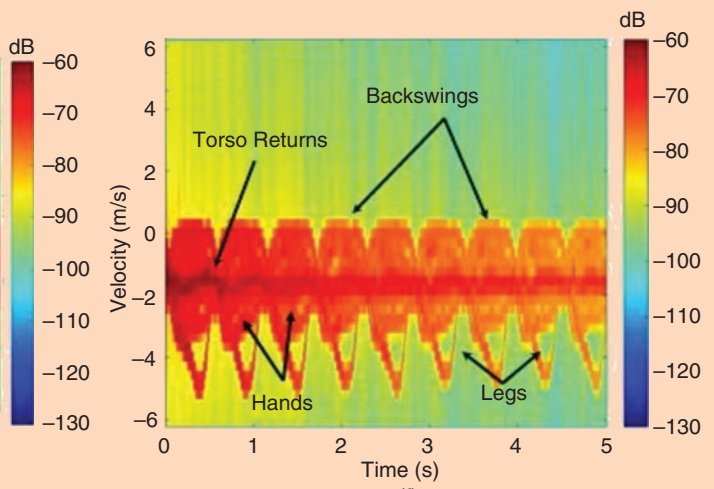
(c)



(d)



(e)



(f)

**FIGURE 5.** The radar signatures generated from the animation models of (a) a small car and (b) a pedestrian using Doppler-resilient 802.11ad standard waveforms [13], [46]. As the targets move radially in front of the radar on the marked trajectories, the movements of the front right (FRWs), front left (FLWs), rear right (RRWs), and rear left wheels (RLWs), respectively, of the car as well as the torso, arms, and legs of the pedestrian are individually observed in (c) and (d) the range-time and (e) and (f) Doppler-time domains.

channel quality. Spectrum cartography methods, which generate a map of spectrum access in different locations and frequencies at different time instances, have been developed in this context [48]. Based on the obtained awareness, the operational parameters of Tx and Rx in each subsystem are adjusted to optimize their performance [3]. Channel-coherence times should be long enough for JRC to apply cognitive actions. Because this duration occurs in nanoseconds for mm-wave environments, compressed sensing-based solutions aid in reducing required samples for cognitive processing [11], [49].

#### Fast waveforms

Algorithms that develop cognitive waveforms should have low computational complexity to redesign waveforms on the fly, typically within a single CPI. This is especially important for mm-wave systems where the fast-time radar waveform can easily have a length of tens of thousands samples. In [50], waveform designs in spectrally dense environments do not exceed a quadratic complexity. In [11] and [20], the mm-wave radar based on sub-Nyquist sampling adaptively transmits in disjoint subbands, and the vacant slots are used by vehicular communications.

#### Machine learning

To facilitate the fast configuration of mm-wave JRC links with low latency and high efficiency, machine learning is useful for acquiring situational awareness. This involves learning the spectrum state's evolution over time (including classifying radar target responses or other waveforms occupying the spectrum), acquiring the channel responses, identifying an underutilized spectrum, and exploiting it in an opportunistic manner. The deep-learning methods are widely applied for tasks such as target classification, automatic

waveform recognition, and determining optimal antennas and RF chains [51]. Optimal policies for coexisting systems may be learned using reinforcement learning approaches such as a partially observable Markov decision process and a restless multiarm bandit [52].

#### Game-theoretic solutions

The interaction between radar and communications systems sharing a spectrum can be analyzed from a game theory perspective [53]. The two systems (i.e., players) form an adversarial, noncooperative game because of conflicting interests in sharing the spectrum. The game is also dynamic due to continuously evolving spectral states over time. The utility function is designed to reflect possible strategies based on the respective players' requirements. The solutions result in a Nash or

Stackelberg equilibrium, which are the game states with the property that none or one of the players can do better, respectively. In comparison to sub-6 GHz, the solution space for mm-wave is several gigahertz wide with much lower maximum transmit power.

#### Summary

We outlined various aspects of implementing JRC systems at mm-wave. The sheer number of mm-wave antennas and huge bandwidth pose new challenges in waveform design and Rx processing that were not seen in other bands. The dynamic and highly variable environments of mm-wave applications require continuous cognition of the mm-wave channel by both radar and communications. While there are still many open problems in this area, mm-wave JRC is a precursor to an emerging frontier of sub-mm-wave or terahertz JRC where terahertz communications would coexist with the promising

**The performance tradeoff between communications and radar is quantified in terms of a weighted combination of the scalar quantities.**

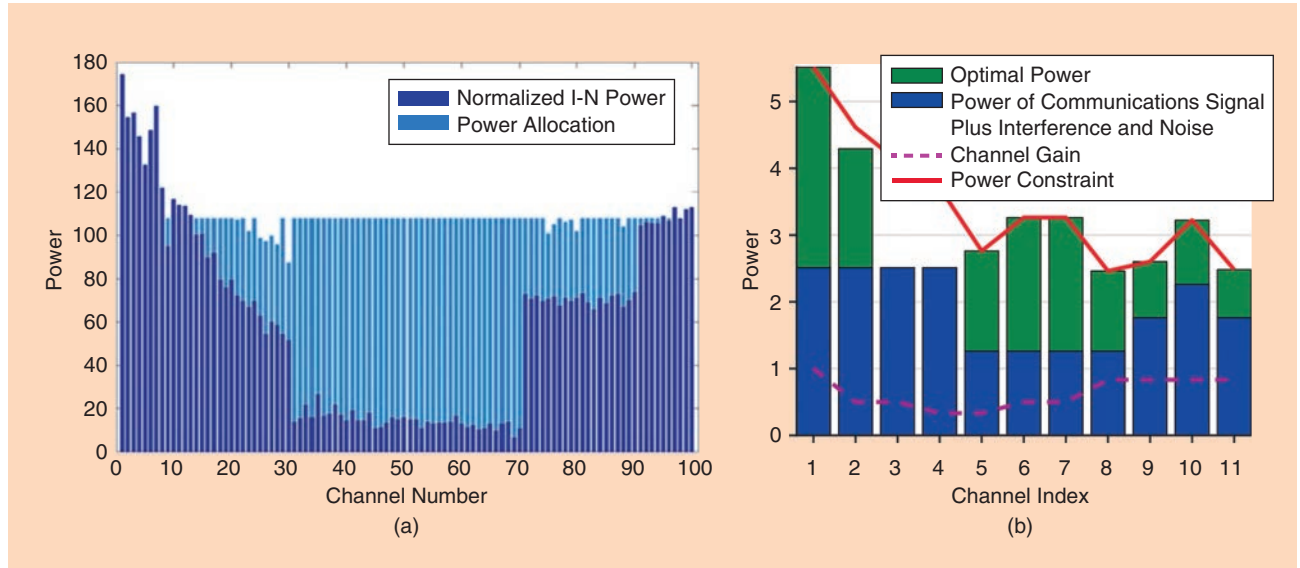


**FIGURE 6.** Power-allocation solutions for JRC carrier exploitation via (a) the water-filling and (b) Neyman-Pearson tests [47].

technology of low-terahertz (0.1–1-THz) automotive and imaging radars.

## Acknowledgments

This work is partially funded by the European Research Council grant Actively Enhanced Cognition based Framework for Design of Complex Systems and Luxembourg National Research Fund Project Adaptive mmWave Radar Platform for Enhanced Situational Awareness: Design and Implementation.

## Authors

**Kumar Vijay Mishra** (kumarvijay-mishra@uiowa.edu) received his B.Tech. degree, summa cum laude (gold medal, honors) in electronics and communications engineering from the National Institute of Technology, Hamirpur, India, in 2003, his M.S. degree in electrical and computer engineering from Colorado State University, Fort Collins, in 2012, and his Ph.D. degree in electrical and computer engineering and M.S. degree in mathematics from the University of Iowa, Iowa City, in 2015. Currently, he is the technical advisor to the automotive radar start-up Hertzwell, Singapore; a research fellow at the Interdisciplinary Centre for Security, Reliability and Trust, University of Luxembourg, Luxembourg City; and the Harry Diamond Distinguished Postdoctoral Fellow at the U.S. Army Research Laboratory, supported by the U.S. National Academies of Sciences, Engineering, and Medicine. He is a Senior Member of the IEEE.

**M.R. Bhavani Shankar** (bhavani.Shankar@uni.lu) received his bachelor of engineering degree from the National Institute of Technology, Tiruchirappalli, India, in 1998 and his M.S. and Ph.D. degrees in electrical communication engineering from the Indian Institute of Science, Bangalore, in 2000 and 2007, respectively. He joined the Interdisciplinary Centre for Security, Reliability and Trust at the University of Luxembourg, Luxembourg City, in 2009 where he is currently a research scientist. He was a postdoctoral researcher at the Signal Processing Lab, the Royal Institute of Technology, Stockholm, Sweden. He serves on the Executive Committee of the IEEE Benelux Joint Chapter on Communications and Vehicular Technology, is the handling editor of *Elsevier Signal Processing*, and is a member of the European Association for Signal Processing Special Area Team on the theoretical and methodological trends in signal processing. He is a Senior Member of the IEEE.

**Visa Koivunen** (visa.koivunen@aalto.fi) received his D.Sc. degree in electrical engineering from the University of Oulu, Finland. He has been a full professor of signal processing at Aalto University, Espoo, Finland, since 1999. He received the academy professor position in 2010. Since 2006, he has also been a part-time visiting fellow at Princeton University, New Jersey, and spent full sabbaticals there. He received the 2007 and 2017 IEEE Signal Processing Society Best Paper Awards. He has served on the editorial boards of multiple IEEE journals, on the Fourier Award Board and Fellow Evaluation Committee, and as a general chair for the IEEE International Workshop on

Signal Processing Advances in Wireless Communications and Asilomar Conference on Signals, Systems, and Computers. His research interests include statistical signal processing, radar, communications, data science, and machine learning. He is a Fellow of the IEEE.

**Björn Ottersten** (bjorn.ottersten@uni.lu) received his M.S. degree in electrical engineering and applied physics from Linköping University, Sweden, in 1986 and his Ph.D. degree in electrical engineering from Stanford University, California, in 1990. Currently, he is the director for the Interdisciplinary Centre for Security, Reliability and Trust at the University of Luxembourg, Luxembourg City. He coauthored papers that received an IEEE Signal Processing Society Best Paper Award in 1993, 2001, 2006, and 2013 and eight IEEE conference papers that received best paper awards. In 1991, he became a professor of signal processing at the Royal Institute of Technology, Stockholm, Sweden. In 2011, he received the IEEE Signal Processing Society Technical Achievement Award. He received the European Research Council Advanced Research Grant twice, 2009–2013 and 2017–2021. He is a Fellow of the IEEE and of the European Association for Signal Processing.

**Sergiy A. Vorobyov** (sergiy.vorobyov@aalto.fi) received his M.Sc. and Ph.D. degrees in systems and control from the Kharkiv National University of Radio Electronics, Ukraine, in 1994 and 1997, respectively. He is a professor with the Department of Signal Processing and Acoustics, Aalto University, Espoo, Finland. He was previously with the University of Alberta, Canada, as a full professor. He has held various research and faculty positions at the Institute of Physical and Chemical Research, Tokyo, Japan; McMaster University, Canada; the University of Duisburg-Essen, Germany; the Darmstadt University of Technology, Germany; and Heriot-Watt University, Edinburgh, Scotland. He received the 2004 IEEE Signal Processing Society Best Paper Award and other awards. His research interests include optimization and multi-linear algebra methods; statistical, array and sparse signal processing; estimation and detection theory; and multiantenna, large-scale, cooperative, and cognitive systems. He is a Fellow of the IEEE.

## References

- [1] B. Paul, A. R. Chiriyath, and D. W. Bliss, "Survey of RF communications and sensing convergence research," *IEEE Access*, vol. 5, pp. 252–270, Dec. 2017.
- [2] A. Hassanien, M. Amin, Y. Zhang, and F. Ahmad, "Signaling strategies for dual-function radar communications: An overview," *IEEE Aerosp. Electron. Syst. Mag.*, vol. 31, no. 10, pp. 36–45, 2017.
- [3] D. Cohen, K. V. Mishra, and Y. C. Eldar, "Spectrum sharing radar: Coexistence via Xampling," *IEEE Trans. Aerosp. Electron. Syst.*, vol. 54, no. 3, pp. 1279–1296, 2018.
- [4] President's Council of Advisors on Science and Technology, "Report to the president: Realizing the full potential of government-held spectrum to spur economic growth," PCAST, Washington, D.C., Rep. ADA565091, 2012. [Online]. Available: <https://apps.dtic.mil/docs/citations/ADA565091>
- [5] T. S. Rappaport, G. R. MacCartney, M. K. Samimi, and S. Sun, "Wideband millimeter-wave propagation measurements and channel models for future wireless communication system design," *IEEE Trans. Commun.*, vol. 63, no. 9, pp. 3029–3056, 2015.
- [6] R. C. Daniels and R. W. Heath Jr., "60 GHz wireless communications: Emerging requirements and design recommendations," *IEEE Veh. Technol. Mag.*, vol. 2, no. 3, 2007.

- [7] S. H. Dokhanchi, B. S. Mysore, K. V. Mishra, and B. Ottersten, "A mmWave automotive joint radar-communications system," *IEEE Trans. Aerosp. Electron. Syst.*, 2019. doi: 10.1109/TAES.2019.2899797.
- [8] J. Lien, N. Gillian, M. E. Karagozler, P. Amihood, C. Schwesig, E. Olson, H. Raja, and I. Poupyrev, "Soli: Ubiquitous gesture sensing with millimeter wave radar," *ACM Trans. Graph.*, vol. 35, no. 4, pp. 142:1–142:19, 2016.
- [9] K. V. Mishra, A. Gharanjik, M. R. B. Shankar, and B. Ottersten, "Deep learning framework for precipitation retrievals from communication satellites," in *Proc. European Conf. Radar Meteorology & Hydrology*, 2018, pp. 1–9.
- [10] N. Decarli, F. Guidi, and D. Dardari, "A novel joint RFID and radar sensor network for passive localization: Design and performance bounds," *IEEE J. Sel. Topics Signal Process.*, vol. 8, no. 1, pp. 80–95, 2014.
- [11] K. V. Mishra and Y. C. Eldar, "Sub-Nyquist channel estimation over IEEE 802.11ad link," in *Proc. IEEE Int. Conf. Sampling Theory Applications*, 2017, pp. 355–359.
- [12] G. Fortino, M. Pathan, and G. Di Fatta, "BodyCloud: Integration of cloud computing and body sensor networks," in *Proc. IEEE Int. Conf. Cloud Computing Technology Science*, 2012, pp. 851–856.
- [13] K. V. Mishra, S. S. Ram, S. Vishwakarma, and G. Duggal, Doppler-resilient 802.11ad-based ultra-short range automotive radar. 2019. [Online]. Available: arxiv:1902.01306
- [14] K. V. Mishra and Y. C. Eldar, "Sub-Nyquist radar: Principles and prototypes," in *Compressed Sensing in Radar Signal Processing*, A. D. Maio, Y. C. Eldar, and A. Haimovich, Eds. Cambridge, U.K.: Cambridge Univ. Press, 2019, pp. 1–50.
- [15] R. Méndez-Rial, C. Rusu, N. González-Prelcic, A. Alkhateeb, and R. W. Heath, "Hybrid MIMO architectures for millimeter wave communications: Phase shifters or switches?" *IEEE Access*, vol. 4, pp. 247–267, Jan. 2016.
- [16] G. R. MacCartney Jr., S. Sun, T. S. Rappaport, Y. Xing, H. Yan, J. Koka, R. Wang, and D. Yu, "Millimeter wave wireless communications: New results for rural connectivity," in *Proc. ACM Workshop All Things Cellular*, 2016, pp. 31–36.
- [17] P. Kumari, J. Choi, N. Gonzalez-Prelcic, and R. W. Heath, Jr., "IEEE 802.11ad-based radar: An approach to joint vehicular communication-radar system," *IEEE Trans. Veh. Technol.*, vol. 67, no. 4, pp. 3012–3027, 2018.
- [18] M. I. Skolnik, *Radar Handbook*, 3rd ed. New York: McGraw-Hill, 2008.
- [19] M. Bică, K. Huang, V. Koivunen, and U. Mitra, "Mutual information based radar waveform design for joint radar and cellular communication systems," in *Proc. IEEE Int. Conf. Acoustic Speech Signal Processing*, 2016, pp. 3671–3675.
- [20] K. V. Mishra, A. Zhitnikov, and Y. C. Eldar, "Spectrum sharing solution for automotive radar," in *Proc. IEEE Vehicular Technology Conf.*, 2017, pp. 1–5. doi: 10.1109/VTCSpring.2017.8108413.
- [21] G. R. Muns, K. V. Mishra, C. B. Guerra, Y. C. Eldar, and K. R. Chowdhury, "Beam alignment and tracking for autonomous vehicular communication using IEEE 802.11ad-based radar," in *Proc. IEEE Infocom Workshops—Hot Topics Social and Mobile Connected Smart Objects*, 2019, to be published.
- [22] B. Donnet and I. Longstaff, "Combining MIMO radar with OFDM communications," in *Proc. IEEE European Radar Conf.*, 2006, pp. 37–40.
- [23] Z. Geng, R. Xu, H. Deng, and B. Himed, "Fusion of radar sensing and wireless communications by embedding communication signals into the radar transmit waveform," *IET Radar Sonar Navig.*, vol. 12, no. 6, pp. 632–640, 2018.
- [24] T. Shi, S. Zhou, and Y. Yao, "Capacity of single carrier systems with frequency-domain equalization," in *Proc. IEEE Circuits and Systems Symp. Emerging Technologies: Frontiers of Mobile and Wireless Communication*, 2004, vol. 2, pp. 429–432.
- [25] K. Takizawa, M. Kyrö, K. Haneda, H. Hagiwara, and P. Vainikainen, "Performance evaluation of 60 GHz radio systems in hospital environments," in *Proc. IEEE Int. Conf. Communications*, 2012, pp. 3219–3295.
- [26] W.-C. Liu, F.-C. Yeh, T.-C. Wei, C.-D. Chan, and S.-J. Jou, "A digital Golay-MPIC time domain equalizer for SC/OFDM dual-modes at 60 GHz band," *IEEE Trans. Circuits Syst. I, Reg. Papers*, vol. 60, no. 10, pp. 2730–2739, 2013.
- [27] S. A. Vorobyov, "Adaptive and robust beamforming," in *Array and Statistical Signal Processing* (Academic Press Library in Signal Processing, Volume 2) A. M. Zoubir, M. Viberg, R. Chellappa, and S. Theodoridis, Eds. Waltham, MA: Elsevier, 2014, pp. 503–552.
- [28] A. Ayyar and K. V. Mishra, "Robust communications-centric coexistence for turbo-coded OFDM with non-traditional radar interference models," in *Proc. IEEE Radar Conf.*, 2019, to be published.
- [29] J. A. Mahal, A. Khawar, A. Abdelhadi, and T. C. Clancy, "Spectral coexistence of MIMO radar and MIMO cellular system," *IEEE Trans. Aerosp. Electron. Syst.*, vol. 53, no. 2, pp. 655–668, 2017.
- [30] Y. Cui, V. Koivunen, and X. Jing, "Interference alignment based spectrum sharing for MIMO radar and communication systems," in *Proc. IEEE Int. Workshop Signal Processing Advanced Wireless Communications*, 2018, pp. 1–5. doi: 10.1109/SPAWC.2018.8445973.
- [31] D. W. Bliss, "Cooperative radar and communications signaling: The estimation and information theory odd couple," in *Proc. IEEE Radar Conf.*, 2014, pp. 50–55.
- [32] P. Kumari, S. A. Vorobyov, and R. W. Heath Jr., Adaptive virtual waveform design for millimeter-wave joint communication-radar. 2019. [Online]. Available: arxiv:1904.05516.
- [33] P. Kumari, D. H. N. Nguyen, and R. W. Heath, "Performance trade-off in an adaptive IEEE 802.11ad waveform design for a joint automotive radar and communication system," in *Proc. IEEE Int. Conf. Acoustic Speech Signal Processing*, 2017, pp. 4281–4285.
- [34] D. Ciuonzo, A. De Maio, G. Foglia, and M. Piezzo, "Pareto-theory for enabling covert intrapulse radar-embedded communications," in *Proc. IEEE Radar Conf.*, 2015, pp. 0292–0297.
- [35] N. Levanon, "Multifrequency radar signals," in *Proc. IEEE Int. Radar Conf.*, 2000, pp. 683–688.
- [36] M. Bică and V. Koivunen, "Frequency agile generalized multicarrier radar," in *Proc. Annu. Conf. Information Sciences Systems*, 2014. doi: 10.1109/CIS.2014.6814069.
- [37] M. Bică and V. Koivunen, "Generalized multicarrier radar: Models and performance," *IEEE Trans. Signal Process.*, vol. 64, no. 17, pp. 4389–4402, 2016.
- [38] A. Hassani, M. Amin, Y. Zhang, and F. Ahmad, "Dual-function radar communication: Information embedding using sidelobe control and waveform diversity," *IEEE Trans. Signal Process.*, vol. 64, no. 8, pp. 2168–2181, 2016.
- [39] A. Hassani, E. Aboutanios, M. Amin, and G. Fabrizio, "A dual-function MIMO radar-communication system via waveform permutation," *Dig. Signal Process.*, vol. 83, pp. 118–128, Dec. 2018.
- [40] A. Hassani, C. Sahin, J. Metcalf, and B. Himed, "Uplink signaling and receive beamforming for dual-function radar communications," in *Proc. IEEE Int. Workshop Signal Processing Advanced Wireless Communications*, 2018, pp. 1–5. doi: 10.1109/SPAWC.2018.8445858.
- [41] T. Aittomäki and V. Koivunen, "Hybrid optimization method for cognitive and MIMO radar code design," in *Proc. European Signal Processing Conf.*, 2017, pp. 2226–2229.
- [42] B. Li, A. Petropulu, and W. Trappe, "Optimum co-design for spectrum sharing between matrix completion based MIMO radars and a MIMO communication system," *IEEE Trans. Signal Process.*, vol. 64, no. 17, pp. 4562–4575, 2016.
- [43] W. Zhang, S. A. Vorobyov, and L. Guo, "DOA estimation in MIMO radar with broken sensors by difference co-array processing," in *Proc. IEEE Int. Workshop Computational Advances in Multi-Sensor Adaptive Processing*, 2015, pp. 321–324.
- [44] Y. Cui, V. Koivunen, and X. Jing, "Interference alignment based precoder-decoder design for radar-communication co-existence," in *Proc. 51st Asilomar Conf. Signals, Systems and Computers*, 2017, pp. 1290–1295.
- [45] S. H. Dokhanchi, M. R. Bhavani Shankar, Y. A. Nijssure, T. Stifter, S. Sedighi, and B. Ottersten, "Joint automotive radar-communications waveform design," in *Proc. IEEE Int. Symp. Personal Indoor Mobile Radio Communications*, 2017, pp. 1–7. doi: 10.1109/PIMRC.2017.8292466.
- [46] G. Duggal, S. S. Ram, and K. V. Mishra, "Micro-Doppler and micro-range detection via Doppler-resilient 802.11ad-based vehicle-to-pedestrian radar," in *Proc. IEEE Radar Conf.*, 2019, to be published.
- [47] M. Bică, K. Huang, U. Mitra, and V. Koivunen, "Opportunistic radar waveform design in joint radar and cellular communication systems," in *Proc. IEEE Global Communications Conf.*, 2015, pp. 1–7. doi: 10.1109/GLOCOM.2015.7417624.
- [48] S.-J. Kim, E. Dall'Anese, and G. B. Giannakis, "Cooperative spectrum sensing for cognitive radios using Kriged Kalman filtering," *IEEE J. Sel. Topics Signal Process.*, vol. 5, no. 1, pp. 24–36, 2011.
- [49] K. V. Mishra and Y. C. Eldar, "Performance of time delay estimation in a cognitive radar," in *Proc. IEEE Int. Conf. Acoustic Speech Signal Processing*, 2017, pp. 3141–3145.
- [50] Y. Li and S. A. Vorobyov, "Fast algorithms for designing multiple unimodular waveform(s) with good correlation properties," *IEEE Trans. Signal Process.*, vol. 66, no. 5, pp. 1197–1212, 2018.
- [51] A. M. Elbir and K. V. Mishra, "Deep learning design for joint antenna selection and hybrid beamforming in massive MIMO," in *Proc. IEEE Int. Symp. Antennas Propagation*, 2019, to be published.
- [52] J. Lunden, V. Koivunen, and H. V. Poor, "Spectrum exploration and exploitation for cognitive radio: Recent advances," *IEEE Signal Process. Mag.*, vol. 32, no. 3, pp. 123–140, 2015.
- [53] K. V. Mishra, A. F. Martone, and A. I. Zaghloul, "Power allocation games for overlaid radar and communications," in *Proc. Int. Union Radio Science Asia-Pacific Radio Science Conf.*, 2019, to be published.

Aboulnasr Hassani, Moeness G. Amin,  
Elias Aboutanios, and Braham Himed

# Dual-Function Radar Communication Systems

*A solution to the spectrum congestion problem*



To get the most use out of scarce spectrum, technologies have emerged that permit single systems to accommodate both radar and communications functions. Dual-function radar communication (DFRC) systems, where the two systems use the same platform and share the same hardware and spectral resources, form a specific class of radio-frequency (RF) technology. These systems support applications where communication data, whether as target and waveform parameter information or as information independent of the radar operation, are efficiently transmitted using the same radar aperture and frequency bandwidth. This is achieved by embedding communication signals into radar pulses. In this article, we review the principles of DFRC systems and describe the progress made to date in devising different forms of signal embedding. Various approaches to DFRC system design, including downlink and uplink signaling schemes, are discussed along with their respective benefits and limitations. We present tangible applications of DFRC systems and delineate their design requirements and challenges. Future trends and open research problems are also highlighted.

## Introduction and historical perspective

The limited availability of the radio spectrum and the explosion in commercial communications services are putting other essential systems of electromagnetic sensing modalities, such as radar, under immense pressure [1]. Recently, intensive research has focused on the problems of RF spectrum congestion and contention between radar and communications [2]. In this high-stakes game, radar is losing out to the commercial interests driving the communications revolution. One of the most pressing challenges in the area of spectral congestion and dynamic frequency allocation is to provide uncontested shared bandwidth between radar and communications or among various RF systems at large. As such, there is a growing and strong need for new bold concepts for making the use of the radio spectrum more efficient while offering protection from interfering services [3]. This has spurred extensive efforts to devise ways to simultaneously operate radar target illuminations and wireless services using the same frequency bandwidth, a drive

that is referred to as *coexistence* [4], [5]. The direct approach for easing the competition over bandwidth is through dynamic spectrum allocations (e.g., using cognitive radio [6] and radar [7]) and interference-management techniques. Alternatively, the two systems can cohabit, in which case the design of the radar waveform may be constrained to avoid interfering with legacy communication systems. Interference mitigation, however, consumes system resources and limits the available spatiotemporal degrees of freedom.

A different approach to coexistence, referred to as *codesign*, enables the two systems to operate in concert and jointly optimize their performances [8], [9]. One codesign technique, DFRC, integrates the two functions on one platform [10], [11]. This is also known as *intentional modulation on a pulse* [12] or *CoRadar* [13]. A DFRC system can be defined as a system that simultaneously performs radar and communication functions using a common transmit/receive aperture, the same bandwidth, and joint dual-function waveforms. The overarching objective of the DFRC approach is to allow the communication service to capitalize on the resources of the radar infrastructure while striving to be transparent to the radar operation and mission. In traditional applications, these resources may include large bandwidth, multisensor beamforming, high-quality hardware, high power, and high-gain antennas. In many emerging applications, DFRC systems are an important part of a new paradigm for meeting, with limited resources, the demand for increased functionality and protection from interfering services. DFRC systems (Figure 1) can be useful in, for example, vehicles in an intelligent transportation system that need to share information in a rapidly changing environment [14], synthetic aperture radar systems that seek to transmit

sensed data to ground stations, radars in a network communicating scheduling and target information with one another, and radar communicating Doppler and range information to the same target it tracks.

Technologies enabling radar platforms to house voice and data transmission and reception are poised to deliver technological advances in both radar and communications systems. Equipment that shares an aperture and spectrum for both radar and communications, besides making efficient use of scarce spectrum, consumes less power and can be made more compact and lightweight than independent pieces of equipment serving the same purpose [13]. In defense applications, equipment that enables the aperture and spectrum for radar and communications to be shared represents a shift away from independent systems and dedicated components and allows command and control systems to be integrated and sensors to be more efficiently managed.

The concept of designing a system capable of simultaneously performing radar and communication tasks while sharing hardware, power, and bandwidth resources was introduced decades ago [15]. But only recently has the idea become a reality, thanks to advancements in waveform design and diversity, the maturity of software-defined radio platforms, implementations of digital beamforming, and the development of efficient methods for solving constrained minimization problems based on convex optimization and relaxation [11], [12], [16]–[18]. Whether operating independently or within a network, information embedding into radar pulses can take the form of amplitude-shift keying (ASK), phase-shift keying (PSK), or index modulation (IM), such as code-shift keying (CSK), frequency IM, or spatial modulation. Consequently, DFRC

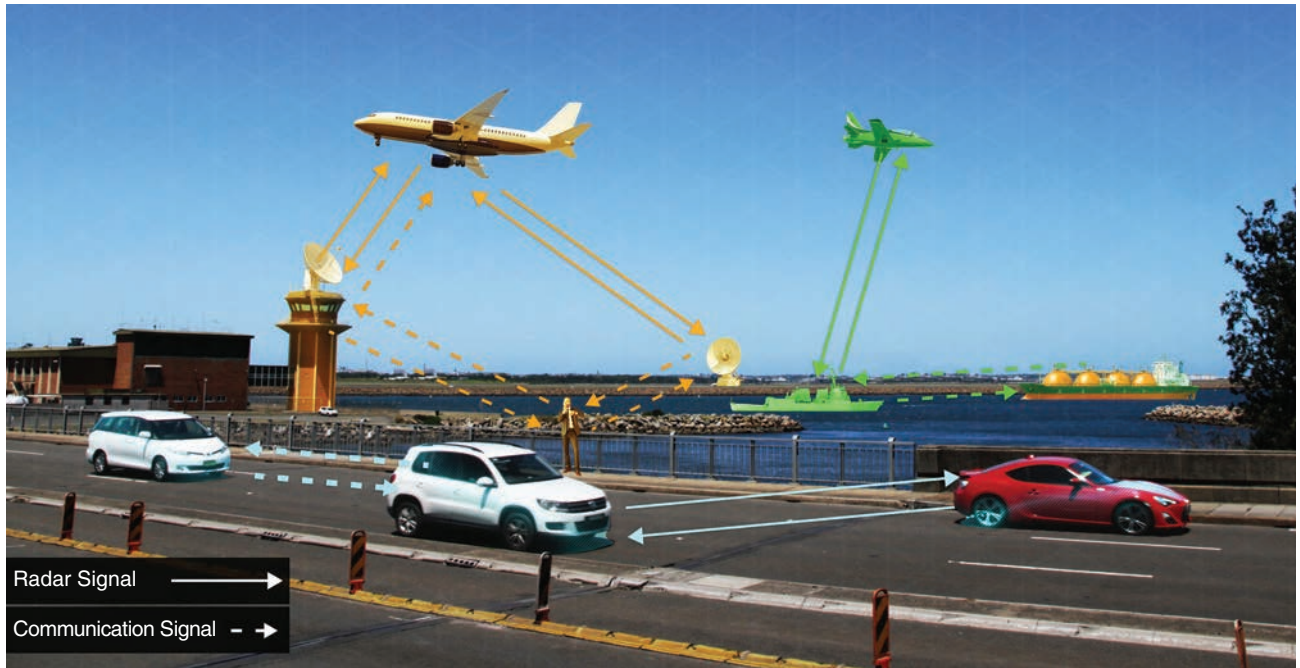


**FIGURE 1.** A photo illustration showing applications for DFRC. Solid lines indicate radar function. Dashed lines represent communications links.

research stands to benefit greatly from the marriage of knowledge accumulating in the communications literature and state-of-the-art radar techniques. This article presents an overview of DFRC systems from the information-embedding perspective, and discusses the various techniques and implementation strategies that define the state of the art. We describe different approaches to DFRC based on radar beampattern and radar-waveform modulation, and we consider both phased-array and multiple-input, multiple-output (MIMO) configurations, along with uplink and downlink communications. The article concludes by highlighting several challenges in DFRC systems and outlining some possible future research directions.

## DFRC configuration and signal model

To develop DFRC systems, researchers needed to devise signaling strategies and modulations of the radar pulse and beam that would lead to the integrated operation and improved use of the finite RF spectrum. With this goal in mind, researchers recognized that communication signals emitted from a radar platform may convey radar signal and target characteristics to other cooperating radars. To create a unified aperture and bandwidth system in an RF-restricted environment, it is desirable to embed such information into radar pulses. The information data rate is determined by the radar pulse repetition frequency (PRF), whether the system uses a phased-array or MIMO configuration, and the permissible incremental changes in radar waveform structure and bandwidth.

In downlink communications, information is transmitted from the DFRC platform toward one or more communication users (Figure 2). The essence of downlink communications is to embed messages into the radar emissions, preferably without disturbing the radar operation. Unless otherwise stated, we assume that the communication symbol duration equals the pulse repetition interval (PRI) of the radar. To illustrate, we consider the baseband transmit signal vector in two common types of radar configurations: single-input, multiple-output (SIMO) and MIMO.

### SIMO radar

Consider a radar system with a linear transmit array comprising  $M$  antennas. The bandwidth and total transmit power budget available to the DFRC system are denoted as  $B$  and  $P$ , respectively. For a SIMO radar, the  $M \times 1$  baseband transmit signal vector during the  $\tau$ th radar pulse can be defined as

$$\mathbf{s}_{\text{SIMO}}(t; \tau) = \sqrt{P} \mathbf{w}^* \phi(t), \quad (1)$$

where  $t$  and  $\tau$  denote the fast time and pulse number, respectively,  $(\cdot)^*$  is the conjugate operation,  $\mathbf{w}$  the unit-norm transmit beamforming weight vector, and  $\phi(t)$  is the radar waveform. The radar signal  $\phi(t)$  is assumed to have unit energy, i.e.,  $\int_{T_\phi} |\phi(t)|^2 dt = 1$ , where  $T_\phi$  is the waveform duration.

### MIMO radar

Let  $\{\phi_m(t)\}$ ,  $m=1, \dots, M$  be a predesigned set of orthogonal waveforms that satisfy the condition  $\int_{T_\phi} \phi_m(t) \phi_m^*(t) dt =$

$\delta(m - m')$ , where  $\delta(\cdot)$  denotes the Kronecker delta function. During the  $\tau$ th pulse, the MIMO radar baseband transmit signal vector can be expressed as a linear combination of the individual orthogonal waveforms as

$$\mathbf{s}_{\text{MIMO}}(t; \tau) = \sqrt{\frac{P}{M}} \sum_{m=1}^M \mathbf{w}_m^* \phi_m(t) = \sqrt{\frac{P}{M}} \mathbf{W} \phi(t), \quad (2)$$

where  $\mathbf{w}_m$  is the  $M \times 1$  transmit beamforming weight vector associated with the  $m$ th orthogonal waveform,  $\phi(t) \triangleq [\phi_1(t), \dots, \phi_M(t)]^T$  is the vector of orthogonal waveforms, and  $(\cdot)^T$  stands for the transpose operation. The  $M \times M$  transmit beamforming weight matrix  $\mathbf{W} \triangleq [\mathbf{w}_1^*, \dots, \mathbf{w}_M^*]$  is assumed to be normalized such that  $\text{tr}\{\mathbf{W}^H \mathbf{W}\} = M$ , with  $\text{tr}\{\cdot\}$  being the trace of a square matrix and  $(\cdot)^H$  the Hermitian transpose.

In the transmit signal model (1), it is assumed that the transmit beamforming weight vectors  $\mathbf{w}$  and transmit waveform  $\phi(t)$  satisfy the transmit beampattern and range-Doppler resolution as mandated by the SIMO radar. Similarly, the transmit beamforming matrix  $\mathbf{W}$  and vector of orthogonal waveforms  $\phi(t)$  in (2) are assumed to be optimized to satisfy the requirements mandated by the MIMO radar. In practice, perfectly orthogonal waveforms with common spectral content are not realizable. Instead, several techniques for the design and realization of waveforms with low cross-correlations are reported in the literature (see [19] and references therein). Typically, the operating parameters of the radar need to remain fixed within a coherent processing interval (CPI). Communications, being secondary to the primary radar function of the system, can be incorporated by modulating the transmit beampattern, the radar waveforms, or both. Several schemes for embedding information into radar emissions have recently been reported. In principle, those that minimize the impact on the radar operation can be grouped into three categories: beampattern modulation, IM, and fast-time

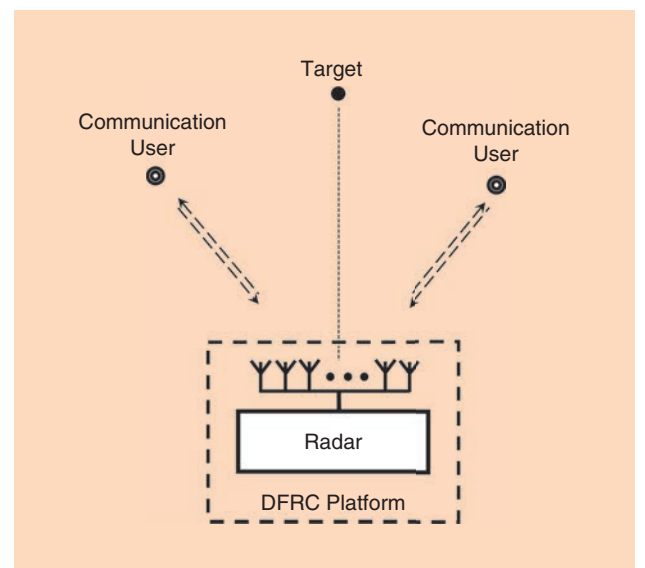


**FIGURE 2.** A diagram of a DFRC system.

modulation. Schemes that redesign the radar waveforms have also been proposed.

## Information embedding using beampattern modulation

This type of information embedding uses the exact same waveform for radar and communications, but changes the radar beampattern, possibly in amplitude and phase, depending on the transmitted information [16]–[18], [20]. The SIMO radar transmit beampattern can be written as

$$G_{\text{SIMO}}(\theta) = \mathbf{a}^T(\theta) \mathbb{E}\{\mathbf{s}_{\text{SIMO}}(t; \tau) \mathbf{s}_{\text{SIMO}}^H(t; \tau)\} \mathbf{a}(\theta) \\ = P |\mathbf{w}^H \mathbf{a}(\theta)|^2 = P |g(\theta)|^2, \quad (3)$$

where  $\theta$  represents the spatial angle,  $\mathbf{a}(\theta)$  is the transmit array steering vector,  $\mathbb{E}\{\cdot\}$  denotes the expectation operator, and  $g(\theta) \triangleq \mathbf{w}^H \mathbf{a}(\theta)$  is the beamformer complex response in the direction  $\theta$ . For the MIMO radar signal model (2), the covariance matrix of the signal vector  $\mathbf{s}_{\text{MIMO}}(t; k)$  is given by

$$\mathbf{R}_s \triangleq \mathbb{E}\{\mathbf{s}_{\text{MIMO}}(t; \tau) \mathbf{s}_{\text{MIMO}}^H(t; \tau)\} = \frac{P}{M} \mathbf{W} \mathbf{W}^H. \quad (4)$$

The MIMO radar transmit beampattern then becomes

$$G_{\text{MIMO}}(\theta) = \mathbf{a}^T(\theta) \mathbf{R}_s \mathbf{a}(\theta) = \frac{P}{M} \mathbf{a}^T(\theta) \mathbf{W} \mathbf{W}^H \mathbf{a}(\theta) \\ = \frac{P}{M} \sum_{m=1}^M |\mathbf{w}_m^H \mathbf{a}(\theta)|^2 = \frac{P}{M} \sum_{m=1}^M |g_m(\theta)|^2, \quad (5)$$

where  $g_m(\theta) \triangleq \mathbf{w}_m^H \mathbf{a}(\theta)$  is the beamformer complex response associated with the  $m$ th waveform.

The essence of beampattern modulation is to retain the magnitude of the beampattern within the radar mainbeam while allowing for controlled variations in the sidelobe region. Hence, information can be embedded into the radar emissions via amplitude modulation (AM) of the radar transmit gain in the sidelobe region and/or phase modulation (PM) of the transmit beampattern in the entire spatial domain. Let  $\tilde{G}_{\text{SIMO}}(\theta, \mathcal{S}(\tau))$  and  $\mathcal{S}(\tau)$  be the modulated beampattern and embedded communication symbol during the  $\tau$ th radar pulse. Then, the radar and communication functions can be performed simultaneously by designing the modulated beampattern such that the following condition is satisfied:

$$\tilde{G}_{\text{SIMO}}(\theta, \mathcal{S}(\tau)) = P |\tilde{g}(\theta, \mathcal{S}(\tau))|^2 \simeq G_{\text{SIMO}}(\theta), \\ \forall \theta \in \Theta_{\text{SIMO}}, \quad \mathcal{S}(\tau) \in \mathbb{D}_{\text{com}}, \quad (6)$$

where  $\tilde{g}(\theta, \mathcal{S}(\tau))$  is the modulated transmit gain,  $\Theta_{\text{SIMO}} \triangleq [\theta_0 - (1/2)\Theta_{\text{bw}}, \theta_0 + (1/2)\Theta_{\text{bw}}]$ ,  $\theta_0$  is the angle at the center of the radar mainbeam,  $\Theta_{\text{bw}}$  indicates the width of the SIMO radar mainbeam, and  $\mathbb{D}_{\text{com}}$  denotes the communication symbol constellation. Satisfying constraint (6) means that the radar mainbeam remains unchanged during the entire processing time, and therefore limits the disturbance to the radar functionality due to the communication symbol embedding. The radar operation may also require the imposition of

additional constraints while designing the modulated beampattern  $\tilde{G}_{\text{SIMO}}(\theta, \mathcal{S}(\tau))$ , e.g., minimum sidelobe attenuation level. For the MIMO radar case, DFRC can be achieved by designing the MIMO transmit beampattern such that

$$\tilde{G}_{\text{MIMO}}(\theta, \mathcal{S}(\tau)) = \frac{P}{M} \sum_{m=1}^M |\tilde{g}_m(\theta, \mathcal{S}_m(\tau))|^2 \simeq G_{\text{MIMO}}(\theta), \\ \forall \theta \in \Theta_{\text{MIMO}}, \quad \mathcal{S}_m(\tau) \in \mathbb{D}_{\text{com}}, \quad m = 1, \dots, M, \quad (7)$$

where  $\tilde{G}_{\text{MIMO}}(\theta, \mathcal{S}(\tau))$  is the overall modulated transmit beampattern,  $\mathcal{S}(\tau) \triangleq [\mathcal{S}_1(\tau), \dots, \mathcal{S}_M(\tau)]^T$  is the vector of embedded communication symbols,  $\tilde{g}_m(\theta, \mathcal{S}_m(\tau))$  and  $\mathcal{S}_m(\tau)$  are, respectively, the modulated transmit gain and embedded communication symbol associated with the  $m$ th waveform during pulse  $\tau$ , and  $\Theta_{\text{MIMO}}$  is the mainbeam region of the MIMO radar. Similar to the SIMO radar case, MIMO radar may require additional constraints in designing the overall modulated beampattern. These constraints may apply, for example, to the sidelobe attenuation level, the uniform virtual array structure, and/or transmit rotational invariance property [17].

Note that, although (6) and (7) show that the MIMO radar formulation enables embedding  $M$  times more communication symbols than the SIMO radar, the transmit power assigned to each orthogonal waveform in the MIMO radar case is reduced by a factor  $M$ , compared to the SIMO radar case. The remainder of this section provides an overview of several techniques reported in the literature for the embedding of downlink communication symbols via beampattern modulation.

### Beampattern AM

Beampattern AM enables information delivery to a communication receiver located within the sidelobes of the radar beam, say in direction  $\theta_c$ . The underlying principle is to modulate the sidelobe level (SLL) of the radar beampattern toward the spatial angle of the communication receiver such that, during each radar pulse, a communication symbol  $\mathcal{S}(\tau)$  is represented by a specific SLL. This requires the construction of an AM constellation of size  $N_{\text{SLL}}$ , denoted as  $\mathbb{D}_{\text{AM}} = \{\delta_1, \dots, \delta_{N_{\text{SLL}}}\}$ . For the SIMO radar case, achieving this number of distinct SLLs requires the design of  $N_{\text{SLL}}$  transmit beamforming weight vectors  $\mathbf{q}_n, n = 1, \dots, N_{\text{SLL}}$  such that

$$P |\mathbf{q}_n^H \mathbf{a}(\theta_c)|^2 = \delta_n, \quad n = 1, \dots, N_{\text{SLL}}. \quad (8)$$

One way to design the beamforming vectors  $\mathbf{q}_n, n = 1, \dots, N_{\text{SLL}}$  while satisfying the radar operation condition (6) and the communication SLLs (8) is to minimize the difference between the desired and actual transmit radiation patterns under the constraints that the sidelobe attenuation is kept above a certain predefined level. This can be formulated as the following optimization problem [18]:

$$\min_{\mathbf{q}_n} \max_{\theta} |d(\theta) - |\mathbf{q}_n^H \mathbf{a}(\theta)||, \quad \theta \in \Theta_{\text{SIMO}} \quad (9)$$

$$\text{subject to } |\mathbf{q}_n^H \mathbf{a}(\theta)| \leq \delta_{\text{SLL}}, \quad \theta \in \bar{\Theta}_{\text{SIMO}}, \quad (10)$$

$$\mathbf{q}_n^H \mathbf{a}(\theta_c) = \delta_n, \quad n = 1, \dots, N_{\text{SLL}}, \quad (11)$$

where  $d(\theta)$  is the desired transmit beampattern,  $\Theta_{\text{SIMO}}$  denotes the sidelobe region, and  $\delta_{\text{SLL}} > 0$  is a design parameter used to control the sidelobe attenuation level. Since  $\delta_{\text{SLL}}$  is the highest SLL as mandated by the radar operation, the condition  $\delta_n \leq \delta_{\text{SLL}}, n = 1, \dots, N_{\text{SLL}}$  should be satisfied. An alternative approach to beampattern sidelobe modulation using time-modulated arrays is developed in [16].

Let  $\delta(\tau) \in \mathbb{D}_{\text{AM}}$  be the communication symbol to be embedded during the  $\tau$ th radar pulse. The corresponding transmit beamforming weight vector,  $\mathbf{w}(\tau)$ , is selected from the set of weight vectors  $\{\mathbf{q}_1, \dots, \mathbf{q}_{N_{\text{SLL}}}\}$ , and the baseband signal at a single-antenna communication receiver becomes

$$y_{\text{com}}(t; \tau) = \alpha_{\text{ch}} \sqrt{P} \underbrace{\mathbf{w}^H(\tau) \mathbf{a}(\theta_c)}_{\delta(\tau)} \phi(t) + n(t; \tau), \quad (12)$$

where  $\mathbf{w}(\tau) \in \{\mathbf{q}_1, \dots, \mathbf{q}_{N_{\text{SLL}}}\}$ . The channel coefficient,  $\alpha_{\text{ch}}$ , summarizes the propagation environment between the transmit array and the communication receiver and  $n(t; \tau)$  is the additive white Gaussian noise with zero mean and power spectral density  $N_0$ . Matched-filtering the communication received signal (12) by the transmitted waveform yields

$$y_{\text{AM}}(\tau) = \int_{T_\phi} y_{\text{com}}(t; \tau) \phi^*(t) dt = \alpha_{\text{ch}} \sqrt{P} \delta(\tau) + n(\tau), \quad (13)$$

where the additive noise term,  $n(\tau)$ , at the output of the matched filter has the same statistics as  $n(t; \tau)$ . Then, the embedded communication symbol can be detected by performing the comparison test

$$\hat{\delta}(\tau) = \delta_n, \text{ if } T_n \leq |y_{\text{AM}}(\tau)| < T_{n-1}, \quad n = 1, \dots, N_{\text{SLL}}, \quad (14)$$

where  $T_0 = 0 < T_1 < \dots < T_{N_{\text{SLL}}-1} < \delta_{N_{\text{SLL}}}$  denote a set of appropriately selected thresholds.

For the MIMO radar case,  $M$  symbols can be embedded during the  $\tau$ th pulse; one per orthogonal waveform. Using the waveform orthogonality at the communication receiver, the embedded symbols can be detected in a way similar to (13) and (14).

Beampattern ASK [18] uses multiple orthogonal waveforms and employs two SLLs in the communication direction to embed one bit per waveform per pulse corresponding to a symbol dictionary  $\mathbb{D}_{\text{ASK}} = \{\Delta_H, \Delta_L\}$ , where  $\Delta_H > \Delta_L$ . Let  $\Delta_m(\tau)$  be the binary bit that needs to be embedded in the  $m$ th waveform during pulse  $\tau$ . Then, the signal at the output of the matched filter of the communication receiver is

$$y_{\text{ASK}}^{(m)}(\tau) = \begin{cases} \alpha_{\text{ch}} \sqrt{P} \Delta_H + n(\tau), & \Delta_m(\tau) = 1, \\ \alpha_{\text{ch}} \sqrt{P} \Delta_L + n(\tau), & \Delta_m(\tau) = 0, \end{cases} \quad m = 1, \dots, M. \quad (15)$$

The receiver detects the symbol  $\Delta_m(\tau)$  by performing the test  $|y_{\text{ASK}}^{(m)}(\tau)| \leq T$ , given an appropriate threshold  $T$ .

To illustrate, Figure 3 shows a realization of the optimum beampattern with  $P = 1$ ,  $\Delta_H^2 = 10^{-2}$ , and  $\Delta_L^2 = 10^{-5}$ , giving SLLs of  $-20$  and  $-50$  dB, respectively. The communication

direction is  $-50^\circ$  and the radar mainbeam is  $\Theta_{\text{SIMO}} = [-15^\circ, 15^\circ]$ . It is evident that the two beampatterns are almost identical within the mainbeam, ensuring that the radar operation is not affected by the information embedding. Figure 4 shows the probability density functions of  $|y_{\text{ASK}}^{(m)}(\tau)|$ . The shaded areas represent the probability of bit error.

### Beampattern PM

This technique embeds information by controlling the phase of the transmit beampattern in the direction of the communication receiver. Information embedding using PSK, recently reported in [17], requires the construction of a PSK dictionary denoted as  $\mathbb{D}_{\text{PSK}} = \{\Omega_1, \dots, \Omega_{N_{\text{PSK}}}\}$ . The PSK

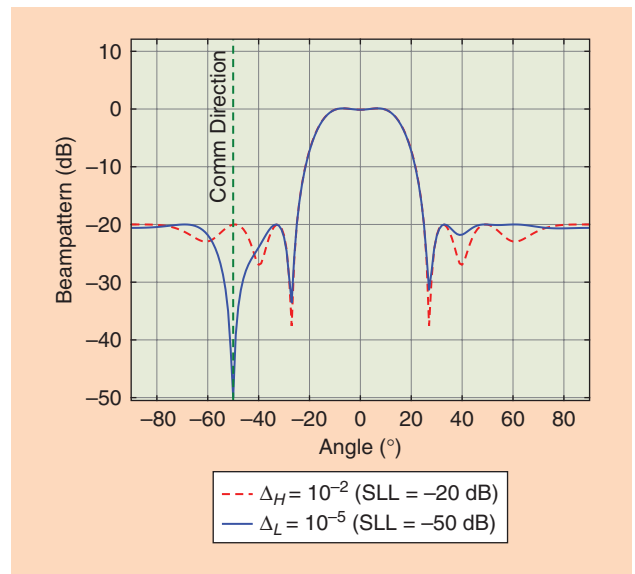


**FIGURE 3.** A transmit beampattern with two distinct SLLs toward the communication direction. Comm: communication.

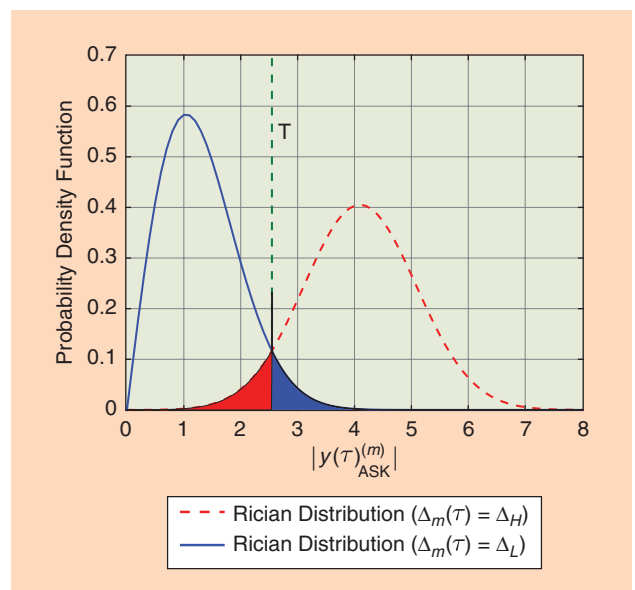


**FIGURE 4.** A graph showing probability distribution of the magnitude of signal at output of the matched filter.

symbols can be chosen to be uniformly distributed on the unit circle. Each PSK symbol represents a unique sequence of  $N_{\text{bit}} = \log_2(N_{\text{PSK}})$  binary bits. The beamforming weight vectors associated with the PSK-modulated beampatterns can be designed using the formulation (9)–(11) but with (11) replaced by the following set of constraints:

$$\mathbf{q}_n^H \mathbf{a}(\theta_c) = d(\theta_c) e^{j\Omega_n}, \quad n = 1, \dots, N_{\text{PSK}}. \quad (16)$$

Here,  $\Omega_n$  denotes the  $n$ th PSK symbol in the constellation  $\mathbb{D}_{\text{PSK}}$ , and  $d(\theta_c)$  is the desired transmit gain in the communication direction. The constraints in (16) dictate the phase of the beampattern, which then permits communications within the mainbeam of the radar.

Let  $\Omega(\tau) \in \mathbb{D}_{\text{PSK}}$  be the symbol embedded during the  $\tau$ th pulse. Then, the signal at the output of the matched filter of the communication receiver can be modeled as

$$y_{\text{PSK}}(\tau) = \alpha_{\text{ch}} \sqrt{P} d(\theta_c) e^{j\Omega(\tau)} + n(\tau). \quad (17)$$

The embedded PSK symbol can be extracted from the phase of  $y_{\text{PSK}}(\tau)$ . For coherent communications, the phase of the channel coefficient  $\alpha_{\text{ch}}$  should be known or accurately estimated. However, noncoherent PSK-based communications is also possible by transmitting two waveforms simultaneously. The PSK symbol is embedded as a phase rotation of one of the two waveforms with respect to the other [17].

Figure 5 shows a comparison between the bit error rate performance versus  $E_b/N_0 \triangleq 10 \log_{10}(|\alpha_{\text{ch}}|^2 \Delta_H^2 / N_{\text{bit}} N_0)$ , where  $E_b$  denotes the energy per bit. The figure compares the performances of the beampattern AM, ASK, and PSK methods for a SIMO radar with a 10-element array. The communication direction is  $\theta_c = -50^\circ$  and the radar mainbeam is focused toward  $0^\circ$ . The number of bits per pulse is fixed at  $N_{\text{bit}} = 2$  bits

for all methods. The figure shows that the ASK method using two SSLs and two orthogonal waveforms outperforms the AM method with four SLLs and a single waveform. The PSK approach offers the best performance of all three methods.

Beampattern modulation techniques may result in reduced aperture efficiency of the radar transmit array. As a result, the transmit coherent processing gain of the radar may be decreased, leading to a reduction in the signal-to-noise ratio (SNR) of the radar target signal. This can make target detection less reliable and/or reduce the parameter-estimation accuracy.

### Information embedding using IM

IM refers to a wide class of modulation approaches where the information is represented by the index of some quantity from a set of available values for that quantity. Unlike traditional modulation schemes, where the symbol belongs to a constellation, IM can include nontraditional symbol sets, such as the index of an antenna from a set of antennas. A number of IM techniques have been proposed in the context of DFRC. In [21], waveform shuffling was used to embed information using the association of a waveform with an antenna. Initially proposed in [10], was recently employed in [22] to embed communications symbols into the radar waveforms in emission-constrained scenarios.

### DFRC using CSK

Advances in waveform design and generation are enabling technologies that change radar waveforms from pulse to pulse. This has opened up the possibility of employing the waveform itself as a means of embedding communication symbols [10], [22]. Such a scheme is referred to as CSK as each waveform is akin to a code representing a particular symbol. Suppose that a dictionary of  $M_c$  orthogonal waveforms is available, with  $M_c$  assumed to be a power of two. Then, using each waveform as a communication symbol,  $N_{\text{bit}}$  per pulse can be transmitted, where

$$N_{\text{bit}} = \log_2 M_c. \quad (18)$$

For a code comprising  $N_c$  chips and a chip duration  $t_c$ , the maximum achievable bit rate becomes  $N_{\text{bit}}/N_c t_c$ , with the actual bit rate being given by  $R = N_{\text{bit}} f_{\text{PRF}}$ , where  $f_{\text{PRF}}$  is the PRF of the radar.

Implementing such a CSK scheme in the context of radar demands careful waveform design to ensure that the radar operation is not compromised. This requires that the autocorrelation across pulses, that is for different waveforms, remains constant despite the change in waveform. However, as pointed out in [10], changing the waveforms from pulse to pulse leads to undesirable range sidelobe modulation (RSM). To address this issue, mismatched filters were developed. From the communications operation perspective, the cross correlation between different pairs of waveforms should be as small as possible. Gold and Kasami codes are pseudorandom sequences that possess desirable cross-correlation values. They are proposed in [22] for emission-constrained scenarios to implement the

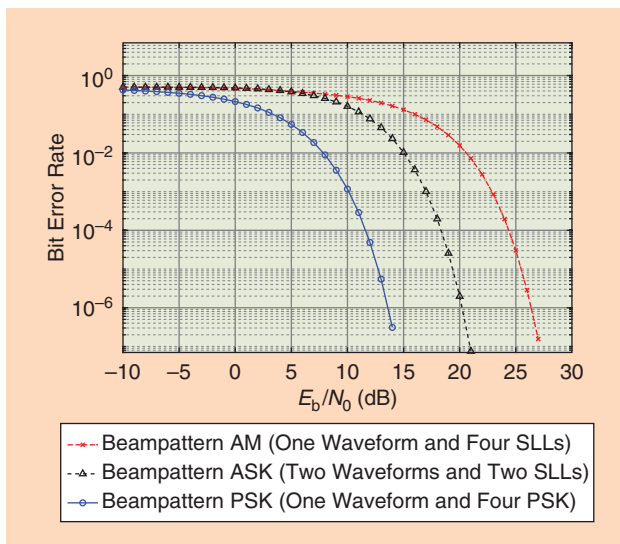


**FIGURE 5.** A graph showing the bit error rate versus signal-to-noise ratio for three beampattern modulation methods for a SIMO radar with 10-element transmit array;  $N_{\text{bit}} = 2$  and  $\theta_c = -50^\circ$ .

communications function while providing a low probability of intercept (LPI) feature. These codes can be PSK-modulated to increase the bit rate. For binary PSK (BPSK) modulation, the bit rate becomes  $R = f_{\text{PRF}}(\log_2 M_c + 1)$ .

The Gold and Kasami codes were evaluated in terms of their symbol error rate and found to be comparable to the codes for M-ary frequency-shift keying. Their radar performances were assessed against random binary phase coded radar using range and Doppler resolutions as well as range and Doppler sidelobes. The zero-delay cut of the periodic ambiguity function (AF) of a 255-bit BPSK-modulated Kasami code is shown in Figure 6(a) while the zero-Doppler cut is shown in Figure 6(b). The Kasami code exhibits a sharp autocorrelation function and low sidelobes on the zero-delay cut.

#### DFRC via frequency-hopping code selection

An alternative IM technique employs frequency-hopping (FH) code selection to embed information into the radar signal [23]. Suppose we have a MIMO radar with  $M$  antennas and  $K$  frequencies that can be used to generate the frequency-hopped waveforms. For each hop, we can use the frequencies associated with the  $M$  antennas as the code. Therefore, we are able to embed  $Q$  symbols per pulse, where  $Q$  is the number of hops. Given  $K$  frequencies for the hops, the number of possible combinations—that is, the number of symbols—is  $L = \binom{M}{K}$ . The achievable bit rate is, therefore,

$$R = |\log_2 L| Q f_{\text{PRF}}. \quad (19)$$

This method is simple to implement and achieves higher bit rates than the previous approaches at the expense of changing the fast-time structure of the radar pulse.

#### DFRC using waveform permutations

In multiple antenna systems employing a MIMO configuration, the antenna–waveform pairing can be used to convey information to a communications receiver at a known direction [21]. Although the antenna–waveform pairing must be known

in a MIMO radar, the association of a particular waveform to a specific antenna is arbitrary. Swapping waveforms between different antennas does not affect the operation of the radar, provided this swap is reflected at the radar receiver. Thus, using the antenna–waveform pairing to embed information into the radar signal is a form of IM that is entirely transparent to the radar.

In a MIMO system with  $K$  antennas and an associated set of  $M$  orthogonal waveforms, shuffling the waveforms between the transmit antennas provides a constellation of  $M!$  symbols, where  $\bullet!$  denotes the factorial. This allows the transmission of  $\lfloor \log_2(M!) \rfloor$  bits per PRI. Let  $\mathbf{P}$  be a  $M \times M$  permutation matrix. Applying  $\mathbf{P}$  to the waveform matrix  $\phi(t)$  gives the shuffled waveform matrix  $\psi(t) = \mathbf{P}\phi(t)$ . The MIMO transmit signal then becomes

$$\mathbf{s}_{\text{MIMO}}(t; \tau) = \sqrt{\frac{P}{M}} \mathbf{W} \psi(t). \quad (20)$$

The communications receiver is assumed to have perfect knowledge of the radar waveforms,  $\phi(t)$ . Upon correlation with the unshuffled set of waveforms  $\phi(t)$ , the received signal becomes

$$\mathbf{r}_c(t) = \alpha_{\text{ch}} \mathbf{P}^T \mathbf{W}^H \mathbf{a}(\theta_c) + \mathbf{n}(t), \quad (21)$$

where  $\mathbf{a}(\theta_c)$  is the steering vector in the direction of the communication receiver,  $\theta_c$ , which is assumed to be known. Setting  $\mathbf{a}_s(\theta_c) = \mathbf{P}^T \mathbf{W}^H \mathbf{a}(\theta_c)$ , we observe that the shuffling matrix  $\mathbf{P}$  can be recovered from the received signal by comparing the received steering vector  $\mathbf{a}_s(\theta_c)$  to the unshuffled vector  $\mathbf{a}_u = \mathbf{W}^H \mathbf{a}(\theta_c)$ . The achievable bit rate of this scheme is  $\lfloor \log_2(M!) \rfloor f_{\text{PRF}}$  bits/s.

#### Information embedding in fast time

These approaches operate on a pulse basis and their achievable bit rates are limited to the order of the PRF of the radar. To overcome this limitation, information embedding in fast time is needed where the radar waveform is modulated from pulse to pulse [12], [24]. However, increased data rates come at the expense of reduced radar performance.

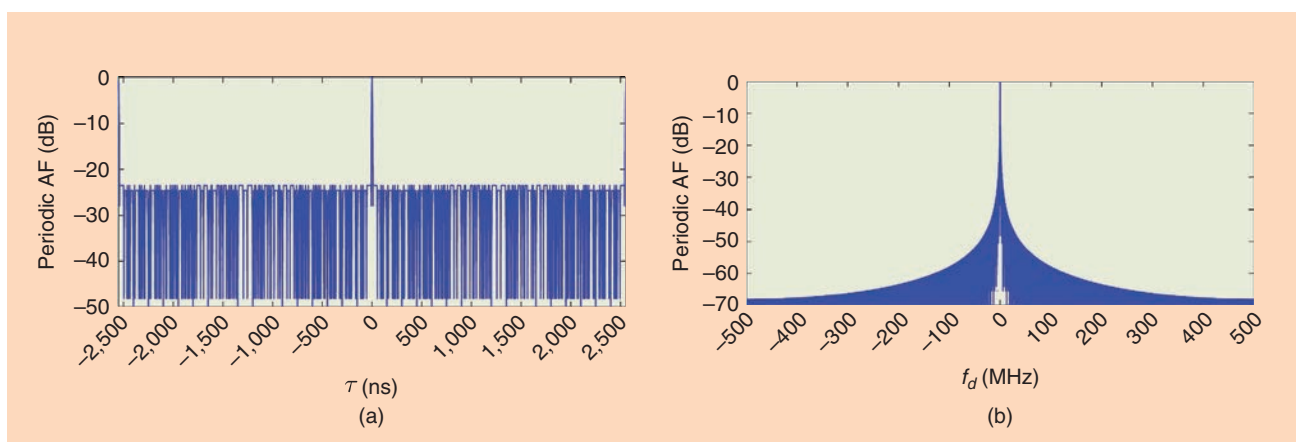


**FIGURE 6.** Two graphs showing (a) a zero-delay cut and (b) a zero-Doppler cut of the periodic AF of a 255-bit BPSK-modulated Kasami code [22].

## Communications via waveform modulation

The first approach to fast-time information embedding in DFRC systems assumes that the waveforms are already designed to optimize the radar operation. The radar pulse is then divided into a number of subpulses and a communication symbol is embedded into each subpulse. To preserve the constant envelope feature of the original radar pulse, each subpulse is multiplied by a complex scalar of unit magnitude and PSK phase symbol [12].

In [24], each subpulse is modulated using continuous phase modulation symbols. This modulation preserves the constant modulus of the original radar waveform and enables frequency bandwidth confinement. The techniques in [12] and [24] and waveform-modulation techniques, in general, alter the modulus and/or phase profile of the predesigned waveforms. This change, in turn, affects the power and spectral efficiency of the radar operation. Reduced power efficiency may lead to deterioration in radar performance, leading to lower target-detection probability or increased probability of a false alarm. In addition, waveform modulation changes the AF of the waveform and its associated range-Doppler characteristics. This is similar to the CSK scheme described in the section “DFRC Using CSK.” A mismatched filter design method is proposed in [25] to address the RSM issue. The highest data rate is obtained if the communication symbol duration is equal to the inverse of the bandwidth of the DFRC system. In this case, the disturbance to the radar would be the maximum.

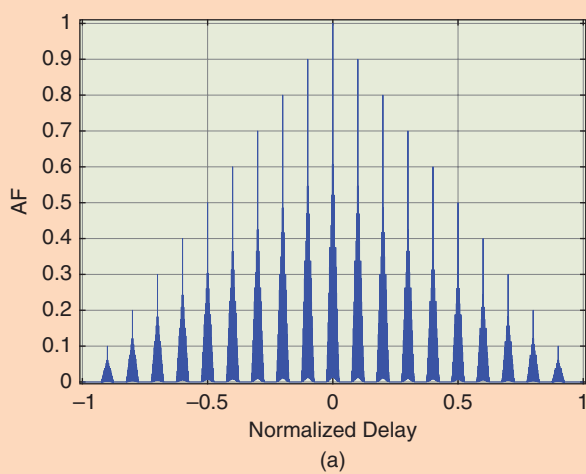
In [26], a fast-time DFRC method using FH waveforms and PSK signaling is proposed and analyzed. Generally, one expects that embedding communication symbols will hinder radar operation. However, it was shown that modulation of the FH radar pulse can benefit both radar and communications. Analysis of the impact of PSK symbol embedding on the AF of a MIMO radar revealed that symbol embedding yields a reduction in the SLLs of the AF of the original FH waveforms. A comparison of the AF with and without the PSK symbol embedding affirmed the benefit of communication embedding. Figure 7(a) and (b) shows the zero Doppler cut of the AF

for a series of 10 pulses of FH waveforms where each pulse comprises 16 hops [26]. It is evident that embedding quaternary PSK symbols into each hop of the radar pulses significantly reduces the sidelobe peaks of the AF.

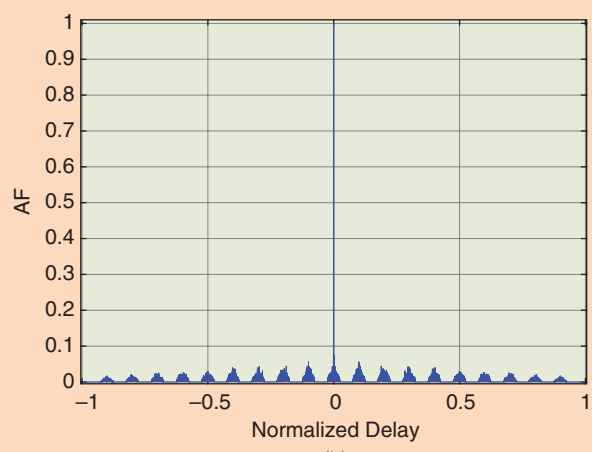
## Waveform design for DFRC systems

An alternative fast-time information embedding approach involves designing dual-function waveforms that can be used simultaneously to probe the radar targets and deliver communication symbols. In [27], a method was proposed for designing a set of physical multifunction waveforms that realize far-field radar and communication signals at the same time using a common MIMO transmit structure and the same spectral support. The essence of this method is to employ space-division multiple-access such that the radar and communication signals are concurrently generated in the far field in the target and communication receiver directions, respectively. A similar approach to waveform design for DFRC is developed in [28], where a MIMO configuration is used for simultaneous target detection and downlink communications. The idea behind this approach is to design transmit waveforms that approximate the required communication symbols at the communication receiver, which is achieved by minimizing the multiuser interference. The radar operation is assured by enforcing the mutual orthogonality of the waveforms. Both methods in [27] and [28] optimize the transmitted waveforms on a pulse-to-pulse basis while satisfying radar-specific constraints, such as constant modulus structure and waveform similarity.

Another waveform design approach to DFRC, recently proposed in [13], exploits the quasiorthogonality of different chirp rates to embed communication symbols into the radar emissions, while at the same time preserving the performance of a linear-frequency modulation (LFM) pulse radar. The scheme uses the fractional Fourier transform (FrFT), allowing chirp subcarriers to be used in place of sinusoids, as in the case of orthogonal frequency-division multiplexing (OFDM) waveforms. The FrFT waveform performs in a way similar



(a)



(b)

**FIGURE 7.** Two graphs showing AF zero-Doppler cut for a series of 10 pulses of FH waveforms (a) without information embedding and (b) with quaternary PSK symbol embedding.

to that of an LFM pulse in terms of probabilities of detection and false alarm, while maintaining a comparable communication performance with respect to the OFDM waveform. This, however, comes at the expense of slightly worse range and Doppler resolution.

The FrFT is a generalization of the Fourier transform that gives a representation of the signal at some angle  $\phi$  in the time–frequency plane. The FrFT of order  $\alpha$  of a length- $N$  signal  $s[k]$ , is given by

$$S_\alpha[n] = \sum_{k=-\frac{N}{2}}^{\frac{N}{2}} K_\alpha[n, k] s[k]. \quad (22)$$

Here,  $K_\alpha[n, k]$  is the FrFT kernel of fractional order  $\alpha$  given in terms of the angle of rotation as  $\alpha = 2\phi/\pi$ .

To embed information into the LFM radar, different linear chirps corresponding to equispaced values of the order  $\alpha$  are used as subcarriers. Then,  $N$  bits to be transmitted can be used to modulate the carrier using some minimum-shift keying scheme to give the signal  $s_i[n]$ , which can then be “rotated” to the required  $\phi$  using (22). Thus, given  $N_c$  subcarriers,  $N_c$  blocks of  $N$  bits can be used to generate MPSK-modulated signals  $s_i[k]$  for  $i = 1 \dots N_c$ . The resulting information-bearing radar pulse is then obtained as [13]

$$x[n] = \sum_{k=-\frac{N}{2}}^{\frac{N}{2}} K_\alpha[n, k] s_i[k]. \quad (23)$$

In this manner, the achievable bit rate is  $N_c \times N \times f_{\text{PRF}}$  b/s.

## Uplink communications for DFRC systems

In most practical situations, communicating is a two-way process. However, very little work has been reported on uplink communications in DFRC systems. Uplink communications, in this context, involves transmitting data from remote users to a radar platform. In this section, we discuss the importance of achieving uplink communications in DFRC systems and highlight the challenges involved. We then present a review of recent work in this area.

Consider a cooperative communication user transmitting in the field of view of a MIMO radar with a colocated receive array operating in the same frequency band as the user. Receive beamforming can be used to detect and extract the communication signal if it impinges on the receive array from a direction other than that of the radar target(s) of interest. However, when the communication signal and target returns arrive from the same direction, the problem of separating them becomes far more challenging.

### DFRC uplink signaling

A new approach to uplink communications within the main-beam of a DFRC system, recently developed in [29], uses the same waveforms of the DFRC system to link to the remote communications user. The DFRC platform simultaneously re-

ceives target reflections as well as uplink signals emitted by the user. Perfect synchronization is assumed between the DFRC system and communication user in slow time and fast time, i.e., both systems use the same time reference, PRI, and fast-time sampling. Uplink signaling is then achieved by transmitting a linear combination of the MIMO radar orthogonal waveforms. Each column of the mixing matrix represents a virtual spatial signature that can be used to embed a communication symbol. The uplink communication signals may be separated from the target returns as the spatial signature of the uplink signal is designed to be orthogonal to the spatial steering vector of the target. This enforced orthogonality allows beamforming techniques at the DFRC receiver to separate the communication signal from the target return even if they both arrive from the same direction. Thus, cross-interference between the received communication signal and reflected radar signals can be effectively mitigated.

Now let the communication function of the DFRC system be half duplex, i.e., when uplink communications take place, the DFRC system does not embed downlink data into the same pulse and vice versa. Let the radar transmitter have a conventional MIMO configuration, with  $M$  orthogonal waveforms  $\phi_m(t)$ ,  $m = 1, \dots, M$ . Furthermore, assume that during the  $\tau$ th pulse, there are  $Q_{\text{ul}}$  contiguous symbol durations available for uplink transmission (Figure 8). In this respect, the maximum number of time intervals available depends on the ratio of the PRI to the pulse duration, that is,  $Q_{\text{ul}} = \lfloor T_{\text{PRI}}/T_\phi \rfloor - 1$ , where  $T_{\text{PRI}}$  is the PRI.

Let  $\beta_{m,q}(\tau) \in \mathbb{D}_{\text{ul}}$ ,  $m = 1, \dots, M$ ,  $q = 1, \dots, Q_{\text{ul}}$  denote the uplink communication symbols to be transmitted during the  $\tau$ th pulse, where  $\mathbb{D}_{\text{ul}}$  denotes the uplink symbol constellation of size  $N_{\text{ul}}$ . Let the start of the radar pulse be the fast-time reference. The first  $T_\phi$  seconds of the pulse is reserved for MIMO radar transmission. Then, the complex envelope of the uplink signal transmitted by a single-antenna remote user during the  $\tau$ th pulse can be expressed as

$$c_q(t; \tau) = \sqrt{P_{\text{ul}}} \boldsymbol{\beta}_q^T(\tau) \mathbf{U}^T \boldsymbol{\phi}(t), \\ qT_\phi \leq t \leq (q+1)T_\phi, \quad q = 1, \dots, Q_{\text{ul}}, \quad (24)$$

where  $P_{\text{ul}}$  is the power of the uplink transmitter,  $\boldsymbol{\beta}_q^T(\tau) \triangleq [\beta_{1,q}(\tau), \dots, \beta_{M,q}(\tau)]^T$  is the  $M \times 1$  vector of communication

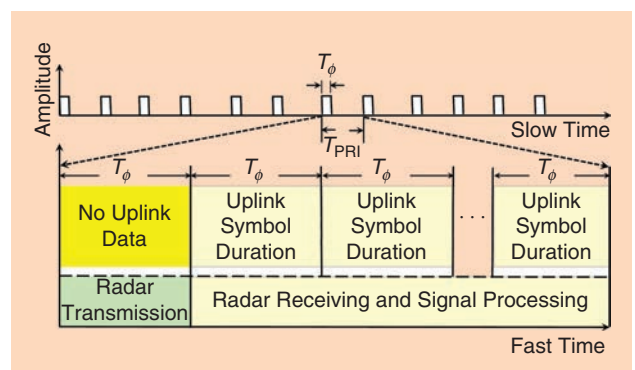


**FIGURE 8.** A diagram showing transmit and receive timing for uplink communications in DFRC systems.

symbols associated with the  $q$ th symbol duration, and  $\mathbf{U} \triangleq [\mathbf{u}_1, \dots, \mathbf{u}_{\tilde{M}}]$  is the  $M \times \tilde{M}$  uplink spatial signature matrix comprising the virtual uplink steering vectors  $\mathbf{u}_m, m = 1, \dots, \tilde{M}$ .

The uplink communication signal together with the returns of  $L$  radar targets impinge simultaneously on the radar receiver, which is assumed to comprise  $N$  antennas arranged in a linear array. Using (2) and (24), the received baseband signal vector can be modeled as

$$\begin{aligned} \mathbf{x}(t; \tau) = & \sqrt{\frac{P}{M}} \sum_{\ell=1}^L \gamma_\ell(\tau) (\mathbf{a}^T(\theta_\ell) \boldsymbol{\phi}(t)) \mathbf{b}(\theta_\ell) \\ & + \alpha_{\text{ch}} c_q(t; \tau) \mathbf{b}(\theta_c) + \mathbf{z}(t; \tau), \end{aligned} \quad (25)$$

where  $\gamma_\ell(\tau)$  is the reflection coefficient of the  $\ell$ th target during the  $\tau$ th pulse,  $\mathbf{b}(\theta_\ell)$  is the  $N \times 1$  steering vector of the receive array toward direction  $\theta_\ell$ ,  $\mathbf{z}(t; \tau)$  is the vector of additive white Gaussian noise with zero mean, and covariance  $\sigma_z^2 \mathbf{I}_N$ , and  $\mathbf{I}_N$  is the  $N \times N$  identity matrix. Matched-filtering the received signal vector  $\mathbf{x}(t; \tau)$  to the vector of orthogonal waveforms yields the  $MN \times 1$  extended complex vector

$$\chi(\tau) = \text{vec}\left(\int_{T_\phi} \mathbf{x}(t; \tau) \boldsymbol{\phi}^H(t) dt\right) = \chi_{\text{radar}}(\tau) + \chi_{\text{com}}(\tau) + \chi_z(\tau), \quad (26)$$

where  $\chi_{\text{radar}}(\tau)$ ,  $\chi_{\text{com}}(\tau)$ , and  $\chi_z(\tau)$  denote the radar return, uplink communications, and additive noise, respectively, at the output of the matched filter. The radar signal term in (26) can be expressed as

$$\chi_{\text{radar}}(\tau) = \sqrt{\frac{P}{M}} \sum_{\ell=1}^L \gamma_\ell(\tau) [\mathbf{a}(\theta_\ell) \otimes \mathbf{b}(\theta_\ell)], \quad (27)$$

where  $\otimes$  denotes the Kronecker product. Similarly, for the uplink communication component we have

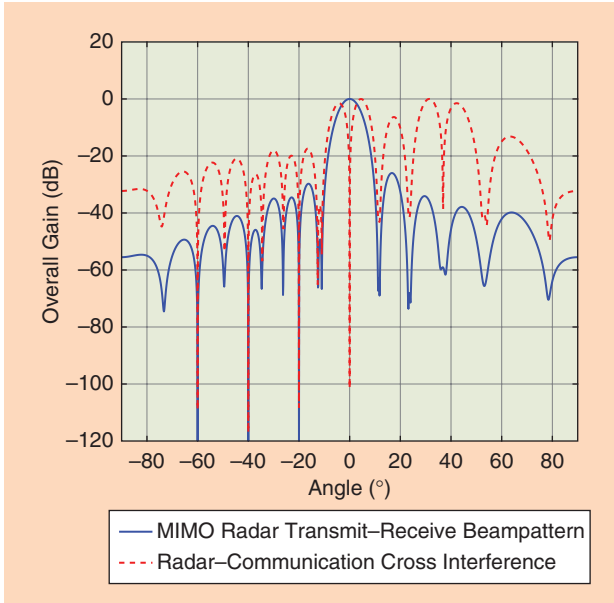


**FIGURE 9.** A graph showing the MVDR beampattern relative to angle for radar receive beamforming as well as radar-communication cross interference.

$$\chi_{\text{com}}(\tau) = \alpha_{\text{ch}} \sqrt{P_{\text{ul}}} \sum_{m=1}^{\tilde{M}} \beta_{m,q}(\tau) [\mathbf{u}_m \otimes \mathbf{b}(\theta_c)], \quad m = 1, \dots, \tilde{M}. \quad (28)$$

To separate the radar signal from the uplink communication signal, two receive beamformers can be used. These can draw on both conventional nonadaptive and adaptive beamforming techniques. To avoid intersymbol interference, the uplink virtual steering vectors can be designed to be orthogonal to one another; that is,

$$\mathbf{u}_m^H \mathbf{u}_{m'} = 0, \quad m, m' = 1, \dots, \tilde{M}, m \neq m'. \quad (29)$$

Furthermore, when  $\theta_{\text{tar}} = \theta_c$ , the uplink communication interference cannot be effectively separated from the radar signal unless the steering vector of the uplink signal is predesigned to be orthogonal to the steering vector of the target. That is,

$$\mathbf{u}_m^H \mathbf{a}(\theta_c) = 0, \quad m = 1, \dots, \tilde{M}. \quad (30)$$

The number of uplink communication symbols that can be transmitted toward the DFRC receiver during one radar pulse is  $\tilde{M} Q_{\text{ul}}$ . Therefore, the uplink data rate in bits per second is given by

$$R_{\text{ul}} = \log_2(N_{\text{ul}}) \cdot \tilde{M} \cdot Q_{\text{ul}} \cdot f_{\text{PRF}}. \quad (31)$$

For medium-to-high radar PRF, uplink data rates of tens of megabits per second are achievable.

To illustrate, we consider a DFRC system with a 10-element MIMO radar. The same array is used for transmitting the radar waveforms and receiving returns from four targets located at  $-60^\circ$ ,  $-40^\circ$ ,  $-20^\circ$ , and  $0^\circ$ , and  $\tilde{M} = 5$  simultaneous uplink symbols arriving from direction  $0^\circ$ . Figure 9 shows the beampattern of the MVDR radar beamformer with the mainbeam focused at  $0^\circ$ . The figure demonstrates that the beamformer adaptively nulls the returns from other targets while using the orthogonality between the target and uplink steering vectors to suppress the uplink interference within the mainbeam.

In [29], spatial diversity is used to separate the target signal from the uplink communication signal. However, if the uplink user is allowed to use different waveforms to the MIMO radar, then the target signal can be separated from the uplink signal using waveform diversity. However, in this case, the cross correlation between the uplink and radar signals would give rise to range-sidelobe modulations that may affect radar performance. More research is needed to examine the impact of uplink communications on radar performance.

### Intrapulse radar-embedded communications

The work on intrapulse radar-embedded communication in [30] implements the communications function over fast time by reradiating a modulated version of the pulse upon scattering from an RF tag or transponder. In this sense, this approach does not use a common transmitter for radar and communications, nor does it employ the same waveform for both systems. Yet it is of interest here as it provides uplink

capability. The proposed novel signal embedding uses the subspace composition of the ambient scattering of the transmitted radar waveform. It achieves LPI by hiding the communication symbols in high-dimensional space defined by the scattering environment and obtained by oversampling the radar signal beyond its Nyquist frequency. Therefore, without prior knowledge of the nature of the embedded signal, it is difficult to separate the communication signal from a masking interference signal, especially if there is a strong masking brought about by inducing partial correlation between the communication signal and clutter. In performing eigendecomposition of the data matrix, which is composed of shifted replicas of the radar pulse, one can use eigenvectors or their combinations to generate orthogonal waveforms for different communication symbols. This leads to small probability of symbol errors when implementing maximum likelihood estimation at the communication receiver.

## Challenges and future trends

The principal challenge in the design of DFRC systems is achieving high data rates with minimum or no distortion to the radar spatiotemporal signal characteristics. Signal embedding for high data rates must account for wireless channel sensing, impairments, and equalization. For example, ship-to-ship communications must deal with fading and multipath effects that are different from those typical of land communications. The SNR needed for combating channel interference must be examined in view of the radar equation and power requirements. Channel-coding techniques would demand additional bits, which may need more radar pulses to communicate the intended message, thus reducing the information rate. In cases where the message changes from one CPI to another, e.g., when communicating target or scheduling information, the code length should be set in relation to the CPI, especially when the communication describes rich information pertaining to the scene. In other cases, messages may not be related to the radar operation, e.g., where the DFRC system is used as a backup to maintain the wireless link when the original designated communication system is no longer operational [20]. In either instance, choosing the most appropriate coding technique for a DFRC system, including linear block codes or convolutional codes, depends on the communication channel and whether the intent is to only detect errors or to both detect and correct them.

Channel estimation in a single-function communication receiver may require a training sequence to be transmitted from the DFRC system. If a separate link between the DFRC transmitter and a single-function communication receiver is to be avoided, this sequence must also be embedded into the radar waveforms. On the other hand, if the situation is reversed and the receiver is dual function, then separating the radar return from the received communication signal becomes vital for both signal demodulation and channel estimation. Further, joint carrier phase and delay estimation at the dual-function receiver must be robust to the radar backscattering.

Bistatic and multistatic DFRC systems present additional challenges compared to monostatic DFRC platforms. A monostatic configuration, which was the subject of this review article, assumes knowledge of the communication symbols transmitted from a common platform. As such, it can opt to restore the radar signal upon receipt, prior to performing matched filtering of the original radar waveform. The monostatic receiver can also implement matched filtering to the modified radar waveform, i.e., to the transmitted signal-embedded radar waveform. The receiver in the bistatic radar configuration, on the other hand, lacks knowledge of the communication signal and, therefore, cannot separate or remove it from the original radar waveform, nor can it perform proper matched filtering. In addition, clutter cancellation in DFRC can be challenging due to beampattern sidelobe modulation, RSM, and/or fast-time structure variation of the radar waveform. Signal-dependent interference due to clutter scattering may also affect communication symbol detection [9].

Notwithstanding the significant strides that have already been made, DFRC systems stand to benefit greatly from the wealth of knowledge in the communications literature. Advances in symbol coding, symbol detection, channel estimation, multiuser interference mitigation, synchronization, and error detection and correction should be informed by the state of the art in the communications area.

## Authors

**Aboulnasr Hassanien** (hassanien@ieee.org) received his B.Sc. and M.Sc. degrees in electronics and communications engineering from Assiut University, Egypt, in 1996 and 2001, respectively, and his Ph.D. degree in electrical engineering from McMaster University, Canada, in 2006. He has been with the Department of Electrical Engineering at Wright State University, Dayton, Ohio, since 2016. He is the recipient of the 2017 IEEE Aerospace and Electronic Systems Society Harry Rowe Mimno Award. He is an associate editor of *IEEE Transactions on Signal Processing*. He served as the lead guest editor of the *Digital Signal Processing* special issue on cooperation and joint design of communications and radar systems and as guest editor of the *International Journal of Antennas and Propagation* special issue on advances in direction-of-arrival estimation and source localization.

**Moeness G. Amin** (moeness.amin@villanova.edu) received his B.Sc. degree in electrical engineering from the Faculty of Engineering, Cairo University, Egypt, in 1976, his M.Sc. degree in electrical engineering from the University of Petroleum and Minerals, Saudi Arabia, in 1980, and his Ph.D. degree in electrical engineering from the University of Colorado, Boulder, in 1984. Since 1985, he has been on the faculty of the Department of Electrical and Computer Engineering at Villanova University, Pennsylvania, where he is currently a professor and the director of the Center for Advanced Communications. He is a recipient of the 2017 Fulbright Distinguished Chair in Advanced

Science and Technology, the 2016 Humboldt Research Award, the 2016 Institution of Engineering and Technology Achievement Medal, the 2015 IEEE Warren D. White Award for Excellence in Radar Engineering, the 2014 IEEE Signal Processing Society Technical Achievement Award, the 2009 European Association for Signal Processing Technical Achievement Award, and the IEEE Third Millennium Medal. He is a Fellow of the IEEE, European Association for Signal Processing, the Society of Photo-Optical Instrumentation Engineers, and the Institution of Engineering and Technology.

**Elias Aboutanios** ([elias@ieee.org](mailto:elias@ieee.org)) received his bachelor degree in electrical engineering in 1997 from the University of New South Wales, Australia, and his Ph.D. degree in 2003 from the University of Technology Sydney, Australia. From 2003 to 2007, he was a research fellow with the Institute for Digital Communications, University of Edinburgh. He is currently associate professor at the University of New South Wales, Australia. He is an associate editor of *IEEE Transactions on Signal Processing* and *IET Signal Processing*. His research interests are in statistical signal processing, in particular signal detection and parameter estimation, for applications such as radar, the Global Navigation Satellite System, smart grids, and nuclear magnetic resonance spectroscopy. He established and led the University of New South Wales EC0 CubeSat Project, which culminated in the launch of the satellite in 2017.

**Brahim Himed** ([brahim.himed@us.af.mil](mailto:brahim.himed@us.af.mil)) received his degree in electrical engineering from the Ecole Nationale Polytechnique of Algiers, El Harrach, Algeria, in 1984 and his M.S. and Ph.D. degrees, both in electrical engineering, from Syracuse University, New York, in 1987 and 1990, respectively. He is a division research fellow with the Air Force Research Laboratory, Sensors Directorate, Multispectral Sensing and Detection Division, in Dayton, Ohio, where he is involved with several aspects of radar development. He is the recipient of the 2001 IEEE Region 1 Award for his work on bistatic radar systems, algorithm development, and phenomenology. He received the 2012 IEEE Warren White Award for excellence in radar engineering. He is a past chair of the IEEE Aerospace & Electronics Systems Society Radar Systems Panel. He is a Fellow of the IEEE and of the Air Force Research Laboratory.

## References

- [1] H. Griffiths, L. Cohen, S. Watts, E. Mokole, C. Baker, M. Wicks, and S. Blunt, "Radar spectrum engineering and management: Technical and regulatory issues," *Proc. IEEE*, vol. 103, pp. 85–102, Jan. 2015.
- [2] H. T. Hayaci and B. Tavli, "Spectrum sharing in radar and wireless communication systems: A review," in *Proc. Int. Conf. Electromagnetics in Advanced Applications*, Aug. 2014, pp. 810–813.
- [3] J. M. Chapin, "Shared spectrum access for radar and communications (SSPARC)," Defense Advanced Research Projects Agency, Arlington, VA, Tech. Rep. DARPA BAA-13-24, Feb. 2013.
- [4] A. R. Chiriyath, B. Paul, and D. W. Bliss, "Radar-communications convergence: Coexistence, cooperation, and co-design," *IEEE Trans. Cogn. Commun. Netw.*, vol. 3, no. 1, pp. 1–12, Mar. 2017.
- [5] S. D. Blunt and E. S. Perrins, eds., *Radar and Communication Spectrum Sharing*. Stevenage, U.K.: Institution of Engineering and Technology, 2018.
- [6] E. Biglieri, A. J. Goldsmith, L. J. Greenstein, H. V. Poor, and N. B. Mandayam, *Principles of Cognitive Radio*. Cambridge, U.K.: Cambridge Univ. Press, 2013.
- [7] J. R. Guerci, *Cognitive Radar: The Knowledge-Aided Fully Adaptive Approach*. Norwood, MA: Artech House, 2010.
- [8] B. Li, A. P. Petropulu, and W. Trappe, "Optimum co-design for spectrum sharing between matrix completion based MIMO radars and a MIMO communication system," *IEEE Trans. Signal Process.*, vol. 64, no. 17, pp. 4562–4575, Sept. 2016.
- [9] J. Qian, M. Lops, L. Zheng, X. Wang, and Z. He, "Joint system design for coexistence of MIMO radar and MIMO communication," *IEEE Trans. Signal Process.*, vol. 66, pp. 3504–3519, July 2018.
- [10] S. D. Blunt, M. R. Cook, and J. Stiles, "Embedding information into radar emissions via waveform implementation," in *Proc. Int. Waveform Diversity and Design Conf.*, Aug. 2010, pp. 195–199.
- [11] A. Hassanien, M. G. Amin, Y. D. Zhang, and F. Ahmad, "Signaling strategies for dual-function radar communications: An overview," *IEEE Aerospace and Electron. Syst. Mag.*, vol. 31, pp. 36–45, Oct. 2016.
- [12] M. Nowak, M. Wicks, Z. Zhang, and Z. Wu, "Co-designed radar-communication using linear frequency modulation waveform," *IEEE Aerospace and Electron. Syst. Mag.*, vol. 31, pp. 28–35, Oct. 2016.
- [13] D. Gaglione, C. Clemente, C. V. Ilioudis, A. R. Persico, I. K. Proudlar, J. J. Soraghan, and A. Farina, "Waveform design for communicating radar systems using fractional Fourier transform," *Dig. Signal Process.*, vol. 80, pp. 57–69, 2018.
- [14] C. Sturm and W. Wiesbeck, "Waveform design and signal processing aspects for fusion of wireless communications and radar sensing," *Proc. IEEE*, vol. 99, pp. 1236–1259, July 2011.
- [15] R. M. Mealey, "A method for calculating error probabilities in a radar communication system," *IEEE Trans. Space Electron. Telemetry*, vol. 9, pp. 37–42, June 1963.
- [16] J. Ezuière, R. Guinvarc'h, M. Lesturgie, B. Uguen, and R. Gillard, "Dual function radar communication time-modulated array," in *Proc. Int. Radar Conf.*, Oct. 2014. doi: 10.1109/RADAR.2014.7060416.
- [17] A. Hassanien, M. G. Amin, Y. D. Zhang, and F. Ahmad, "Phase-modulation based dual-function radar-communications," *IET Radar, Sonar Navigation*, vol. 10, pp. 1411–1421, Oct. 2016.
- [18] A. Hassanien, M. G. Amin, Y. D. Zhang, and F. Ahmad, "Dual-function radar-communications: Information embedding using sidelobe control and waveform diversity," *IEEE Trans. Signal Process.*, vol. 64, pp. 2168–2181, Apr. 2016.
- [19] S. D. Blunt and E. L. Mokole, "Overview of radar waveform diversity," *IEEE Aerospace and Electron. Syst. Mag.*, vol. 31, pp. 2–42, Nov. 2016.
- [20] A. de Oliveira Ferreira, R. Sampaio-Neto, and J. M. Fortes, "Robust sidelobe amplitude and phase modulation for dual-function radar-communications," *Trans. Emerging Telecommunications Technologies*, Mar. 2018. doi: 10.1002/ett.3314.
- [21] A. Hassanien, E. Aboutanios, M. G. Amin, and G. A. Fabrizio, "A dual-function MIMO radar-communication system via waveform permutation," *Dig. Signal Process.*, vol. 83, pp. 118–128, 2018.
- [22] T. W. Tedesco and R. Romero, "Code shift keying based joint radar and communications for EMCON applications," *Dig. Signal Process.*, vol. 80, pp. 48–56, 2018.
- [23] W. Baxter, E. Aboutanios, and A. Hassanien, "Dual-function MIMO radar-communications via frequency-hopping code selection," in *Proc. 52nd Asilomar Conf. Signals, Systems and Computers*, Oct. 2018.
- [24] C. Sahin, J. Jakabosky, P. M. McCormick, J. G. Metcalf, and S. D. Blunt, "A novel approach for embedding communication symbols into physical radar waveforms," in *Proc. IEEE Radar Conf.*, Seattle, WA, May 2017, pp. 1498–1503.
- [25] C. Sahin, J. G. Metcalf, and S. D. Blunt, "Filter design to address range sidelobe modulation in transmit-encoded radar-embedded communications," in *Proc. IEEE Radar Conf.*, Seattle, WA, pp. 1509–1514, May 2017.
- [26] I. P. Eedara, A. Hassanien, M. G. Amin, and B. D. Rigling, "Ambiguity function analysis for dual-function radar communications using PSK signaling," in *Proc. 52nd Asilomar Conf. Signals, Systems and Computers*, Oct. 2018.
- [27] P. M. McCormick, S. D. Blunt, and J. G. Metcalf, "Simultaneous radar and communications emissions from a common aperture, Part I: Theory," in *Proc. IEEE Radar Conf.*, Seattle, WA, May 2017, pp. 1685–1690.
- [28] F. Liu, L. Zhou, C. Masouros, A. Li, W. Luo, and A. Petropulu, "Toward dual-functional radar-communication systems: Optimal waveform design," *IEEE Trans. Signal Process.*, vol. 66, pp. 4264–4279, Aug. 2018.
- [29] A. Hassanien, C. Sahin, J. G. Metcalf, and B. Himed, "Uplink signaling and receive beamforming for dual-function radar communications," in *Proc. IEEE Int. Workshop Signal Processing Advances in Wireless Communications*, June 2018. doi: 10.1109/SPAWC.2018.8445858.
- [30] S. D. Blunt, P. Yatham, and J. Stiles, "Intrapulse radar-embedded communications," *IEEE Trans. Aerosp. Electron. Syst.*, vol. 46, pp. 1185–1200, July 2010.

Danilo P. Mandic, Petar M. Djurić, Andrzej Cichocki,  
Clive Cheong-Took, Saeid Sanei, and Lajos Hanzo

# Quo Vadis ICASSP: Echoes of 2019 ICASSP in Brighton, United Kingdom

*Signal Processing Meets the Needs of Modern Humankind*

**T**rue to the words of the old English saying, “Time and tide wait for no man,” the world has moved on, and

the dust, mostly of the intellectual kind, has settled. Like all things, a new circus is about to come to town. However, it is our hope that you have returned home from ICASSP 2019, held 12–17 May 2019 in Brighton, United Kingdom,

with fond memories, ranging from the welcome reception on the magnificent Brighton Pier to the Royal Pavilion. Remember the “scientific discourse” we were having with the seagulls (over the rights to fish and chips for dinner) while

*Digital Object Identifier 10.1109/MSP.2019.2923339  
Date of publication: 9 September 2019*

## The Welcome Reception



The welcome reception on Brighton Pier. The ICASSP delegates and the local seagulls liked our one-course menu equally, while the local brew ensured high spirits among the delegates.

we were absorbing the magic of the sunset at Brighton Pier?

Now that ICASSP 2019 is in the rear-view mirror and receding slowly but unwaveringly, we hope that you will join us in reflection. If you were unable to attend, you were sorely missed. Because more than 50% of the states in the United States have at least one place called “Brighton,” for many delegates, the stay was really like a home away from home. For those interested in heritage, there were more than 3,360 listed buildings in Brighton and Hove, more than 500 to choose from for every day of ICASSP.

Brighton has a historic connection to electrical engineering. In 1911, the first-ever cargo flight in Britain took place, and it transported OSRAM electric light bulbs. And do you know where? Yes, you guessed it right: from Brighton to Hove, a good 2 mi away and a step in the long association of this city with electricity and electrical engineering! Whether it is this connection with electrical engineering that tipped the scales when the IEEE Signal Processing Society (SPS) bestowed upon us the job of organizing ICASSP 2019 is sure to be debated by future historians of the subject, but for us, this challenging experience did require quite a few “lightbulb moments.” Indeed, no career experience can prepare one to become an ICASSP organizer, which is a monumental task. We owe our sincere thanks to our pre-

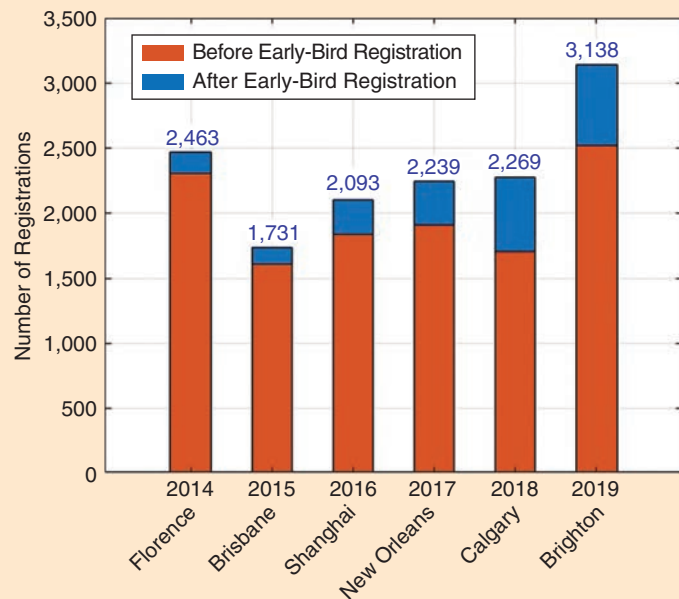


**FIGURE 1.** Participation in the ICASSP series of conferences since 2014. Sincere thanks are given to our delegates.

decessors in this role for sharing their experiences while we were preparing for our eventful journey.

### ICASSP 2019 in numbers

This was the first ICASSP held in England and only the second ever in the United Kingdom, a mere 30 years after the 1989 ICASSP in Glasgow. This is also the largest ICASSP in the history of this conference series (for a glimpse on participation in ICASSP for the past few years, see Fig-

ure 1). There were 3,510 submissions and 1,732 accepted papers, at an acceptance rate of 49.3%, and 41 presentations of journal papers recently published in the Society’s transactions and letters. Overall, the breakdown of attendees is as follows:

- 3,138 participants (including complementary registrations)
- 1,300 spread across 11 tutorials
- 200 at the MATLAB workshop
- 2,200 at the welcome reception
- 630 at the banquet

### The Banquet at the Grand Brighton Hotel



The Grand Brighton Hotel, built in 1864, offered a unique atmosphere for the banquet. Among other advanced engineering characteristics, the hotel featured a “vertical omnibus,” the first lift (or elevator as it is known in the United States) in the United Kingdom that was built outside London.

## Lecture and Poster Sessions



The 18 parallel sessions (seven lecture and 11 poster) were very well attended.

- 132 at the Women in Signal Processing (WiSP) event
- 138 at the Young Professionals development workshop
- 80 at the Young Professional networking event.

We are grateful to our extended team of technical committee chairs, special interest group chairs, and area chairs for helping us to organize a memorable ICASSP.

### The review process

The entire IEEE SPS mobilized to handle the reviews. Indeed, 97% of the submitted papers received three or more reviews, which is a whopping 10,500 total. Our most heartfelt thanks go to our authors and reviewers from all over the world, whose technical expertise and sheer dedication made our task so much more pleasurable. Therefore, it comes as little surprise that our first “lightbulb moment” was to introduce the Outstanding Reviewer Award, which recognized colleagues who gave the most valuable help toward ensuring the highest technical quality at our meeting:

- Ivan Bajic, Simon Fraser University, Canada
- Waheed Bajwa, Rutgers University
- Danilo Cominello, La Sapienza University, Italy

- Wong-Seng Gan, Nanyang Technological University, China
- Yuantao Gu, Tsinghua University, China
- Xinze Guan, eBay
- Antoine Liutkus, INRIA, France
- Anh-Huy Phan, Skolkovo Institute of Science and Technology, Russia
- Tirza Routtenberg, Ben-Gurion University of the Negev, Israel
- Konstantinos Slavakis, State University of New York at Buffalo
- Dirk Slock, EURECOM, France
- Palghat Vaidyanathan, California Institute of Technology.

### Trends in ICASSP 2019

In our Society, progress goes much further than just changing the SPS's logo. We live in exciting times for signal processing, an era of real revolution in artificial intelligence, machine learning, big data analytics, smart environments, and the Internet of Things. Advances in signal processing are at the heart of this revolution. We are proud to say that the

2019 ICASSP technical program not only kept up with the times but its many forward-looking contributions also rekindled ongoing and set new fires in these spaces. These changes were inevitably reflected in the numbers of submitted papers. Indeed, just within the scope of “Machine Learn-

ing for Signal Processing,” the number of papers nearly doubled in two years, from 261 papers in 2017 to 336 papers in 2018 and then to 497 papers in 2019. We are also delighted that our authors have kept a close eye on the practical relevance of their work: the number of papers in the “Design and Implementation of Signal Processing Systems” has more than doubled since last year.

### Innovation starts with education

At the very core of its activities, ICASSP 2019 promoted signal processing education, as innovation starts with education. It is fortunate that our 2018–2020 ICASSPs coincide with the anniversaries of the conception or publication of some of our most celebrated mathematical tools:

- 60 years of the least-mean-square algorithm
- 60 years of the Kalman filter
- 60 years of I.J. Good's prime-factor fast Fourier transform
- 55 years of Cooley–Tukey's fast Fourier transform
- 25 years of the particle filter

to mention only a few. Our “Back to the Future” events proudly featured an education panel and two special sessions on digital signal processing (DSP) education, which both celebrated the success of our discipline and charted ways to teach DSP in the modern curriculum. The attendance of approximately 200 for the education panel and 125 for the special sessions on DSP education both speak for themselves regarding the timeliness of this initiative

**We live in exciting times for signal processing, an era of real revolution in artificial intelligence, machine learning, big data analytics, smart environments, and the Internet of Things.**

## The Education Panel



The education panel in full swing. The past, present, and future of DSP education were discussed under the motto “innovation starts with education.”

and the entire Society’s interest in better establishing our identity through education drives.

Mónica F. Bugallo (Stony Brook University), Andreas Spanias (Arizona State University), and Dani-  
lo Mandic (Imperial College London) organized the education stream, with additional words of wisdom coming from Petar M. Djurić (Stony Brook University), while the panel was moderated by Victor Solo (University of New South Wales, Australia) and Maria Sabrina Greco (University of Pisa, Italy). More details about the education panel can be found in the

“SP Forum” column article in this issue of *IEEE Signal Processing Magazine* [1].

The panel was a very dynamic 2-h session. The discussions were so deep that the audience was mesmerized; in fact, we were kicked out of the conference center for breaching all allowed time limits. Many thanks to our moderators Victor Solo and Maria Sabrina Greco, who skillfully navigated

the maze of various burning issues addressed in the panel discussion. The panelists included

■ Alan V. Oppenheim the Massachusetts Institute of Technology

■ Fred Harris, University of California at San Diego

■ Anthony Constantinides, Imperial College, London, United Kingdom

■ Athina Petropulu, Rutgers University

■ Scott C. Douglas, Southern Methodist University

■ Waheed Bajwa, Rutgers University.

We extend our thanks to our pioneers Anthony Constantinides, Fred Harris, and Alan V. Oppenheim for being the pillars of our ICASSP 2019 education panel and for their roles in educating generations of researchers who are carrying the torch of our discipline well into the 21st century.

Our DSP Education initiative would not have been complete without recognizing our distinguished educators.

## At the very core of its activities, ICASSP 2019 promoted signal processing education, as innovation starts with education.

## Next-Generation Researchers



Our future is in safe hands! The younger generation demonstrated knowledge, technical maturity, and passion beyond their age that impressed all the attendees.

## Socializing at the Evening Sessions



ICASSP participants thoroughly enjoyed the evening sessions.

This year's Education Innovation Awards went to

- Anubha Gupta and Akansha Farswanm, IIIT-Delhi, India
- Zhe Li, Xiangyu Chen, Wei Deng, Wenjian Pei, and Yili Xia, Southeast University, China
- James McClellan and Gregory Kudrysz, Georgia Institute of Technology
- Roberto Togneri and Sally Male, University of Western Australia.

### Next-generation DSP researchers at ICASSP 2019

Our emphasis was to promote ICASSP as a must-go venue for postgraduate researchers. We are delighted that this was reflected in 797 student participants, 750 of whom attended the full tutorials on Sunday and Monday. This is a 40% increase over ICASSP 2018 and involved the tutorial price for students of only US\$25 (which our finance chair approved without even blinking an eye), a trend we would encourage our successors to follow when organizing ICASSP 2020.

Andrzej Cichocki chaired our awards committee. He, with the help of Toshihisa Tanaka, Sergio Cruces, Bao-Liang Lu, Felipe Tobar, Ayush Bhandari, and Anh Huy Phan, had the truly difficult task of selecting 12 Best Student Papers. Alan V. Oppenheim and Anthony Constantinides presented the awards at the beginning of our education panel. Our warmest congratulations go to

- Hayato Ito, University of Tokyo, Japan
- Yang Li, University of Rochester
- Sarit Khirirat, Royal Institute of Technology, KTH, Sweden
- Deqing Wang, Dalian University of Technology, China, and University of Jyväskylä, Finland
- Yousef El-Laham, Stony Brook University
- Xurong Xie, Chinese University of Hong Kong
- Stefan Braun, University of Zürich and ETH Zürich, Switzerland
- Rui Zhang, Georgia Institute of Technology
- Longhao Yuan, Saitama Institute of Technology and RIKEN Advanced Intelligence Project, Japan
- Tom Véniat, Sorbonne Université, France
- Shayan Aziznejad, École Polytechnique Fédérale de Lausanne, Switzerland
- Olga Graf, Technical University, Munich, Germany.

For complete information about the awards, please visit <https://2019.ieeeicassp.org/program#awards/>.

This ICASSP offered numerous opportunities for young researchers to get together and discover ways to expand their research and networks. These events included Student Career Luncheon, Young Professional Net-

working Event, Young Professionals Development Workshop, a workshop on Authors Best Practices, and IEEE Author Tools workshop.

### Quantum leap toward signal processing futures

Other forward-looking intellectual sparks included the promotion of quantum information science, an activity driven by Lajos Hanzo, including a tutorial, special session, and panel dedicated to this emerging area. Special thanks are given to Angela Sara Cacciapuoti and Mar-

cello Caleffi, who played a key role in these well-attended events, as well as to Soon-Xin Ng and Massimo Panella, who dedicated their valuable time to or-

**It, therefore, comes as no surprise that quantum technologies have become one of the IEEE's institute-level flagship programs.**

ganizing the special session. Robert Malaney's contribution to the panel discussion was also greatly appreciated. Driven by increasingly sophisticated DSP solutions, the radical advances in nanoscale integration have reached 7 nm. Like it or not, this means that we are approaching the limits of Moore's law and entering the world of quantum effects. It, therefore, comes as no surprise that quantum technologies have become one of the IEEE's institute-level flagship programs, with the SPS expected to play a pivotal role in this new era.

There is another innovation that falls into rather an “under-the-lightbulb” category. For the first time in the history of ICASSP, there were two evening sessions. These sessions allowed the delegates to present their work while mingling with their colleagues in a more relaxed setting, enhanced by catering. It was our impression that the delegates approved of this experiment.

### **Another innovation: ETON-Primers**

We have also introduced a new stream of the experts-to-nonexperts (ETON)-Primer lecture series, which is designed to include easy-to-digest but brilliant-to-inspire 45-min overviews of topics du jour that help the participants decide on future directions for their research. These discussions, held during the lunch breaks on Wednesday and Thursday, were very well attended not only by students but also by academics and engineers of all experience levels. We are grateful to

our inaugural lunchtime ETON-Primer speakers for simultaneously looking after our waistlines and keeping our intellectual appetite well satisfied. The feedback was that the courses on the ETON-Primer menu were each worth at least one scholarly Michelin star, with the lecture on information theoretic deep learning attracting well over 300 attendees. The ETON-Primer speakers and their topics were

- Jose C. Principe, University of Florida, “Understanding Dynamics of Deep Learning With Information Theory”
- Nuria González-Prelcic, University of Vigo and University of Texas at Austin, “Signal Processing for 5G Communications”
- Sergios Theodoridis, University of Athens, “Challenges in Deep Learning”
- Urbashi Mitra, University of Southern California, “Sensing, Commu-

nication and Control: Opportunities for Signal Processing for Biological Systems”

- Yun Nung (Vivian) Chen, National Taiwan University, “Learning for Language Generation and Understanding”
- DeLiang Wang, The Ohio State University, “The Cocktail Party Problem: A Case Study in Deep Learning”
- Georgios Giannakis, University of Minnesota, “Data and Network Sciences: SP Challenges and Opportunities”
- Mahesan Niranjan, University of Southampton, “Recent Developments in Machine Learning With a Focus on Communication Systems.”

### **Plenary talks, tutorials, special sessions, and other events**

With our plenary cochairs, Jonathon Chambers, Zoran Cvetkovic, and Geoffrey Li, we lined up a list of plenary speakers of

### **Inspiring Plenary Sessions**



The plenary sessions were an inspiration to the riveted audience.

## Tutorial Sessions



Attendance was outstanding for the tutorial sessions.

the highest stature who delivered gripping talks that excited many in the audience, especially our youngest colleagues. The speakers and their plenaries were

- Sir David Spiegelhalter, University of Cambridge, “Understanding Uncertainty”
- Corinna Cortes, Google Research, “Machine Learning”
- Mischa Dohler, King’s College London, “Internet of Skills”
- Hermann Ney, RWTH Aachen University, “Automatic Speech Recognition.”

We also take this opportunity to congratulate John Treichler, the 2018 winner of the Norbert Wiener IEEE SPS award. Our delegates thoroughly enjoyed his keynote.

Our tradition of offering full-blown 3-h tutorials continued with 15 exciting topics covered by globally acclaimed international experts. A big thank you goes to our tutorial co-chairs, Dave Bull, Patrick Naylor, and Mark Plumley.

### Special sessions

We initially accepted 40 proposals for special sessions. The peer review of the special session papers was of the same rigor as for regular papers, and we were delighted to eventually accept 30 special sessions with 184 papers. We extend our gratitude to our special session cochairs, Simon Godsill and Stephan Weiss, and to all special session chairs, for spicing up our ICASSP program.

## Show-and-tell events

We continued with the tradition of hosting show-and-tell demonstrations of innovative work by industrial and academic researchers. Our delegates had the opportunity to visit the demo booths to experience first-hand the potential of state-of-the art products and advanced prototypes that use DSP as an enabling technology, to meet and greet fellow researchers who “got their hands dirty” on successful practical applications, or even just to collect some giveaways.

### Sponsor and patrons

There were 28 exhibitors from industry, including Samsung, Google, and JD.com. The spectrum of sponsors was quite diverse, in terms of geography

## Show-and-Tell Booths and Exhibitor Areas



The show-and-tell booths and exhibitor areas presented another opportunity for engaging with cutting-edge applications of our discipline.

(from Japan to the United States), size (from multinational companies such as Facebook to smaller ones), and scope (from speech transcription by Speech Ocean to Internet Services by LINE Corporation). Despite such diversity, the sponsors were quite in unison in using ICASSP 2019 as a platform to 1) recruit bright and talented students, such as Apple hosting the Apple Mixer at Revolution Brighton or 2) showcase their products, such as ByteDance demonstrating their emotion-recognition software. These opportunities have proven to be of real value to our young delegates, providing them with exposure to a wealth of industrial connections. We are particularly grateful to Apple, our Diamond Patron, whose large team was always at hand to attend to numerous queries from ICASSP delegates.

## WiSP

The ICASSP 2019 program also included a WiSP lunch and panel discussion, which took place on Wednesday at noon. Its overarching theme was “From Grad-School to IEEE Fellow and Beyond.” The panel consisted of

- Yonina Eldar, Weizmann Institute of Science, Israel
- Dilek Hakkani-Tur, Amazon
- Athina Petropulu, Rutgers University
- Isabel Trancoso, IST-Lisbon, Portugal

The panel was moderated by the WiSP committee chair, Namrata Vaswani of Iowa State University. The discussion revolved around various issues including what is needed to be successful in practice within the IEEE and the SPS, the important criteria for becoming an IEEE Fellow, visibility within the Society, and the types of useful service and leadership.

## The banquet

The 630 participants at the ICASSP 2019 banquet enjoyed a music-fueled banquet for all ages and appetites and a floor for



**FIGURE 2.** Over to you, our Spanish counterparts. Nos vemos el año que viene en Barcelona.

3 h of celebration and fun. The live band also performed songs by the celebrated Swedish pop group ABBA, which launched its journey to music stardom in Brighton by winning the Eurovision Song Contest with “Waterloo” in 1974.

With the technical program full to the brim, we take responsibility for making the delegates work so hard, as if our participants needed any encouragement in this direction! Sunset in Brighton at this time of the year was around 9:00 p.m., which gave the participants plenty of time to meet colleagues (and join in the English love of discussing the weather) between and after the technical sessions. DSP researchers can be night owls, and

Brighton provided plenty of opportunities for the delegates to reflect on the technical sessions in the city’s numerous establishments until the wee hours. To feed our spirits, the Brighton Festival (<https://brightonfestival.org/>) coincided with our conference, offering theater, music, comedy, outdoor and family events, and more. For those who were still suffering from jetlag, there were an estimated 614.6 million pebbles that waited to be counted along the six miles of beach.

**We are indebted to our next-generation DSP researchers, who volunteered to make the experience of holding the first ICASSP in England a unique one.**

What a wonderful opportunity for a collaborative DSP project that was.

Last but not least, we are indebted to our next-generation DSP researchers, who volunteered to make the experience of holding the first ICASSP in England a unique one. The first cargo plane took off from Brighton, and it is our hope that ICASSP 2019 will also become a runway, helping many budding research careers to take off. We very much hope that our delegates at ICASSP 2019 in Brighton, a venue where signal processing meets the needs of modern humankind, enjoyed the experience.

As the curtain for ICASSP 2019 in Brighton has come down and the lights faded away, our message to the organizers of ICASSP 2020 in Spain is a heartfelt “You Will Never Walk Alone,” an English song that was sung so loudly and proudly in Madrid just two weeks after ICASSP. In another paraphrase of F. Nietzsche’s *Thus Spoke Zarathustra* (“you great star ...”), what would our happiness be but for our successors, ICASSP 2020 in Barcelona, to surpass the heights of any previous ICASSP? Hasta luego, ICASSP 2020 (see Figure 2)!

## Reference

- [1] Solo et al., “Innovation starts with education: ICASSP 2019 Education Panel” [SP Forum], *IEEE Signal Process. Mag.*, vol. 36, no. 5, pp. 135–137, Sept. 2019.

Victor Solo, Maria Sabrina Greco, Danilo Mandic, Petar Djurić, Andreas Spanias, and Mónica F. Bugallo

## Innovation Starts With Education

*ICASSP 2019 Education Panel*

The anniversary of a number of significant signal processing algorithms from the 1960s, including the least mean square algorithm and the Kalman filter, provided an opportunity at ICASSP 2019 to reflect on the links between education and innovation. This led ultimately to the proposal of some special sessions as well a panel session that would provide some insight, via a historical perspective, consideration of the current status, and an assessment of the emerging educational future.

The panel was organized by Prof. Mónica F. Bugallo (Stony Brook University), Prof. Andreas Spanias (Arizona State University), Prof. Danilo Mandic (Imperial College), and Prof. Petar Djurić (Stony Brook University) and was moderated by Prof. Victor Solo (University of New South Wales, Sydney) and Prof. Maria Sabrina Greco (University of Pisa). The discussion was part of a special program “Celebrating Signal Processing Education” and consisted of this 90-min forum and two special sessions: “Half a Century of Adaptive and Statistical Signal Processing Education” and “Traditional and Emerging Signal Processing Teaching Practices.”

The panel, with six discussants (Figure 1), was preceded by presentations of best student paper awards and best education paper awards and was well attended,

with about 200 people. The two complementary sessions also drew many people—approximately 125 each. (See the “Conference Highlights” column article on page 127 in this issue for more on these sessions.)

The objective of the panel was to address the link between innovation and the educational process. This intersection arises at many levels, such as in the mode of supervision of a Ph.D. degree student, new ways of teaching traditional concepts, bringing insights from research into the classroom, offering projects as part of a university course, approaches to teaching that put more emphasis on class involvement, and taking electrical engineering education into high schools.

To inject some structure into our discussion, the idea was to look at the past, present, and future. Furthermore,

the early involvement of the audience was enabled by opening up the program for comments and questions after each two speakers’ presentations. A panel that could address such issues as those just mentioned needed a mix of scholars—some senior; some with an overall view of current practices, such

as a former department chair; and some who would take a disruptive approach to teaching. The invited panelists and their relevant topics were

- Prof. Waheed Bajwa (associate professor, Rutgers University) on flipped classrooms
- Prof. Scott Douglas (professor, Southern Methodist University) on signal processing for middle and high school education
- Prof. Fred Harris (professor, University of California, San Diego) on novel approaches to standard material



**FIGURE 1.** The panelists of ICASSP 2019 (from left): Prof. Waheed Bajwa, Prof. Scott Douglas, Prof. Fred Harris, Prof. Alan V. Oppenheim, Prof. Tony G. Constantinides, and Prof. Athina Petropulu.

- Prof. Alan V. Oppenheim (professor, Massachusetts Institute of Technology) on reflections and advice on teaching for the future
- Prof. Tony G. Constantinides (professor, Imperial College) on research pressures and women in engineering
- Prof. Athina Petropulu (professor, Rutgers University) on viewpoints from a former department chair.

Some questions were asked of the panel, but the speakers were free to pick and choose those they would respond to, given their expertise and interests. The following three themes emerged: teaching, research pressures, and women in engineering.

## Teaching

Prof. Oppenheim opened with the startling admission, “Teaching: I did it all wrong for 50 years.” (This is quite something coming from a distinguished scholar who has won numerous teaching awards!) He went on to contrast what he called the before online technology (BOT) approach to teaching with the after online technology (AOT) technique, which he now advocates. The BOT method consists of lectures, followed by homework, while the AOT approach involves homework/

preparation before the lecture plus technology-enabled interaction and no student multitasking (e.g., texting) during the lecture.

Prof. Harris sketched an integrated approach to the fast Fourier transform (FFT). His mostly visual presentation allowed a unified and easy-to-follow treatment of both discrete- and continuous-time Fourier transforms. It further enabled the dismissal of some myths about the limitations of the FFT.

Prof. Bajwa recounted his experience with flipped teaching of digital signal processing (DSP). He opened by noting the pluses and minuses of the traditional approach (Prof. Oppenheim’s BOT), including the fact that it assumes that all students learn in the same way. He was critical of massive open online

courses, otherwise known as *MOOCs*, as an alternative; they have a place, he said, but will not dominate the new classroom. So far, their 10-year history seems to bear this out.

The flipped approach (more or less Prof. Oppenheim’s AOT) depends on prelecture preparation, then tests and error correction during the lecture to improve student knowledge, followed by testing after the lecture. But such a method needs some nontrivial infrastructure: “good-quality instructional videos, teaching assistants active during the lecture, and special classroom structures,” according to Prof. Bajwa. His strong conclusion was that this is not practical for “research-active faculty in state schools.”

In 2016, Prof. Bajwa and colleagues ran Rutgers’s first flipped class; it was a junior-level (third-year) DSP course. One unexpected positive result was that many of the weaker students did a lot better. For further details, see [1].

Prof. Douglas described the Infinity Project at Southern Methodist University’s Engineering College, which has now been running for two decades and aims to increase enrollment by taking engineering instruction into high schools and middle schools. Each Engineering College department

has developed instructional materials for specific projects that can be taught and implemented in a middle or high school setting. For example, one of the electrical engineering/signal processing projects involves developing “Wearable Technology for Personal Health Tracking.” The Infinity Project has now trained more than 1,000 middle and high school teachers.

Prof. Petropulu drew attention to a recent report from the U.S. National Academy of Engineering, which classifies the challenge of engineering education into four cross-disciplinary themes: sustainability, health, security, and the joy of living; see <https://www.nae.edu/20742/Frontiers-of-Engineering-Education> for this and other very interesting reports. She further observed that,

while we’re good at teaching engineering students how to solve problems, we also need to be teaching them how to formulate them. The workplace is becoming more interdisciplinary, so multidisciplinary training must be rapidly expanded. This will require big changes in the way engineering is taught and will encounter much resistance. A part of this will come from the necessity for the engineers of the future to be much better at articulating what their technology has to offer. She pointed out that signal processing can help here. The modeling paradigm integral to DSP can help to conceptualize problems outside of DSP.

## Research pressures

Prof. Oppenheim began his commentary on research with the challenging assertion that “the research enterprise, including its educational mission, has been hijacked by the funding mechanisms, the metrics, and media hype.” This led to a discussion about how to manage a research career in the presence of pressure from evaluation based on metrics and the need to acquire research funding.

Prof. Oppenheim’s forcefully stated advice, strongly seconded by Prof. Constantinides, was that one needs to pursue what one thinks is important, not what somebody else does. If you don’t do that, they asserted, you won’t be able to generate the kind of intensity needed to solve hard problems, and you will neither achieve the kind of success you aim for nor be fulfilled [2]. However, Prof. Oppenheim said, there is room for pragmatism. There are usually several compelling projects, ideas, or directions vying for one’s attention; the right strategic choice of which one to pursue can have a great impact on making or hindering a career. This is one place where advice from mentors can help.

Prof. Constantinides recalled the early days of DSP. Its widespread utility in communications seems obvious now, he said, but, in the 1950s and early 1960s, many major communication technology companies could not see it, failed to invest in it, and fell by the wayside. Some things may not have changed much since then. Metrics were treated very skeptically by the panel, and much more needs to be done to clarify what role they should

**While we’re good at teaching engineering students how to solve problems, we also need to be teaching them how to formulate them.**

play, if any (see the 2015 U.K. government report, “The Metric Tide” [4]).

## Women in engineering

The panelists’ consensus was that women’s participation in engineering remains a significant challenge for the field in general and for signal processing in particular. The panelists emphasized two aspects. The first was the overly slow ebbing of prejudice and implicit bias against women already in the profession. It was suggested that this is partly a matter of socialization, which means it will change slowly. The second point was the difficulty of attracting women into all areas of engineering. This is related to a worldwide trend of declining interest in science, technology, engineering, and mathematics subjects.

Prof. Constantinides illustrated the old principle that a good place to start changing things is in your own backyard. He mentioned some initiatives he encouraged at Imperial College—in particular, a DSP ambassador program led by Dr. Paulina Chen, formerly with Bell Labs. She gives talks, organizes meetings, and mentors young women in engineering. The Department of Electrical and Electronic Engineering at the college also has a number of related projects.

Prof. Petropulu observed that only 11% of B.S. degrees in electrical engineering are earned by women and that only 11% of IEEE Signal Processing Society members are women. She pointed out that this means the profession misses out on a vast reservoir of talent, the perspective of the other half of humanity, and the wisdom of a more diverse population. Rutgers also has a number of women in engineering initiatives. (For more from a former department chair, see [3].)

## Conclusions

ICASSP is dominated by research and application, as it should be. But, to state the obvious, the educational role of academics and universities is a necessary complement to the research role. And, of

course, there is feedback between the two. This means that ICASSP also needs to continue to address educational issues. Since the environment keeps changing (is time varying), educational innovation, like research, is an ongoing process. ICASSP 2019 was held 12–17 May in Brighton, United Kingdom. The education panel described in this article, and its two complementary special sessions, were a small part of addressing some aspects of that process. We look forward to the next round of ICASSP educational activities and the new insights that future organizers will enable.

## Authors

**Victor Solo** (v.solo@unsw.edu.au) received his B.Sc. degree from the University of Queensland, Brisbane, Australia; two degrees (both first class honors) from the University of New South Wales (UNSW), Sydney, Australia: a B.Sc. degree in statistics and a B.E. degree in mechanical engineering; and his Ph.D. degree from the Australian National University, Canberra. He is a professor of electrical engineering at UNSW. He is also a faculty member in the Massachusetts General Hospital—

Massachusetts Institute of Technology—Martinos Center for Biomedical Imaging, a part of the Radiology Department at Harvard Medical School. He has been an associate editor of *IEEE Transactions on Automatic Control*, *IEEE Transactions on Pattern Analysis and Machine Intelligence*, *IEEE Signal Processing Magazine*, *Journal of the American Statistical Association*, and *Journal of Econometric Theory*. He is a Fellow of the IEEE and American Statistical Association.

**Maria Sabrina Greco** (m.greco@iet.unipi.it) received her M.S. degree in electronic engineering in 1993 and her Ph.D. degree in information engineering in 1998. She is a full professor in the Department of Information Engineering, University of Pisa, Italy. She is a corecipient of the 2001 and 2012 IEEE

Aerospace and Electronic Systems Society’s (AESS’s) Barry Carlton Award for Best Paper and a recipient of the IEEE AEES 2008 Fred Nathanson Young Engineer of the Year award. She has been general chair, technical program chair, and organizing committee member of many international conferences. She is an associate editor of *IET Radar, Sonar, and Navigation* and *Journal of Advances in Signal Processing*, a senior editorial board member of *IEEE Journal of Selected Topics in Signal Processing*, and a senior area editor of *IEEE Transactions on Signal Processing*. Her general interests are in the areas of statistical signal processing, estimation, and detection theory. She is a Fellow of the IEEE.

**Danilo Mandic** (d.mandic@imperial.ac.uk) is a professor of signal processing at Imperial College London, United Kingdom. He has a keen interest in signal processing education and is a member of the IEEE Signal Processing Society Education Technical Committee. His contributions were recognized with the President’s Award for Excellence in Postgraduate Supervision at Imperial College in 2014. He is a Fellow of the IEEE.

**Petar Djurić** (petar.djuric@stonybrook.edu) received his B.S. and M.S. degrees in electrical engineering from the University of Belgrade, Serbia, and his Ph.D. degree in electrical engineering from the University of Rhode Island. He is currently a distinguished professor in the Department of Electrical and Computer Engineering at Stony Brook University, New York. His research has been in signal and information processing, with an emphasis on Monte Carlo-based methods, signal processing over networks, applications in wireless sensor networks, and radio-frequency identification. He received the IEEE Signal Processing Magazine Best Paper Award in 2007 and the EURASIP Technical Achievement Award in 2012. He is a Fellow of the IEEE and EURASIP.

**Andreas Spanias** (spanias@asu.edu) received his B.S. degree in electrical engineering from the Cyprus University

(continued on page 147)

# Audio-Based Search and Rescue With a Drone

*Highlights From the IEEE Signal Processing Cup 2019 Student Competition*

Increasing interest in unmanned aerial vehicles (UAVs), commonly referred to as *drones*, has occurred in recent years. Search and rescue scenarios where humans in emergency situations need to be quickly found in difficult-to-access areas constitute an important field of application for this technology. Drones have already been used by humanitarian organizations in countries such as Haiti and the Philippines to map areas after a natural disaster using high-resolution embedded cameras, as documented in a recent United Nations report [1]. Although research efforts have focused mostly on developing video-based solutions for this task [2], UAV-embedded audio-based localization has received relatively less attention [3]–[7]. However, UAVs equipped with a microphone array could be of critical help to localize people in emergency situations, especially when video sensors are limited by a lack of visual feedback due to bad lighting conditions (such as at night or in fog) or obstacles limiting the field of view (Figure 1).

This motivated the topic of the sixth edition of the IEEE Signal Processing (SP) Cup: a UAV-embedded sound-source localization (SSL) challenge for search and rescue. The SP Cup is a student competition in which undergraduate students form teams to work on real-life challenges. Each team should include

1) one faculty member (the supervisor), 2) at most, one graduate student (the mentor), and 3) at least three, but no more than ten, undergraduate students. (An undergraduate student is a student without a four-year university degree at the time of submission.) Participation in the SP Cup is open to all teams from around the world that satisfy the aforementioned eligibility criteria. The top three finalist teams were selected to present and compete at the final stage of competition, which was held at the ICASSP 2019 in Brighton, United Kingdom, on 13 May 2019. We will overview the IEEE SP Cup experience, including competition setup, technical approaches, and statistics.

## Drone-embedded SSL

Estimating the direction of a sound source given audio measurements from an array of two or more microphones is a long-standing research topic referred to

**UAVs equipped with a microphone array could be of critical help to localize people in emergency situations.**

as *sound source localization (SSL)* [8]. The most common approach to this problem is to estimate the sound time difference of arrival (TDOA) in a microphone pair, which can be approximately mapped to an angle of arrival when the source-to-microphones distance is large compared to the intermicrophone distance. For arrays containing more than

two microphones and having known geometry, the angles of arrival of different pairs can be combined to estimate the 2D (azimuth and elevation) direction of arrival of the source in the array's coordinate frame. A large number of methods for robustly estimating TDOAs from signal pairs in the presence of noise, reverberation, or interfering sources has been developed, including generalized cross-correlation methods [9] and subspace methods [10], [11]. Alternatively, a number of machine-learning-based SSL methods have recently emerged (see [12] and [13]). However, because acquiring sufficiently large real-world data sets to train SSL models for specific arrays is very costly, most learning-based approaches rely on simulated data sets [13], which do not always generalize well to real-world conditions.

The specific task of UAV-embedded SSL comes with a number of challenges. One major issue is the noise produced by the UAV itself, generically referred

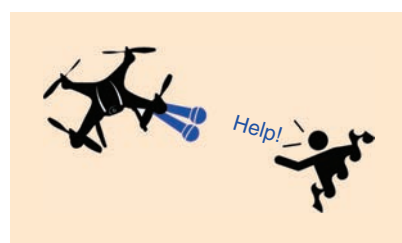


**FIGURE 1.** Microphones embedded in a UAV may help localize people for search and rescue in disaster areas.

to as *ego noise* in robotics [14]. Due to the quickly changing speed of motors to stabilize the vehicle in the air or change its position, the noise profile is harmonic but also nonstationary. Additionally, because the microphones are mounted on the drone itself, they are very close to the noise sources, leading to high noise levels. Because of this, the signal-to-noise ratio (SNR) can easily reach  $-15$  dB or lower, making SSL very difficult. Another factor impacting localization performance is wind noise. The wind is produced by the rotating propellers and the UAV movement in the air, and it may also occur naturally in outdoor scenarios.

This wind noise has high power and is of low frequency. Thus, it easily overlaps with speech signals, which typically occur in a similar frequency range. Finally, SSL must be performed using relatively short time

windows due to the fast movements of the UAV relative to potential sound sources. All of these challenges need to be tackled at the same time and nearly in real time when considering the real-world SSL application of search and rescue. On the bright side, however, UAVs may be equipped with other embedded sensors (such as gyroscopes, motor controllers, inertial measurement units, compasses, and cameras), which may provide useful additional information. In the particular case of the SP Cup, the rotational speeds of each of the drone's propellers at all times were provided along with the audio recordings, and they could optionally be used by the participants for ego-noise estimation.

### *The Drone Egonoise data set*

The SP Cup data were built from a subset of the recently released Drone Ego-noise (DREGON) data set [7]. The release of parts of the DREGON data set, including ground truth annotations, was delayed for the SP Cup to take place in fair conditions. The entire data set is now publicly available for download at

<http://dregon.inria.fr>. It consists of annotated audio recordings acquired with a specifically designed 3D-printed cube-shaped eight-microphone array rigidly attached under a quadrotor UAV, as shown in Figure 2. The 8SoundsUSB microphones and sound card designed by Sherbrooke University, Canada, were used. Specifications can be found at [https://sourceforge.net/p/eightsoundsusb/wiki/Main\\_Page](https://sourceforge.net/p/eightsoundsusb/wiki/Main_Page). The quadrotor UAV was the MK-Quadro from MikroKopter (HiSystems GmbH, Moormerland, Germany). The data set includes both static and in-flight recordings with or without the presence of a sound

source emulated by a loudspeaker emitting either speech from the TIMIT data set [15] or white noise. Recordings were made inside large rooms with mild reverberation times (lower than 150 ms) and negligible background noise.

The synchronized five degrees of freedom coordinates of both the UAV and loudspeaker were obtained using a Vicon motion-capture system, yielding ground-truth source-direction annotation errors of lower than  $2^\circ$  for the entire data set.

### **Tasks in the 2019 SP Cup**

The goal of the competition was for teams to build a system capable of localizing a sound source based on audio recordings made with a microphone array embedded in a UAV. Teams had to use their signal processing expertise to process the audio signals to extract relevant spatial cues to estimate the direction of arrival of a speech source. Key challenges were the large amounts of noise present in the recordings due to the UAV's rotors and wind as well as the dynamics of realistic flights involving fast movements. To help noise estimation, the mean rotational speeds of each of the four propellers were provided for each localization task. The microphone array geometry and coordinate frame were also available.



**FIGURE 2.** The quadrotor UAV used for the SP Cup, equipped with a 3D-printed eight-microphone array. The circled areas highlight two of the microphones.

### *The open competition: Static task*

For this task, 300 eight-channel audio recordings at 44.1 kHz and of approximately 2 s each were provided in the form of waveform audio file format (WAV) files. All recordings were obtained by adding together a clean recording of a static loudspeaker emitting random utterances from the TIMIT database [15] by an unknown (azimuth and elevation) direction in the UAV microphone array's frame and a recording of UAV noise of the same length in various flight conditions and using various SNRs, from  $-20$  to  $5$  dB. The goal of this task was to retrieve the azimuth and elevation angles of the static speech source for each of the 300 recordings. A source was considered correctly localized when the great-circle distance between the estimated and ground-truth directions was lower than  $10^\circ$ . One point was given for each correctly localized static file, for a total of 300 points.

### *The open competition: Flight task*

For this task, 36 eight-channel audio recordings at 44.1 kHz lasting precisely 4 s each were provided in the form of WAV files. All recordings were made during flight. In the first 16 recordings, the source was a loudspeaker emitting speech, whereas in the last 20 recordings, the source was a loudspeaker emitting white noise. A white noise source is considered easier to localize because it has a much broader frequency range than speech. The average SNR was approximately  $-15$  dB. Although the source (loudspeaker) was static during flights, the microphone array was moving with the drone. Thus,

the (azimuth and elevation) source direction in the array's frame was constantly changing over time. For each of the 4-s recordings, 15 regularly spaced time stamps were defined. The goal of this task was to retrieve the mean azimuth and elevation angles of the source within a 500-ms window centered on each of these time stamps for each of the 32 recordings. Similarly to the static task, one point was given for each correctly localized time stamp, for a total of 540 points.

### *The open competition—Bonus task:*

#### *Data collection*

On top of the 840 points that could be gained by correctly localizing all of the sources, participating teams were encouraged to send their own audio recordings obtained from one or several microphones embedded in a flying UAV. The recordings had to be made either outdoors or in an environment with mild reverberation, and they weren't to feature sound sources other than the UAV's noise or wind. A report detailing the microphones and

UAV used as well as the recording conditions and including pictures of the setup and experiments had to be given with the audio files. Sixty extra points were granted to teams submitting such data. A novel UAV ego-noise data set was created from the teams' contributions to this bonus task, and it is now freely available for research and educational purposes at <http://dregon.inria.fr>.

#### *The baseline*

A baseline method was provided for the competition. The method, implemented in MATLAB, is based on the open source Multi-channel BSS Locate toolbox ([http://bass-db.gforge.inria.fr/bss\\_locate](http://bass-db.gforge.inria.fr/bss_locate)) and available at <https://github.com/Chutlhu/SPCUP19>. Although the baseline as provided used the steered-response power phase-transform (SRP-PHAT) method as described in [16], the MBSS Locate toolbox implements 12 different source localization methods,

which are detailed in [17] and were also sometimes used by participants. The method chosen as the baseline ranked among the best-performing methods in the single-source localization tasks of the recent IEEE acoustic source localization and tracking challenge [18].

#### *Final competition*

The three highest-scoring teams from the open competition stage were selected as finalists invited to compete in the final competition at ICASSP 2019. Teams gave a 5-min presentation of their method followed by 5-min of questions in front of a jury composed of SP Cup organizers and a MathWorks representative. Presentations were marked by the jury according to clarity, content, originality, and answers to the questions. Then, the

teams were given previously unseen recordings made with the same UAV as in the open competition, i.e., 20 static speech recordings of roughly 2 s each and one long in-flight speech recording of 20 s. The average SNRs for

both tasks were similar to the lowest SNRs encountered during the open competition—approximately -17 dB. The teams had 25 min to run their methods and provide results for these tasks in the same format as in the open stage. Results were evaluated on the spot, and a global score was calculated for each team so that the presentation, the static task, and the flight task each accounted for one-third of the total.

#### *Competition data*

The data of both the open and final stages of the 2019 SP Cup as well as corresponding ground-truth result files and MATLAB scripts can be found at <http://dregon.inria.fr/datasets/signal-processing-cup-2019/>.

#### **2019 SP Cup statistics and results**

As in previous years, the SP Cup was run as an online class through the Piazza platform, which allowed for continuous

interaction with the teams. In total, 207 students registered for the course, and the number of contributions to the platform was more than 150. An archive of the class is available at [https://piazza.com/ieee\\_sps/other/spcup2019/home](https://piazza.com/ieee_sps/other/spcup2019/home). We received complete and valid submissions from 20 eligible teams from 18 different universities in 11 countries across the globe: India, Japan, Brazil, South Korea, New Zealand, China, Germany, Bangladesh, Australia, Poland, and Belgium. The teams had four to 11 members for a total of 132 participants.

Figure 3 summarizes the scores obtained by the 20 participating teams and baseline for all of the open-competition subtasks. Remarkably, 12 teams strictly outperformed the already strong baseline in their overall score (excluding bonus points). As can be seen, near-perfect scores were obtained by the best-performing teams in the static speech and in-flight broadband tasks, with more than 95% of correctly localized sources. In contrast, the in-flight speech task, which formed the heart of the competition and was the closest one to the motivational search and rescue scenario, proved to be extremely challenging. For this task, only one timestamp out of 240 was correctly localized by the baseline. In fact, only nine teams succeeded in localizing more than 5% of the timestamps for this task, while the winning team achieved a stunning 65% score. In addition to the mandatory localization result files, 12 of the teams sent their own UAV recordings for the bonus task, yielding a unique and valuable data set (see the section “The Open Competition—Bonus Task: Data Collection”).

#### **Highlights of the technical approaches**

In this section, we provide an overview of the methods employed by the top 12 teams that outperformed the baseline. Proposed methods were generally made of at least two components: 1) a preprocessing stage aimed at reducing the noise in the observed signals and 2) an SSL stage. The most popular noise reduction methods used were the multichannel Wiener filter or single channel variations of it (see [19] for a review). These approaches

require estimates of the noise statistics, which were obtained using many different techniques. Half of the teams used the motor speeds provided along with the audio files to do so via some form of interpolation among the corresponding individual motor recordings available as development data. Others used voice activity detection to isolate noise-only parts and estimate the statistics on them, or they made use of recursive averaging. In addition to Wiener filtering, several teams used various bandpass filters to reduce the impact of wind noise. Notable alternatives to Wiener filtering included noise reduction methods based on nonnegative matrix factorization or deep neural networks. One

team also used spatial filtering to reduce noise in the directions of the four rotors based on the provided UAV geometrical model. Two of the teams developed methods to adaptively remove microphone pairs for which the noise was too important. Many teams combined several of the aforementioned strategies to further reduce the noise.

For SSL, most of the teams built on the SRP-PHAT method implemented in the baseline. Some others used nonlinear

variations of it, beamforming-based methods, or subspace methods. A number of teams used some form of postprocessing on the angular spectra provided by these methods, for instance, by ignoring regions associated to the drone's rotor directions or by clustering local minima. An approach that proved particularly successful for in-flight tasks was

to smooth estimated source trajectories. This was done by using Kalman filtering or handcrafted heuristics. Overall,

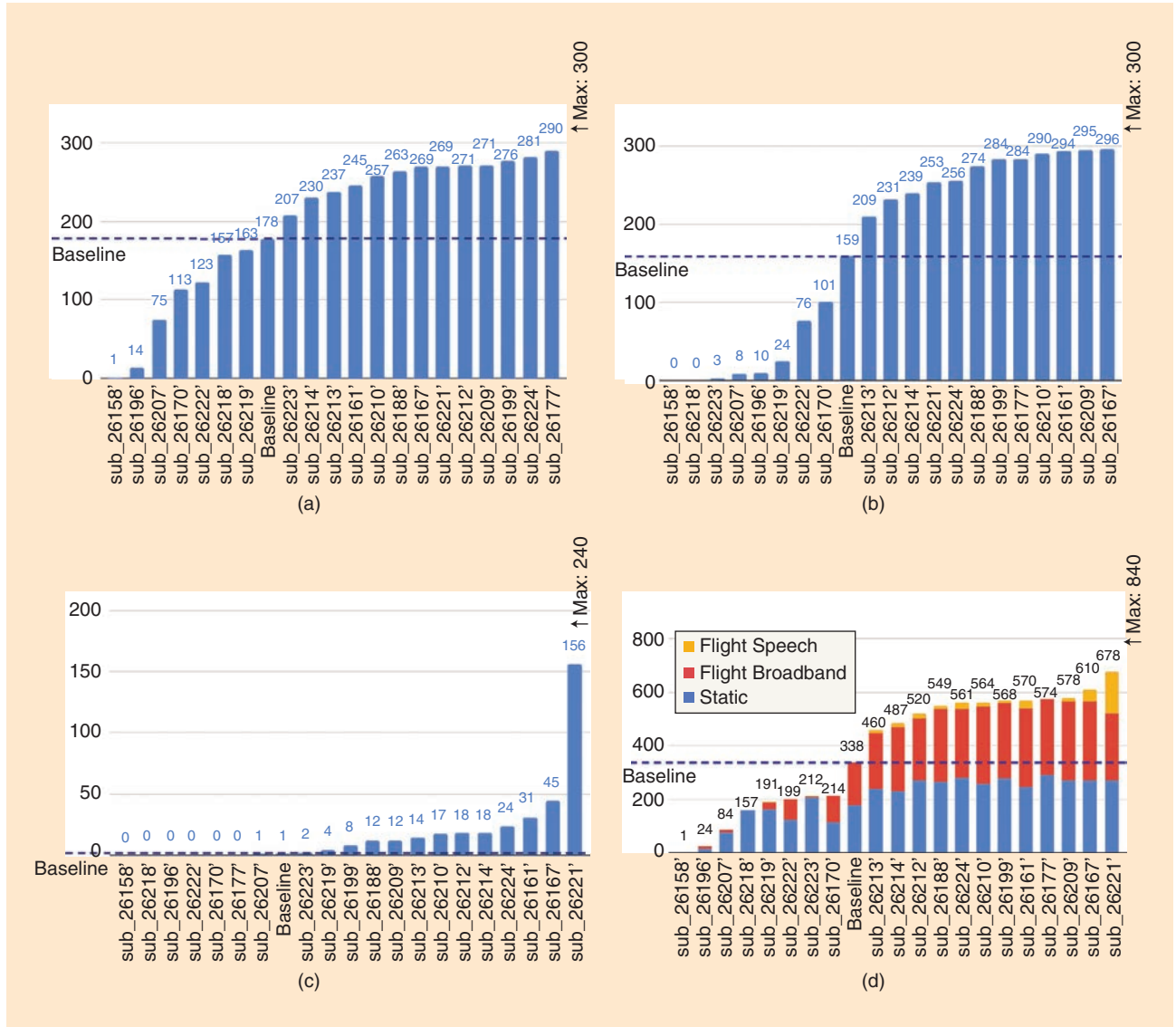


**FIGURE 3.** The anonymized scores of the 20 teams and the baseline for the three open-competition subtasks: (a) the static speech localization task, (b) in-flight broadband localization task, (c) the in-flight speech localization task, and (d) the total scores.



**FIGURE 4.** The members of the three finalist teams after the final competition at ICASSP 2019: (a) first place, Team AGH; (b) second place, Team SHOUT COOEE!; and (c) third place, Team Idea!\_SSU.

the finalist teams proved that combining several techniques carefully designed for the task at hand was the only way to achieve good performance on the competition data. This suggests that even better results could be obtained by combining the best ideas from the different competitors.

### The winning teams

In the section, we provide details about the three winning teams as well as an overview of some feedback and perspectives received from them. Team members at the final competition are shown in Figure 4.

#### Team AGH

- **Affiliation:** Akademia Górnictwa i Hutnicza, University of Science and Technology, Kraków, Poland
- **Undergraduate students:** Piotr Walas, Mateusz Guzik, and Mieszko Fraś
- **Tutor:** Szymon Woźniak
- **Supervisor:** Jakub Gałka
- **Approach:** The team preprocessed the signals using multichannel Wiener filtering, where the noise covariance matrices were estimated by averaging across several frames as well as across the whole signals. To perform localization, the team combined estimates from the SRP-PHAT baseline and the multiple signal classification based on generalized eigenvalue decomposition [11] methods via  $k$ -means clustering in the angular-spectrum domain. Angular spectra were presmoothed using a max filter. Finally, a Kalman filter was employed to smooth out estimated trajectories in flight tasks.

#### Opinions

- “Leading a group of undergrads was a challenging as well as rewarding task. It gave me a perspective on how hard it is to efficiently organize research work in team, even though the team was small in number. During the competition, I especially enjoyed discussing out-of-the-box ideas of undergrads and studying state of the art alongside them. The tricky part of this competition was to figure out how to evaluate accuracy of tested methods, since without ground truth, you never know. On the other hand, the most exciting moments were the announcement of the results of the first phase and incontestably taking part in the final competition at ICASSP. This kind of competition gives an excellent opportunity for undergraduates to try their hands at solving challenging research problem.”

—Szymon Woźniak

- “I chose to join the Signal Processing Cup competition because I searched for a project outside of regular studies that would allow me to develop myself in the field of signal processing. During the work, I got to develop state-of-the-art SSL methods and also had a chance to experience working in a great team. I enjoyed the most the moments when we got some improvements after testing a new idea. Unfortunately, due to the lack of development data, we often had to rely on our intuition in deciding between two solutions, which was the hardest part of the competition. I

think those types of events are a great chance for students to get an idea of how the scientific community works and meet like-minded people from around the world.”

—Mateusz Guzik

- “I chose to participate in SP Cup as I saw the opportunity to create a solution which could be potentially used for helping others. During the competition, the most enjoyable and exciting part was studying state-of-the-art algorithms, merging them into one solution, and observing the results. The difficulty of the competition itself was connected to the lack of development data, which made challenging to choose between different solutions. After all, I believe that the most important of taking part in this competition was the knowledge and hands-on experience which we gained.”

—Piotr Walas

#### Team SHOUT COOEE!

- **Affiliation:** The University of New South Wales, Kensington, Australia
- **Undergraduate students:** Antoni Dimitriadis, Alvin Wong, Ethan Oo, Jingyao Wu, Prasanth Parasu, Qingbei Cheng, Hayden Ooi, and Kevin Yu
- **Supervisor:** Vidhyasaharan Sethu
- **Approach:** The team preprocessed the signals using multichannel Wiener filtering, where the noise covariance matrices were estimated from linear combinations of the provided individual motor recordings, weighted according to the current propeller’s

speed. A nonlinear generalized cross-correlation (GCC-NONLIN) method [17] was used to localize the sound source. And, for flight tasks, source trajectories were smoothed using a heuristic method inspired by the Viterbi algorithm.

## Opinions

- “I learned a lot from this SP Cup competition, from how directions of arrival can be determined using signal processing techniques to how a Wiener filter can be applied to reduce the noise in recordings. Furthermore, I learned the importance of testing and validation and how it can be utilized to evaluate the effectiveness of strategies as well as determine optimal parameters to produce an algorithm that is accurate and robust. It was an intellectually stimulating and challenging experience. I really enjoyed doing research on various strategies that could be employed in producing more accurate sound source localization results. It was always exciting whenever new strategies developed from our research led to improved performance of our system. I chose to join the competition as I have a passion for signal processing and saw this competition as an opportunity to develop my signal processing skills. Furthermore, I believed I would gain a deeper understanding of how I could apply signal processing methods and techniques to solve practical, real-world problems.”

—Prasanth Parasu

- “The whole experience has been unlike any other that I have been a part of and was very much worth the time spent on the competition. Much was learned during the SP Cup, including the importance of teamwork, clear communication, and (particularly in our team’s case) running programs on multiple computers to ensure that we safeguard against unforeseen problems. The UNSW team were all collaborative and supportive of each other, and we have grown closer as a result. The competition gave us the opportunity to chal-

lenge ourselves intellectually and gain knowledge and experience that will serve us well in the future. I’d like to thank my team members for being so awesome and particularly our team coordinator, who introduced us to the competition and supported us throughout the whole adventure.”

—Ethan Oo

- “It was great to work in the team SHOUT COOEE! and compete with other brilliant teams all over the world. I love the idea of solving real-world problems. It’s challenging and also attractive. Thanks to the SP Cup, I gained a new understanding of speech processing. It provided a good opportunity to learn about the multichannel Wiener filter incorporated with acoustic noise statistics of the drone. We also had chances to research and play around with different DOA estimation algorithms and seek for the best. It’s an exciting and unforgettable experience.”

—Jingyao Wu

## Team Idea!\_SSU

- **Affiliation:** Soongsil University, Seoul, South Korea
- **Undergraduate students:** Donggun Lee, Myeonghun Jeong, Minjae Park, Youngjae Lee, and Jinyoung Son
- **Tutor:** Beomhee Jang
- **Supervisor:** Sungbin Im
- **Approach:** The team preprocessed the signals using a combination of single-channel speech enhancement techniques and multichannel Wiener filtering, for which noise statistics were estimated from noise-only segments using voice-activity detection. Wind noise was also reduced by cutting frequencies below 100 Hz. The SSL methods used were SRP-PHAT for the static task and GCC-NONLIN for the flight tasks. To reduce outliers on flight tasks, the team used a two-step procedure: 1) compute a global source direction on

a 4-s segment and 2) estimate directions every 250 ms on 1-s segments by limiting the angular search space around the global estimated direction.

## Future steps and the upcoming SP Cup

The SP Cup’s organizing team hopes that this edition will foster research in the emerging topic of UAV-embedded audition for search and rescue, notably because of its unique data set, which is now publicly available. Participants of the 2019 SP Cup as well as other researchers in this field are encouraged to submit their work to the upcoming special issue of *EURASIP Journal on Audio, Speech, and Music Processing* with the topic “Advances in Audio Signal Processing for Robots and Drones.” The submission deadline is 1 December 2019. For details, please visit <https://asmp-eurasipjournals.springeropen.com/call-for-papers--advances-in-audio-signal-processing-for-robots->.

The seventh edition of the SP Cup will be held at ICASSP 2020. The theme of the 2020 competition will be announced in September. Teams who are interested in the SP Cup competition may visit <https://signalprocessingsociety.org/get-involved/signal-processing-cup>. In addition to the SP Cup, the IEEE Signal Processing Society (SPS) also organizes the Video and Image Processing (VIP) Cup. The third edition of the VIP cup will be held at the 2019 IEEE International Conference on Image Processing, in Taipei, Taiwan, on 22–25 September 2019. The theme of this edition is “Activity Recognition From Body Cameras.” For details, visit <https://signalprocessing-society.org/get-involved/video-image-processing-cup>.

## Acknowledgment

The organizers of the 2019 SP Cup would like to express their utmost gratitude to all who made this adventure a reality, including, but not limited to, the participating teams, the local organizers,

and the IEEE SPS Membership Board. In addition, great appreciation goes to MathWorks and its representative Kirthi Devleker, who came to the final competition as a member of the jury. Since its inception, the SP Cup has received generous support from MathWorks, the maker of the popular MATLAB and Simulink platforms. MathWorks kindly provided funding support to the SP Cup, including travel grants and monetary prizes for the finalists. Finally, special thanks go to Pol Mordel, Victor Miguet, Vincent Drevelle, and François Bodin from the Institut de Recherche en Informatique et Systèmes Aléatoires, Rennes, France), without whom obtaining such valuable UAV-embedded recordings would not have been possible.

## Authors

**Antoine Deleforge** (antoine.deleforge@inria.fr) received his engineering B.Sc. degree in 2008 and his research M.Sc. degree in computer science and mathematics in 2010 from the École Nationale Supérieure d'Informatique et de Mathématiques Appliquées de Grenoble, France, and the Université Joseph Fourier, Grenoble, France, and his Ph.D. degree in computer sciences and applied mathematics from the University of Grenoble. He is a tenured research scientist with INRIA Nancy-Grand Est, France, with the team MULTISPEECH. He serves as a member of the IEEE Audio and Acoustics Signal Processing Technical Committee (AASP TC) and the IEEE Autonomous System Initiative (ASI). He initiated, coordinated, and chaired this edition of the Signal Processing Cup, endorsed by the AASP TC and ASI. He is a Member of the IEEE.

**Diego Di Carlo** (diego.di-carlo@inria.fr) is a Ph.D. student with INRIA Rennes-Bretagne Atlantique, France, with the team PANAMA. He was in charge of the competition evaluation and wrote the baseline and evaluation scripts. He is a Student Member of the IEEE.

**Martin Strauss** (martin.strauss@fau.de) received his B.Sc. degree in sports science in 2013 from the Technical University of Munich and his B.Sc. degree in medical engineering in 2016

from the Friedrich-Alexander University of Erlangen-Nuremberg, Germany, where he is currently a master's student. He is the main author of the Drone Egonoise data set [7], which served as a basis for the competition, and he participated in the early design of the tasks. He is a Student Member of the IEEE.

**Romain Serizel** (romain.serizel@loria.fr) received his M.Eng. degree in automatic system engineering from the Ecole Nationale Supérieure d'Electricité et de Mécanique, Nancy, France, in 2005, his M.Sc. degree in signal processing from the Université Rennes 1, France, in 2006, and his Ph.D. degree in engineering sciences from the Katholieke Universiteit Leuven, Belgium, in 2011. He is an associate professor at Université de Lorraine, France, doing research with Laboratoire Lorrain de Recherche en Informatique et Ses Applications with the team MULTISPEECH. He contributed to the Signal Processing Cup competition design and evaluation and presided over the final jury. He is a Member of the IEEE.

**Lucio Marcenaro** (lucio.marcenaro@unige.it) received his degree in electronic engineering and his Ph.D. degree in computer science and electronic engineering from the University of Genova, Italy, in 1999 and 2003, respectively. He is an assistant professor in the Department of Electrical, Electronics and Telecommunication Engineering and Naval Architecture, University of Genoa, Italy. He chairs the Student Service Committee of the IEEE Signal Processing Society, supporting the Signal Processing Cup. He is a Member of the IEEE.

## References

- [1] D. Gilman, "Unmanned aerial vehicles in humanitarian response," United Nations Office for the Coordination of Humanitarian Affairs, 2014. [Online]. Available: <https://docs.unocha.org/sites/dms/Documents/Unmanned%20Aerial%20Vehicles%20in%20Humanitarian%20Response%20OCHA%20July%202014.pdf>
- [2] L. Lopez-Fuentes, J. van de Weijer, M. González-Hidalgo, H. Skinnemoen, and A. D. Bagdanov, "Review on computer vision techniques in emergency situations," *Multimedia Tools Appl.*, vol. 77, no. 13, pp. 17,069–17,107, 2018. doi: 10.1007/s11042-017-5276-7.
- [3] M. Basiri, F. Schill, P. U. Lima, and D. Floreano, "Robust acoustic source localization of emergency signals from micro air vehicles," in *Proc. 2012 IEEE/RSJ Int. Conf. Intelligent Robots and Systems*, pp. 4737–4742.
- [4] T. Ohata, K. Nakamura, T. Mizumoto, T. Taiki, and K. Nakadai, "Improvement in outdoor sound source detection using a quadrotor-embedded microphone array," in *Proc. 2014 IEEE/RSJ Int. Conf. Intelligent Robots and Systems*, pp. 1902–1907.
- [5] K. Hoshiba, K. Washizaki, M. Wakabayashi, T. Ishiki, M. Kumon, Y. Bando, D. Gabriel, K. Nakadai, et al., "Design of UAV-embedded microphone array system for sound source localization in outdoor environments," *Sensors*, vol. 17, no. 11, article no. 2535, 2017. doi: 10.3390/s17112535.
- [6] L. Wang, R. Sanchez-Matilla, and A. Cavallaro, "Tracking a moving sound source from a multi-rotor drone," in *Proc. 2018 IEEE/RSJ Int. Conf. Intelligent Robots and Systems*, pp. 2511–2516.
- [7] M. Strauss, P. Mordel, V. Miguez, and A. Deleforge, "DREGON: Dataset and methods for UAV-embedded sound source localization," in *Proc. 2018 IEEE/RSJ Int. Conf. Intelligent Robots and Systems*. doi: 10.1109/IROS.2018.8593581.
- [8] C. Rascon and I. Meza, "Localization of sound sources in robotics: A review," *Robotics Autonomous Syst.*, vol. 96, pp. 184–210, Oct. 2017. doi: 10.1016/j.robot.2017.07.011.
- [9] C. Knapp and G. Carter, "The generalized correlation method for estimation of time delay," *IEEE Trans. Acoust., Speech, Signal Process.*, vol. 24, no. 4, pp. 320–327, 1976. doi: 10.1109/TASSP.1976.1162830.
- [10] S. Argentieri and P. Danes, "Broadband variations of the MUSIC high-resolution method for sound-source localization in robotics," in *Proc. 2007 IEEE/RSJ Int. Conf. Intelligent Robots and Systems*, pp. 2009–2014.
- [11] K. Nakamura, K. Nakadai, F. Asano, Y. Hasegawa, and H. Tsujino, "Intelligent sound source localization for dynamic environments," in *Proc. 2009 IEEE/RSJ Int. Conf. Intelligent Robots and Systems*, pp. 664–669.
- [12] A. Deleforge, F. Forbes, and R. Horaud, "Acoustic space learning for sound-source separation and localization on binaural manifolds," *Int. J. Neural Syst.*, vol. 25, no. 1, p. 1440003, 2015. doi: 10.1142/S0129065714400036.
- [13] C. Gaultier, S. Kataria, and A. Deleforge, "Vast: The virtual acoustic space traveler dataset," in *Proc. Int. Conf. Latent Variable Analysis and Signal Separation*, 2017, pp. 68–79.
- [14] H. W. Löllmann, H. Barfuss, A. Deleforge, S. Meier, and W. Kellermann, "Challenges in acoustic signal enhancement for human-robot communication," in *Proc. 11th ITG Symp. Speech Communication*, 2014, pp. 1–4.
- [15] J. S. Garofolo, "TIMIT acoustic-phonetic continuous speech corpus," Linguistic Data Consortium, 1993. [Online]. Available: <https://catalog.ldc.upenn.edu/LDC93S1>
- [16] R. Lebarbenchon, E. Camberlein, D. di Carlo, C. Gaultier, A. Deleforge, and N. Bertin, Evaluation of an open-source implementation of the SRP-PHAT algorithm within the 2018 LOCATA challenge. 2018. [Online]. Available: <https://arxiv.org/abs/1812.05901>
- [17] C. Blandin, A. Ozerov, and E. Vincent, "Multi-source TDOA estimation in reverberant audio using angular spectra and clustering," *Signal Process.*, vol. 92, no. 8, pp. 1950–1960, 2012. doi: 10.1016/j.sigpro.2011.09.032.
- [18] H. W. Löllmann, C. Evers, A. Schmidt, H. Mellmann, H. Barfuss, P. A. Naylor, and W. Kellermann, "The LOCATA challenge data corpus for acoustic source localization and tracking," in *Proc. 2018 IEEE 10th Sensor Array and Multichannel Signal Processing Workshop*, pp. 410–414.
- [19] S. Gannot, E. Vincent, S. Markovich-Golan, and A. Ozerov, "A consolidated perspective on multi-microphone speech enhancement and source separation," *IEEE/ACM Trans. Audio, Speech, Language Process.*, vol. 25, no. 4, pp. 692–730, 2017. doi: 10.1109/TASLP.2016.2647702.

Please send calendar submissions to:  
Dates Ahead, Att: Samantha Walter, E-mail: [walter.samantha@ieee.org](mailto:walter.samantha@ieee.org)

## 2019

### SEPTEMBER

#### **IEEE International Conference on Advanced Video and Signal-Based Surveillance (AVSS)**

18–21 September, Taipei, Taiwan.

General Cochairs: Rama Chellappa, Ming-Hsuan Yang, and Hanseok Ko  
URL: <http://avss2019.org/>

#### **IEEE International Conference on Image Processing (ICIP)**

22–25 September, Taipei, Taiwan.

General Chairs: C.-C. Jay Kuo, Homer H. Chen, and Hsueh-Ming Hang  
URL: <http://2019.ieeeicip.org>

#### **IEEE 21st International Workshop on Multimedia Signal Processing (MMSP)**

27–29 September, Kuala Lumpur, Malaysia.

General Chairs: Jenq-Neng Hwang, Chee Seng Chan, and Wen-Huang Cheng  
URL: <http://mmsp2019.org>

### OCTOBER

#### **IEEE International Workshop on Machine Learning for Signal Processing (MLSP)**

13–16 October, Pittsburgh, Pennsylvania, United States.

General Chair: Murat Akcakaya  
URL: <https://www.ieemlsp.cc/>

#### **IEEE Workshop on Applications of Signal Processing to Audio and Acoustics (WASPAA)**

20–23 October, New Paltz, New York, United States.  
General Chairs: Augusto Sarti and Boaz Rafaeli  
URL: <https://www.waspaa.com/>

#### **IEEE International Workshop on Signal Processing Systems (SiPS)**

20–23 October, Nanjing, China.  
General Chairs: Zhongfeng Wang and Chuan Zhang  
URL: <http://sips2019.org/>

### NOVEMBER

#### **Asilomar Conference on Signals, Systems, and Computers**

3–6 November, Pacific Grove, California, United States.  
General Chair: Gerald Matz  
URL: <http://www.asilomarssc.org>



©ISTOCKPHOTO.COM/J2R

ICASSP 2020 will be held 4–9 May 2020, in beautiful Barcelona, Spain.

#### **IEEE Global Conference on Signal and Information Processing (GlobalSIP)**

11–14 November, Ottawa, Ontario, Canada.

General Cochairs: Fabrice Labeau and Sreeraman Rajan  
URL: <https://2019.ieeglobalsip.org/>

#### **Asia-Pacific Signal and Information Processing Association Annual Summit and Conference (APSIPA ASC)**

18–21 November, Lanzhou, China.

General Cochairs: Thomas Fang Zheng, Hongzhi Yu, Jianwu Dang, Wan-Chi Siu, and Hitoshi Kiya  
URL: <http://www.apsipa2019.org/>

### DECEMBER

#### **IEEE International Workshop on Information Forensics and Security (WIFS)**

9–12 December, Delft, The Netherlands.

General Chair: Zekeriya Erkin  
URL: <https://wifs2019.tudelft.nl/>

#### **IEEE International Symposium on Signal Processing and Information Technology (ISSPIT)**

10–12 December, Ajman, United Arab Emirates.

General Cochairs: Khaled Assaleh and Adel Elmaghreby  
URL: <http://www.isspit.org/isspit/2019/index.html>

#### **IEEE Automatic Speech Recognition and Understanding Workshop (ASRU)**

14–18 December, Sentosa, Singapore.

General Chair: Haizhou Li  
General Cochair: Eric Fosler-Lussier  
URL: <http://www.asru2019.org/>

#### **IEEE International Workshop on Computational Advances in Multisensor Adaptive Processing (CAMSAP)**

14–18 December, Guadeloupe, West Indies.

General Chairs: David Brie and Jean-Yves Tourneret  
URL: <https://camsap19.ig.fpms.ac.be>

## 2020

### APRIL

#### **IEEE International Symposium on Biomedical Imaging (ISBI)**

4–8 April, Iowa City, Iowa, United States.

General Chairs: Mathews Jacob and Jong Chul Ye  
URL: <http://2020.biomedicalimaging.org/>

### MAY

#### **IEEE International Conference on Acoustics, Speech, and Signal Processing (ICASSP)**

4–9 May, Barcelona, Spain.

General Chairs: Ana I. Pérez Neira and Xavier Mestre  
URL: <https://2020.ieeeicassp.org>

# IN THE SPOTLIGHT

(continued from page 148)

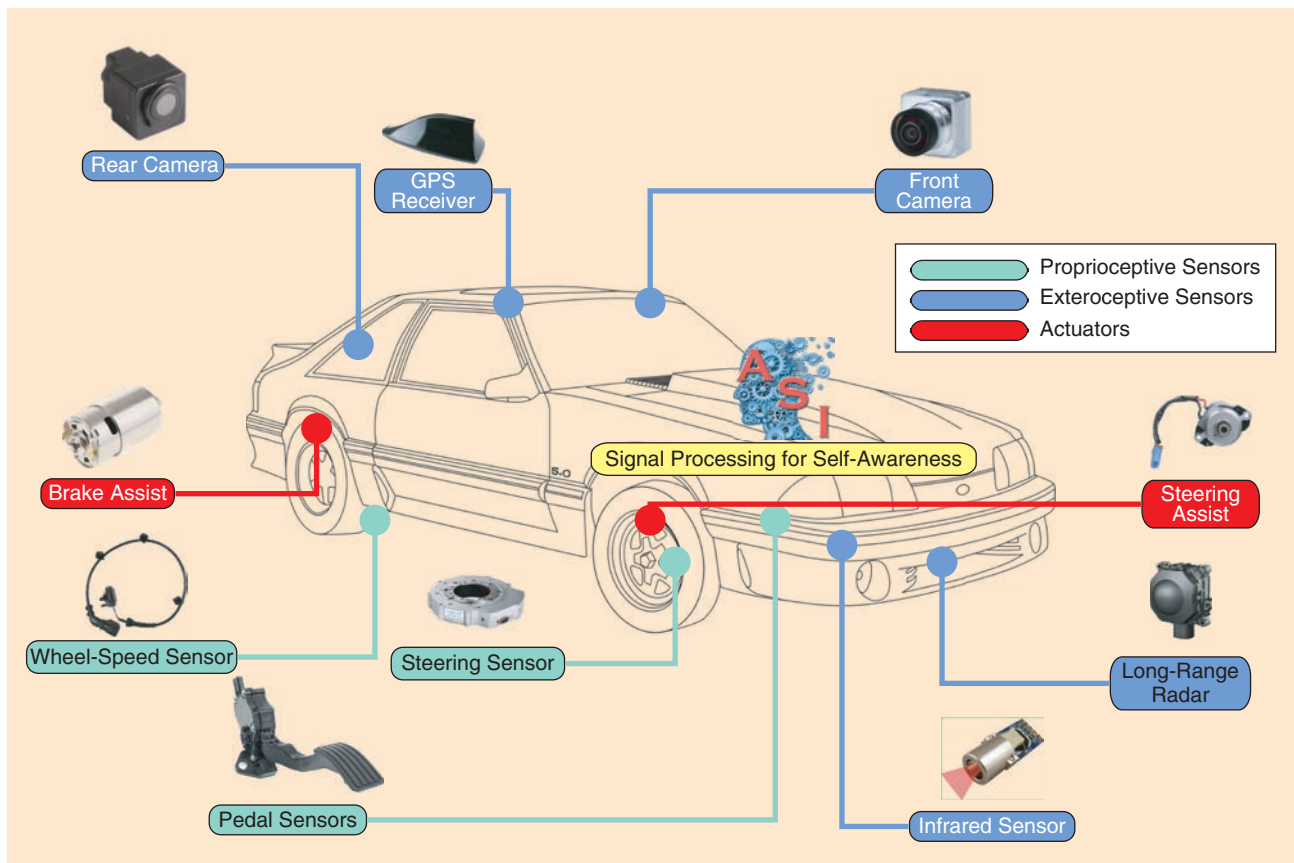


**FIGURE 1.** An architecture for a self-aware autonomous system. The autonomous vehicle observes the surrounding environment with exteroceptive sensors (blue) and its internal state with proprioceptive sensors (green). It translates its autonomous decisions into actions through actuators (red). The self-awareness core is able to forecast the next state of the environment and of the system itself to detect anomalies and execute the derived actions.

- perception modalities, e.g., visual, sonar/ultrasound, laser, or radio/GPS.
- In autonomous system communications, signal (e.g., video) compression, transmission, and error resilience are very important aspects.
- In autonomous system action, adaptive signal processing can play an important role in command and control.

The IEEE Signal Processing Society (SPS) recognized the immensity of the challenges ahead and the research potential and launched the Autonomous Systems Initiative (ASI) during the 2018 IEEE International Conference on Image Processing. From a scientific point of view, ASI can cover the following areas:

- perception
- sensor-information processing

- mission planning and control
- machine learning for perception and control
- robust, secure mobile communications
- embedded systems
- security
- societal issues, e.g., data protection and privacy.

From an industrial/sectorial point of view, it can cover autonomous systems operating in any environment, whether on land, underwater, in the air, underground, or in space. More specifically, this includes

- autonomous cars
- autonomous robotic systems
- marine, underwater vessels
- drones and unmanned aircraft.

ASI is expected to draw significant interest within the SPS constituency

but also in the wider scientific community and related industries. To this end, it will cooperate with all relevant SPS technical committees, which will have representatives in ASI. The creation of SPS megatrend ASI will boost SPS involvement in this important and expanding area and allow interaction with other IEEE Societies. Furthermore, it will allow interfacing with other related scientific communities and industrial bodies.

In the last year, ASI has established its bylaws and built an organizational structure (steering committee, members, and associate members). The ASI website (<https://ieeeari.signalprocessingsociety.org/>) and a Google docs drive have been created and populated, where a wealth of various ASI activities (special issues, special sessions, tutorials,

and workshops) are detailed. Any interested engineer or scientist is welcome to join as an ASI member, associate member, or volunteer by following the procedures described on the ASI website and to contribute to ASI activities.

Proposals on ASI-related activities (e.g., courses, special sessions/issues, workshops, or competitions) for synergies within SPS, IEEE Societies, and other scientific communities and relevant industrial bodies are welcome from anyone who can send an email to ASI Chair Prof. Ioannis Pitas and/or ASI Vice Chair Prof. Carlo Regazzoni.

## Authors

**Carlo Regazzoni** (carlo.regazzoni@unige.it) received his M.S. and Ph.D. degrees from the University of Genova, Italy, in 1987 and 1992, respectively. Currently, he is a professor at the Polytechnic School of the University of Genova, Italy. He has been involved in

research on signal and video processing and data fusion since 1988. His current research interests are cognitive dynamic systems, adaptive and self-aware data fusion, machine learning, software, and cognitive radio. He is one of the pioneering researchers in intelligent video surveillance. In 1998, he created the IEEE International Conference on Advanced Video and Signal-Based Surveillance. He is author or coauthor of more than 100 journal papers and 400 conference papers and book chapters (his Google Scholar h-index is 40). He has served within the IEEE Signal Processing Society in various positions including vice president-Conferences (2015–2017). He is currently vice chair of the IEEE Autonomous Systems Initiative. He is a Senior Member of the IEEE.

**Ioannis Pitas** (pitas@csd.auth.gr) received his diploma and Ph.D. degree in electrical engineering, both from the

Aristotle University of Thessaloniki, Greece, where, since 1994, he has been a professor in the Department of Informatics. He has published more than 1,090 papers, contributed to 50 books in his areas of interest, and edited or (co)authored another 11 books. He has also been member of the program committee of many scientific conferences and workshops, an associate editor or coeditor of nine international journals, and the general/technical chair of four international conferences. He participated in 69 R&D projects, primarily funded by the European Union. He has more than 29,000 citations to his work, and his h-index is 79+ (Google Scholar). He leads the big European H2020 R&D project MULTIDRONE and is the chair of the IEEE Autonomous Systems Initiative. He is a Fellow of the IEEE and EURASIP as well as an IEEE Distinguished Lecturer.



## SP FORUM *(continued from page 137)*

of Technology, Limassol, and his M.S. and Ph.D. degrees in electrical and computer engineering from West Virginia University, Morgantown. He is a professor in the School of Electrical, Computer, and Energy Engineering at Arizona State University, Tempe, where he also directs the Sensor Signal and Information Processing (SenSIP) center and founded the SenSIP industry consortium. He has served as an associate editor of *IEEE Transactions on Signal Processing* and as general cochair of ICASSP 99. He is a corecipient of the 2002 IEEE Donald G. Fink Paper Prize Award. His research interests are in the areas of adaptive

signal processing, speech processing, machine learning, and sensor systems. He is a Fellow of the IEEE.

**Mónica F. Bugallo** (monica.bugallo@stonybrook.edu) received her B.S., M.S., and Ph.D. degrees in computer science and engineering from the University of A Coruña, Spain. She is a full professor of electrical and computer engineering and the faculty director of the Women in Science and Engineering program at Stony Brook University, New York. Her research interests are in the field of statistical signal processing, with emphasis on the theory of Monte Carlo methods and their application to

different disciplines including biomedicine, sensor networks, and finance. She has authored and coauthored two book chapters and more than 150 journal papers and refereed conference articles. She is a Senior Member of the IEEE.

## References

- [1] W. Bajwa, "On 'flipping' a large signal processing class [SP Education]," *IEEE Signal Process. Mag.*, vol. 34, no. 4, pp. 158–170, 2017.
- [2] A. V. Oppenheim, "One plus one could equal three (and other favorite clichés)," *IEEE Signal Process. Mag.*, vol. 23, no. 6, pp. 10–12, 2006.
- [3] S. K. Mitra, "Reminiscences of a department chair," *IEEE Signal Process. Mag.*, vol. 23, no. 3, pp. 10–13, 2006.
- [4] Responsible Metrics, "The metric tide." [Online]. Available: <https://responsiblemetrics.org/the-metric-tide/>



## Perspectives in Autonomous Systems Research

**T**oday, many devices (e.g., cars and other vehicles) we operate for various tasks (e.g., to go from place A to place B) are changing: in the past, they were characterized by a body and control actuators that allowed us to perform these tasks. These days, they are not simply passive recipients of our instructions; rather, they have become proactive tools performing the assigned task (or parts of it) by making autonomous decisions based on signals from their sensors.

Therefore, more of these devices can be classified as *autonomous systems*. The level of autonomous decision making can be device dependent but, in every case, involves efficient multimodal signal processing capabilities. Such devices become our agents and have to relate multisensorial data representations to their actions and to the action context. Such a context includes the target of the agent's task, i.e., the action motivation and the user, in cases in which the task is only partially automated.

What is our role as signal processing researchers in autonomous systems research? For many years, our community has developed theories and methods to obtain optimal representations of received/observed heterogeneous signals. Optimality concepts often have been expressed at the signal level, as the signal representation was just a filtered version of the signal itself; in other cases, we had to provide optimal discrete variables or labels as signal processing output. Segmentation

of video sequences or speech can be such examples. Some of us are used to working up to the semantic signal analysis level by providing semantic labels to signal segments and associating a meaning to such labels. This moves toward pattern recognition, which, for many of us, is just a mapping of signals to discrete variable domains or label sets. When signal processing is used within an autonomous system, the optimization functional changes again. Here, the optimality is often related to the fact that signals are processed within the agent perception–action cycle aiming at agent decision making for reaching an optimal dynamic equilibrium with the environment and the agent's user.

Autonomous cars, drones, robots, cognitive radios and radars, and intelligent buildings (and much more to come) will be the agents for which we have to provide solutions. Video, acoustic, tactile, and radio signals will be just some of the sensorial signals that should be processed by an agent in real time, for example,

- to interpret the external situation in which it operates
- to relate a situation to its internal state, by observing it with other proprioceptive sensors, so that it becomes self-aware
- to use representations to help its own control blocks to drive its actuators
- to be able to explain at subsymbolic and symbolic levels the reasons for its own choices (see Figure 1).

Over the last decade, researchers have been proposing and investigating computing systems with advanced levels of autonomy to manage the ever-increasing

requirements in complexity. An autonomous system is an artificial system able to perform a certain number of tasks with a high degree of autonomy. Many real-world systems frequently experience nonstationary conditions (i.e., unknown situations) due to uncertain interactions with the environment (including human agents) and users, failures, or structural changes. Autonomous systems aim at building up behavior rules over time by learning, through interactions with the environment with complex perception–action cycles, to deal with environment changes and uncertainties.

A fully autonomous system can

- gain information about the environment
- work for an extended period without human intervention
- move either all or part of itself throughout its operating environment without human assistance
- avoid situations that are harmful to people, property, or itself unless those are part of its design specifications.

An autonomous system may also learn or gain new knowledge, such as adjusting for new methods of accomplishing its tasks or adapting to changing surroundings. From an industrial point of view, autonomous systems have exhibited impressive growth in the last decade, notably in autonomous cars, robots, and drones.

Signal processing plays an important role in the perception–action cycle of autonomous systems.

- In autonomous system perception, signal analysis is important for any

## Call for Papers -- IEEE Journal of Selected Topics in Signal Processing

Deep Learning for Multi-modal Intelligence across Speech, Language, Vision, and Heterogeneous Signals

[Deadline Extended: September 15, 2019]

In the past years, thanks to the disruptive advances in deep learning, significant progress has been made in speech processing, language processing, computer vision, and applications across multiple modalities. Despite the superior empirical results, however, there remain important issues to be addressed. Both theoretical and empirical advancements are expected to drive further performance improvements, which in turn would generate new opportunities for in-depth studies of emerging novel learning and modeling methodologies. Moreover, many problems in artificial intelligence involve more than one modality, such as language, vision, speech and heterogeneous signals. Techniques developed for different modalities can often be successfully cross-fertilized. Therefore, it is of great interest to study multimodal modeling and learning approaches across more than one modality. The goal of this special issue is to bring together a diverse but complementary set of contributions on emerging deep learning methods for problems across multiple modalities.

Topics of interest in this special issue include (but are not limited to):

- Fundamental problems and methods for processing multi-modality data including language, speech, image, video, and heterogeneous signals.
- Pre-training, representation learning, multitask learning, low-shot learning, and reinforcement learning of multimodal problems across natural language, speech, image, and video.
- Deep learning methods and applications for cross-modalities, such as image captioning, visual question answering, visual story-telling, text-to-image synthesis, vision-language navigation, *etc.*
- Evaluation metrics of multimodal applications.

### Important Dates

Submissions due: 15-Sept-2019

First review: 01-Nov-2019

Revised manuscript due: 15-Dec-2019

Second review: 1-Feb-2020

Final manuscripts due: 15-Mar-2020

### Guest Editors:

Xiaodong He, JD AI - Beijing, China (Lead Guest Editor), [xiaodong.he@jd.com](mailto:xiaodong.he@jd.com)

Li Deng, Citadel, USA, [l.deng@ieee.org](mailto:l.deng@ieee.org)

Minlie Huang, Tsinghua University, China, [aihuang@mail.tsinghua.edu.cn](mailto:aihuang@mail.tsinghua.edu.cn)

Richard Rose, Google AI, USA, [rickrose@google.com](mailto:rickrose@google.com)

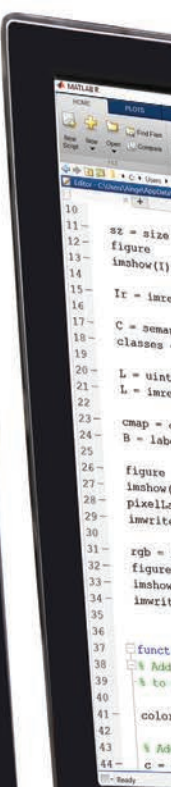
Isabel Trancoso, IST (University Lisbon), Portugal, [isabel.trancoso@inesc-id.pt](mailto:isabel.trancoso@inesc-id.pt)

Chao Zhang, JD AI Research & University of Cambridge, UK, [chao.zhang@jd.com](mailto:chao.zhang@jd.com)

# MATLAB SPEAKS DEEP LEARNING

With just a few lines of MATLAB® code, you can use CNNs and training datasets to create models, visualize layers, train on GPUs, and deploy to production systems.

[mathworks.com/deeplearning](http://mathworks.com/deeplearning)



```
10 sz = size
11 figure
12 imshow(I)
13
14 Ir = imre
15
16 C = seman
17 classes
18
19 L = uint
20 L = imre
21
22 cmap =
23 B = lab
24
25
26 rgb =
27 figure
28 imshow(
29 pixels)
30 imwrit
31
32
33
34
35
36
37
38
39
40
41
42
43
44 c =
```